Synthesis and cell adhesion studies of linear and hyperbranched poly(butyl methacrylate) and poly(t-butyl acrylate)

Kayleigh J Cox-Nowak

Submitted for the degree of Doctor of Philosophy

Department of Chemistry

October 2013

Contents

Acknowledgements

Abbreviations

(semi-)IPN	(Semi-)Interpenetrating polymer network
ACVA	4,4'-azobiscyanovaleric acid
BMA	Butyl methacrylate
CAM	Cell adhesion molecule
CTA	Chain transfer agent
DMEM	Dulbecco's modified Eagle's medium
DMSO	Dimethyl sulfoxide
EDC	1-Ethyl-3-(3-dimethylaminopropyl)carbodiimide
EDTA	Ethylenediaminetetraacetic acid
FBS	Feotal bovine serum
FT-IR	Fourier transform infra-red spectroscopy
GPC	Gel permeation chromatography
HBP	Hyperbranched polymer
HDF	Human dermal fibroblast
IR	Infra-red
NMR	Nuclear magnetic resonance
OD	Optical density
PBS	Phosphate buffered saline
PEG-PEI-PBLG	Poly(ethylene glycol)–polyethylenimine–poly(γ-benzyl l-glutamate)
PLGA	Poly(lactide-co-glycolic acid)
pnipam	Poly(n-isopropylacrylamide)
RAFT	Radical addition-fragmentation chain transfer polymerisation
REpC	Human renal epithelial cells
SEC	Size exclusion chromatography
tBuAc	Tertiary-butyl acrylate
UV	Ultraviolet
VBA	4-vinyl benzoic acid

Abstract

A library of polymers/oligomers with three different architectures was synthesised. Short chain, linear oligomers were produced by performing oxidative cleavage on a poly(butyl methacrylate-co-butadiene) polymer. Although butadiene is a gaseous monomer, it was found that careful control over the reaction conditions led to successful copolymerisation in an unpressurised reactor. Hyperbranched polymers of n-butyl methacrylate and t-butyl acrylate were synthesised by RAFT polymerisation with 4-vinylbenzyl-pyrrolecarbodithioate (CTA1) and 4-vinylbenzyl dithiobenzoate (CTA2). A variety of analytical techniques, such as elemental analysis and NMR, were used to characterise the polymers and confirm the hyperbranched structure. Some variation in monomer conversion and CTA uptake was seen under different polymerisation conditions.

After synthesis and characterisation, it was found that the polymer end groups could be modified through work up with diamine or 4.4'-azobiscyanovaleric acid. Linear oligomers of butyl methacrylate were functionalised with amines whilst hyperbranched polymers were given acid functional end groups. FT-IR and elemental analysis were used to monitor the success of the end group reactions.

As the polymers could be applied as films, they were assessed as cell culture substrates using Human dermal fibroblasts (HDF) and Human renal epithelial cells (HREp). A linear butyl methacrylate-co-4-vinyl benzoic acid copolymer was also assessed in comparison to the hyperbranched structures. It was observed that the two cell types had different responses to each of the polymers. Fibroblast cells showed better rates of adhesion and proliferation on acid-functionalised polymers, whilst epithelial cells performed best on the amine-functionalised moieties.

This work provides useful information for the synthesis and preparation of new biomaterials. It has been found that polymer functionality must be considered when compatibility with a specific cell type is desired, and polymers with the potential to be incorporated into future biomaterials are highlighted.

1 - Introduction

Context

Today, teams of polymer chemists and cell biologists are working together in an effort to create evermore practical and functional materials for use in tissue engineering, cell re-growth and therapy and agent delivery. The purpose of this introduction is to review and correlate the work carried out in the areas of controlled polymer architecture and biocompatibility. Many potential bio-interactive polymers have been identified, but rarely are cell culture experiments performed which would provide adherence and toxicity information. Any commercial material must be able to fit within a narrow specification range. HBPs are attractive biomaterials as they can be synthesised with high control and within narrow polydispersities[1]. The use of HBPs in biomaterials ranges from carriers to degradable materials. A HBP with tertiary amino groups was synthesised by Park *et al.*[2] that was able to efficiently transfect DNA with low toxicity. In addition, protein immobilisation has been demonstrated by Shen[3], [4] and Cosulich[5] which opens the possibility of 'enzyme-based bioobjects'. Lin and Zhang *et al.* created a biodegradable blend material with enhanced properties by combining HBPoly(ester amide) with polylactide[6], and Chen *et al.* reported the successful synthesis of an inherently biodegradable cationic HBP of PEG-PEI-PBLG[7]. These polymers all show positive bio-interactions and indicate that the amine functionality may be a positive inclusion for increasing cell adherence and culture.

Polymers with carboxylic acid functionality are also considered to have a degree of biocompatibility[8]. Observations by MacNeil *et al.* have indicated that a polymer containing *ca.* 3% acid promotes the attachment of keratinocytes and osteoblast-like cells[9], [10]. The MacNeil group have also utilised the technique of electrospinning to form polymers with acid functionality, that can be used for tissue regeneration and drug release [11], [12].

This project investigated the emulsion polymerisation of P(BMA-BD) and the biocompatibility of oligomers after being cleaved with ozone and functionalised with amine or acid. Also explored was the synthesis of and biocompatibility of HBP(BMA) and HBP(tBuAc). Some polymers were reacted with 4,4'-azobis4-cyanovaleric acid (ACVA) or diamines in order to observe the effect of end group functionality on cell adhesion.

To our knowledge this is the first known use of RAFT to form hyperbranched polymers using *t*-butyl acrylate and butyl methacrylate monomers. It was investigated what effect varying the amount of chain transfer agent (CTA) had on the polymerisation and also on the final product. The original aim was to synthesise a range of hyperbranched polymers, and then use

these to build a library of semi-interpenetrating polymer networks. However, the HBPs did not have high enough molecular weights to stay entrapped in the networks.

In order to investigate the polymers' biocompatibility, they were cast into films so that cells could be grown in direct contact, where it was found that introducing acid functionality was advantageous. Amino groups have been considered to be more cell interactive than carboxylic acid and OH functionality [13], [14]. The evidence provided by this work indicates that the cell-interactivity of a functional group is also dependent on the cell type tested against. With carefully planned experiments, it is possible to observe the effect of molecular weight, branching and end group modifications on HBPs. The observations described within indicate that non-mesenchymal cells show a preference for amine and dithioate functional polymers over acids. This knowledge is essential for the creation of future materials that possess both the necessary physical and chemical properties for continued healthy cell adhesion and proliferation *in vivo*. This introduction will discuss current methods and trends in RAFT and emulsion polymerisation, followed by an overview of synthetic polymers (specifically hyperbranched or crosslinked) and their uses in modern biomaterials.
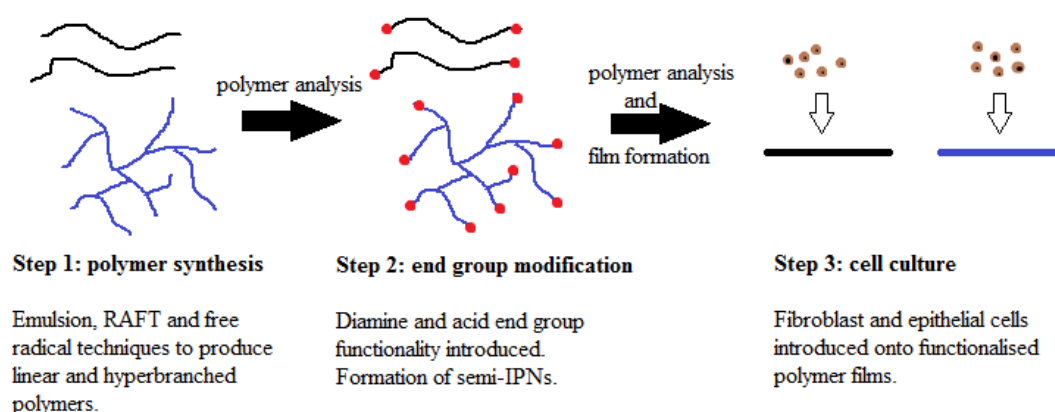
Figure 1.1 – Diagram illustrating the concept and stages of the project

1.1 Emulsion polymerisation

Emulsion polymerisation is used in a variety of applications ranging from adhesives, rubbers, drug delivery and paper additives[15]–[22]. The product obtained from emulsion polymerisation is a polymer dispersed in water and colloidally stabilised by surfactant – called a latex or polymer dispersion. Typically the reaction is free radical and occurs in a

heterophase system, where an immiscible liquid (the monomer) is held in the dispersion medium (water) by a surfactant.

The role of surfactant within the system is to: stabilise monomer in the form of droplets or micelles, influence the polymerisation kinetics and provide colloidal stability for the final product. It is added at levels above the critical micelle concentration, which is the minimum concentration for micelle formation. Surfactants have two domains, a hydrophilic 'head' and a hydrophobic fatty acid 'tail' and it is this amphiphilic nature that allows these compounds to stabilise hydrophobic molecules in aqueous media. Monomer and surfactant can interact to form either large monomer droplets or smaller, and relatively numerous, micelles (figure 1.1.1). The number and size of micelles present in a system depends on the amount of surfactant added, with higher proportions leading to smaller, more numerous micelles. This means that, to some extent, larger particle sizes can be achieved by using less surfactant in the recipe – especially during interval I as will be described on page 14. However, this can lead to the appearance of coagulated polymer as it will not be adequately stabilised later in the reaction.
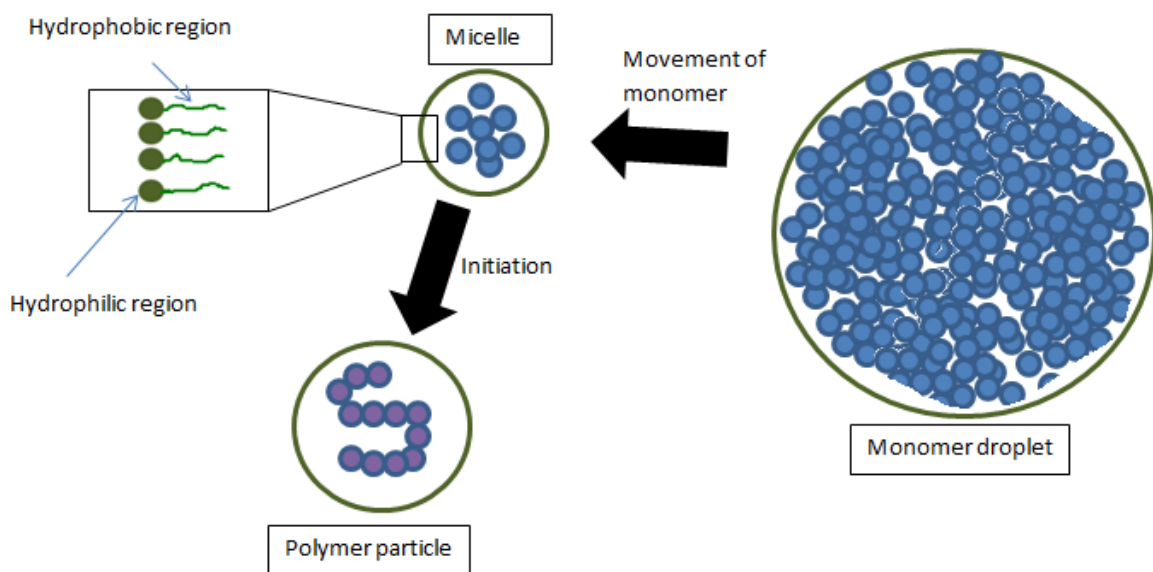
Figure 1.1.1 – The basic constituents in an emulsion polymerisation.

Emulsion recipes can be prepared so that a population of larger sized particles are included at the end of the reaction. The combination of small and large particles enables more efficient ordering of the molecules to occur, and therefore greater solids contents can be achieved than with a single particle size[23].

Many different types of surfactant, or emulsifier, are available to assist the dispersion of monomers in emulsion polymerisation. The most commonly used are those with an anionic head group, such as sulfates, sulfonates, carboxylates and phosphates. Available emulsifiers in this group include sodium dodecyl sulfate and dioctyl sodium sulfosuccinate. There also exist cationic surfactants, these are normally amines or contain a quaternary ammonium cation, and non-ionic stabilisers such as long chain alcohols. However, it is often found that the strongest amphiphilic behaviour exists with molecules up to a chain length of C_{22}, beyond which the hydrophobic domain dominates and prevents solubility in water. A dispersant is a surface-active molecule that is added to an emulsion to aid the dispersal of additives such as pigments. In this case, the dispersant adsorbs directly onto the surface of the pigment molecules in order to prevent clumping and flocculation.

The key property of any monomer for polymerisation is that it must be unsaturated and allow addition across the bond. For a monomer to be suitable for emulsion polymerisation it must only be sparingly soluble in the dispersal medium – usually water. The solubility of some commonly used monomers that are used in emulsion polymerisation is listed in table 1.1.2.

Monomer	Solubility in water g/l^{-1}
Styrene	0.07
Butadiene	0.8
Vinyl Chloride	7
Methyl methacrylate	16
Vinyl acetate	25
Butyl acrylate	2
Butyl methacrylate	3

Table 1.1.2 – Solubility of some common monomers used in emulsion polymerisation.

A typical commercial emulsion contains 30-50% of monomer[24], [25], with the end use of the product determining how much is required. The majority of monomer within the reaction system exists within the large monomer droplets which are stabilised by surfactant molecules. The rest is either present within surfactant micelles, or free within the dispersion medium. To provide a source of radicals, either a redox coupling system or a thermal initiator is employed, although universally the initiator will be water soluble and oil-insoluble. This means that propagation cannot occur on the monomer droplets as previously discussed. The benefit of a redox coupling system is that it can be used to produce radicals at low

temperatures. This means reactions can be performed at 6°C instead of common industrial processes that occur at temperatures of 75°C and above.

Unlike other techniques, emulsion polymerisation is able to attain high molecular weights with no detriment to reaction rates. This is because propagating polymer chains are kept separated by the dispersal medium, reducing the chance of termination by coupling. Employing a chain transfer agent such as *n*-dodecyl mercaptan can keep molecular weight lowered. Chain transfer is the effect that is responsible for lower observed polymer molecular weights than predicted. Chain transfer occurs through the termination of a propagating chain through abstraction of a hydrogen atom, or other species present in the reaction system (for instance monomer, solvent and initiator). If the rate of chain transfer is greater than the rate of propagation, then very short chain polymers are formed. In addition to the termination of a growing chain, chain transfer also releases a free radical which is able to reinitiate polymerisation. If the rate of reinitiation is rapid, then no effect is observed on the rate of polymerisation. However, a slow rate of reinitiation will lead to a decrease in overall rate of polymerisation. The effect of chain transfer on the degree of polymerisation can be calculated using the general form of the Mayo equation (equation 1.1.3)

$$\frac{1}{X_n} = \frac{(2-a)R_i}{2R_p} + C_M + C_S\frac{[S]}{[M]} + C_I\frac{[I]}{[M]}$$

Equation 1.1.3 – General form of the Mayo equation, where X_n= number average degree of polymerisation, R_p = Rate of polymerisation, R_i = rate of initiation, C = chain transfer constant, M = monomer, S = chain transfer agent and I = initiator.

The theory for the mechanism of emulsion polymerisation was first proposed by Harkins, and further developed by Smith and Ewart, in the 1940's based on studies of poly(butadiene) and styrene respectively[26]–[28]. The mechanisms proposed were insightful for the time but it is now known that the migration of the (electronegative) initiator into the micelles was overlooked.

Smith-Ewart-Harkins theory splits the polymerisation into three intervals. The theory states that interval I involves the dispersal of monomer and surfactant into large droplets and smaller micelles. Small amounts of monomer diffuse though the dispersion medium into the micelles, and a water-soluble initiator is added. The initiator forms free radicals that in the first instance begin the polymerisation with monomers present in the aqueous phase. As monomer molecules are added to the growing oligomers, their hydrophobicity increases until they reach a critical length. At this length the oligomers begin to leave the aqueous phase and enter the monomer-swollen micelles. Once inside the micelles, there is plenty of monomer

present to continue the propagation of oligomers and the micelle then becomes a particle nuclei. The embryonic particles continue to grow, and their colloidal stability is maintained by the donation of surfactant molecules from shrinking monomer micelles[29].

The depletion of the monomer micelles marks the end of interval I. An average of about 10^{2-3} micelles are successfully converted into latex particles - this is much greater than the number of monomer droplets, which generally only act as monomer reservoirs and are not converted into particles. The concentration of surfactant contributes strongly to particle nucleation; this is predicted by Smith-Ewart theory that states the number of nucleated particles per unit volume of water is proportional to $[\text{surfactant}]^{0.6}$. Particle nucleation continues until about 10-20% conversion of monomer, and it controls the particles size and particle size distribution of latexes. A seed latex, which bypasses interval I, is commonly used commercially to ensure batch-to-batch repeatability and generally a smaller particle size can be achieved by increasing the amount of surfactant.

The initiator produces two radicals, which react with the monomer in the surfactant micelles to form z-mer oligomeric radicals. The z-mer is the oligomer chain length that is no longer soluble in the continuous phase.

Persulfate molecules initiate polymerisation by undergoing homolysis in the aqueous phase and then adding across the unsaturated bond in the monomer. The radical active site is then regenerated and propagation occurs as this radical adds to further monomer molecules. This is known as interval II. As monomer is added into the polymer chain, more molecules disperse into the micelles from the large droplets of monomer. The radical active site is also constantly regenerated after the addition of each discrete molecule of monomer allowing polymer growth to continue. Interval III is considered to occur when all of the free monomer is present in the polymer particles, and the rate of polymerisation will begin to steadily to steadily decrease. Termination can occur by combination where two growing chains come together to form one dead polymer or by disproportionation, where a growing chain donates a proton to another. This can lead to branched polymers as a result of chain transfer.

Smith-Ewart theory does not account for the homogenous nucleation that occurs when using slightly more water soluble monomers, such as vinyl acetate or methyl methacrylate. In this case because of the higher presence of free monomer in the dispersal medium, it is possible to get z-mer formation in that phase. Therefore, the polymerisation of these monomers can be performed without the use of surfactant.

1.2 RAFT polymerisation

Reversible addition-fragmentation transfer (RAFT) polymerisation is a highly versatile controlled radical polymerisation (CRP) technique that was first reported by Rizzardo, Moad and Thang in 1998[30]. It is intrinsically tolerant to functionality and allows for polymerisation of a wide range of monomers such as acrylic acid, hydroxyethyl methacrylate and dimethylaminoethyl methacrylate[31]–[36]. A variety of polymer architectures have been synthesised using RAFT polymerisation including brushes, stars, hyperbranched and dendrimers[37]. A good review of the versatility of RAFT with regards to polymer architecture has been provided by Chong *et al.*[38] and also by Perrier and Takolpuckdee[39]. RAFT can also be used to synthesise polymers with controlled molecular weights and narrow polydispersities, as evidenced by Moad *et al.*[40], Pelet and Putnam[41] and others [36], [42].

Key to the success of a RAFT polymerisation is the choice of chain transfer agent (CTA, figure 2.2.1), which come in four main classes: dithioesters, trithiocarbonates, xanthates and dithiocarbamates.
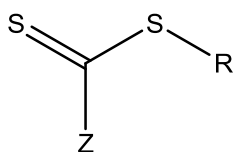
Figure 1.2.1 – General structure of a chain transfer agent, CTA where R = free radical leaving group and Z controls the reactivity of the C=S bond.

The CTA contains an activated double bond and a weak bond, this means thiocarbonyls are often advantageous due to their higher reactivity compared to carbonyls[43]. The choice of Z group is important for the activation of the C=S double bond, and those RAFT agents with low reactivities have electrophilic Z groups with lone pairs of electrons that conjugate with C=S [44]. A summary of the main classes of CTA used in RAFT polymerisation is shown in figure 1.2.2.
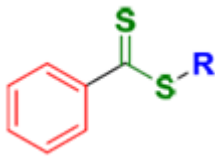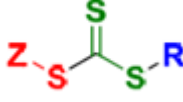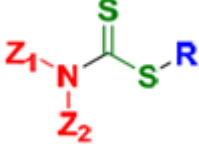
Dithiobenzoates	Trithiocarbonates	Dithiocarbamates
-Very high transfer constants -Prone to hydrolysis -May cause retardation under high concentrations	-High transfer constants -More hydrolytically stable than dithiobenzoates -Cause less retardation	-Activity determined by substituents on N -Effective with electron-rich monomers

Figure 1.2.2 – Summary of the three main classes of RAFT chain transfer agent, and their properties[45].

Addition of the propagating species to the CTA forms an intermediate, which then fragments at the weak bond. The RAFT process induces an equilibrium between propagating and dormant species and it is this, and the subsequent loss of the termination step, that is responsible for its high levels of control (figure 1.2.3). Overall, the process is not kinetically degrading because the fragment radical formed is free to re-enter the reaction cycle. The stability, sterics and polarity of the R group can affect the rate of reaction once equilibrium is reached[46].

$P_c^{\bullet}$ - Propagating species
$R^{\bullet}$ - Fragment radical
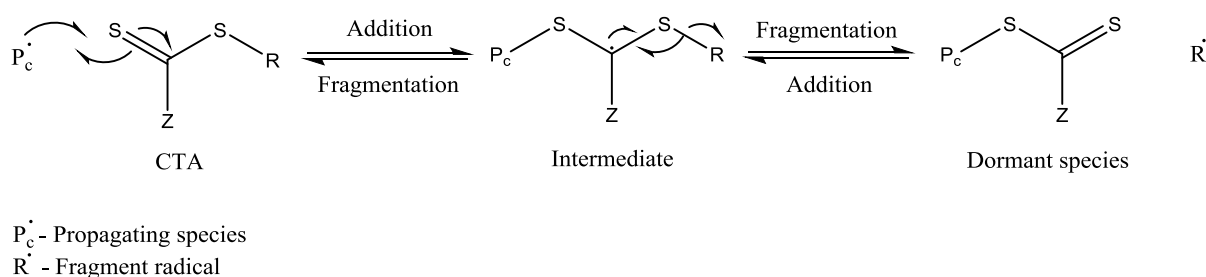
Figure 1.2.3 – Schematic of the addition/fragmentation mechanism within RAFT polymerisation.

The complete mechanism for RAFT polymerisation is shown in figure 1.2.4.
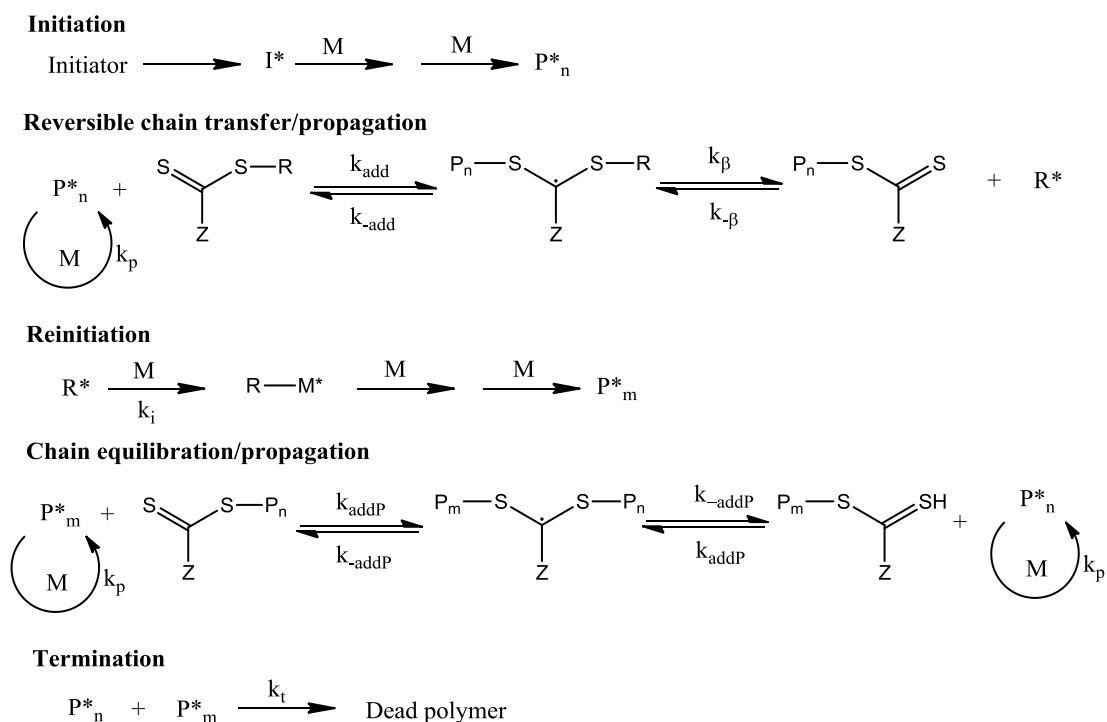
Figure 1.2.4 – Full scheme of RAFT polymerisation[31].

Both initiation and termination are identical to normal radical polymerisations. However, shortly after initiation the propagating chain will add to the CTA forming an intermediate radical, which fragments into a new radical and a polymeric dithiocarbonate. The newly formed radical proceeds to react with monomer to form a new propagating chain which is then subject to the same addition/fragmentation process. As equilibrium is reached between P_n*, P_m* and the dormant species, there is equal opportunity for all chains to grow and therefore low polydispersity is achievable with this technique. Some polymers will retain the CTA end group as a result of RAFT, allowing functional end groups to be applied post-polymerisation.

The main disadvantage of the RAFT procedure is the synthesis of the CTA itself, which often requires an inert atmosphere and the use of hazardous materials, such as CS_2. However, modern syntheses are being published using softer reagents[47] and also report high yields without the need for strict anaerobic conditions[48].

In the presence of a cross-linker RAFT polymerisation enables branching whilst quenching cross-linking[49] and hyperbranched polymers with polydispersities as low as 1.3 have been produced using this system[50]. The amount of CTA present in the system has been seen to control levels of branching, however too high quantities can decrease monomer conversion.

This is a known effect, although if the mechanism is primarily an increase in side reactions, or a decrease in the fragmentation reaction is still the subject of some controversy[51]–[53].

A variety of hyperbranched polymers have thus been synthesised using RAFT polymerisation including poly(*N*-isopropyl acrylamide) (PNIPAM) [54] and poly(methyl methacrylate)[55], with the latter case indicating that monomer concentration plays a role in determining the microstructure of the final product. It has been demonstrated by Sherrington that using a CTA to reduce the primary chain length can lead to a corresponding reduction of gel formation[56]–[61].

Hyperbranched polymers offer the opportunity to functionalise the numerous chain ends imparting, for example, protein binding capabilities[5], [62], [63] and the tolerance of RAFT permits the introduction of biodegradable bonds within a hyperbranched structure[64], [65]. These advantages offer great possibilities for increasing bioconjugation using this technique. The labile C-S bond that is retained in polymers during RAFT allows the introduction of functionality through reaction with amines[30]. Moad *et al.* further expand this by demonstrating the preparation of carboxy- and primary amino functional RAFT polymers[66], after showing that the sulfur-containing end groups of RAFT polymerization can be removed[67].

The CTA can also be used as a source for introducing carboxy functionality, although hydrolytic instability can be a problem[68]–[70].

RAFT and other living polymerisation techniques offer the special ability to grow polymers directly from the surface of a protein. This has been achieved by the conjugation of initiator on cysteine thiol groups that are present on the surface of the protein[71]. RAFT polymerisation also allows the synthesis of block copolymers[72]–[74] and this is an important feature for conjugate polymers, as when one block collapses the other block can remain soluble and prevent phase separation. The introduction of two different end groups on one polymer via RAFT has been used by Kulkarni to improve polymer-protein conjugation[75]. Polymers are attractive protein conjugates as they can be designed across a wide range of compositions, structures and sizes[76]–[78] and potential uses range from markers to enzyme inhibitors.

1.3 Ozonolysis

Ozonolysis is the breakdown of unsaturated organic compounds by the use of ozone. Cleavage of the carbon-carbon bond generates an ozonide and its subsequent work up leads to the formation of two carbonyl compounds. Carl Harries was the son-in-law of the inventor

Werner Siemens who designed some of the earliest ozone generators. Harries first investigated the interaction of ozone with a range of olefins, from ethylene to cycloalkanes[79]–[82] where he found that a 1:1 addition occurs between alkene and ozone to form the ozonide species. By choosing the appropriate work up (for instance, hydrogen peroxide) products with aldehyde, ketone or carboxylic acid functionality were produced. Harries concluded that oxidative cleavage by ozone is an undemanding process with a good degree of manipulation.

Ozone can be generated in the lab by passing oxygen through a high-voltage electrical current[83] and two molecules of ozone are formed for every three of oxygen that enter the system.

The generally accepted mechanism of ozonolysis has been described by Criegee in the 1960s [83]–[86] and proceeds via three discrete steps (figure 1.3.1). The first step is the nucleophilic addition of the alkene to ozone, forming a C-O bond. The other nucleophilic oxygen of ozone then attacks the opposite end of the alkene to form a second C-O bond. The overall process is 1,3-cycloaddition, generating an unstable molozonide 5-membered ring. The second step of the mechanism is the decomposition of the molozonide forming a carbonyl and a zwitterion. Finally, another 1,3-dipolar cycloaddition occurs where the carbonyl and zwitterion recombine. The zwitterion acts similarly to ozone in this situation, and a second ozonide is formed as the first stable product which can be isolated[87].
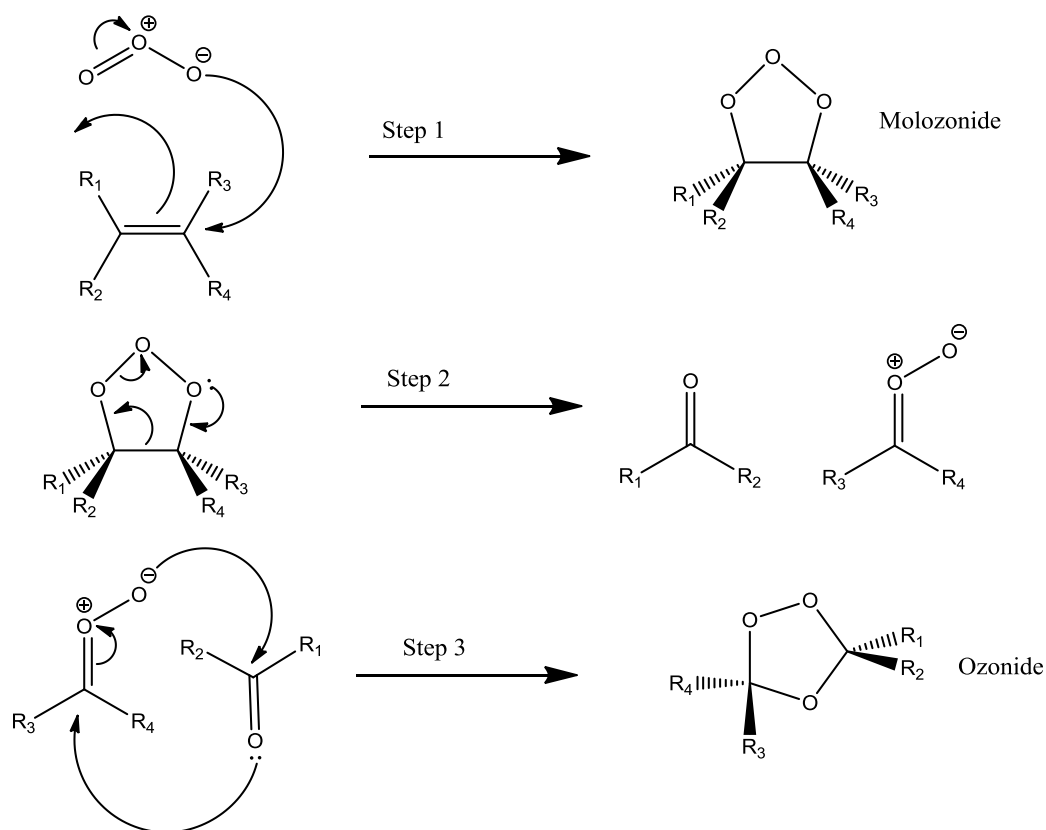
Figure 1.3.1 – Mechanism of ozonolysis.

19

The final ozonide, whilst stable, can be explosive when heated at concentrations in excess of 20 *wt%* and is usually decomposed *in situ*. This can be achieved using a gentle or strong reduction, forming two aldehyde products, or oxidatively to produce carboxylic acids. When ozonolysis is performed under aqueous conditions, the zwitterion formed in step 2 is stabilised and can yield hydroperoxides through reaction with water[88].

In a commercial setting, ozone must compete with methods such as through the use of permanganese and chromic acid that are used to oxidate alkene bonds[89]. However, ozone is often preferred for use in the cosmetic and pharmaceutical industries, where impurities from heavy metals can necessitate complex purification procedures.

1.4 Hyperbranched polymers

The history of hyperbranched polymers can be traced back to the end of 19th, when it was observed that a resin was formed from the combination of tartaric acid (A2B2 monomer) and glycerol, a B3 monomer[90]. In 1901 the results of combining an A2 monomer (phthalic anhydride or phthalic acid) with the B3 monomer glycerol. This reaction was studied by Callahan, Arsem and Kienle *et al.*[91], [92] to reach conclusions about viscosity that are still valid today. The first commercialised plastics, which were phenolic polymers, were introduced in 1909 by Baekeland via the Bakelite Company[93]. The polymerisation between an A2 monomer (formaldehyde) and a B3 monomer (phenol) produces a hyperbranched structure just before gelation occurs. Statistical mechanics was used in the 1940s by Flory[94]–[97] in order to determine the molecular weight distribution of hyperbranched polymers. Flory also developed the concepts of the degree of branching and highly branched species. Flory further developed his theory in 1952 with the synthesis of highly branched polymers without gelation. This could be achieved through the polycondensation of ABn monomers (where n>=2)[98]. In 1982 highly branched polymers were reported by Kricheldorf as the products of an AB + AB2 polymerisation[99]. The term 'Hyperbranched polymer' was first used by Kim and Webster[100] in 1988 after the successful synthesis of HBpolyphenylene. Since that time hyperbranched polymers have seen a boon as an alternative to the more intricate dendrimers; wth applications in coatings, drug delivery, rheology modifiers and biomaterials. Hyperbranched polymers are being researched for many potential uses including host-guest encapsulation[101].

Hyperbranched polymers (HBPs) are macromolecules with a tree-like architecture; they have a high number of end groups with a densely packed and highly branched backbone. HBPs belong to the dendritic molecules, although they display less perfect branching than dendrimers as illustrated in figure 1.4.1. Dendrimers are the ideal hyperbranched polymers, with perfect 100% branching. Both dendrimers and hyperbranched polymers comprise of a central core with repeat units emanating outwards, but the stringent synthetic techniques to produce dendrimers are not well suited to industrial processes. Usually, linear monomers or chains are used to connect the core to further branching molecules like spokes. Each multifunctional branching molecule then acts as an individual core as further bifunctional molecules are added. HBPs are often produced using a simpler one-pot synthesis that produces a range of molecular weight products with random branching. This means that for a given recipe, there will be multiple possible HBP structures but only one dendrimer outcome.

Dendrimer   **Hyperbranched polymer**   **Linear polymer**
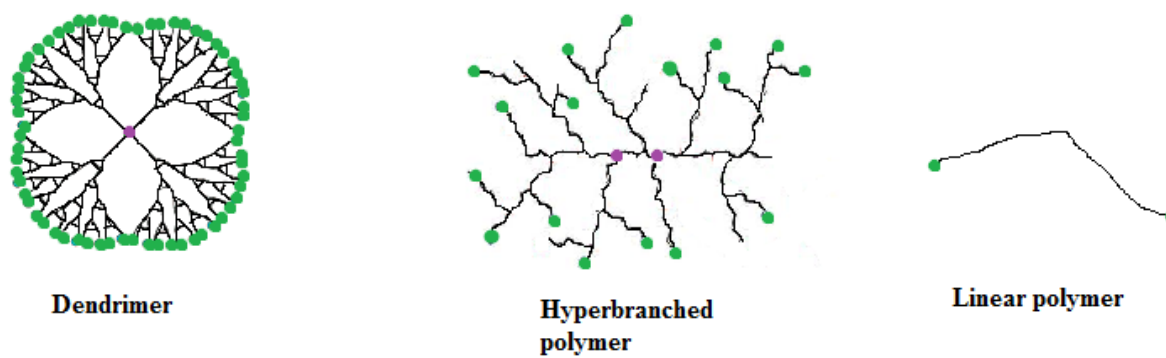
Figure 1.4.1 – Schematic comparison between dendrimers, hyperbranched polymers, and linear polymers. Purple is a core monomer, whilst green represents end groups.

When a polymer is dissolved in a solvent, an increase in viscosity is observed. The intrinsic viscosity (η) of the polymer solution is determined by the interactions between polymer chain and solvent molecules. It is specifically defined as "the ratio of a solution's specific viscosity to the concentration of the solute, extrapolated to zero concentration"[102]. For any given molecular weight, a large diffuse molecule will have a higher intrinsic viscosity than a small and compact molecule. HBPs have different viscosity profiles to linear polymers, often HBPs have a lower viscosity (figure 1.4.2).
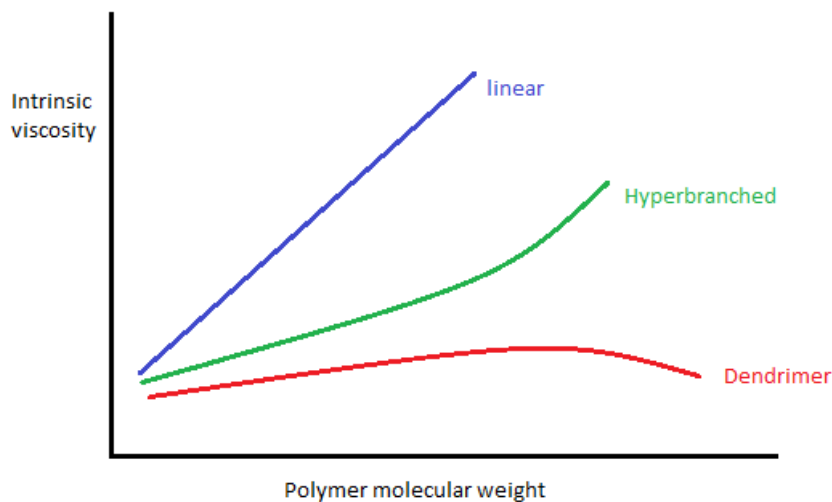
Figure 1.4.2 – Simplified representation of the viscosity profile of different polymer architectures.

When in solution, HBPs reach a maximum of intrinsic viscosity as a function of molecular weight. This occurs as the extended shape of the HBP becomes more compact and globular. Linear polymers show a linear increase in viscosity up to a critical molar mass, whereupon a drastic increase in viscosity is observed as a result of chain interactions and entanglement. In HBPs this effect is a result of the entanglements and interactions of the branch units – longer branches lead to increased interactions between molecules and thus increase the viscosity of the system. By controlling the branch length, HBPs can be used as processing aids to reduce viscosity[103]–[105]. It is this property that is exploited in techniques such as triple detection GPC to obtain molecular weight information. In GPC, polymer is passed through a column packed with beads; the smaller chain molecules enter into and pass through the beads, whilst longer chains have a faster elution time as they pass between the beads. This separation is based on the size of the polymers and not their molecular weight. Commonly, GPC is performed with a single concentration detector such as refractive index. In conventional GPC, a standard sample is run first so that the response and elution time can be calibrated to known molecular weights. As the test polymer often does not have the same chemistry as the standard sample, this can lead to errors as interactions with the column packing affect retention time as well as differences in polymer size. The use of a viscometric detector means that the universal calibration can be used, allowing for a more accurate molecular weight determination. The universal calibration uses a calibration plot of log[n]M against retention time. This plot will look the same independent of the standards used, and it means that the chemical nature of the polymer is no longer influencing the results[106].

As the effect of branching is to decrease the intrinsic viscosity, therefore it can be possible to determine the degree of branching by also performing analysis of a linear analogue.

22

Rheology studies have been successful in characterising the average branching of polyolefins[107], [108] and 1H and 13C melt-state NMR have also been used in the characterisation of starch[109], polyethylene[110] and polyacrylates[111]. HBPs have much greater chemical reactivity than their linear analogues, due to the high proportion of end groups[112]–[114]. The percentage functionality can also be controlled by control over the degree of branching / number of end groups.

1.5 Interpenetrating polymer networks

A note on terminology

Occasionally within the literature the term 'hydrogel interpenetrating network' (hydrogel IPN) is shortened only to hydrogel. The term 'double network hydrogel' is also used to describe a sub-class of interpenetrating polymer network (IPN). Whilst hydrogels and IPNs can share many characteristics it is important to define them as two separate species. A hydrogel is a single, sometimes copolymer, network that is highly swollen in water. Whilst it can, in certain situations, be applicable to call an IPN a hydrogel the reverse does not apply and for clarity this report shall not use the two terms interchangeably.

Interpenetrating polymer networks (IPNs) consist of two or more polymers, in network form, which whilst being heavily intermingled are not chemically bound to each other (figure 1.5.1)[115]. This is not to be confused with a polymer blend or alloy, which is a mixture of non-crosslinked polymers. IPNs are generally considered to be composite materials, and are heterogeneous systems with defined phase boundaries between their component parts. Semi-IPNs refer to a system where one of the polymers is not crosslinked.

Polymer network
Polymer network'
Full IPN

Polymer network
Non-crosslinked polymer
Semi-IPN
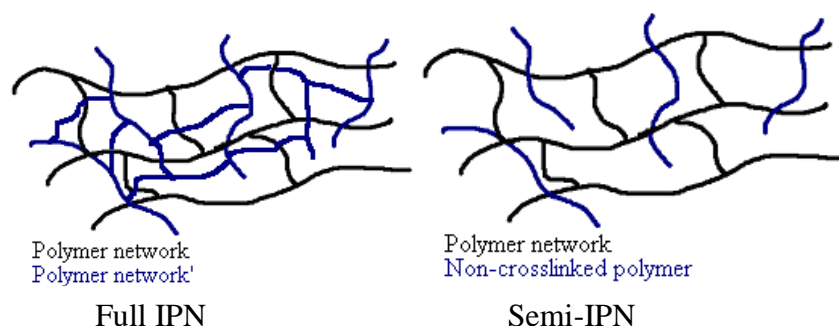
Figure 1.5.1 – Diagram illustrating full and semi-IPNs.

At present, the state-of-the-art mainly describes semi-IPNS in which the non-crosslinked component is linear and there are very few reports of instances where this component is branched. There are two routes to forming an IPN; simultaneous, whereby both networks are formed at the same time[116], [117] or sequential, where the second network is polymerised within an existing, swollen, cross-linked system[118]. The simultaneous method is preferred for its greater integration of networks and simplicity, but it relies upon both sets of monomers being polymerised by different means e.g. radically and via a condensation reaction.

As expected, IPNs have much improved mechanical properties compared to hydrogels due to their double network structure[119]. Even IPNs composed of weak polymers can show strength greater than the sum of the two component networks[120]. For applications within bioengineering this is highly advantageous. Natural tissues such as cartilage are able to combine high water content with good mechanical properties, which is difficult to replicate with most biocompatible hydrogels. By using a two-polymer system, it is proposed that these natural properties will become easier to replicate by combining a functional polymer with a network that has good mechanical strength.

IPNs have a variety of industrial and biomaterial applications silver-loaded IPNs are being investigated as wound dressings with antibacterial capability[121]–[123] and are also showing promise as proton exchange membranes which have applications in both biology and emerging fuel technologies[124], [125].

IPN hydrogels have a variety of properties that make them preferred for biotechnical applications. This includes a relatively straightforward method of production, minimal irritation of surrounding tissues and stability in biological fluids[126]. The structure of the IPN allows for control of the hydrophilicity of the hydrogel, and this property is exploited for the entrapment and release of small molecules like drugs[127]–[130].

1.6 Stimuli responsive interpenetrating polymer networks

The formation of IPNs that can respond to external stimuli is of great interest to researchers. The stimulus can include a pH response that causes network swelling and release of a target molecule, temperature, salt or a change in shape induced by an electrical field. The general principle of a stimulus responsive IPN is to form a product with two different network functionalities that each reacts differently to external stimuli. The use of amphiphilic IPNs is

already showing promise for controlled and targeted drug release[131], where the hydrophobic network acts to quell swelling of its hydrophilic counterpart leading to aggregation around the target molecule.

An example of this is an IPN containing networks of Konjac glucomannan (KGM) and poly(acrylic acid) (PAA). KGM is a fibre derived from the *Amorphophallus konjac* plant[132] , and has been explored as a means to target drug delivery to the colon. Interpenetrating polymer networks formed from KGM and PAA have been loaded with vitamin B12 and then subjected to a model digestive tract system. These IPNs showed significant vitamin release when exposed to colonic conditions, due to the combined enzymatic attack upon the KGM and the pH response of the PAA[133]. In this case, the KGM network acts to prevent degradation in the harsh digestive conditions prior to reaching the bowel, whilst the PAA pH response assists molecule release from the network.

However, homo-IPNs, where both networks are chemically identical, have also been investigated. Poly(*N*-isopropylacrylamide) (PNIPAM) is a well-documented temperature responsive polymer[134] and it is intuitive that this response could be conveyed to an IPN. PNIPAM homo-IPNs show an enhanced trapping of bovine serum albumin (BSA) above the LCST, as well as greater mechanical properties when compared to a single network PNIPAM hydrogel[129]. PNIPAM's temperature response has also been exploited to create an injectable semi-IPN that hardens *in vivo*, to reinforce scleral tissue that has been degenerated by myopia[135]. IPNs that exhibit a bending response when exposed to an electrical field have been synthesised. These IPN systems typically couple a strong electrolyte network, such as PNIPAM[136] and Poly(vinyl sulfonic acid) (PVSA)[137], [138] with a second network that imparts other desirable properties such as pH responsiveness or biodegradability. As the IPN is exposed to an electrical field, the positive ions in the electrolytic network migrate towards the cathode with the result being partial shielding of the sulfonate and carboxylate groups and, ultimately, a reduction in hydration. These IPNs could provide breakthroughs relating to biological switches and sensors.

There is a wide scope for introducing functionality and stimuli response to IPNs, and the examples given above are by no means exhaustive but have been chosen to demonstrate the range of applications and responses that are possible.

1.7 Cell adhesion and biocompatibility

The success of any biomaterial clearly rests upon its biocompatibility. Hydrophilic polymers such as PAA and PNIPAM, and natural polymers such as KGM are considered biocompatible[139] and as a result there is a bias towards these compounds when developing biomaterials.

There are many examples of cell growth upon a hydrogel or IPN scaffold. Neural tissue has been grown upon networks of a tri-block copolymer of ethylene glycol, glycolic acid and lactic acid[140], dextran/gelatin IPNs have exhibited endothelial cell adhesion[141], as have IPNs with a collagen/glycopolymer composition[142].

Antifouling materials also require careful control of biocompatibility to prevent environmental pollution and current work is focussing towards protein resistant networks[143], [144]. Hyperbranched fluoropolymers have been explored as antifouling materials[145], [146] but their unknown toxicity and bioaccumulation data has caused a shift towards networks of poly(isoprene) and poly(*N*-vinylpyrrolidinone)[147] alongside further investigation of the more traditional poly(ethylene glycol) based materials[148], [149]. Surface chemistry, including surface tension[150], hydrophilicity[151], [152] and zwitterionic nature[153], is known to be of considerable importance in antifouling. Polymer networks appear to be a logical solution to the problem of fouling.

When formulating a new biomaterial, there are tactics available to the researcher to improve the chances of cell adhesion, growth and biocompatibility. As previously mentioned there are well-documented polymers that are known to be non-toxic and biocompatible. Early workers considered that controlling the amphilicity of the biomaterials surface would be sufficient to ensure cell adhesion and proliferation. However, although there are clear effects of amphilicity on cell adhesion these strategies have rarely proved effective enough for the clinic. A much more effective technique is to place peptide sequences within the structure; the RGD motif in particular is known to confer cell adhesion[154] (where R = arginine, G = glycine and D = aspartic acid). The modification of materials with specific peptide sequences is an expensive and time-consuming process and an emerging technique is to apply alkyl amines to a material[155]. These act to mimic the lysine functionalities that are modified by extracellular enzymes during cell proliferation[155], [156]. Finally, careful thought must be given to the final structure of any network designed to sustain tissue regeneration, as too narrow a mesh size will inhibit any cell growth. Material architecture is also expressly important in the emerging field of stem cell differentiation[157].

There are four primary cell assays that are undertaken to assess biocompatibility of a new material. These are: cell contact toxicity, cell extract toxicity, cell seeding and cell proliferation. Together these assays build a picture that informs if a material itself is toxic to cells, whether it leaches toxic chemicals, and finally if cells are able to adhere to and proliferate upon the material's surface.

The cells chosen for contact studies in this work were primary dermal fibroblasts (HDF) and renal epithelial cells (REpC). Fibroblast and epithelial cells are often found growing together in the tissues of the body, but they exhibit very different phenotypes and perform different biological roles. The differences in membrane proteins are responsible for each cell type's specific interactions and the movement of small molecules into and out of the cell. Protein typically represents 50% of the plasma membrane, although this value can vary dramatically depending on the cell type. Despite this there is still a high ratio of lipid molecules to protein due to their smaller size (figure 1.7.1). The variances in protein expression are what differentiate fibroblast cells from epithelia and other cell types.
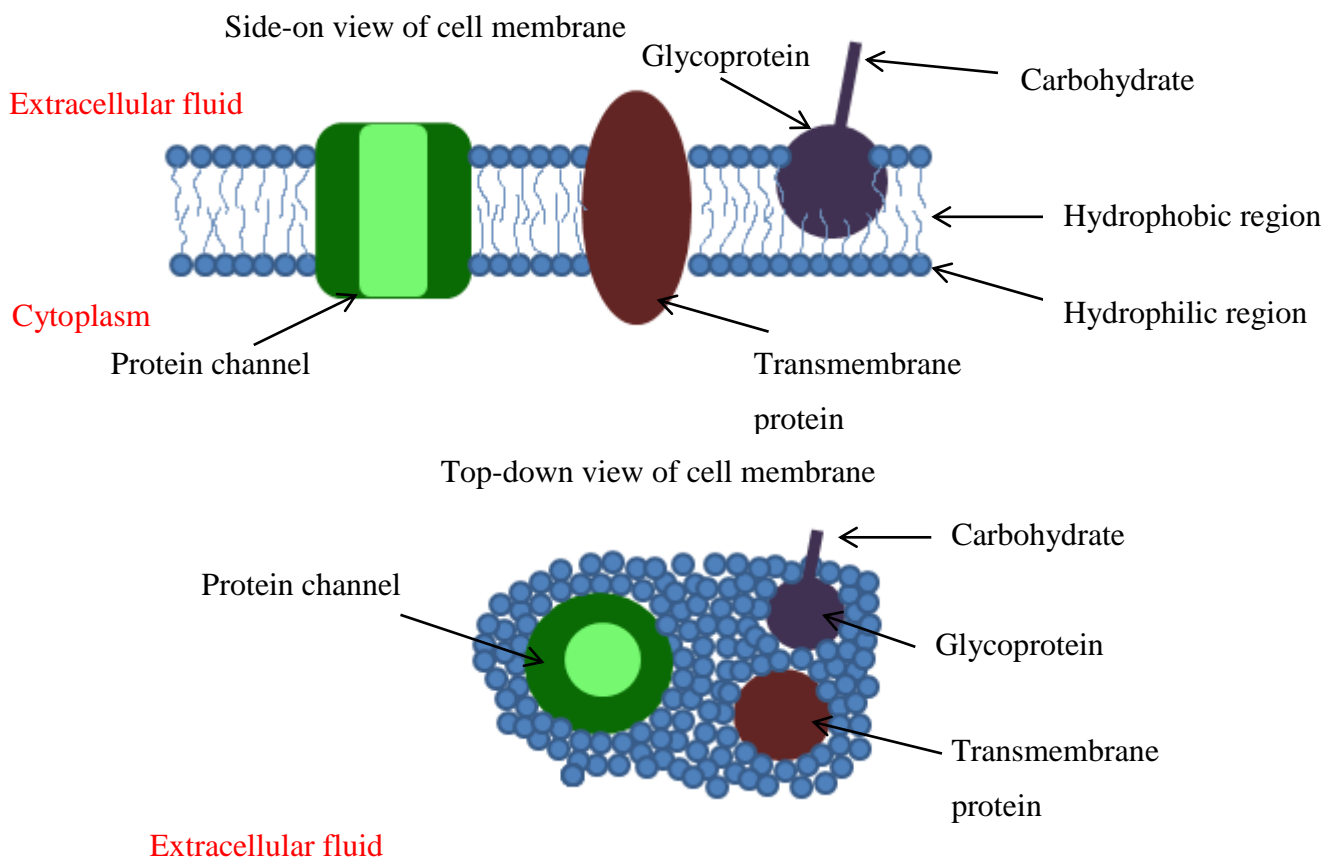
Figure 1.7.1 – Side- (top) and top-down representations of protein and lipids in the cell membrane[158].

This means that due to differences in protein expression and extracellular matrix (ECM) development, the fibroblasts and epithelial cells may have opposite responses to the same material. The extracellular matrix is best imagined as a scaffold that provides sites for cell

attachment and structural support. In addition, it also acts as a store for small signalling molecules that regulate inflammation, cell movement and angiogenesis[159].

The epithelium lines the cavities of many of the body's compartments. As well as forming a physical barrier, the epithelium is responsible for absorption and secretion, as well as detecting changes in environment. Generally, there is little space between individual epithelial cells with physical links through tight cell junctions. This means that the cells are able to form continuous sheets which can act like a barrier (figure 1.7.2).
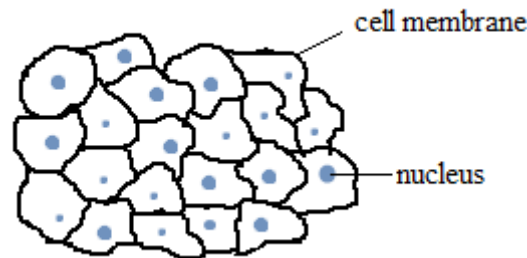
Figure 1.7.2 – Diagram of a continuous epithelial sheet.

Epithelia have a minimal ECM and are linked together at tight junctions between cells that in turn form a tight barrier between body parts. In RePCs, plasma membrane proteins are spatially arranged so that proteins are confined to the apical and basal domains in the membrane (figure 1.7.3)[158]. Tissue polarity is governed by cell interactions – either with the ECM or another cell – and it is this that means the apical and basal layers can perform different functions[160].
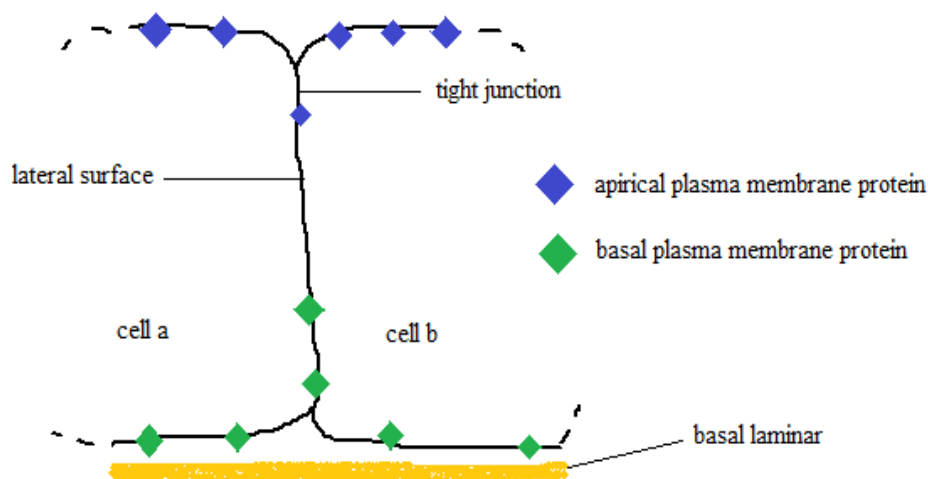
Figure 1.7.3 – Diagram representing the apical and basal plasma membranes, and the tight junctions between epithelial cells.

Underlying epithelial cells is the basal lamina and this connects to a layer of fibroblasts in order to build tissues and organs. Fibroblasts can be seen to have a different structure and growth pattern to epithelia, related to their role as connective tissue (figure 1.7.4)
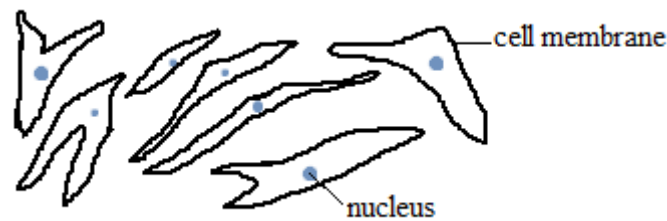
Figure 1.7.4 – Diagram representing normal fibroblast morphology.

As already mentioned, fibroblast cells are critical for the healing of wounds and for structural integrity. Fibroblasts produce precursors of the extracellular matrix, for instance collagen, and many diseases have been related to errors in fibroblast activity[161]–[163]. Fibroblast cells also influence wound healing as mitosis is stimulated by tissue damage, encouraging the production of ECM molecules, for instance glucosaminoglycans and elastic fibres. Unsurprisingly, fibroblast cells show a well-developed extracellular matrix, which is designed to withstand some mechanical stress[158]. However, this has been found to apply only along the length of the cell[164]. Mechanical stress on fibroblasts has also been seen to increase their production of collagen I[165] whilst vocal fold fibroblasts show increased rates of proliferation when subjected to vibration[166].

There are some situations in which fibroblast cells are able to arise from epithelia and this is called an epithelial-mesenchymal transition (EMT). EMT is an essential process during embryonic development but it is also linked with tumours and other diseases[167], [168]. Factors that induce EMT are varied and the pathways involved require much more depth than is necessary for this review. Interested parties are directed to the referenced articles[169]–[172].

Conversely, there are also developmental stages where epithelia are able to arise from sheets of fibroblast cells and this is known as a mesenchymal-epithelial transition (MET). Once again, the reader is directed to the referenced sources for further information about this process[173]–[176].

2 - Synthesis of oligo(*n*-butyl methacrylate) with acid or amine end groups

2.1 Introduction

The purpose of this work was to build upon previous work done within the Rimmer group that showed fibroblast cytocompatibility with acid-ended oligomeric butyl methacrylate with Mn>2700[177]. Initially, reactions were performed to identify the optimal conditions for emulsion polymerisation between butyl methacrylate and butadiene. Ozonolysis was then used to cleave the polymers at the site of butadiene insertion. Work up with selenium dioxide/hydrogen peroxide functionalised the resulting oligomers with carboxylic acid end groups. These activated oligomers were then subject to modification with various alkane diamines as per previous work[178] and their cytocompatibilty with human primary cells was investigated. This work produced butyl methacrylate oligomers of Mn 10,000-22,000Da. The cell culture results indicate that fibroblast cells may prefer acidic functionality whilst epithelial cells are better able to proliferate on amine materials. Optimised oligomers could be used as surface coatings to introduce functionality and improve biocompatibility, whilst the cytotoxicity of these compounds is of interest as oligomeric dispersions are the main product from *in vitro* degradation of aliphatic polyesters[179].

As previously reported, a semi continuous monomer-starved process was adopted for the copolymerisation of *n*-butyl methacrylate and butadiene[177], [178], [180], [181]. A batch polymerisation would not be appropriate as the co-monomer butadiene would volatilize from the system before reaction could occur. In this situation, careful control of the monomer feed rate(s) prevents a monomer flooded system from occurring. Monomer flooded systems resemble a batch polymerisation and butadiene can easily volatilize away. A two-syringe gas pump was used to control the rate of butadiene injection, whilst a calibrated peristaltic pump controlled the liquid monomer feed over the course of 16 hour reactions. Despite this polymerisation having been previously carried out successfully[178], it was found that different reaction conditions were necessary for the incorporation of butadiene into the polymer.

Butadiene is a small, hydrophobic monomer and cyclodextrins were therefore employed as solubilizing agents to decrease the instantaneous vapour pressure during polymerisation.

Cyclodextrins are cyclic oligosaccharides, composed of glucopyranose units seen in figure 2.1.1. These structures adopt a toroidal shape, with a central pore that is less hydrophilic than the surrounding aqueous environment[182] and enable the formation of inclusion complexes with small hydrophobic monomers.
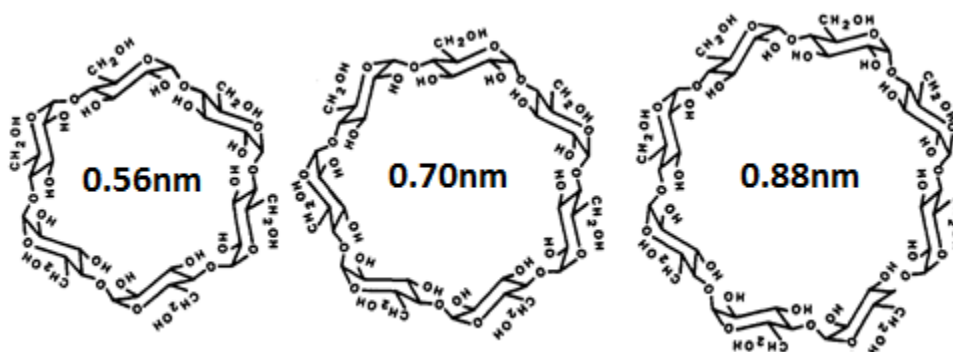
Figure 2.1.1– From left to right, structure of α, β and γ cyclodextrins. Internal diameter (nm) of each cyclodextrin is shown.

Cyclodextrins allow the aqueous phase initiation and Z-mer formation of molecules that are not normally able to undergo emulsion polymerisation[183], [184] and Ritter has notably reported the formation of CD-monomer complexes that have then been polymerised[185]–[189] using such hydrophobic monomers such as styrene and isobornyl acrylate. The use of cyclodextrins in biomaterials is not disadvantageous and several reviews into the pharmaceutical uses of cyclodextrins have been provided by Loftsson[190]–[192]. Studies have also indicated that the cytotoxicity of cyclodextrins follows γ < α < β, where γ is least toxic[193], [194] and cyclodextrins administered orally are practically non-toxic[195].

Oxidative cleavage is a non-selective technique whereby the two alkene carbons of a C=C bond are converted to carbonyl functionality. When polymer molecules are exposed to ozone, both 1,2- and 1,4- orientated alkene bonds are cleaved by the mechanism described in chapter 1.3. For the purposes of the project non-selectivity is not a disadvantage, as any cleavage that does not occur in the polymer backbone will simply give rise to acid functional pendant groups.

Cell studies were performed using primary human dermal fibroblasts (HDF) and human renal epithelial cells (REpC) in direct contact with oligomers over 72 hours. Cell viability and microscopy studies were performed after 24 and 72 hours to assess cell adhesion, growth and health. It was expected that the two cell types might show a preference for oppositely functional materials, due to the differences in their plasma membrane phenotype as previously discussed in chapter 1.

2.2 Results and Discussion

2.2.1 Monomer starve-fed emulsion polymerisation of butyl methacrylate and butadiene
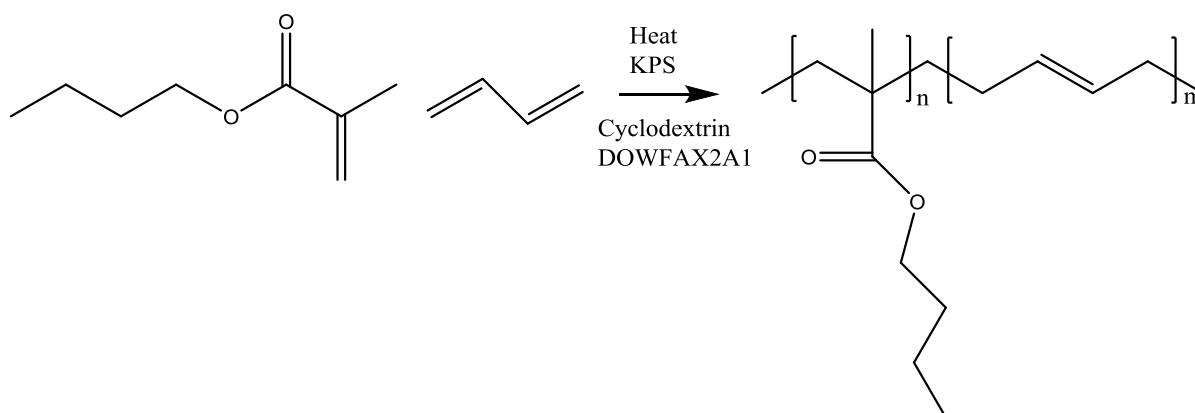
Scheme 2.2.1.1 – Scheme of emulsion copolymerisation of *n*-butyl methacrylate and butadiene. KPS = potassium persulfate.

Initially it was found to be much more difficult than expected to incorporate butadiene into the final product using emulsion polymerisation (scheme 2.2.1.1). This was caused by volatilisation of the co-monomer before it could successfully react within the reaction vessel. A series of emulsion polymerisations were performed at 70 ℃ over 4-16 hours, and the amount of butadiene fed into the reaction was also increased from 0.05 to 2 moles. Despite these efforts, butyl methacrylate polymers still contained negligible butadiene. Without butadiene to provide cleavage sites ozonolysis could not be used to split the polymer backbone into oligomeric segments.

A polymerisation was performed at the higher temperature of 80 ˚C. The rationale for increasing the temperature was to increase the rate of polymerisation: thus creating a monomer starved system. Any butadiene entering the system should, with the aid of cyclodextrins, react before it can be volatilised. Also, any increased loss of butadiene would be minimised by the addition of a new condenser to the reaction vessel, enabling cooling of effluent gases to -14 ˚C.

Figure 2.2.1.2 shows that 1 mole of butadiene fed into the reaction at 80 ˚C (24 mL/min feed rate) led to successful alkene incorporation into the final polymer. All described reactions contained β-cyclodextrin at 1% unless otherwise stated.
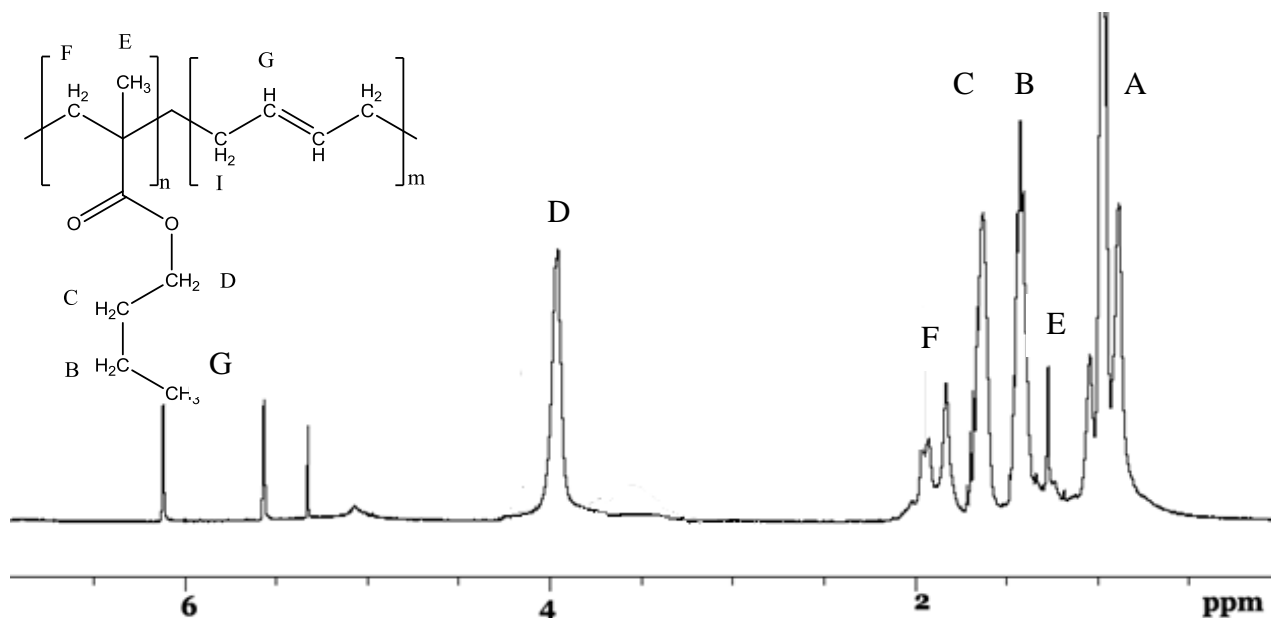
Figure 2.2.1.2 – ^{1}H NMR spectrum of poly(butyl methacrylate-co-butadiene) polymerised at 80°C.

The resonances at 5.57ppm and 6.12ppm indicate the predominant 1,4-insertion of butadiene in the cis and trans configuration. The peak at 5.05ppm is due to 1,2-terminal olefins whilst the signal at 5.45ppm is due to non-terminal 1,2- inserted butadiene[196]. The data obtained here shows some variation from literature values, and this is thought to be due the electron withdrawing effects of the butyl methacrylate co-monomer. The ^{13}C NMR spectrum provides further evidence that the majority of butadiene insertion occurred in a 1,4-configuration.

(figure 2.2.1.3). The 1,2-insertion of butadiene would result in two sp^2 carbon environments, and therefore two opposing peaks would be observed on the ^{13}C spectrum. The single peak shown here correlates well with *cis*-polybutadiene that has been previously characterised[197].

33
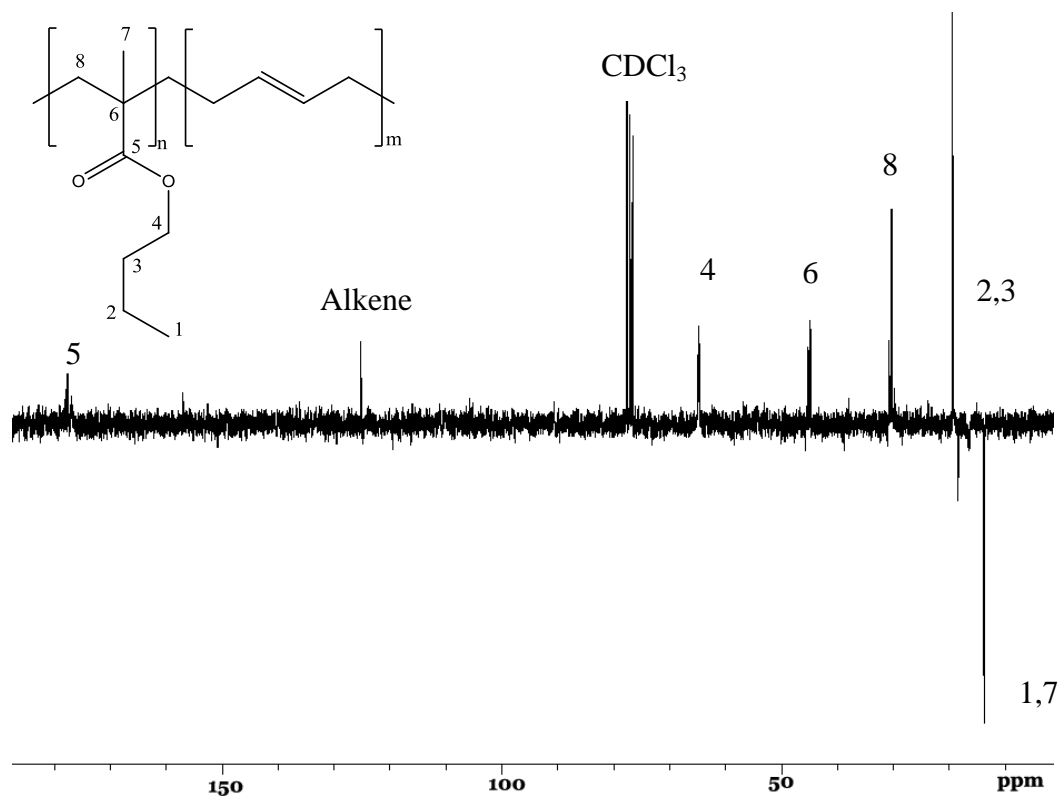
Figure 2.2.1.3 – ^{13}C spectrum of poly(butyl methacrylate-co-butadiene) polymerised at 80°C. Of note is the single alkene peak at 125ppm.

DEPT-spectra: above baseline are even number of protons (CH$_2$) and below baseline is odd number of protons (CH, CH$_3$).

After the successful 1,4-insertion of butadiene at 80°C, the influence of cyclodextrin on the reaction system was investigated. The reaction was repeated in an identical manner but in the absence of cyclodextrin. This product still showed some incorporation of butadiene (figure 2.2.1.5) but less than in the presence of cyclodextrin. Figure 2.2.1.6 provides a comparison of butadiene content of polymerisations performed with and without cyclodextrin stabilisation. These results show that cyclodextrin is essential for successful butadiene incorporation in this type of reactor configuration. Reactions performed at 75°C allow the greatest butadiene incorporation only in the presence of either α- or β-cyclodextrin (0.9% and 0.6% butadiene content in final product respectively). This confirms previous assumptions that cyclodextrin acts as a stabilising molecule that traps butadiene within the reaction system. Reactions performed without cyclodextrin and those performed at the higher temperature 80°C showed little to no incorporation of butadiene. This can be attributed to the volatilisation of butadiene.
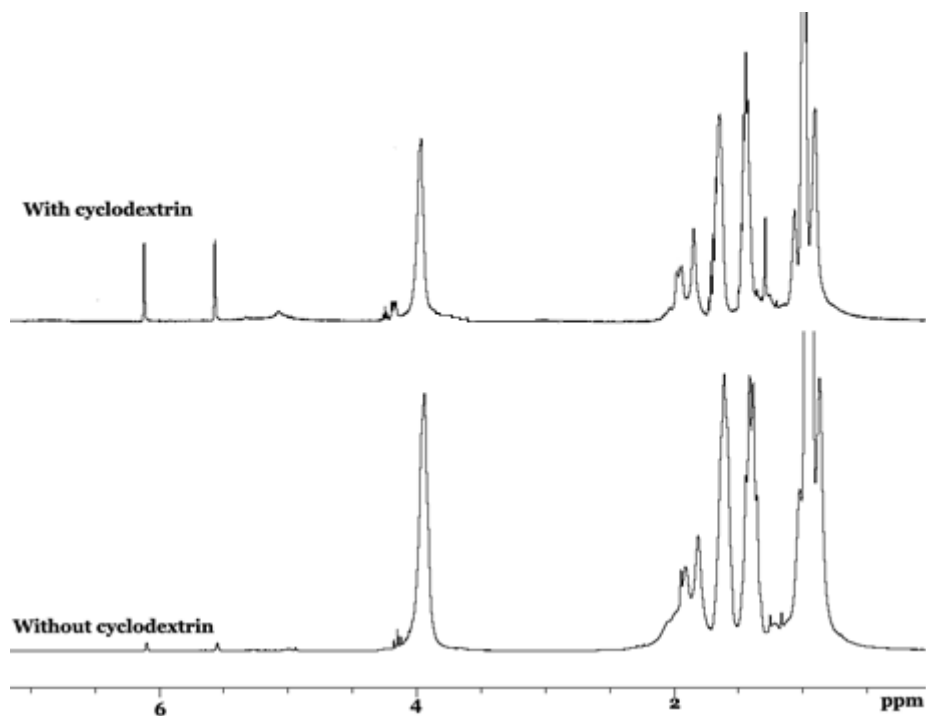
Figure 2.2.1.5 – ^{1}H NMR comparison of poly(butyl methacrylate) prepared in the presence of butadiene with and without cyclodextrin. Polymerisations performed at 80 ˚C.
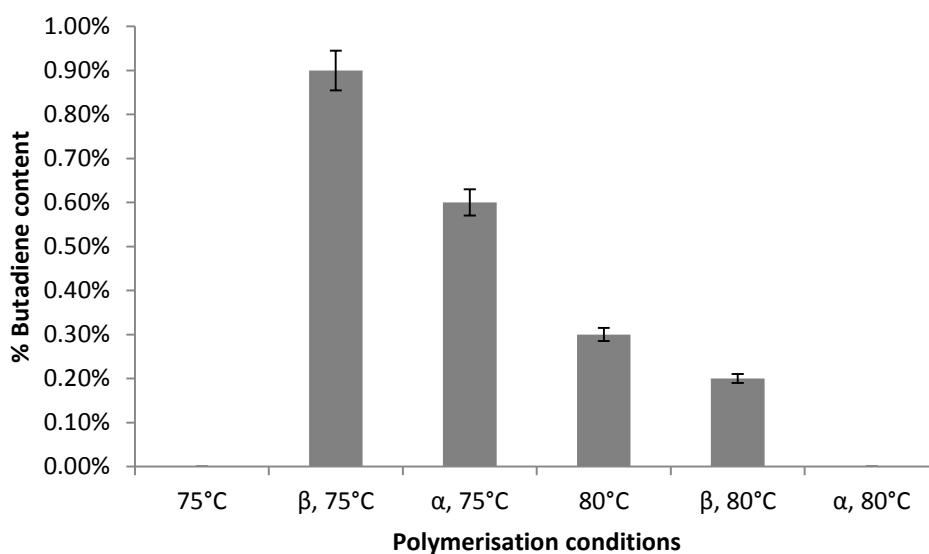
Figure 2.2.1.6 – Graph comparing the butadiene content in poly(butyl methacrylate) under different reaction conditions. % Butadiene calculated using integrations from ^{1}H NMR spectrometry.

Figure 2.2.1.7 shows that butadiene incorporation at 75 °C with β-cyclodextrin displays a simple splitting pattern which is associated with 1,4-insertion. It is suggested that this therefore is the optimal reaction conditions for copolymerisation between butyl methacrylate and butadiene in this unpressurised reactor configuration.
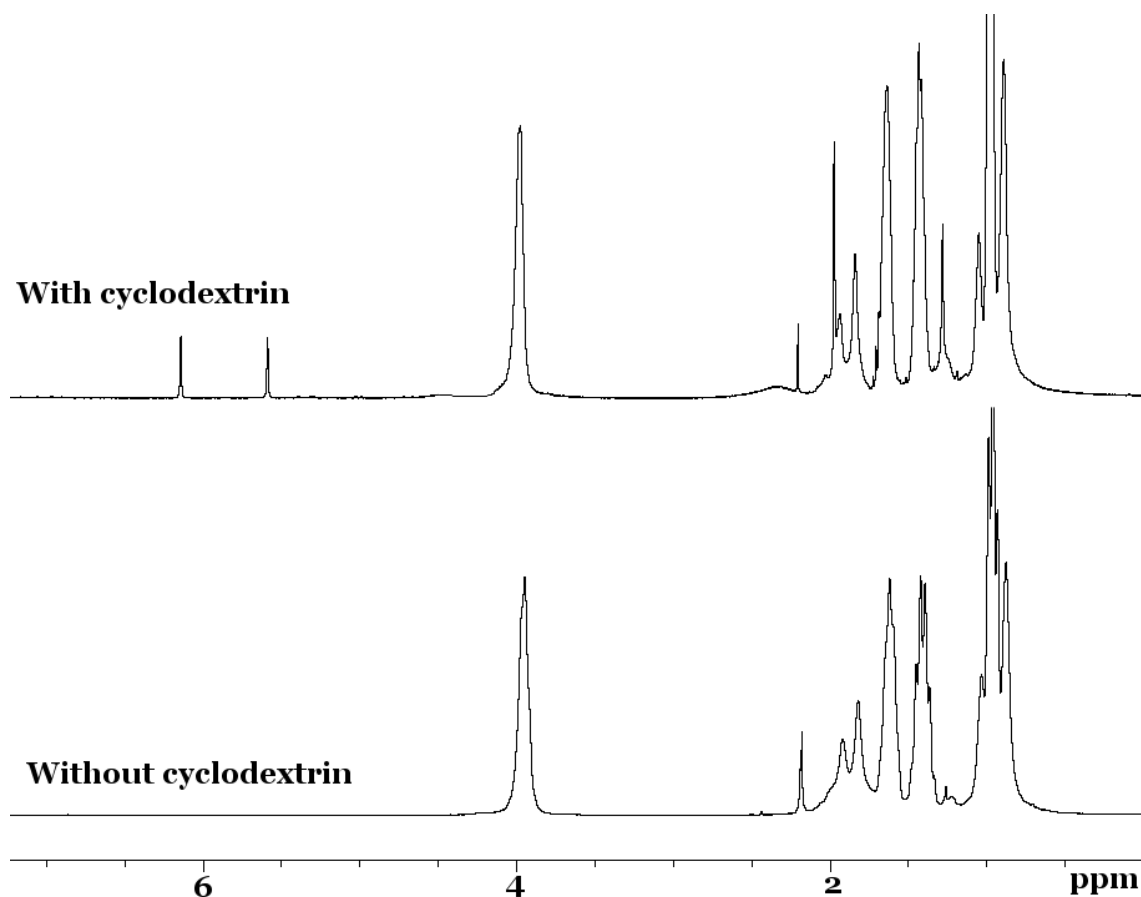
Figure 2.2.1.7 - ^{1}H NMR comparison of poly(butyl methacrylate) prepared in the presence of butadiene with and without cyclodextrin. Polymerisations performed at 75˚C. Alkene proton resonances seen at 5.5 and 6.1ppm.

All polymers were subjected to SEC GPC using tetrahydrofuran as the solvent. Table 2.2.1.8 provides a summary of this analysis. It is possible to see here that β-cyclodextrin produces polymers of slightly lower Mn than α-cyclodextrin. This is because as higher amounts of butadiene are incorporated, the average propagation rate constant ($\overline{kp}$) decreases. The $\overline{kp}$ of *n*-butyl methacrylate at 60 ℃ is 976[198], whilst it is only 0.057×10^{-3} for butadiene at 30 ℃[93].

Reaction Conditions	% Butadiene	$\overline{Mn}$	$\overline{Mw}$	$\overline{Mz}$	PDI
80°C, β-CDX, 1mole BD, 0.63moles BMA	0.2%	16300	44700	89250	2.7
80°C, 1mole BD, 0.63moles BMA	0.3%	40850	124000	252550	3.0
75°C, β-CDX, 1mole BD, 0.63moles BMA	0.9%	18450	57550	129100	3.1
75°C, 1mole BD, 0.63moles BMA	0	35650	80300	183550	2.3
80°C, α-CDX, 1mole BD, 0.63moles BMA	0	22500	57800	112350	2.6
75°C, α-CDX, 1mole BD, 0.63moles BMA	0.6%	40800	88200	153580	2.2

Table 2.2.1.8 – GPC analysis of butyl methacrylate polymers. Where CDX is β-cyclodextrin.

$\overline{Mn}$ and $\overline{Mw}$ given in Daltons.

Figure 2.2.1.9 demonstrates that all butyl methacrylate polymers have approximately the same molar mass distribution (MMD). The molar mass distribution describes the relationship between the number of molecules (LogM) and their molecular weight (dw/dLogM). The presence of β-cyclodextrin can be seen to increase butadiene incorporation and yet their presence decreased the average molar mass. Those polymers synthesised without any cyclodextrins gave high molecular weights contained negligible butadiene and were not suitable for further treatment by ozonolysis. α-Cyclodextrin was found to be a viable alternative at 75 °C, producing a butyl-methacrylate-butadiene copolymer with $\overline{Mn}$ 40800Da. The decrease in molar mass produced by inclusion is probably not due to reactions with the cyclodextrins. Rather, the increased frequency of propagation steps involving butadiene reduces the overall average rate of propagation relative to the rate of termination.
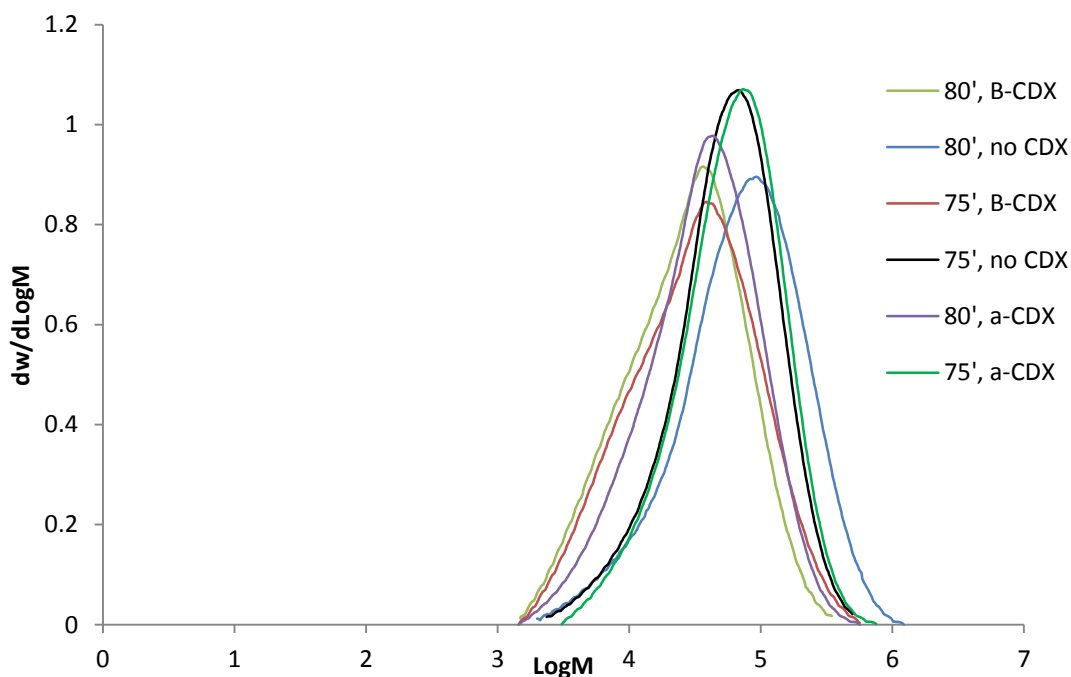
Figure 2.2.1.9 – Molar mass distribution for various poly(butyl methacrylates) synthesised in the presence of butadiene and cyclodextrin (see legend).

2.2.2 Formation of oligo(butyl methacrylate) and end group functionalization
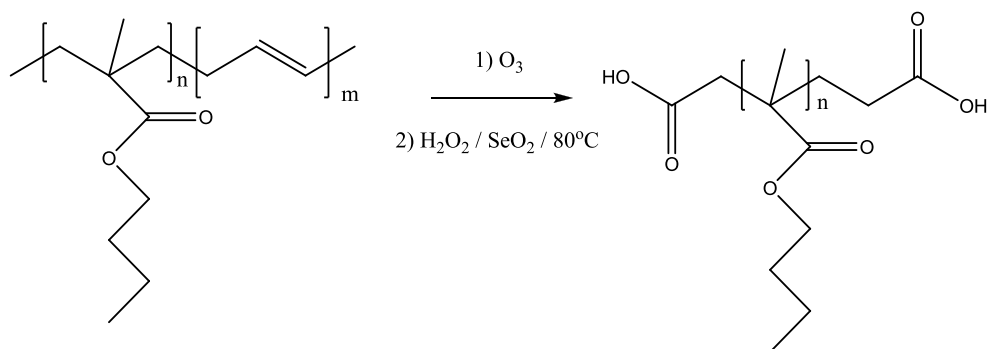
Scheme 2.2.2.1 – Scheme showing ozonolysis of poly(*n*-butyl methacrylate-co-butadiene).
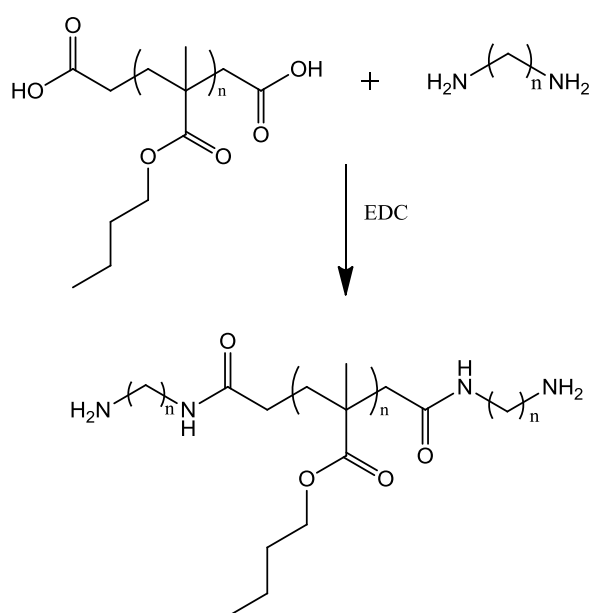
Scheme 2.2.2.2 – Scheme showing amidation of acid ended butyl methacrylate oligomer.

Polymers which had been identified by NMR spectroscopy to contain butadiene were subjected to cleavage by ozonolysis (schemes 2.2.2.1 and 2.2.2.2). As alkene sites along the polymer backbone were cleaved by ozone, oligomers were formed. By varying the work up conditions, the end groups of these oligomers can be functionalised into aldehydes, ketones and carboxylic acids. In this instance, all oligomers were given carboxylic acid end groups as it is then a relatively trivial procedure to further react these oligomers with excess of diamine-functional compounds to produce oligomers with primary amine end groups. The success of the ozonolysis of polymers was observed using GPC and NMR. ^{1}H NMR spectroscopic analysis of the oligomeric product confirmed loss of the alkene moieties (figure 2.2.2.3) whilst GPC showed a significant decrease in molar mass consistent with backbone cleavage (table 2.2.2.4). The molar mass distribution can be seen to become much broader (figure

2.2.2.5) whilst $\overline{Mn}$ has significantly decreased. This is consistent with cleavage of polymer chains that have alkene insertion randomly along the chain. The increase in the breadth of the molar mass distribution is a consequence of changes in the efficiency in the placement of butadiene in the chain as the polymerisation progresses. Further optimisation of the copolymerisation can provide narrower molar mass distributions after ozonolysis and perfect statistical placement in the copolymer chain is predicted to decrease the MMD compared to the non-ozonised material. In this study a broad distribution of molar masses is potentially an advantage as lower molar mass oligomers, with high amine end group content, are expected to diffuse to the surface of the films cast for cell culture while the higher molar mass fractions form the bulk of the coatings. This means that the maximum amount of the imposed functionality should be available for cell-polymer interactions.
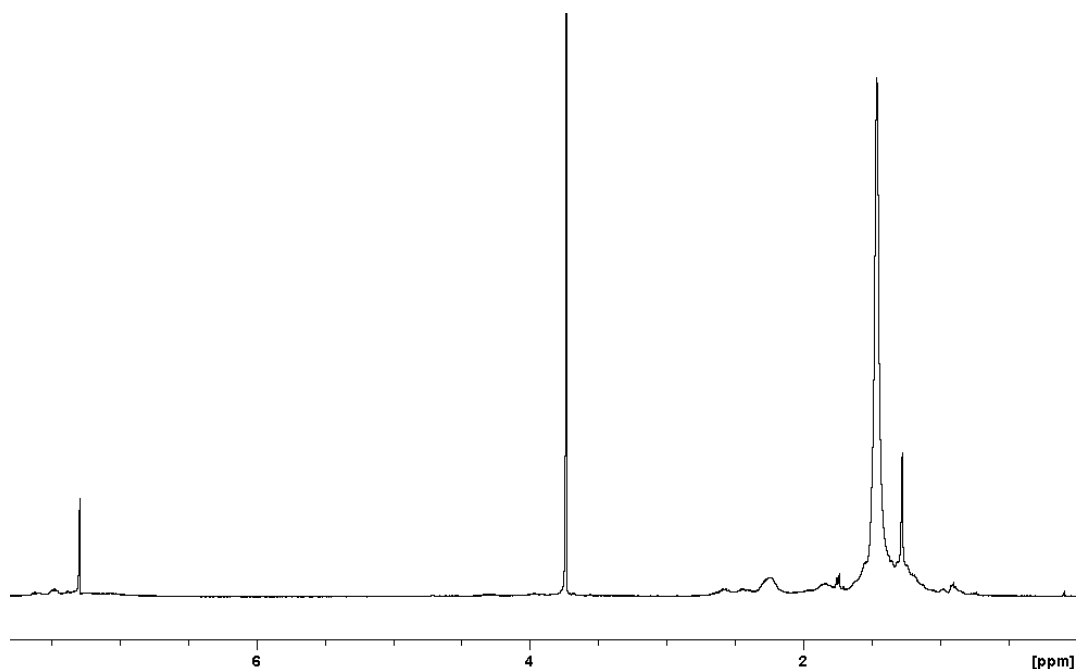
Figure 2.2.2.3 - 1H NMR of poly(BMA-BD) after treatment with ozone demonstrating the loss of resonance in the alkene region (5.5-6.5ppm)

	$\overline{Mn}$	$\overline{Mw}$	$\overline{Mz}$	PDI
Polymer	16300	44700	89250	2.7
Oligomer	1400	14200	52750	10.1

Table 2.2.2.4 - GPC analysis of butyl methacrylate-co-butadiene polymer before and after ozonolysis. Molecular weights given in Daltons.
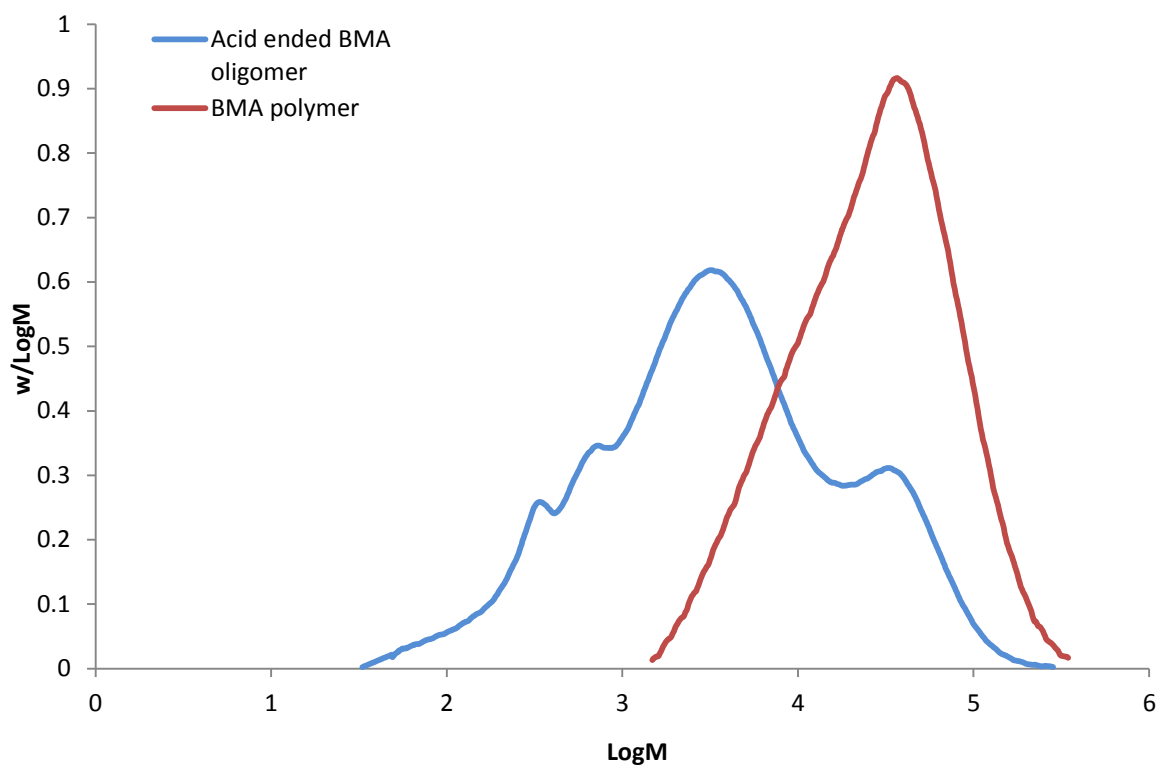
Figure 2.2.2.5 – Molar mass distribution of butyl methacrylate polymer (red) oligomer after ozonolysis (blue). The molar mass distribution has a lower average and broadens after ozone treatment.

Functionalisation with diamine occurs through the formation of an amide linker between CO_2H and NH_2. The carbodiimide EDC (1-Ethyl-3-(3-dimethylaminopropyl)carbodiimide) was used as a coupling agent. The proposed mechanism of amide formation by EDC is shown in scheme 2.2.2.6. Carbodiimides are dehydrating agents that activate carboxylic acids for amide or ester formation. They can also produce unwanted byproducts, however. The mechanism of amide formation by EDC in aqueous solution was investigated by Nakajima and Ikadan[199]. Their work confirmed that the presence of both protons and carboxyl groups is required for amide formation, and determined an optimal pH range of 3.5-4.5. The formation of the side product *N*-acylurea (**5**) in the presence of excess EDC was also confirmed[200]. Amidation reactions were performed in a two-step process whereby oligomer and EDC were first added into the reaction vessel, followed by the slow addition of diamine. The carboxylic acid end groups on the oligomer prevent the hydrolysis reaction in the first step.
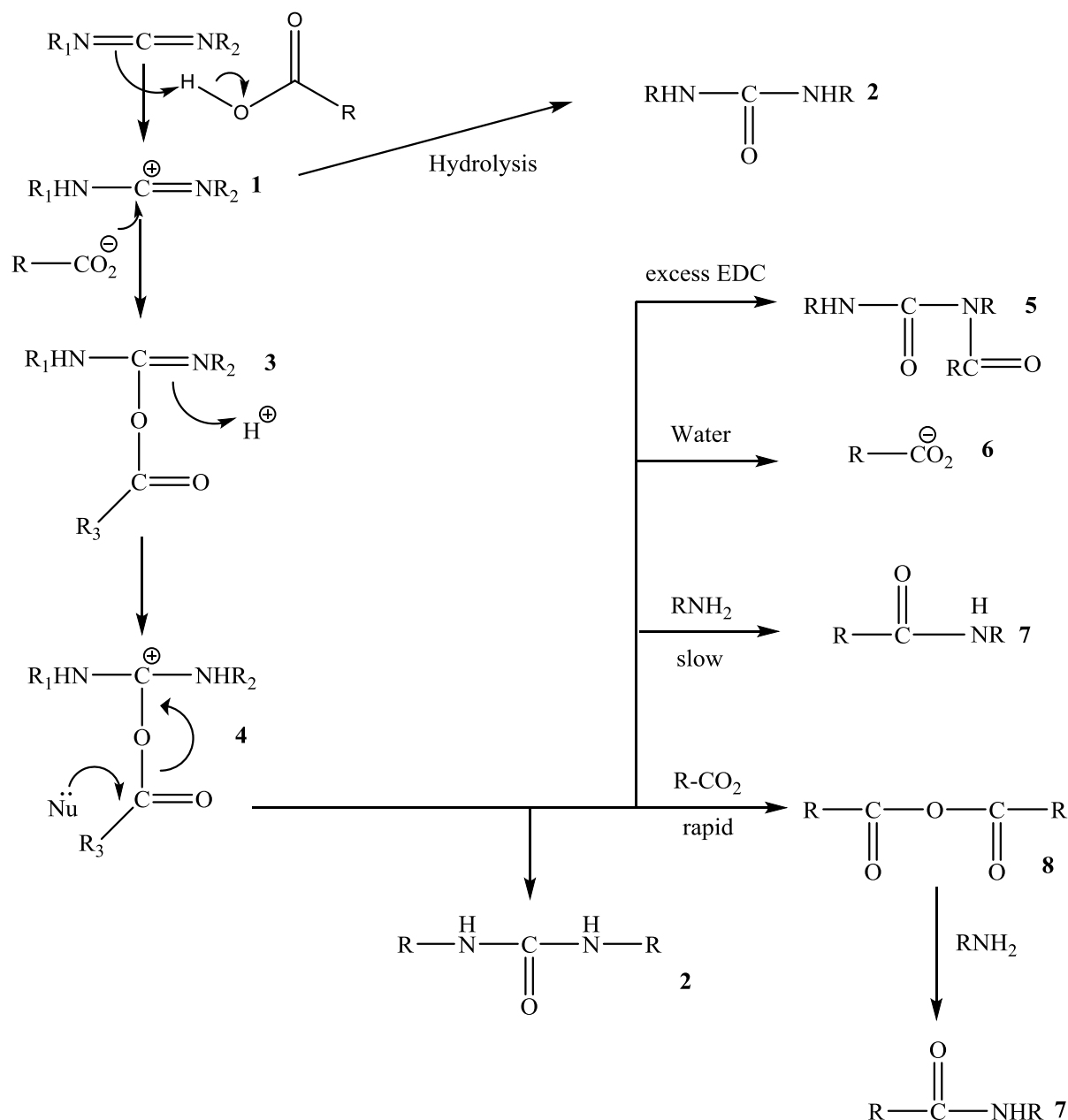
Scheme 2.2.2.6 – Reaction scheme showing the formation of amide (**7**) and by-products using EDC coupling agent. Where **1** = Carbocation derivative of carbodiimide, **2** = urea derivative, **3** = O-acylisourea, **4** = carbocation derivative of O-acylisorea, **5** = N-acylurea, **6** = carboxylate, **7** = amide and **8** = carboxylic anhydride.

2.2.3 Characterisation of functionalised oligomers

After end group modification oligomers were subject to various characterisation techniques. FT-IR studies confirmed that amines and amide linkers were absent from the acidic oligomer but present in those that had been treated with amine. Figure 2.2.3.1 shows that the acidic oligomer has the signature broad absorbance band at ~3400 cm^{-1} due to the OH stretch. The acidic oligomer also displays peaks at the frequencies 1700 cm^{-1} and 1200cm^{-1} which could be caused by C=O and O-C stretches in the BMA pendant groups and/or in the acid end

41

groups. As these stretches are also seen in the aminated oligomers it is reasonable to assume the two functionalities are overlapped in the acid oligomer. All of the oligomers exhibit alkene carbon stretches just under 3000cm^{-1}. The absorbance bands at 1445 cm^{-1} seen in all oligomers are due to CH scissoring; however, some broadness in non-acidic oligomers is to be expected caused by an overlap with N-H stretching expected around 1500cm^{-1}. Finally the oligomers treated with diamines all exhibit activity between 580-650cm^{-1} and 930-980cm^{-1} which can be attributed to NH_2 and NH wag modes.
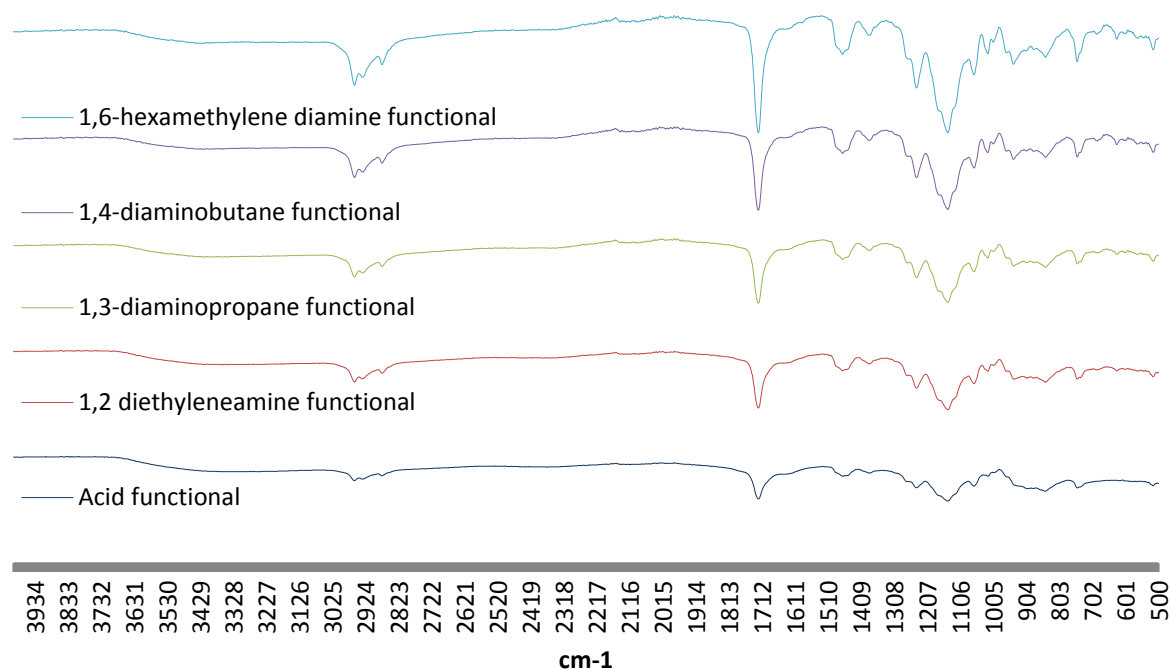
Figure 2.2.3.1 – Combined FT-IR of acidic and aminated oligomers, where 1,2 = reaction with 1,2-diaminoethane through to 1,6- = hexamethylenediamine.

GPC analysis of the functionalised oligomers is summarised in table 2.2.3.2. Here the amine functional oligomers can be seen to have comparable molar masses and table 2.2.3.3 confirms similar molar mass distributions. A noticeable amount of chain extension and narrowing of polydispersity is seen after the reaction with diamine. The increase in molar mass after treatment with diamine is probably the consequence of a single diamine reacting with the acid ends of two different polymer chains and therefore acting as a linker. Additionally, where one end of the diamine has added to the polymer, it is then possible for 'back-biting' to occur, where the free amine end reacts with the other acid group on the opposite end of the polymer.

Oligomer	$\overline{Mn}$	$\overline{Mw}$	$\overline{Mz}$	PDI
Acid	1400	14200	52750	10.1
1,2-NH$_2$	12250	44750	124250	3.7
1,3-NH$_2$	11400	45900	152150	4.0
1,4-NH$_2$	11600	44950	126350	3.9
1,6-NH$_2$	13000	27550	43600	2.1

Table 2.2.3.2- Summary of molar mass (Daltons) and polydispersity for functionalised oligomers.
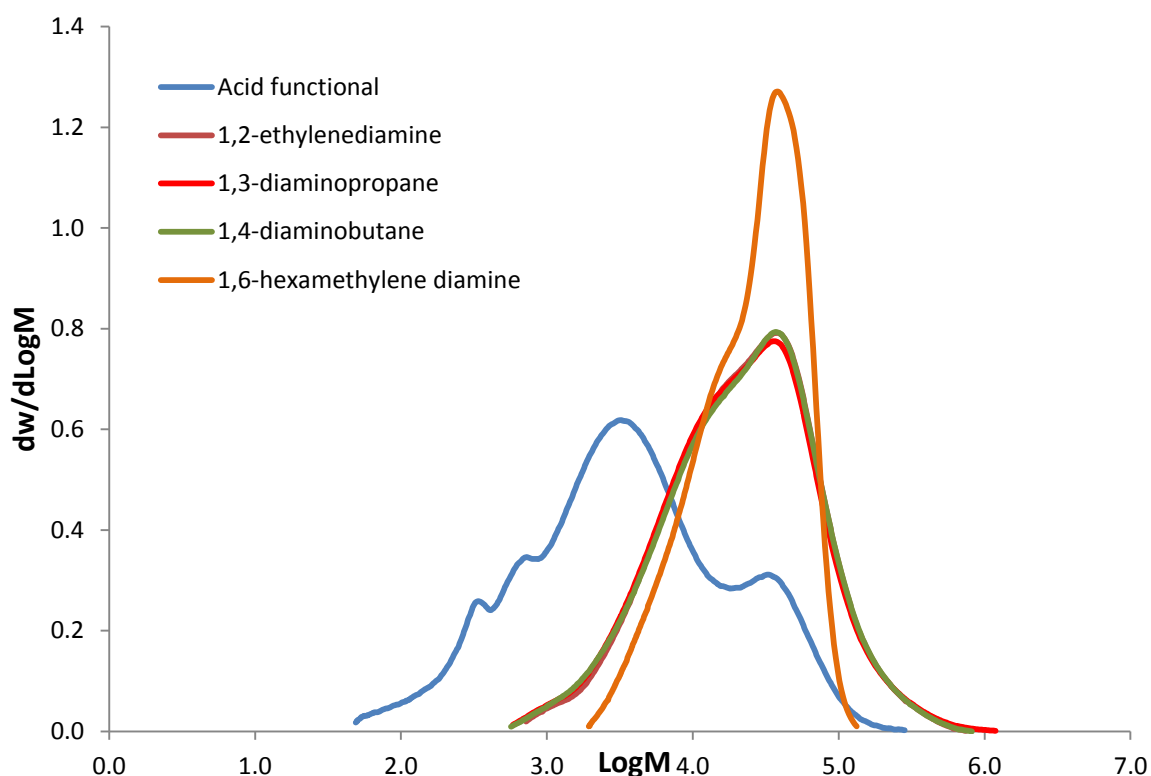
Figure 2.2.3.3 – Combined molar mass distributions (MMD) of poly(butyl methacrylate) subjected to ozonolysis and worked up with H$_2$O$_2$/SeO$_2$ to produce acid end group functionality and then an excess of the relevant diamine plus EDC to give amine end group functionality.

The contact angle measurements were obtained for the acidic oligomer (54.4°±1.2) and the 1,2-diamine functionalised oligomer (4.75°±0.17) but values for the other amine functional oligomers were not easily obtainable as the droplets quickly dispersed on the surface of the material. This is an important result as it indicates a much higher charge separation on the

amidated oligomers. This again confirms the successful coupling reaction with diamine, and the difference in surface properties between acid and amine functional oligomers. These properties are vitally important when developing new biomaterials[201], [202] and it is expected that cell interactions will differ between acid and amine functional oligomers.

2.2.4 Cell contact studies

Human Dermal Fibroblasts

Polymers were dissolved in isopropanol and cast onto a sterile glass coverslip, 22x22mm. 1.5×10^4 cells were then directly seeded onto the polymers and incubated in normal conditions for 72 hours prior to undergoing viability testing and staining. The results from seeding with human dermal fibroblast (HDF) cells are summarised in figure 2.2.4.1.
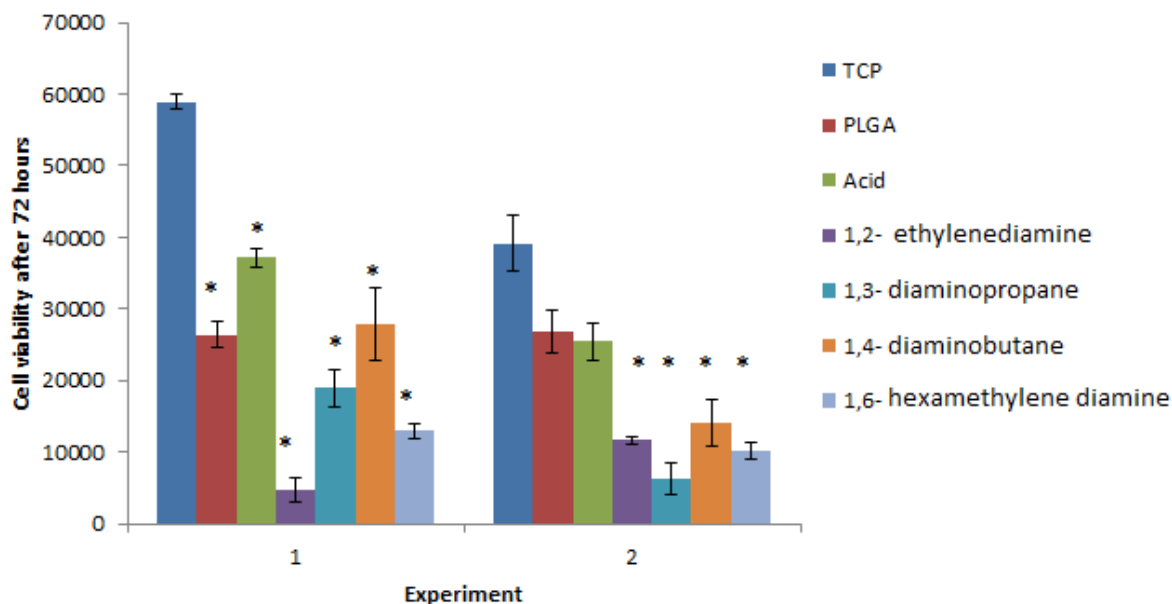
Figure 2.2.4.1 Alamarblue results after incubation of HDF for 72 hours in direct contact with oligomers. Contact experiment repeated on two separate occasions (1and 2). Error calculated to 95% confidence. One way analysis of variance (ANOVA) and post-hoc Tukey's analysis was performed to find statistically significant results (marked with *).

The amidated oligomers performed significantly worse compared to the tissue culture plastic (TCP) standard for fibroblast viability in both experiments presented here. The 1,2-diaminoethane ended polymer also has a significantly lower cell viability in experiment 1. However, based on this one experiment it is unknown if this is due to oligomer toxicity or culture conditions. Taking into account the broad molecular weight distribution of the oligomeric products, these results could be caused by the leeching of toxic short chain molecules. Therefore, a higher molecular weight polymer with acid functionality may show good cell viability. Polymer size and mass have been identified as important properties when investigating the biocompatibility of synthetic materials. Polyethylenimine, which is used as a transfecting agent, has been shown to be much more effective in the linear form[203] and at higher molar masses[204].

45

Of the amidated oligomers, it can be seen that the 1,4- difunctional oligomers are able to withstand slightly higher cell numbers although still not as many as the acid functional and standard materials. This is likely due to the similarities held between the amino terminal residues of the oligomer and the amino acid lysine which has the chemical formula $HO_2CCH(NH_2)(CH_2)_4NH_2$.

Optical microscopy was used to investigate the morphology of the adhered cells (figure 2.2.4.2). In all experiments cells were incubated on oligomer-coated coverslips. These images showed that the oligomers with acid functionality were covered with the largest amount of fibroblasts and these cells were closest in appearance to those on TCP. This could be due to the surface chemistry, or as a consequence of the topography of the cast oligomers. Surface nano-topography may be important in adherent cell cultures[205]–[207] but elucidating the interplay of surface chemistry and topography remains elusive. The acidic oligomer has a smooth surface when viewed by phase contrast microscopy (figure 2.2.4.3). The amidated oligomers appeared slightly rougher and this may have some effect on cell adhesion, as witnessed by microscopy after 24 hours. The 1,6-NH_2 functionalised oligomer is seen to have the greatest fibroblast adhesion out of all the amine functional oligomers via microscopy, but it still performs poorly as a cell culture substrate material. Figure 2.2.4.4 shows higher magnification images of the fibroblast cells after 72 hours culture on functionalised oligomers. These images show a comparable cell morphology and density between TCP and the acid functional oligomer. However, the nuclei of the cells grown on the oligomer are slightly less pronounced. Fibroblast morphology on the amidated oligomers is abnormal with the appearance of spindly cells that are sparsely spaced. This further confirms that oligomers with amine end group functionality are not a suitable fibroblast cell culture substrate. Acid functional oligomers show promise and could be further tailored.
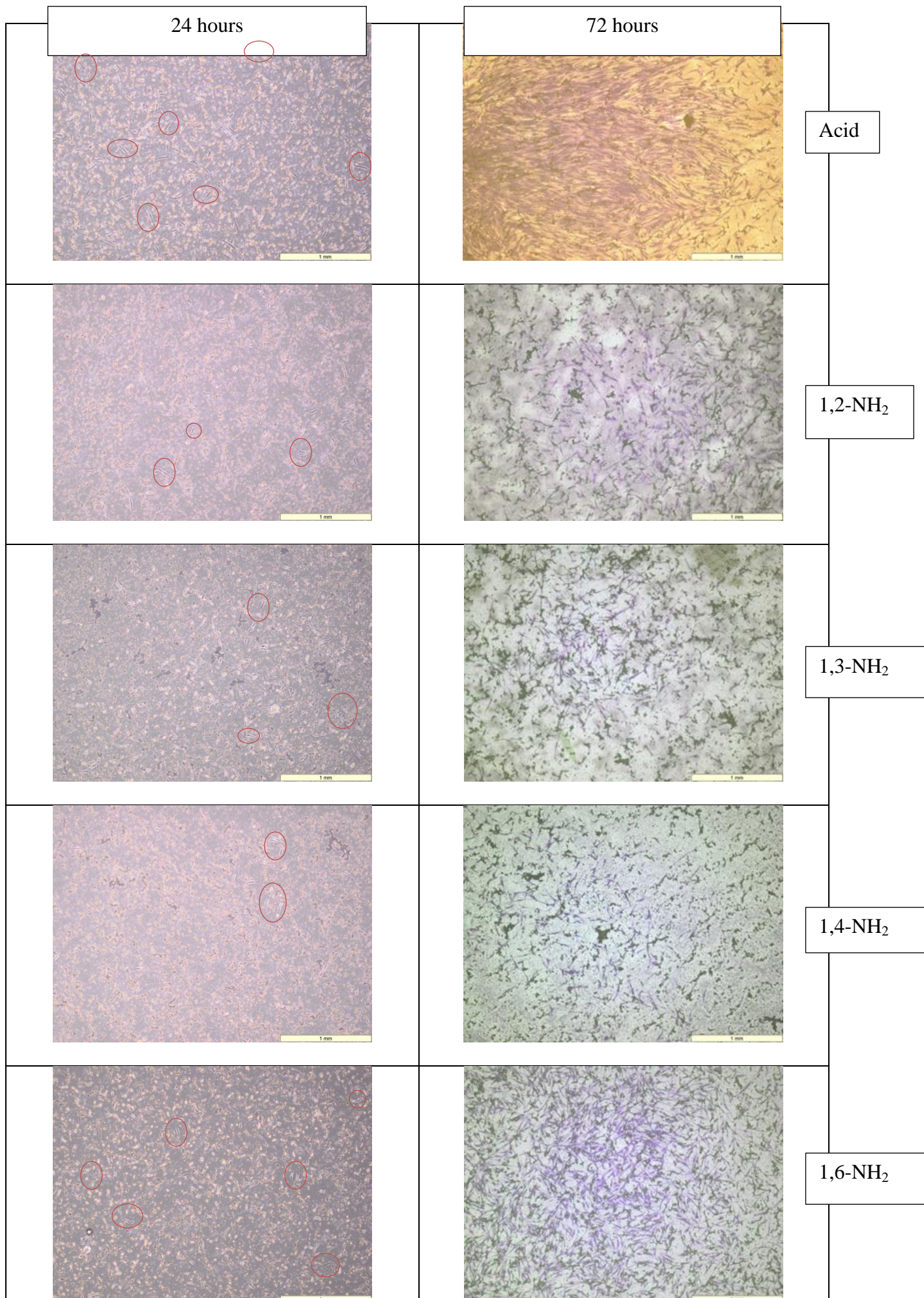
Figure 2.2.4.2 - Images comparing fibroblast adhesion on functionalised oligomers after 24 and 72 hours at 4x magnification. 24 hours= phase contrast, red circles indicate adhered cells. 72 hours = cells fixed and stained with Giemsa solution.
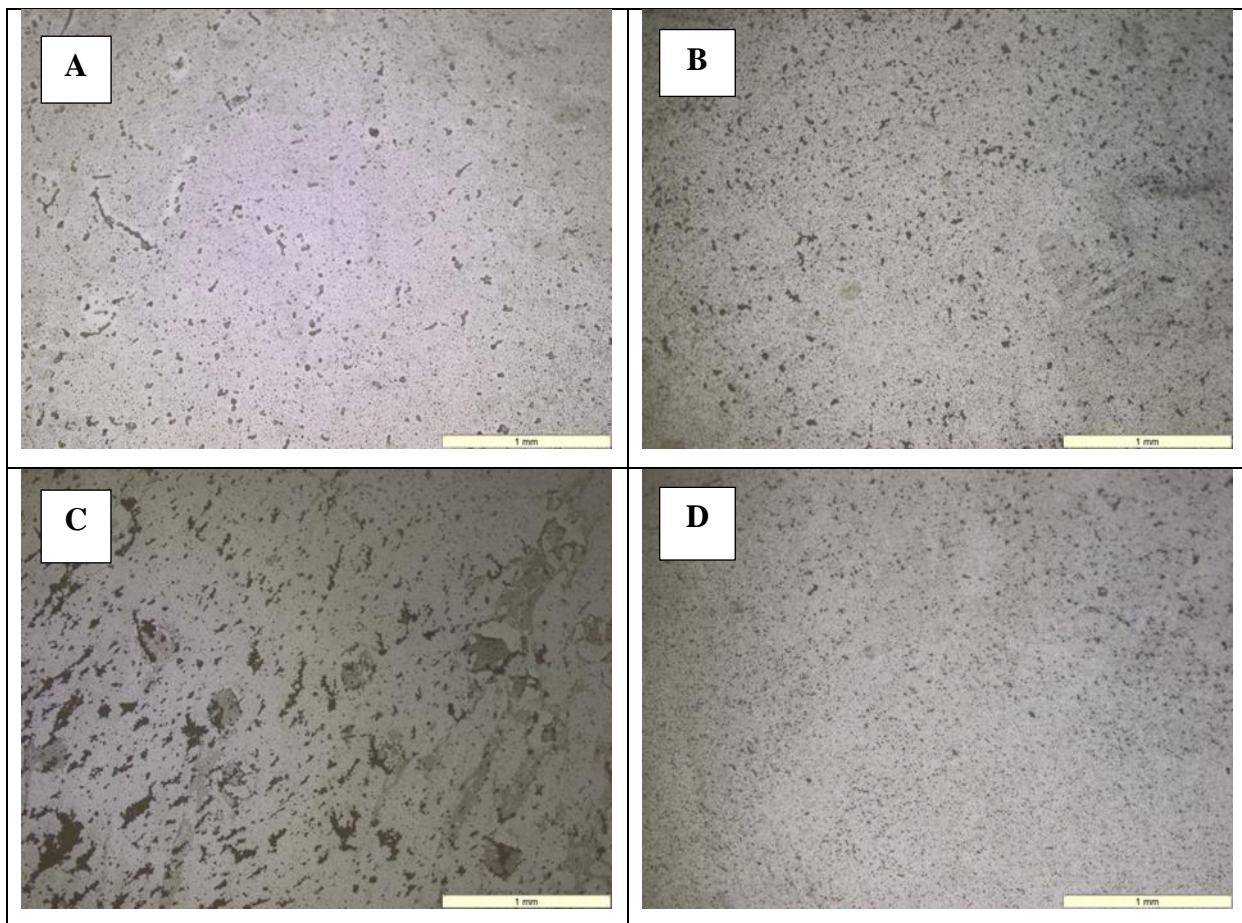
Figure 2.2.4.3 – Phase contrast images of oligomer films after drying. Where A = acid functional end groups and B= 1,NH$_2$, C=1,3-NH$_2$,D=1,4-NH$_2$ amine functional end groups.
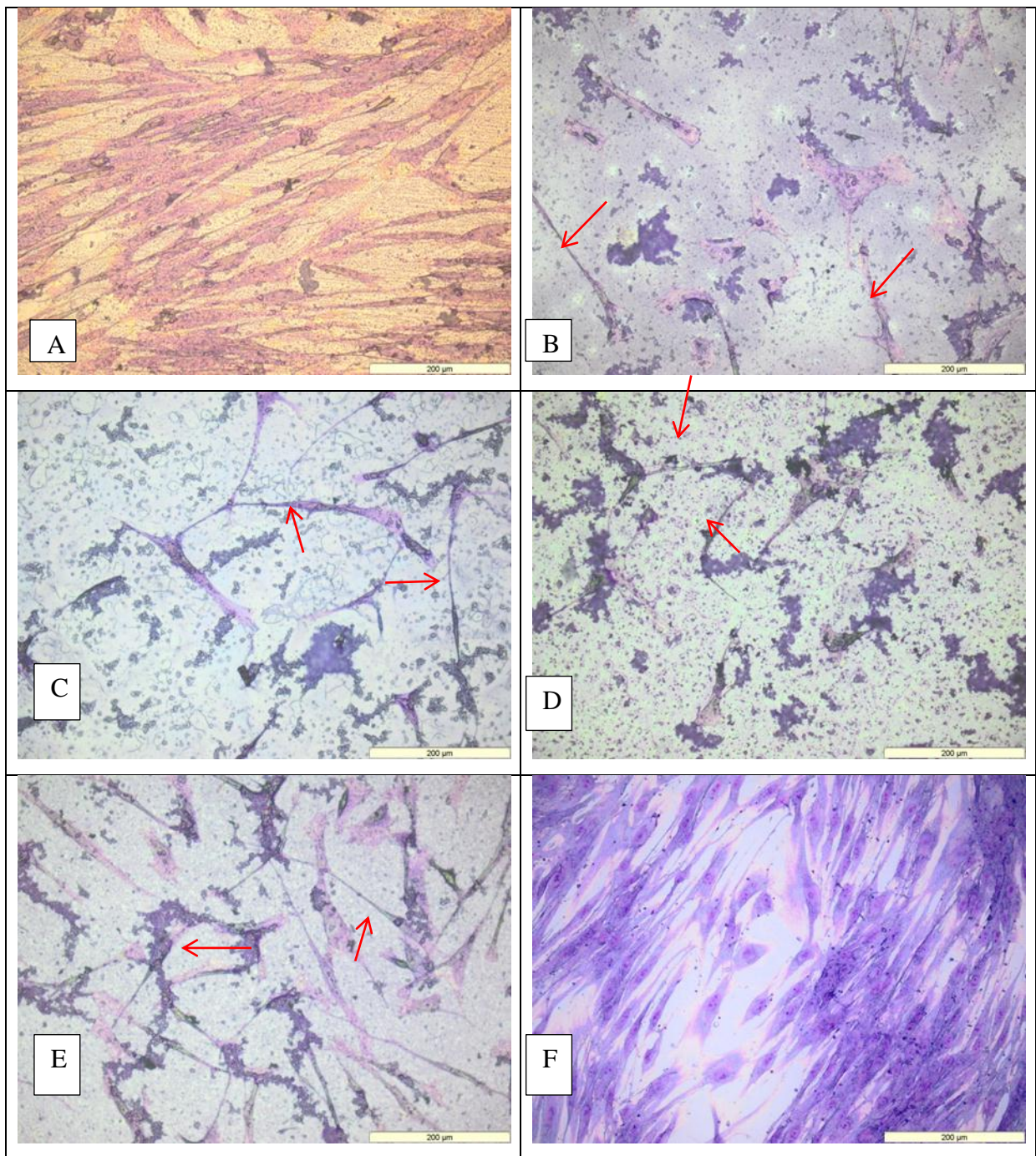
Figure 2.2.4.4 – 20x magnification images comparing fibroblast adhesion and morphology on functionalised oligomers and TCP. Cells cultured on oligomers for 72 hours then fixed with 10% formalin and stained with Giemsa. A= Acid oligomer. B= 1,2-NH$_2$ functional. C= 1,3-NH$_2$ functional. D= 1,4-NH$_2$ functional. E= 1,6-NH$_2$ functional. F= TCP. Arrows mark abnormal spindly cells.

Human Renal Epithelial Cells

Primary renal epithelial cells were cultured in direct contact with oligomer films in an identical manner to the fibroblasts, mentioned above. The viability assay results are shown in figure 2.2.4.5 below.
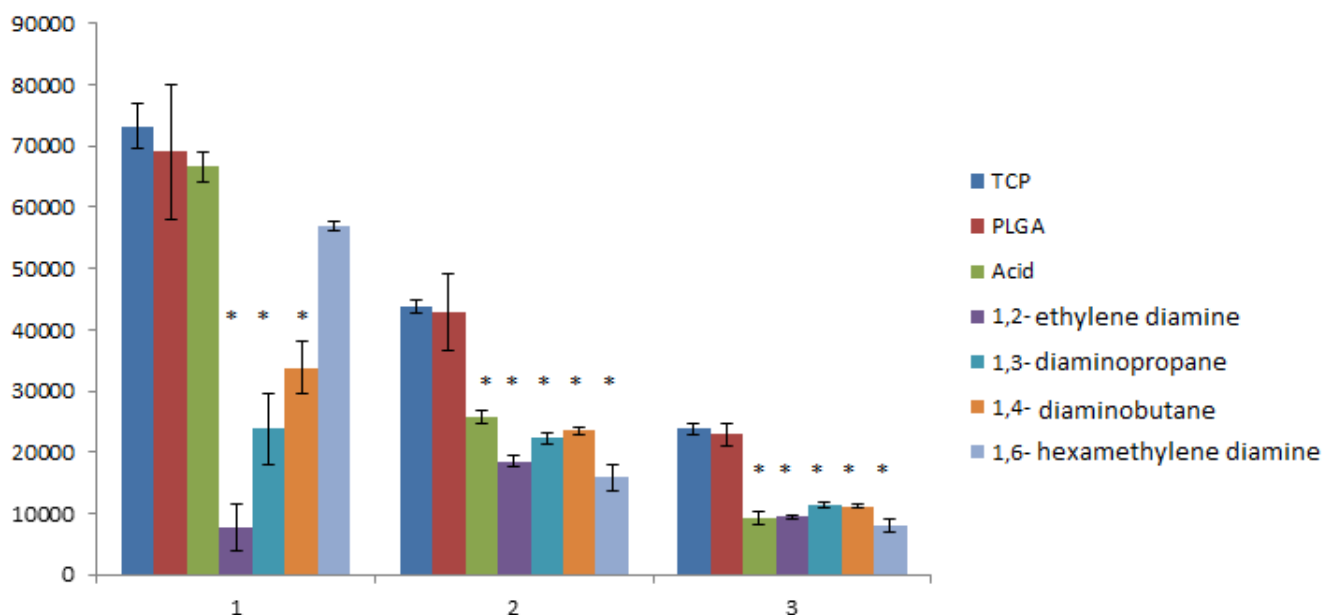
Figure 2.2.4.5 Alamarblue® results of 72 hour HREpC incubation in direct contact with oligomers.

Experiment 1 with the epithelial cells indicate that the acidic and 1,6- ended oligomers are far preferable for cell growth and adhesion when compared to the shorter chain diamines.

This is confirmed clearly by the cell images taken at 24 hours in figure 2.2.4.6 which show little to no cell adhesion on the 1,2-, 1,3- and 1,4- functional oligomers. However, further seeding experiments suggest that such an extreme difference between the different oligomers does not exist and that, whilst not comparable to control materials, all are equally able to provide a suitable substrate for cell culture. For all experiments the healthiest cell morphology, closest to that seen on the TCP controls, and attachment was seen on the 1,6- functional oligomer (figure 2.2.4.7). The cells on the 1,3-NH_2 oligomer can be seen to be underdeveloped with smaller nuclei when compared to those cells on the acid and 1,6- oligomers. The cells on the 1,2 and 1,4- oligomers were too underdeveloped to image effectively and are not shown.
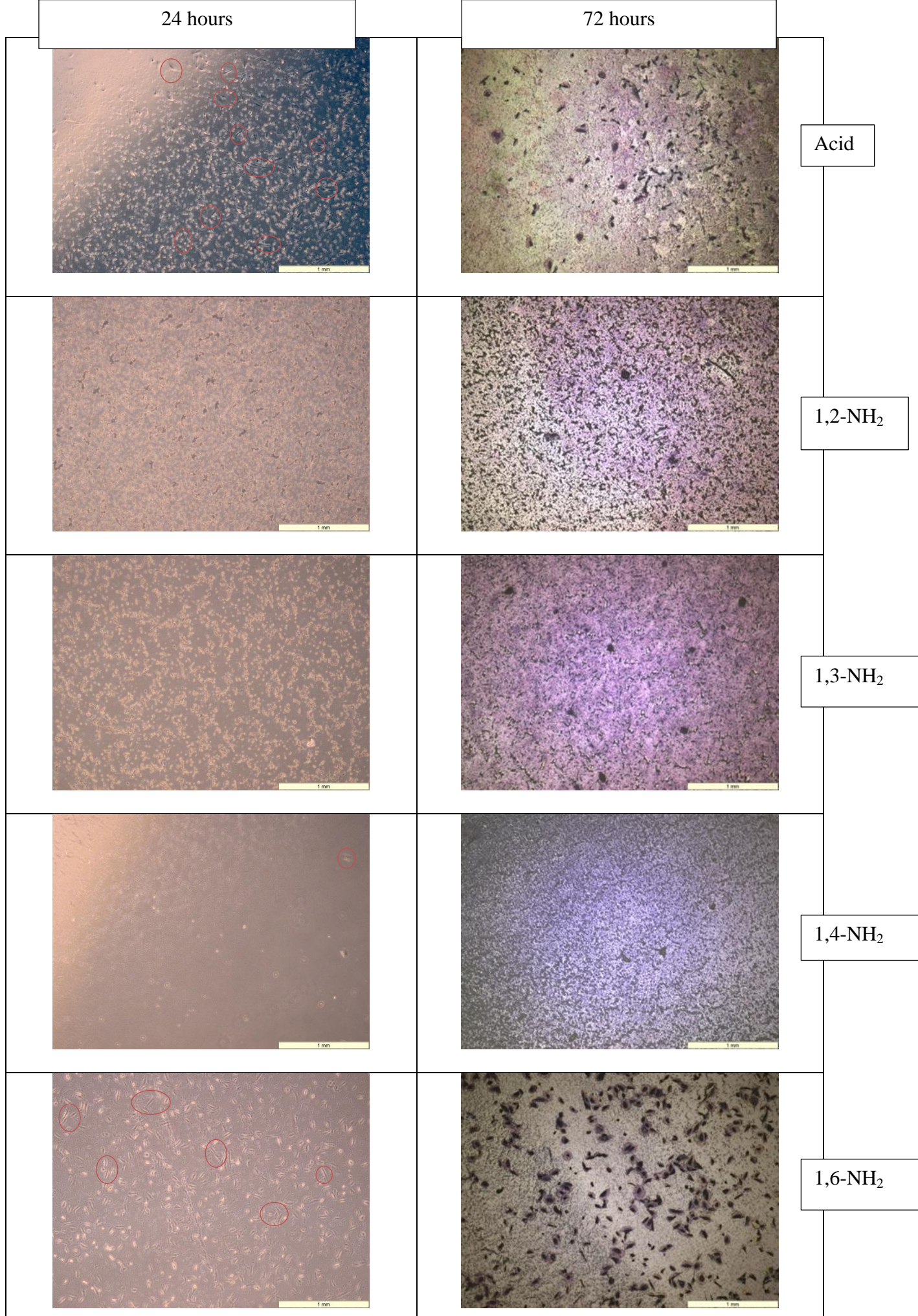
Figure 2.2.4.6 - Images comparing epithelial adhesion on functionalised oligomers after 24 and 72 hours at 4x magnification. 24 hours= phase contrast, red circles indicate adhered cells. 72 hours = cells fixed and stained with Giemsa solution.
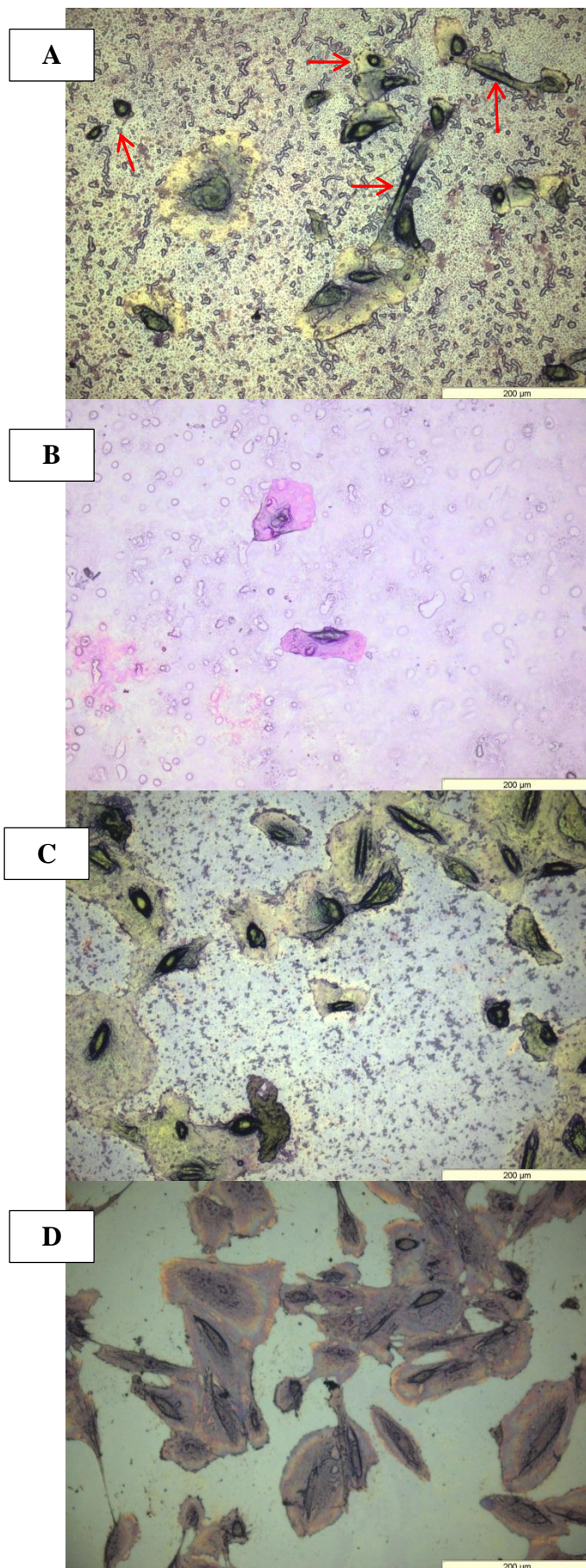
Figure 2.2.4.7 - 20x images of epithelial cells cultured for 72 hours on A= acid, B= 1,3-NH$_2$ and C= 1,6-NH$_2$ functionalised oligomers. D= tissue culture plastic. Cells stained with Giemsa.

The cell morphology on the acid oligomer is erratic. Some cells display good adhesion and prominent nuclei comparable with the TCP control whilst others appear rounded or enlongated (marked with arrows on figure 2.2.4.7 A). This indicates that whilst epithelial cells are able to adhere and proliferate on the acid functional material, this growth is not entirely healthy and normal. Epithelial cells express transglutaminases (Tgase), calcium-dependent enzymes that are able to cross link free amine groups to the gamma-carboxamide group of bound glutamine[208]–[210] Tgases can be extracellular or reside within the cytoplasm and almost since their discovery have been linked to cell morphology and adhesion[211], [212]. They are of interest especially as they have been previously shown to aid the adhesion and mobility of epithelial cells[213]. It is possible Tgases are acting to stabilise the epithelial cells and assist the formation of cell-polymer linkages.

2.3 Conclusions

Through the course of this work it has been identified that cyclodextrins are essential for the successful inclusion of butadiene into an *n*-butyl methacrylate backbone, as is a reaction temperature of 75 °C. However, despite this polymers still showed relatively low levels of butadiene incorporation when compared to the amount of monomer added to the reaction. Copolymers of butyl methacrylate-butadiene were successfully cleaved using ozone and then successfully worked up to contain either acid or amine end group functionality. The successful end group functionalization of the butyl methacrylate oligomer was shown using FT-IR and elemental analysis.

Contact angle measurements were not possible on many of the films formed by the amidated oligomers. This indicates a surface with a high charge separation and provides reassurance that much of the amine functionality was present on the surface of the films.

Fibroblast and epithelial cell culture on the functionalised oligomers showed that overall, no material was a competitor for the standards tissue culture plastic and poly(lactide-glycolic acid). Dermal fibroblast cells showed greatest cell adherence and proliferation on the acid functional oligomer. Optical microscopy showed that these cells were comparable to those cultured on TCP control material. Growth on the amine functional oligomers was sparse and the cells displayed an abnormal spindly morphology. Cell viability results taken in hand with size exclusion chromatography suggest that low molecular weight molecules could leach from the oligomers which could potentially be toxic to cells.

The results of the renal epithelial cell culture in direct contact with functionalised oligomers showed that the 1,6-diamine functional oligomer was the preferred. Some abnormal epithelial growth was observed on the acid functional oligomer. This is in direct contrast to the fibroblast cell culture results, and is probably due to the expression of transglutaminase by epithelial cells. Transglutaminase (tgase) may be able to catalyse the cross-linking of 1,6-diamine groups present in the oligomer film with glutamate residues in extracellular biomolecules.

Fibroblasts, being structural cells, are believed to rely on a different adhesion mechanism. It is proposed that the acid functional polymers are mimicking the negatively charged proteoglycans that reside within the extracellular matrix. The presence of negatively charged species ensures that cells stay hydrated, through the attracted of water and they may also allow the storage of growth factors.

In conclusion, these results suggest the potential for new cell culture substrates using oligo(BMA) functionalised with acid (fibroblast cells) or 1,6-diamine end groups (epithelial

cells). However, both systems require further optimisation through oligomer compositon and their purification. Additionally, longer term culture studies are required and further cell assays: for instance the DNA stain pico green and the fluorescent live/dead staining system can both be used to assess cell health.

2.4 Experimental

Instrumentation

NMR spectra were obtained using either a Bruker AC-250 (operating frequency ^{1}H- 250 MHz, ^{13}C- 62.5 MHz) or a Bruker AMX2-400 (operating frequency ^{1}H- 400 MHz, ^{13}C- 100 MHz) spectrometer depending on the required resolution. Analysis was performed using TopSpin™.

THF Gel permeation chromatography was performed using a Polymer Laboratories LC1150 pump with dual model 481 Lambda-Max LC spectrophotometer UV detector obtained from ERMA and Viscotek RI detector. The stationary phase comprised 2 x 40 cm Polymer Laboratories PL gel mixed-E columns (5 mm particle size, Effective MW range 103 – 0.2 x 106 g mole-1) + guard columns. The flow rate of the mobile phase was 1.0 ml/min. Automatic sampling was performed by a Gilson auto injector and analysis was performed using Cirrus™ GPC software.

Triple detection GPC was performed using a Viscotek TDA 302 complete with a GPCmax autosampler with THF as the mobile phase (flow rate 1.0 ml/min). The stationary phase comprised of 2 x 300 mm Polymer Laboratories PL gel mixed-C columns (effective range 200 – 2 x 106 gmol^{-1}). Analysis was performed using OmniSEC™ software.

Ultrafiltration was performed using a stirred 400 cm^3 Millipore ultrafiltration cell with a regenerated cellulose filter under 4-bar nitrogen pressure.

Colorimetric studies were performed using end point analysis on a Dynex Technologies MRXII plate reader with a 570nm filter and a 600nm reference filter.

Infrared spectra were obtained using a Perkin Elmer Spectrum 100 FT-IR spectrometer with diamond tip ATR.

2.4.1 Monomer starve-fed emulsion polymerisation of butyl methacrylate and butadiene

Materials

Butadiene (99+%, Aldrich), Potassium persulfate (99+%, Aldrich), Potassium hydrogen phosphate (98+%, Aldrich), DOWFAX2A1 surfactant solution (alkyldiphenyloxide disulfonate, Dow Chemical Company USA), sodium chloride (Fisher, Lab reagent grade), Methanol (Fisher, HPLC grade) Beta-cyclodextrin hydrate (Alfa Aesar) and Alpha-cyclodextrin hydrate (Alfa Aesar) were used as received.

Butyl methacrylate (99%, Aldrich) was purified before use to remove any inhibitor present. It was twice washed with equal portions of aqueous 2% sodium hydroxide solution, followed by two equal portions of distilled water. This washed butyl methacrylate was then distilled under reduced pressure, prior to use and stored at –4.5 ˚C.

Distilled water was used throughout.

Equipment

Polymerisations were performed in a 1L double-jacketed glass reactor (Radleys, UK) equipped with an overhead mechanical glass stirrer, a nitrogen inlet, a reflux condenser, a temperature probe and an inlet for gaseous and liquid monomer addition. Liquid monomers were added using a peristaltic pump (Watson Marlow 505S) and gaseous butadiene was added using an infusion pump (Precidor Type 5003, Infors HT). The peristaltic pump was calibrated after every three uses, and tubing was cleaned using successive flows of distilled water and acetone. Monomer addition was controlled so that addition of both liquid and gas was completed at the same time and the butadiene molar feed rate was adjusted to coincide with the liquid monomer. The equipment set up can be seen in figure 2.4.1.1.
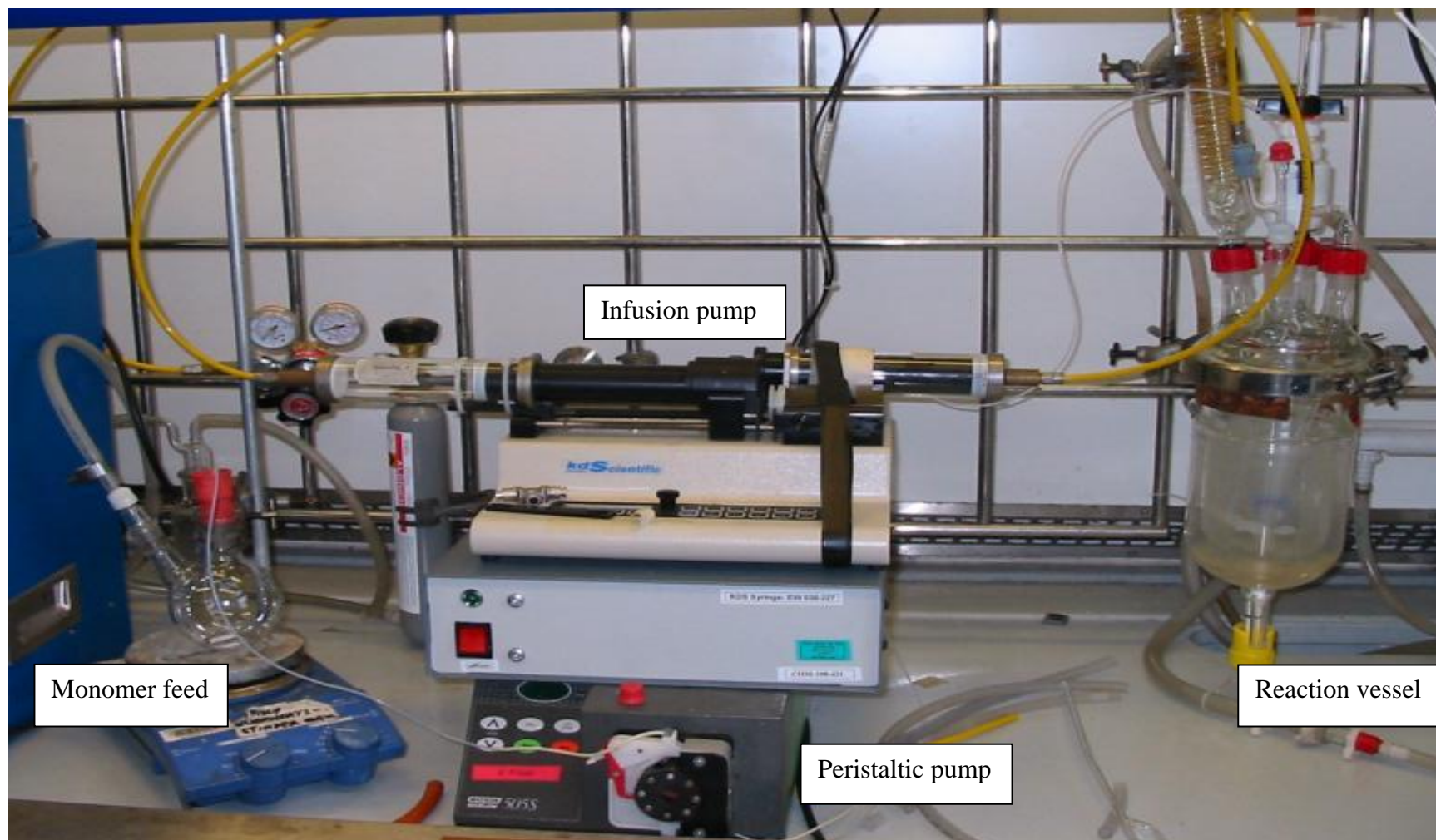
Figure 2.4.1.1 – Photo of 1L reactor, with peristaltic and infusion pumps.

Method

Cyclodextrin, DOWFAX 2A1 (3.6 g) and pH regulator potassium hydrogen phosphate (0.4 g) were added to 450 mL water and stirred until dissolved. The solution was added to the reactor and nitrogen purged for one hour, whilst simultaneously heated to 70 ˚C. At the same time, potassium persulfate was dissolved in 50 mL of water and butyl methacrylate was added to a two-necked round bottom flask. Both were purged with nitrogen for one hour. Once the contents of the reactor had reached the required temperature, the initiator solution was injected into the reactor and the monomer feed was started. Table 2.4.1.2 summarises the quantities and reaction times attempted. Reactions were also performed at 80 ˚C and 75 ˚C using α-cyclodextrin (3.6 g, 0.00317 moles), butyl methacrylate (100 mL, 0.63 moles) and a feed rate of 2 4mL/min of butadiene (1 mole) over 16 hours.

Butyl methacrylate /mL (moles)	Butadiene /mL (moles)	Temperature /˚C	Reaction time /hr	β-Cyclodextrin /g (moles)
75 (0.47)	7600 (0.32)	70	4	3.6 (0.00317)
75 (0.47)	1200 (0.0625)	70	4	3.6 (0.00317)
100 (0.63)	4000 (0.17)	70	4	3.6 (0.00317)
100 (0.63)	4000 (0.17)	70	5	3.6 (0.00317)
100 (0.63)	24000 (1)	70	16	3.6 (0.00317)
100 (0.63)	24000 (1)	70	16	3.6 (0.00317)
100 (0.63)	48000 (2)	70	16	3.6 (0.00317)
100 (0.63)	24000 (1)	80	16	3.6 (0.00317)
100 (0.63)	24000 (1)	80	16	0
100 (0.63)	24000 (1)	75	16	3.6 (0.00317)
100 (0.63)	24000 (1)	75	16	0

Table 2.4.1.2 – Summary of conditions used in poly(butyl methacrylate-co-butadiene) syntheses. Molar values in parentheses.

When both monomers had been consumed, the resulting white latex was removed from the reactor and stored at room temperature.

Solid polymers were retrieved from the latex by using sodium chloride to induce coagulation. The white solid was filtered and washed thoroughly with water and then methanol before being dried in a vacuum oven at 50 ˚C. GPC analysis was performed using tetrahydrofuran (GPC grade, Fisher) eluent.

Results of NMR spectroscopy:

(^{1}**H**, 400 MHz, *CDCl$_3$*) δppm 0.97 (A), 0.98 (E), 1.42 (B), 1.64 (C), 1.96 (F,I), 4.17 (D), 5.57 (G), 6.12 (G)

(^{13}**C**, 100 MHz, *CDCl$_3$*) *δppm* 13.7 (1,7), 19.3 (2,3), 30.2 (8), 44.9 (6), 64.6 (4), 76.5 (CDCl$_3$), 77.2 (CDCl$_3$), 125.1 (Alkene), 180.7-174.4 (5).

2.4.2 Ozonolysis of Poly (Butyl methacrylate-co-Butadiene) and generation of acid end groups

Materials

Hydrogen peroxide (35% v/v, Alfa Aesar), selenium dioxide (98%, Aldrich), toluene (Fisher) and Amberlite IRA 400(Cl) (Aldrich) used as received.

Equipment

Ozone was generated by passing oxygen through an electrical discharge generator (Type BA, Wallace & Tiernan, UK) at a rate of 1.74ghour^{-1}.

Method

The poly(BMA-co-BD) latex (200 mL) was added to a 1L 3-neck round bottom flask, equipped with a magnetic stirrer and dropping funnel. An equal volume of distilled water (200 mL) was added with stirring. Toluene (50 mL) was added dropwise to the diluted latex over 4 hours at room temperature. The swollen latex was then stirred for a further 24hours. After this time a reflux condenser was added to the flask and it was placed in an ice bath. A glass inlet was used to introduce ozone at a rate of 1.74 ghour^{-1} for 6-8 hours, with constant stirring of the latex throughout. The ice bath was topped up as required during this time. On removal of the ozone inlet, a nitrogen inlet was introduced for an hour to remove any residual ozone from within the flask.

Selenium dioxide (4 g, 0.03 moles) and hydrogen peroxide solution (35 % v/v) (100 mL, 1 mole) were then added to the colloidally stable latex with stirring. This was heated to 80$^\text{o}$C and refluxed for 24 hours to generate acid end group functionality.

Purification of acidic poly(BMA-co-BD)

Amberlite IRA 400(Cl) (20 g) was placed into a conical flask with 100mL of latex. The flask was placed onto an orbital shaker with a very low setting and gently shaken. After about 5 hours the latex was decanted into a second conical flask containing fresh Amberlite IRA 400 (Cl) and was shaken gently overnight. The latex was then removed and placed into dialysis visking tubing and placed into distilled water. Twice daily water changes occurred over a period of one week. The latexes were then removed from the dialysis tubing and any toluene present was removed by reduced pressure. The water was then azeotropically removed by addition of ethanol and then removing by reduced pressure.

2.4.3 Diamine Addition to Oligo(BMA-co-BD) with acid end groups

Materials

Ethylenediamine (99%, Aldrich), 1,3-diaminopropane (99%, Aldrich) 1,4-diaminobutane (99%, Aldrich), 1,6-diaminohexane (99%, Aldrich), 1-(3-dimethyl-aminopropyl)-3-ethylcarbodiimide hydrochloride (Alfa Aesar) were used as received. Distilled water was used throughout.

Method

The oligo (BMA) + COOH latex (75 mL) was added to a 3-neck round bottom flask, equipped with a condenser and magnetic stirrer bar. DOWFAX 2A1 was then added to the flask and vigorous stirring was started. At the same time 1-(3-dimethyl-aminopropyl)-3-ethylcarbodiimide hydrochloride (EDC) was weighed out and dissolved in 45mL of water. The stirring solution of latex and surfactant was then submerged into an ice bath; the aqueous solution of EDC was then added slowly, upon completion, of addition, a stable latex remained. The appropriate diamine was then added to the stirring latex slowly over a period of at least an hour. Substantial effervescence was observed at this stage. The reaction was left to warm to room temperature and continued to stir for 24 hours. The quantities used for each reaction are shown in table 2.4.3.2.

Diamine	Amount used	EDC	DOWFAX2A1 (g)
Ethylenediamine	4.651g (0.08 moles)	3.6971g (0.02 moles)	1.210g
1,3-diaminopropane	5.841g (0.08 moles)	3.7123g(0.02 moles)	1.211g
1,4-diaminobutane	6.812g (0.09 moles)	3.6991g(0.02 moles)	1.210g
1,6-diaminohexane	7.941g (0.09 moles)	3.7114g(0.02 moles)	1.202g

Table 2.4.3.2 – Table of reagents used in EDC-mediated diamine-oligomer cross coupling reaction.

1, 6-diaminohexane is a solid and an aqueous solution of this was prepared in 90 mL of water which was then added to the reaction mixture.

The stable emulsions were removed placed into dialysis visking tubing and placed into distilled water for 2 weeks, with daily changes of water taking place.

2.4.4 Culture of fibroblast and epithelial cells

All described protocols performed under sterile conditions in a dedicated laminar flow hood, using 70% alcohol (ethanol or isopropanol) and Virkon® solutions as cleaning agents.

Human dermal fibroblasts

Materials

Primary normal dermal fibroblasts (ATCC), Dulbecco's modified Eagle's medium (HEPES buffered, high glucose, + pyruvate, Life Technologies), fetal bovine serum (FBS; sterile filtered, non-USAorigin, Sigma), penicillin-streptomycin (pen-strep; 10000µ, Life Technologies), trypsin-EDTA (0.25%, Life Technologies), trypan blue stain (Life Technologies).

Equipment

Purecell NU-5100 CO2 Direct Heat Air Jacketed Incubator (Nuaire).

Culture

60 mL of DMEM was removed from the 500 mL bottle, and replaced with 50 mL FBS and 10 mL penicillin-streptomycin. The bottle was agitated before 9 mL of complete medium was removed and placed in a T75 cell culture flask. This aliquot of medium was warmed in the incubator for 30 minutes, whilst the remaining media was stored in the fridge for up to six weeks. After 30 minutes the cryopreserved cells were gently agitated in a water bath at 37 °C for 1 minute, until the frozen 'plug' broke inside the vial. The cells were then quickly transferred to the pre-prepared T75 and gently swirled to thaw completely. The cells were kept in the incubator at 5% CO_2, 37 °C for 24 hours, in order to adhere, before a complete media change was performed. Complete media changes were then performed every 2-3 days, with daily checks of cell health using phase contrast microscopy.

Passage

When cells were observed to be 80-90% confluent, passage was performed to ensure the continued rate of mitosis. The media was aspirated from the cells, and they were washed with 10 mL of PBS. Each T75 was then treated with 3 mL of trypsin-EDTA, tapped and agitated until the cells were observed to be detached from the flask. The trypsin was then neutralised by the addition of an equal amount (3 mL) of complete ^{f}media. The cell suspension was then transferred to a centrifuge tube and spun at 1400rpm for 5 minutes, until a cell pellet could be observed on the bottom of the tube. The supernatant was carefully aspirated from the pellet, which was then resuspended in a known amount of complete ^{f}media. A cell count (described in section 2.4.5) was performed at this stage, and cells were then reseeded into T75 flasks at a density of $2x10^6$ cells. 10 mL of ^{f}media was added to each flask, and cells were then subjected to ordinary incubation and culture.

Human renal epithelial cells

Materials

Primary human renal epithelial cells (ATCC), DMEM/F-12 (no phenol red, HEPES buffered, + L-glutamine, Life Technologies), hydrocortisone (Bioreagent, Sigma) , epidermal growth factor (EGF; recombinant, expressed in *E. coli*, lyophilized powder, Sigma) , penicillin-streptomycin (pen-strep; 10000 µ, Life Technologies), fetal bovine serum (FBS; sterile filtered, non-USAorigin, Sigma), phenol red (Bioreagent, Sigma), insulin-transferrin-selenium supplement A (ITS-A; Life Technologies), GlutaMAX™ (Life Technologies).

100 µg of EGFwas dissolved in 400 µL DMEM/F-12 and stored in the freezer -20 ℃.

18 µg of hydrocortisone was dissolved in 20ul of ethanol, which was then made up to 20 mL with DMEM/F-12. 1 mL aliquots were stored in the freezer at -20 ℃.

FBS and pen-strep were stored in 25 mL and 10 mL aliquots at -20 ℃, respectively.

Preparation of media

40 mL of DMEM/F-12 was removed from each 500mL bottle. To the remaining media was added 5 mL ITS-A, 5 mL pen-strep, 5 mL GlutaMAX™, 5mL pen-strep, 25 mL FBS, 20 µl EGF solution, 20 µl hydrocortisone solution and 5 mg phenol red. The media was gently agitated and stored in the fridge for up to six weeks.

Culture

The culture of HREp cells followed the same protocols as described for fibroblast cells in section 2.4.4, with the use of HREp medium as prepared above used throughout.

Due to the lower amount of FBS present in complete HREp medium, a ratio of 2 mL trypsin : 4 mL neutralising media was used during the passage procedure of epithelial cells.

2.4.5 Culture of cells in direct contact with oligomers

Materials

Functionalised oligomers as synthesised in sections 2.4.2 and 2.4.3, isopropanol (absolute, Fisher), complete media (prepared as described above), trypsin-EDTA (Life Technologies), PLGA (50:50, Polysciences), DMSO (anhydrous, Sigma), Alamarblue® (Life Technologies), phosphate buffered saline (Bioreagent, Sigma), hematoxylin solution according to Weigert (parts A and B, Aldrich), eosin y (99%, Sigma Aldrich), 10% neutral buffered formalin solution (Sigma), giemsa stain modified solution (Sigma), ethanol (absolute, Fisher), glacial acetic acid (99%, Fisher).

Distilled water was used throughout unless otherwise specified.

Equipment

IR spot lamp 75W (Exo Terra).

Preparation of polymer films

Polymers were dissolved in isopropanol at a concentration of 5 mg in 1 mL solvent, whilst the PLGA was dissolved in DMSO at the same concentration. The polymer solutions were well agitated and sonicated for 30 seconds if required. 100 mL of polymer solution was then pipetted onto each sterile glass coverslip. An IR lamp was used to heat treat the polymer films until the solvent appeared visibly removed. At this point, each coverslip-with-film was placed into its own well of a six well plate and washed with sterile PBS to remove any residual solvent.

Fibroblasts or epithelial cells were treated with trypsin as previously described, but instead of re-seeding into T-75 flasks, they were seeded directly onto the films at a density 1×10^4 cells/well. 2 mL of complete media added was to each well and the cells were incubated for 24 hours at 37 ºC, 5%CO_2. After 24 hours phase contrast imaging and a full media change was performed. After 72 hours cells were assayed and fixed for staining.

Cell counting and seeding

To ensure that approximately the same density of cells was cast onto each film, cell counting was performed after resuspension of the cell pellet.

20 µL of cell suspension was agitated with 20 µL of trypan blue stain. 15 µL of this solution was pipetted into each of the chambers of a haemocytometer cell counter. The hemocytometer has a known volume of 0.1 µl for each large square. The number of live (non-stained) cells were counted within the marked squares on figure 2.4.5.1.
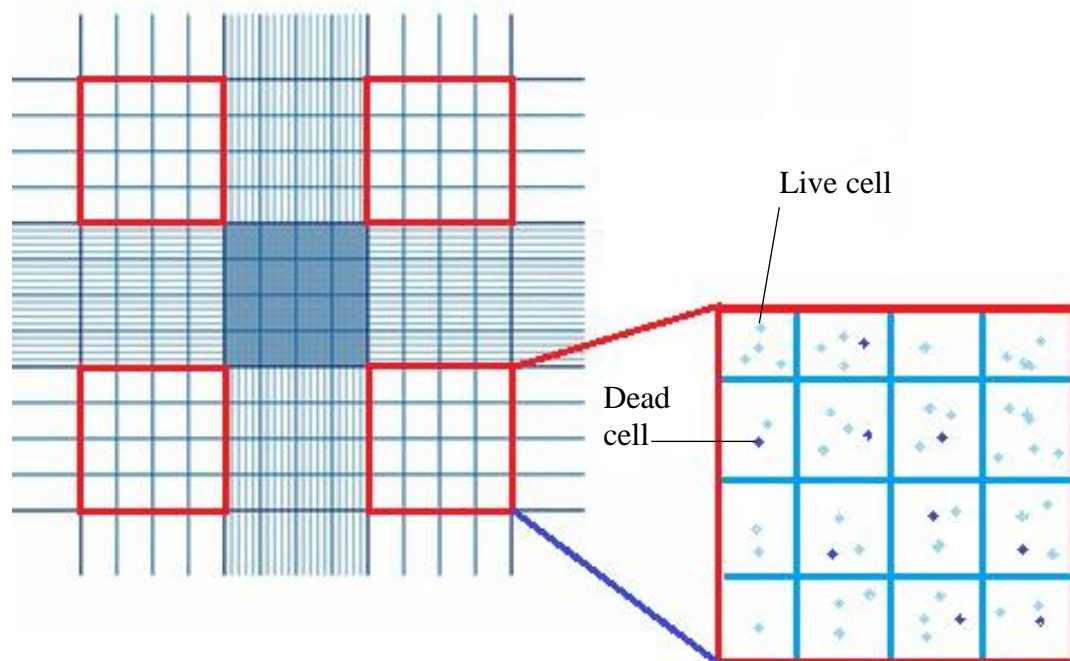
Figure 2.4.5.1 – Diagram illustrating the counting squares of a hemocytometer. Pale blue dots represent live cells, whilst dark blue dots represent dead cells stained with trypan blue.

As there are two counting chambers on a hemocytometer, a total of 8 cell counts are obtained and an average per 0.1µl can be obtained. By using equation 2.4.5.2 the number of cells in suspension can be calculated.

$$Number\ of\ cells = 2\ x\ n\ x\ m\ x\ 10000$$

Equation 2.4.5.2 - Equation used to calculate total number of cells in m mLs of solution after obtaining average cell count (n) from hemocytometer. It is necessary to multiply by 2 due to the half dilution with trypan blue in the counting chamber.

After obtaining a total cell count it was then possible to seed the cells at the required density.

Alamarblue® Assay

The Alamarblue® assay was performed as per the manufacturer's instructions[214]. As colorimetric analysis was being used to assess the colour change of rezasurin to resorufin, an incubation period of 16 hours with 10% Alamarblue® was found to be optimal for the cell types used. A typical standard curve obtained for the Alamarblue® assay is shown in figure 2.4.5.3.

y = 6E-07x + 0.1225
R² = 0.9425
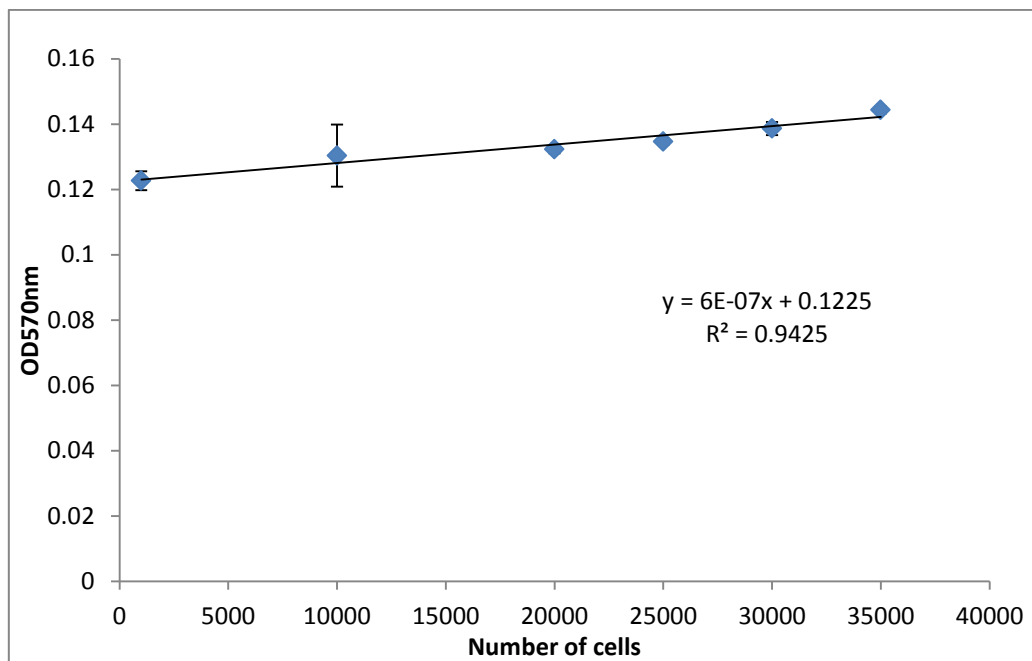
Figure 2.4.5.3 - Typical Alamarblue® standard curve.

The number of cells present in each well was then calculated using the following equation:

$$Number\ of\ cells = \frac{OD_{570nm} - c}{m}$$

Equation 2.4.5.4 - Equation used to find number of cells from optical density (OD_{570nm}). C= constant from standard curve and m = gradient of standard curve.

Cell visualisation

After performing viability assays, each glass coverslip was washed with sterile PBS. The slips were then submerged in 10% formalin for 10 minutes to fix the cells and then washed again with sterile PBS.

Giemsa

Coverslips were then submerged into the giemsa stain solution for 5 minutes and then washed with distilled water until clear. The coverslips were allowed to air dry before imaging.

This stain has the following characteristics:

Feature	Colour
Micro-organisms, fungi, parasites	Purple/blue
Starch and cellulose	Sky blue
Nuclei	Dark blue/violet
Erythrocytes	Salmon pink
Cytoplasm	Various light blues
Collagen, muscle, bone	Pale pink

Hematoxylin and Eosin Y

Equal parts of the hematoxylin reagents A and B were mixed fresh to form the working Weigert's solution. Each coverslip submerged into the Weigert's solution for 5 minutes and then washed with tap water until clear. The coverslips were then submerged into a 1% aqueous solution of Eosin Y for 5 minutes. The coverslips were then submerged into 0.5% acetic acid for 1 minute and then rinsed again with tap water. Finally, each coverslip was washed with ethanol and allowed to air dry.

This stain has the following characteristics:

Feature	Colour
Nuclei	Blue (hematoxylin)
Erythrocytes	Very bright pink (eosin Y)
Muscle, cytoplasm	Deep pink (eosin Y)
Collagen	Pale pink (eosin Y)

3 - Hyperbranched poly(*n*-butyl methacrylate) and linear analogues with acid or amine end groups: synthesis and cytocompatibility

3.1 Introduction

The purpose of this part of the work was to synthesise novel hyperbranched (HB) butyl methacrylate (BMA) polymers using RAFT polymerisation and to observe cell-polymer interactions on coatings derived from these polymers. To our knowledge, the synthesis of hyperbranched poyl(BMA) using RAFT has not been reported to date. Experiments were performed to ascertain the optimal ratio of monomer:chain transfer agent to produce hyperbranched polymers with end groups capable of being modified. These materials, if they exhibit satisfactory properties, might be suitable as cell-adhesive coatings for tissue implants. The addition of acid monomers in tissue scaffolds has been shown to enhance wound healing and promote angiogenesis[215], [216]. This is due to the differences in hydrophilicity and hydrophobicity between comonomers creating the right amphiphilic environment for cell growth. Also important for cell adhesion are the proteins and molecules that are present on the cell surface, known as cell adhesion molecules (CAMs). Ruoslahti has published popular reviews on both integrins and proteoglycans in cell adhesion[217], [218]. A review of the role of peptides has been been provided by LeBaron *et al.*[219] and these have been utilised by members of the Rimmer group to improve cell adhesion[220]–[222]. CAMs are also discussed in chapter 1 section 7.

One objective was to test the hypothesis that a hyperbranched polymer with multiple acid end groups would be a good substrate for cell adhesion and proliferation. This would then allow future projects to optimise these materials for use as tissue scaffold coatings. This would involve using a polymer coating to introduce cell-adhesive functionality onto an inert structural material. In order to assess the performance of the hyperbranched polymers, they were compared with linear BMA polymers that had been copolymerised with 4-vinyl benzoic acid. These acid functional polymers were then reacted with diamines to investigate if this would provide enhanced cell adhesion. Diamines were chosen to functionalize the polymers

due to simplicity of the amidation reaction at the carboxylic acid groups[155], [199], [223], [224] and because of the chemical similarity to the amino acid lysine. Lysine is the eighth most abundant amino acid and is present in all proteins[225]. As it is a positively charged amphiphile, lysine is often involved in salt-bridges with negatively charged amino acids (e.g. aspartate) and this has a stabilising effect on protein structure[226], [227]. Additionally, the action of lysyl oxidase on lysine in the extracellular matrix forms the derivative allysine (figure 3.1.1) which is then used in the synthesis and crosslinking of collagen and elastin[228], [229].
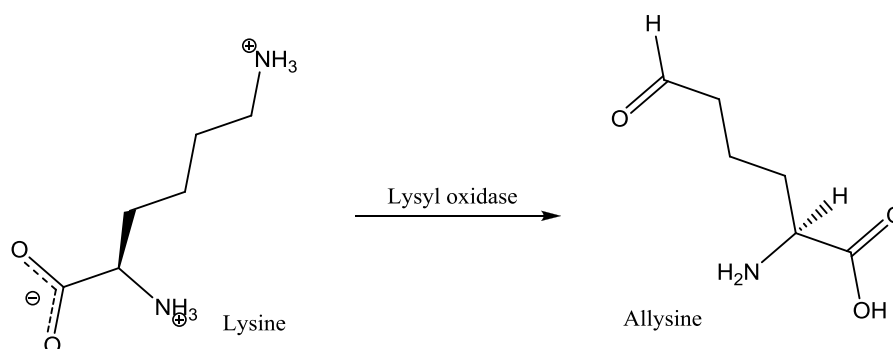
Figure 3.1.1 – The conversion of lysine into allysine by lysyl oxidase. Allysine is a precursor for the ECM components collagen and elastin.

It was hypothesised that the diamine functional polymers will promote the action of lysyl oxidase through mimicking lysine, and thus encourage the formation of cross-links and the extracellular matrix.

The synthesised polymers (BMA1-4) were analysed using standard characterisation techniques such as triple detection GPC and ^{1}H NMR spectroscopy and the results are discussed with a critical view of the RAFT polymerisation. A successful polymerisation should produce highly branched polymers showing good conversion of both methacrylate monomer and CTA1, with little evidence of cross-linking in the final polymer. Severe cross-linking, or gelation, is evident by insolubility in all solvents. The hyperbranched polymers were also analysed after reaction with excess 4,4'-azobiscyanovaleric acid (ACVA) in order to judge if the acid functionality had successfully added to the end groups. The linear *n*-butyl methacrylate polymers were prepared in three different monomer ratios and characterised by Sarah Canning in the course of her Master's project[230] prior to functionalization. In this document, the linear polymers shall be referred to as LIN1, 2 or 3 where 1 = 4:1 molar ratio *n*-butyl methacrylate:4-vinylbenzoic acid, 2 = 8:1 ratio and 3 = 12:1 ratio of monomers.

These polymers were assessed for their suitability as analogues to the BMA library and also the outcomes of diamine coupling reactions were studied.

As these polymers are intended for use as surface coatings, they were cast upon glass coverslips before cell seeding was carried out as described in chapter 2. Primary dermal fibroblast and renal epithelial cells were used for direct contact studies, at a density of 1.5×10^4 cells per film. Cells were grown on each polymer in triplicate in each experiment and each experiment was repeated on three separate occasions using identical methods and conditions (experiments 1, 2 and 3). The cell viability on the polymers after 72 hours was assessed using the Alamarblue® assay and optical microscopy.

3.2 Results and Discussion

3.2.1 Hyperbranched polymer synthesis and functionalisation

The first step of the RAFT polymerisation was the synthesis of the RAFT agent 4-vinylbenzyl pyrrole carbodithioate chain transfer agent (CTA1). This is shown in scheme 3.2.1.1 and described in detail in chapter 3.4.1.
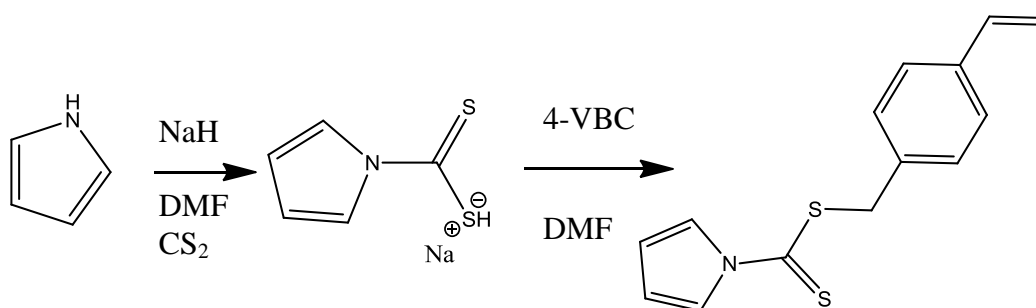
Scheme 3.2.1.1 – Scheme of 4-vinylbenzyl-pyrrolecarbodithioate synthesis. 4-VBC = 4-Vinylbenzyl chloride.

Hyperbranched polymers of butyl methacrylate were produced in four molar ratios with pyrrole carbodithioate (CTA 1) and 4-4'azobis cyanovaleric acid was used as a free radical initiator in RAFT polymerisation (scheme 3.2.1.2 and table 3.2.1.5). The synthesis was performed using a freeze-pump-thaw technique with an aprotic solvent. Polymers with higher quantities of *n*-butyl methacrylate were sensitive to gelling in the ampoule, probably caused by cross-links through bimolecular termination. It was found that this effect could be lessened by minimising the amount of initiator present in the system, thus decreasing the total number of radicals present.
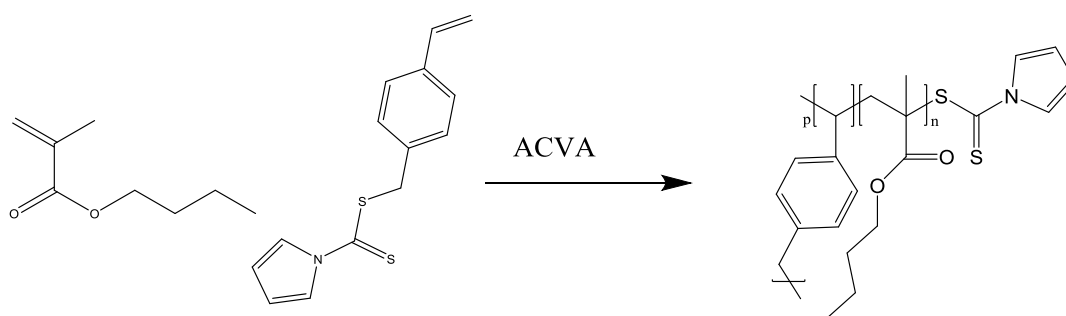
Scheme 3.2.1.2 – RAFT polymerisation of *n*-butyl methacrylate using ACVA initiator.

The successful incorporation of the chain transfer agent into poly(butyl methacrylate) was first observed using ^{1}H NMR. Figure 3.2.1.3 shows that in addition to the usual peaks associated with poly(butyl methacrylate), signals associated with aromatic protons were observed at 6.5-8ppm. The most intense resonances observed are those that arise from the alkyl protons of butyl methacrylate between 1-2ppm– this is expected as it is the monomer present in the greatest amount.
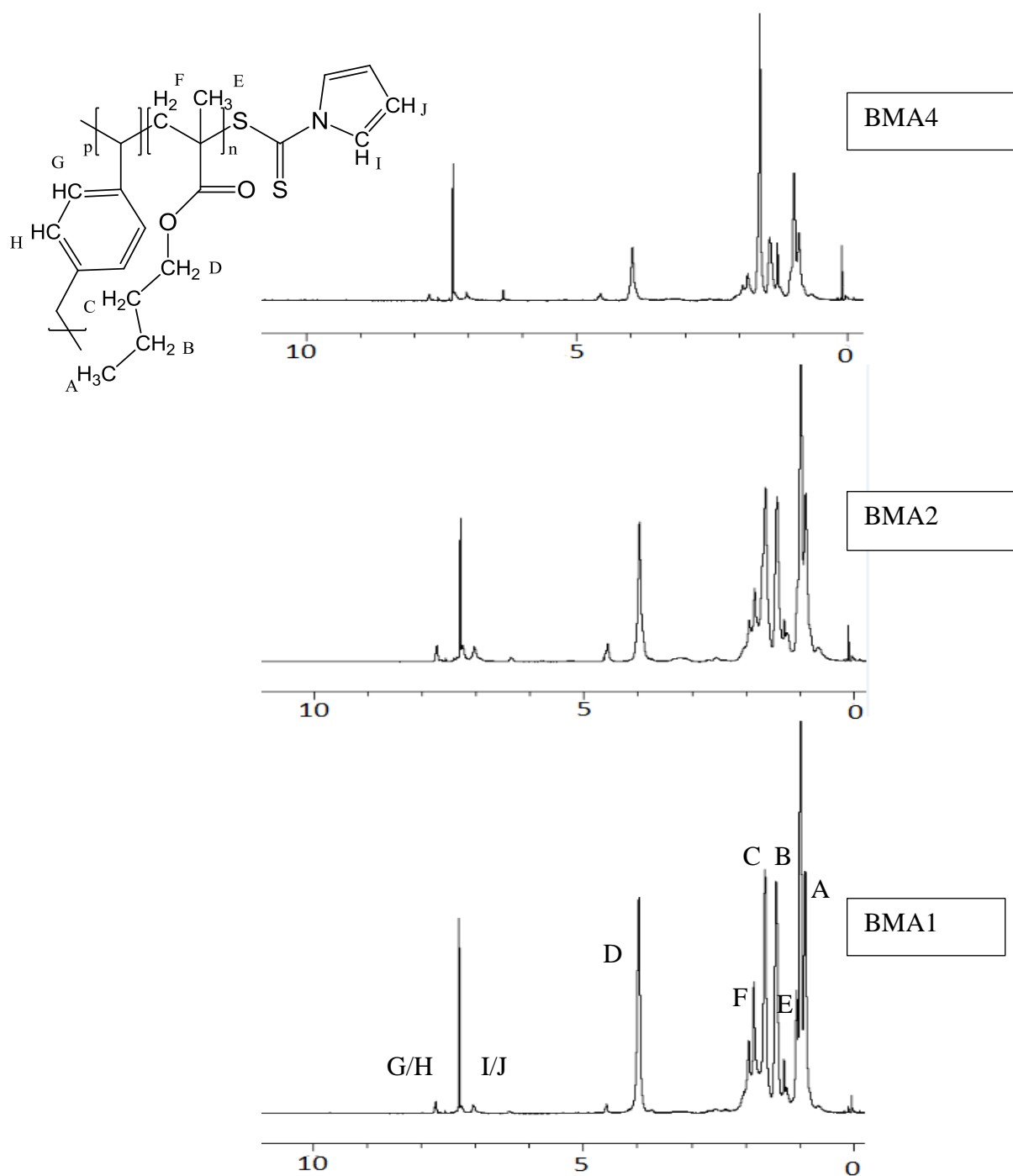
Figure 3.2.1.3 - ^{1}H NMR spectra of hyperbranched polymers BMA1-4. (BMA3 insoluble).

Approximate values for the percentage incorporation of carbodithioate can be calculated by comparison of the integrations in the proton NMR spectra. This is achieved using equation 3.2.1.4 which compares the integrals of the pendant alkyl protons from the *n*-butyl methacrylate (H_A) and pyrrolidine protons (H_J).

$$\% \, Dithioate = 100 \; x \; \frac{\int \frac{H_J}{2}}{\int \frac{H_A}{3}}$$

Equation 3.2.1.4 - Equation used to calculate the percentage dithioate in each polymer using ^{1}H NMR integrals.

The observed incorporation of carbodithioate as calculated by the equation above is summarised for each polymer in table 3.2.1.5.

	BMA added (mL)	ACVA added (g)	CTA1 added (mL)	Moles BMA	Moles ACVA	Moles CTA 1	Maximum % dithioate	Observed % dithioate
BMA1	5	1.29	1	0.03	0.004	0.004	12.26	2.3
BMA2	10	1.29	1	0.06	0.004	0.004	6.13	4.0
BMA3	15	0.645	1	0.09	0.002	0.004	4.09	n/a
BMA4	20	0.645	1	0.13	0.002	0.004	3.3	3.06

Table 3.2.1.5 – Comparison of the different ratios of *n*-butyl methacrylate (BMA) and 4-vinylbenzyl-pyrrolecarbodithioate RAFT agent (CTA1) in each of the polymers synthesised (BMA1-4). Analysis of ^{1}H NMR spectra used for calculated % dithioate.

With the exception of BMA3, that was not suitably soluble in deuterated solvents for NMR analysis, there appears to be an increase in the efficiency of the polymerisation as the percentage of CTA1 decreases. As expected, the observed incorporation carbodithioate of all polymers was lower than the theoretical maximum if 100% conversion had occurred. However, BMA4 does seem to show the closest correlation between calculated and theoretical percentage of dithioate: 3.06 and 3.3% respectively. The decrease in efficiency with CTA1 is most pronounced for BMA1:- to which 12% CTA1 was added but only 2% appears to have been incorporated into the hyperbranched polymer. Using greater amounts of

monomer in the starting mixture, that is to decrease the proportion of CTA1, appears to have led to the easier incorporation of CTA1 into the polymer product.

Using less initiator in the BMA3 and 4 feeds was successful in reducing most of the crosslinking that had been observed. As each mole of ACVA generates two moles of radicals, in theory each CTA1 molecule could still have been activated during the reaction. The percentage monomer conversion for each of the polymer compositions is shown in table 3.2.1.6.

Polymer	Conversion %	Time in 60°C bath
BMA1	74.3±2.5	16 hours
BMA2	100.0 ±11.6	16 hours
BMA3	34.6±4.2	6 hours
BMA4	20.9±3.8	4 hours

Table 3.2.1.6 – Calculated conversion of monomer for each of the hyperbranched butyl methacrylate polymers.

Here it can be seen that monomer conversion reaches a maximum for the BMA2 polymer at almost 100%, but then tapers off strongly for the BMA3 and BMA4 polymers. This is probably at least in part due to the decreased time spent in the water bath at 60'C (4 hours compared to 16), however, longer reaction times led to a highly crosslinked product. It is reasonable to assume the $\overline{kp}$ of the divinyl R group of CTA1 is approximate to styrene, ~162M^{-1}s^{-1}. It is therefore expected that the rate of propagation drops significantly as this styrene derivative is added to a *n*-butyl methacrylate polymerisation which has a $\overline{kp}$ in the region of 573M^{-1}s^{-1} [231]. However, the design of these experiments are rather complex given that the molar percentage of monomer, initiator and CTA1 varies for the different polymers as well as the reaction times. Thus, it is perhaps not too surprising that the trends in the conversion data would be complex and difficult to fully rationalise.

It can be seen through elemental analysis (table 3.2.1.7) that decreasing the amount of ACVA did not prevent copolymerisation with the RAFT agent. The main aim in this work is to develop polymeric coatings for improving epithelial cell adhesion. Since these polymerisations were successful in generating target polymers no further work on the detail of the kinetics of these polymerisations was carried out.

	Predicted Elemental Analysis	Observed Elemental analysis	% CTA1
BMA1	C 66.6%, H 8.9%, N 1.5%, S 6.7%	C 66.8%, H 9.2%, N 1.0%, S 4.0%	2.0%
BMA2	C 67.0%, H 9.1%, N 0.8%, S 3.8%	C 66.9%, H 9.9%, N 0.6%, S 2.1%	1.05%
BMA3	C 67.9%, H 9.3%, N 0.7%, S 3.0%	C 67.3%, H 9.4%, N 0.5%, S 3.5%	1.75%
BMA4	C 68.5%, H 9.6%, N 0.5%, S 2.0%	C 67.0%, H 9.3%, N 0.5%, S 3.3%	1.65%

Table 3.2.1.7 – Summary of theoretical (calculated) and observed elemental analysis for hyperbanched(butyl methacrylate) (BMA1-4). CTA1= carbodithioate chain transfer agent.

The elemental analysis results provide data that is contrary to the end group analysis that was performed using the ^{1}H NMR spectra. It is considered that elemental analysis is much more sensitive for the quantitative analysis of these polymers and is thus more reliable. Here, the polymer BMA2 can be seen to contain the lowest amount of carbodithioate (1.05%) whilst NMR spectroscopic analysis suggested that it actually contained the highest amount of chain transfer agent (4%). This indicates that care must be taken when using techniques such as NMR spectroscopy to quantitatively analyse samples such as this, although NMR can still be successfully employed as an indicator of successful copolymerisation. The polymer BMA1 can be seen to contain the highest amount of CTA1 (2.0%), and this is in line with expectations given the molar ratio of monomers used in this polymer (0.1 CTA1:BMA). Polymers BMA3 and BMA4 show approximately the same observed CTA1 content by elemental analysis (1.75 and 1.65 %, respectively). Interestingly, these polymers appear to show better incorporation of the chain transfer agent than the 10:1 ratio polymer. This again suggests that for optimal efficiency, it may be preferred to use a lower ratio of chain transfer agent to monomer. However, when taken in hand with the other results so far presented, especially the percentage conversion of monomer, it seems that BMA2 is the optimal feed ratio in terms of producing polymer with the highest functionality.
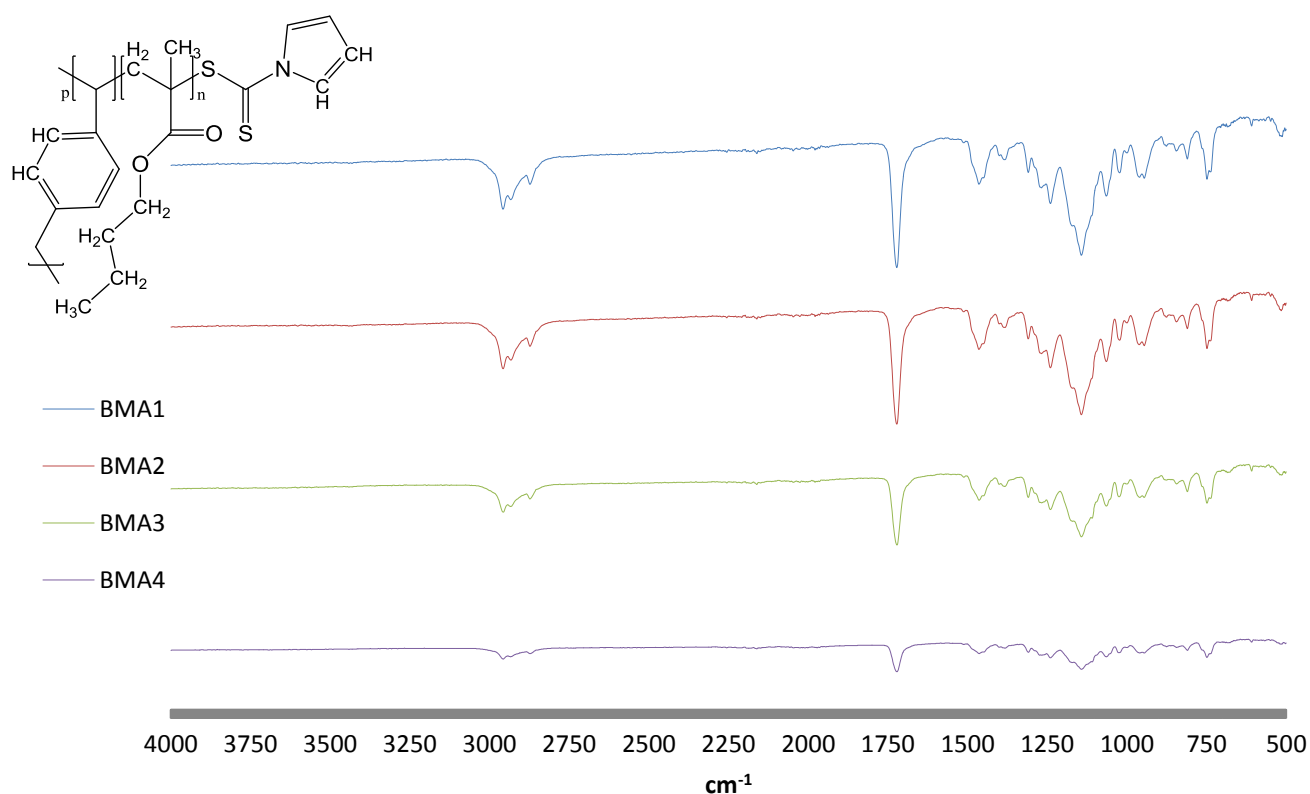
Figure 3.2.1.8 – Combined FT-IR spectra of hyperbranched polymers BMA1-4.

Figure 3.2.1.8 provides the FT-IR comparison of the hyperbranched polymers. The strong stretches at 1710 and 1490cm^{-1} can be attributed to the C=O and C-O of the ester linkage in butyl methacrylate. The sharp stretch at 1160 is due to the C=S thiocarbonyl bond. The stretches seen between 2920 and 3030 are due to sp^3 C-H bonds. The weak aromatic stretch expected around 1600cm^{-1} can't be observed because it is coincident with the C=O signal, but aromatic overtones can be seen between 1800 and 2200cm^{-1} in addition to the aromatic C=C signal at 1450cm^{-1} that confirm the successful inclusion of the RAFT agent.

	$\overline{Mn}$	$\overline{Mw}$	$\overline{Mz}$	PDI	α
BMA1	14300	39700	90100	2.8	
BMA1 TD	17600	43750	160850	2.5	0.5
BMA2	21250	62900	164700	3.0	
BMA2 TD	66050	210600	4840000	3.2	0.4
BMA3	21300	57800	140800	2.8	
BMA3 TD	68400	220550	2402000	3.2	0.5

Table 3.2.1.9 – Molar mass averages (gmol^{-1}) for HB(nBMA) polymers as determined by GPC using tetrahydrofuran as the mobile phase. TD= triple detection GPC results, also performed with tetrahydrofuran mobile phase.

Table 3.2.1.9 shows that BMA2 and BMA3 polymers have comparable $\overline{Mn}$s, but BMA1 has almost half the molar mass. The molar mass distribution in figure 3.2.1.10 also shows that the BMA1 distribution is marginally broader with a slight shoulder, suggesting the presence of lower molar mass fractions.
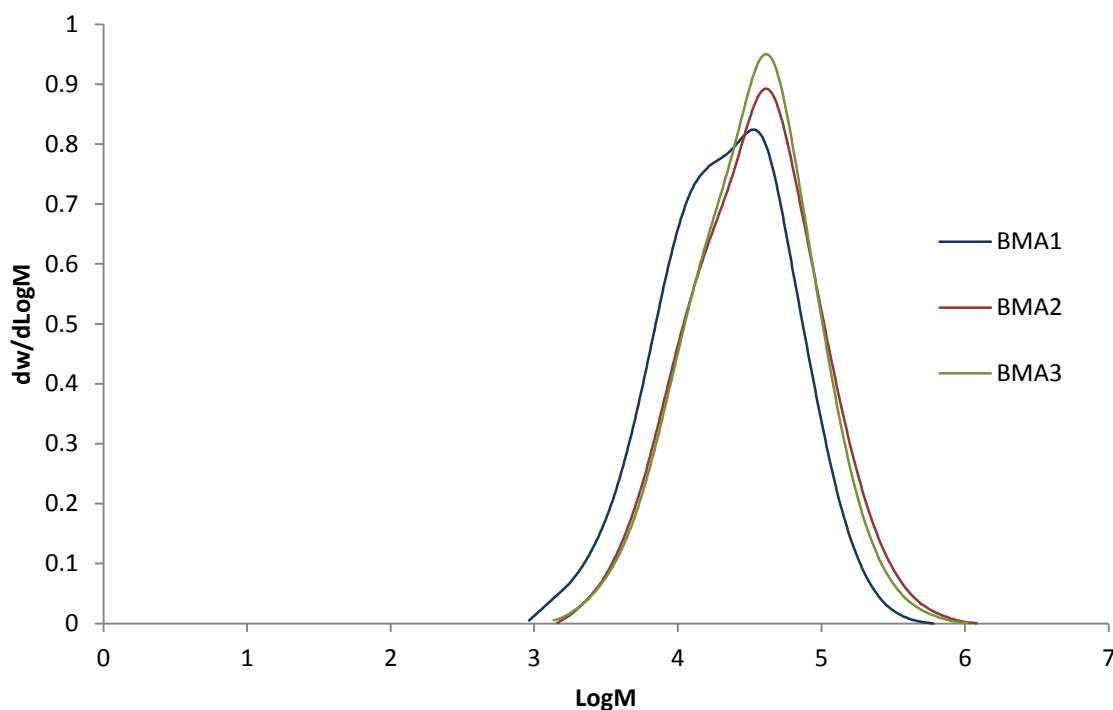
Figure 3.2.1.10 – Molar mass distribution of hyperbranched polymers BMA1-3. BMA4 was not sufficiently soluble for GPC analysis.

The Mark Houwink equation describes the dependence of a polymer's intrinsic viscosity on its molar mass and is shown in equation 3.2.1.11.

$$[\eta] = KM_r^{\alpha}$$

Equation 3.2.1.11 – Mark-Houwink equation, where [ŋ] is intrinsic viscosity, K and α are polymer-dependent constants (α being the Mark-Houwink exponent) and Mr is the viscosity molar mass average.

The value for α can vary between 0 for solid spheres and 2 for rod shaped structures, and an α of 0.4 to 0.5 indicates a random coil structure[232]. By using triple detection GPC, which incorporates the measuring of viscosity, it was possible to calculate α for the HB poly(butyl methacrylate)s (table 3.2.1.9). Table 3.2.1.9 shows $\overline{Mn}$ correlates relatively well between the two GPC techniques, in that the trend in molar mass averages is the same. As expected, the absolute values of molar mass differ between the two GPC techniques with almost three-fold higher $\overline{Mn}$ reported for polymers BMA2 and 3 using the triple detector set up. This effect is a clear indication of the branched nature of the polymers, as increased branching decreases the hydrodynamic volume of the coil at a constant molar mass, and it is this parameter that controls the retention time in a GPC experiment. Calculations suggested that ~74% monomer was converted in polymerisation BMA1 (table 3.2.1.6), but the low molar mass results suggest much of this was converted into more numerous polymers with lower chain length. This is to be compared with polymers BMA2 and 3 which exhibited monomer conversions of 100 and 35%, respectively, and much higher molar masses. It is clear, as expected, that as the amount of CTA1 and initiator increased in the reaction the rate of chain growth decreased providing lower molar mass averages and lower monomer conversion. In order to maintain relative ratios of CTA1 to initiator, as the CTA1 was increased the initiator concentration was also increased: the latter increases the rate of conversion, whilst increasing the former decreases conversion.

The α values quoted above indicate that the synthesised polymers all have a tight random coil structure. Our observed values for α correspond well with the α values previously reported for hyperbranched polystyrene[233], polyesteramide[234] and polymethyl methacrylate[235]. However, the values of α are higher than the previously reported values when a similar CTA was copolymerised with *N-iso*propyl acrylamide. This suggests that the branching self-condensation process is less effective with this class of chain transfer agent when polymerising methacrylates, such as BMA. Despite this, the α values still suggest branched structures. It is also important to note that the system with the highest conversion (BMA2) had the lowest α, which is an indication of increased branching.

3.2.2. Characterisation of hyperbranched polymers with acid end groups

The hyperbranched polymers were reacted with ACVA in order to replace the pyrrole carbodithioate end groups with acid functionality. After extensive purification, the polymers were subjected to characterisation by ^{1}H NMR and FT-IR spectroscopies. Gel permeation chromatography was not available to these functionalised polymers as they were not suitably soluble in the required solvents, but it is reasonable to assume without the evidence of chain disintegration that the molar mass of each polymer is comparable to its unfunctionalised precursor.
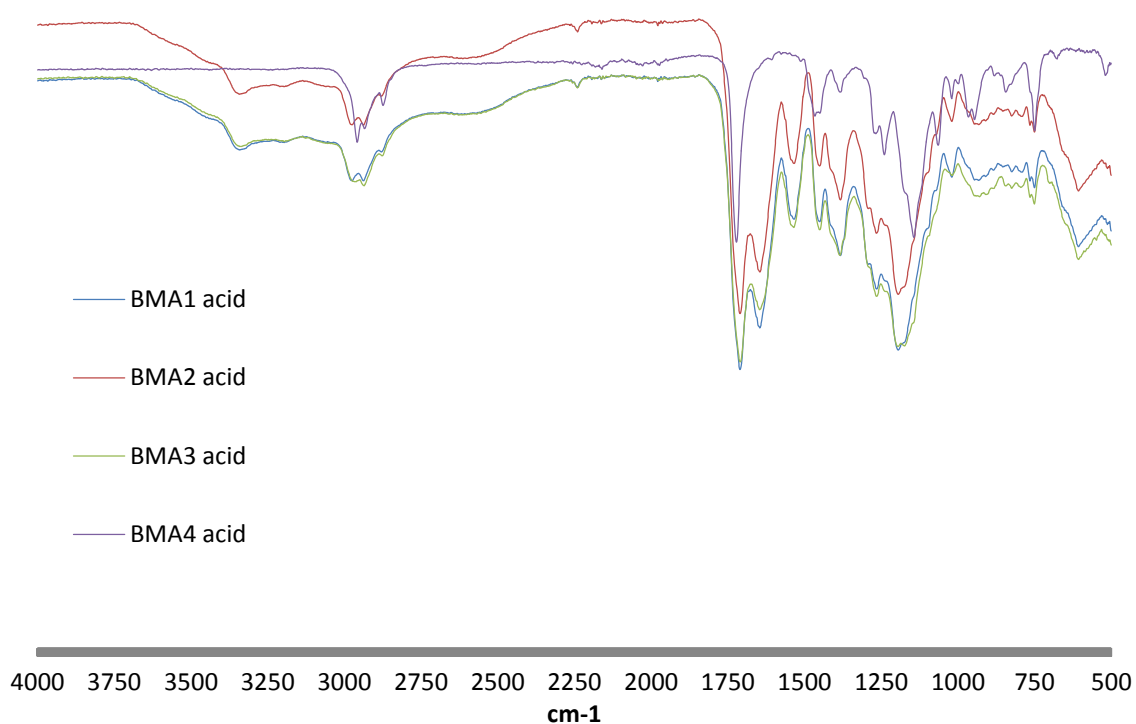
Figure 3.2.2.1 FT-IR of hyperbranched polymers after reaction with excess ACVA to form acid functional end groups.

The FT-IR spectra in figure 3.2.2.1 shows that there is a much greater response from the acid functional polymers in the region 1100-1700cm^{-1}. The strong absorbance band at 1650cm-1 can be attributed to the C=O of ACVA, which has shifted due to the presence of a nitrile group which is observable at 2200cm^{-1}. The conservation of the C=O peak at 1700cm^{-1}

indicates that the butyl methacrylate polymer backbone remains intact. This is a good indicator of the successful reaction with ACVA, replacing the carbodithioate groups with acid functionality. Further evidence for this can be seen in the absorbance band at 2220cm^{-1} which arises from the C≡N in the ACVA molecule, the broad stretch at 3200-3400cm^{-1} due to hydrogen bonding between O-H groups and at 1390cm^{-1} from the C-O-H bend, as well as the new N-H stretch at 1520cm^{-1}. It is worth noting that BMA4 does not appear to be successfully functionalised by this reaction, with none of these signals present. This could be due to inaccessibility of the carbodithioate groups, or crosslinking, as further reactions with ACVA were fruitless. If polymer BMA4 has been crosslinked, this would also explain its insolubility in analytical solvents such as THF and CDCl$_3$.
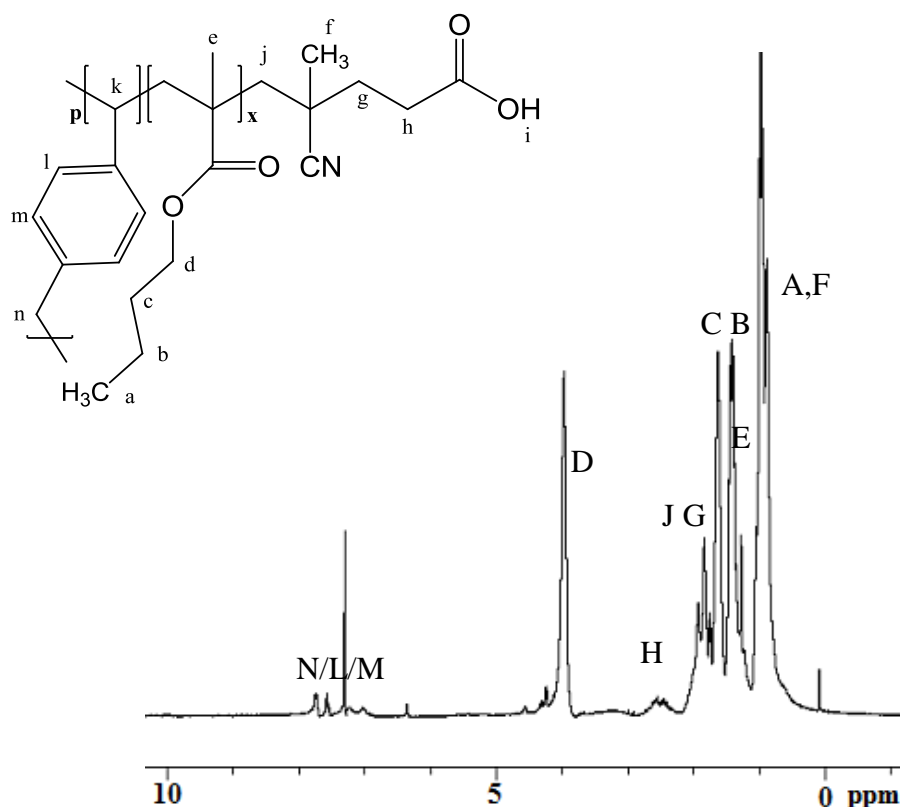
Figure 3.2.2.2 – Representative ^{1}H NMR of hyperbranched butyl methacrylate polymer after treatment with excess ACVA.

Figure 3.2.2.2 shows a representative ^{1}H NMR spectra of polymers BMA1-3 after the reaction with excess ACVA. Polymer BMA4 was too insoluble for NMR analysis, again indicating that it had crosslinked during the course of the reaction. The success of this reaction is noted by a new peak at 8ppm that is due to OH of the carboxylic acid. Two further

peaks are evident at 2.8 and 3ppm, which can be assigned to the CH$_2$ of ACVA and indicates the successful introduction of ACVA onto the polymer chain ends. The signals seen between 1-3ppm are a result of the alkyl protons present within the P(BMA).

3.2.3 Linear polymer characterisation

Linear polymers, analogous to the HB polymers, were supplied by Masters student Sarah Canning. These were copolymers of butyl methacrylate and 4-vinyl benzoic acid in various ratios (LIN1, 2 and 3 being 4:1, 8:1, and 12:1 molar ratios, respectively) in order to mimic the hyperbranched functionality after reaction with ACVA. These polymers were fully characterised and reacted with an excess of diamines, before being used as substrates in direct culture with epithelial and fibroblast cells.

The reaction with 1,6-diaminohexane produced much more effervescence than the reaction with other diamines, and the amount of recovered polymer was not sufficient to perform cell culture and all analysis techniques. Due to limited amounts of the supplied acid-functional polymers, instead of repeating the reaction greater amounts of the other amidated polymers were produced so that cell culture and analysis could be comfortably performed.

In figure 3.2.3.1 the sharp signal at 1740cm^{-1} exhibited by the acid polymer is the C=O stretch. This stretch is notable by its shift to 1677cm^{-1} in the amidated polymers, as is usual for an amide bond. This shows that the reactions with excess amine and EDC were successful in adding diamines to a copolymer of butyl methacrylate and 4-vinyl benzoic acid.
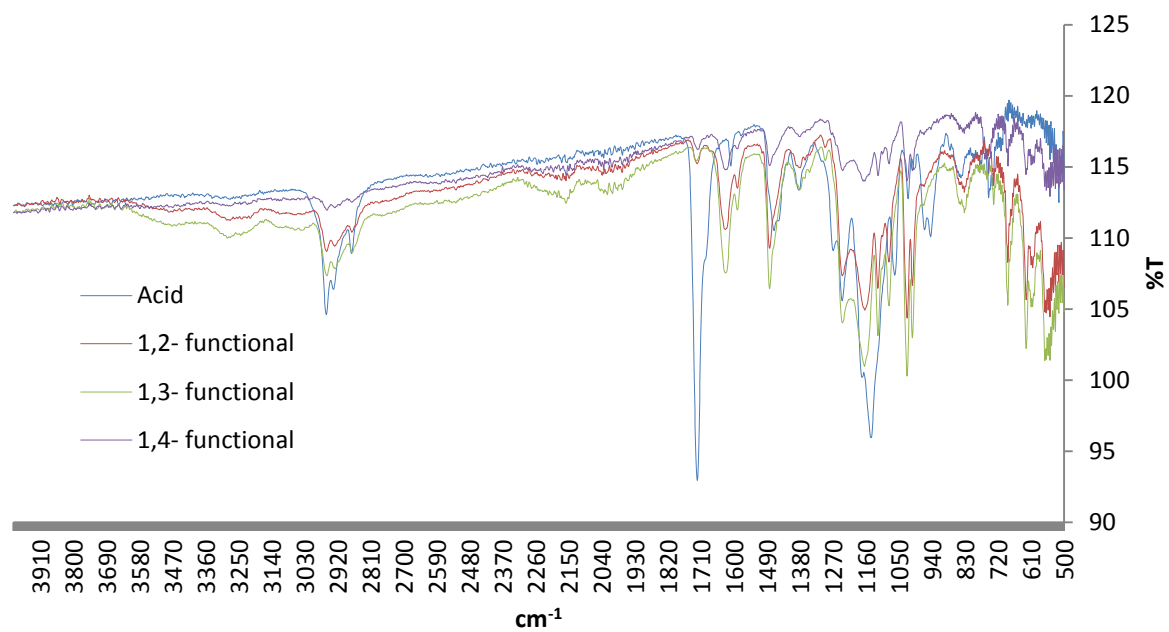
Figure 3.2.3.1 –Combined FT-IR of Poly(BMA-co-4-vinylbenzoic acid) and amidated derivatives which has been subsequently reacted with an excess of various diamines as previously described.
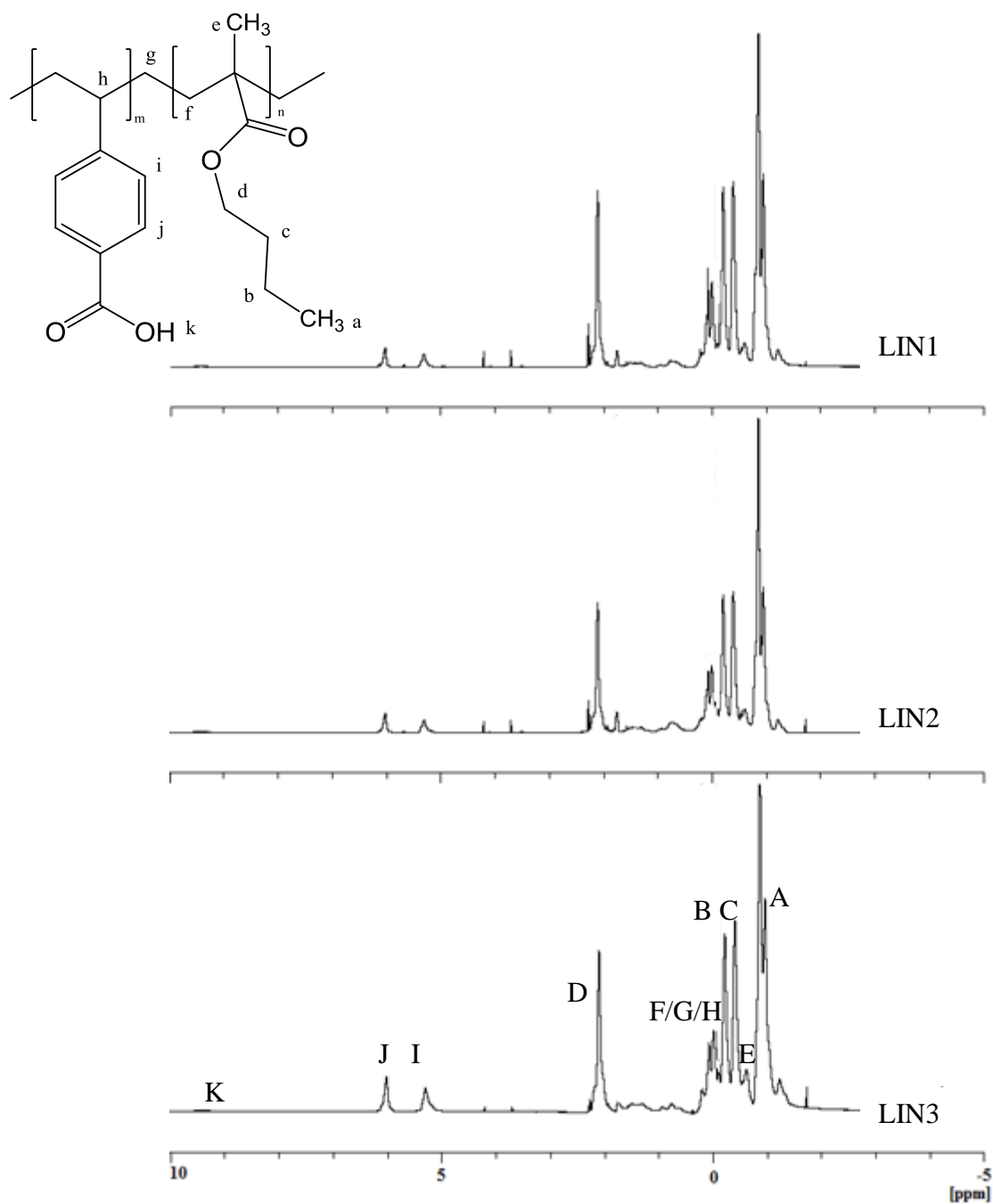
Figure 3.2.3.2 – ^{1}H NMR of linear butyl methacrylate-co-4-vinyl benzoic acid polymers. (LIN1-3)

As previously described the linear polymers were analysed by triple detection GPC and the Mark-Houwink principle was applied (table 3.2.3.3). This enabled us to make a good approximation of the size of the polymers supplied.

	$\overline{Mn}$	$\overline{Mw}$	$\overline{Mz}$	PDI	α
LIN1	81350	113000	192900	1.4	0.5
LIN2	97700	143500	278000	1.5	0.6
LIN3	126700	176250	291300	1.4	0.7

Table 3.2.3.3 – Triple detection GPC molar masses and Mark-Houwink exponent for linear butyl methacrylate-co-4-vinylbenzoic acid polymers (LIN1-3).

The Mark-Houwink exponent for these polymers increases in value as the amount of *n*-butyl methacrylate increases relative to 4-vinyl benzoic acid (4-VBA). α is a measure of the openness of the coils across the molar mass range and thus increases in α reflect an increase in solvency and coil expansion. This also means that as the amount of 4-VBA in the polymer decreases, the solvency increased in THF. These data agree with one aspect of the observations with the highly branched polymers, which is that the solvency decreases as the amount of carboxylic acid increases. The HBPs became insoluble in THF when the dithioate end groups were converted to carboxylic acid. The variation in solubility and method of casting the polymer films means that a uniform film of equal thickness may not always be achieved. However, as this work is a proof of concept regarding cell adhesion to polymers with different architecture and end group functionality, the film formation was considered to be sufficient.

3.2.4 Cell contact studies

Two types of primary cells, normal human dermal fibroblasts and human renal epithelial cells, were cultured on polymer films cast on glass coverslips for 72 hours to observe cell adherence and proliferation. Cells were imaged after 24 hours using phase contrast optical microscopy in order to observe initial cell adherence before any potential cell death due to polymer toxicity.

Human Dermal Fibroblasts
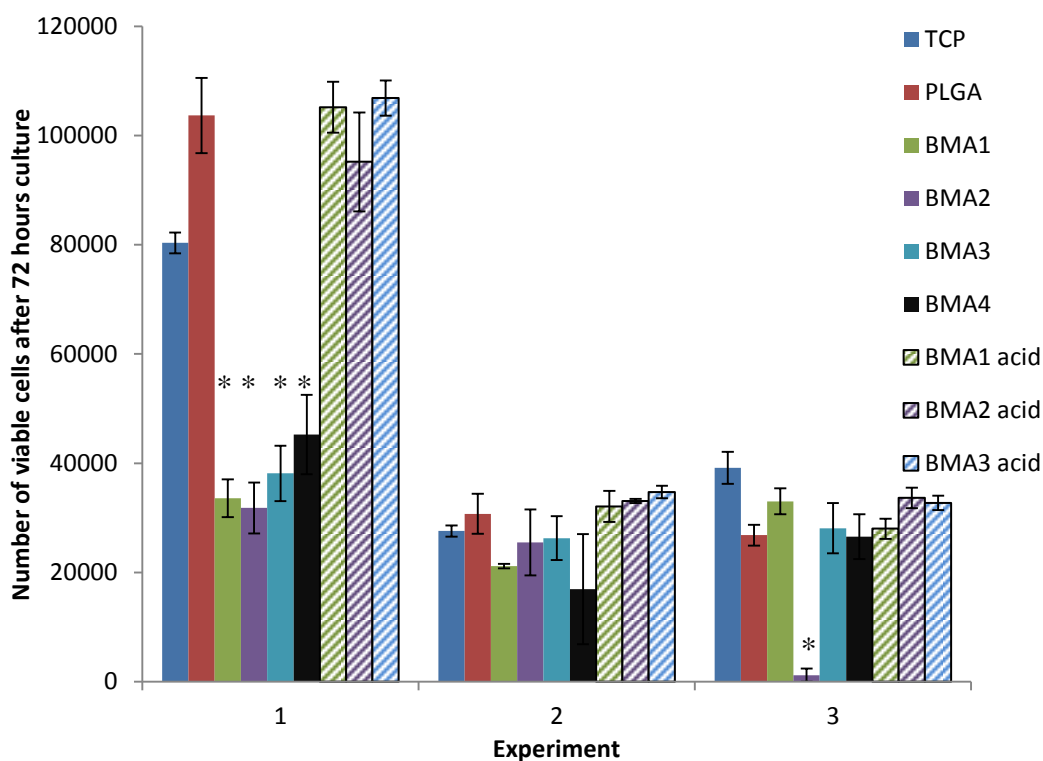
Figure 3.2.4.1 - Human dermal fibroblast cell viability after 72 hour culture in direct contact with hyperbranched(BMA)s over 72 hours. One-way analysis of variance and post-hoc Tukey's statistical analysis performed, significant values relative to TCP marked with *.

Figure 3.2.4.1 shows that in experiment 1 there was a pronounced preference for the acid functional polymers (BMA1-3 acid) and the results are slightly better than tissue culture plastic (TCP). This is again repeated in experiment 2, except the cells were also maintained on the dithioate functional polymers (BMA1-4). In experiment 3, TCP was a slightly better substrate (cells showing improved viability) and the dithioate from BMA4 was a particularly

poor substrate. It is unclear from these experiments if any of the acid functional polymers are more preferred for cell adhesion and proliferation, although they do perform better than the native carbodithioate functional HBPs (BMA1-4). The carbodithioate polymers also appear to perform similarly as cell culture substrates, partly due to the variances in cell viability between samples.

The fibroblast cells were stained and imaged using an inverted microscope. Figure 3.2.4.2 demonstrates that all carbodithioate polymers showed fibroblast adhesion after 72 hours culture, with growth patterns extremely similar to the TCP control. Initial cell adhesion is observed on the polymers BMA1-4 after 24 hours culture, and the polymers BMA2 and 4 appear to have an initial fibroblast confluence that exceeds the control substrate.

Figure 3.2.4.3 shows the cell adhesion after 24 and 72 hours on the acid functional HBPs (BMA1-3 acid). Cell adhesion is visible after 24 hours and the acid functional polymers all show cell adherence and proliferation similar to TCP; there does not appear to be any variation between the polymers and the cells have normal patterns of growth.

Examination images taken at increased magnification (figure 3.2.4.4) reveals that the cells grown in contact with carbodithioate functional polymers exhibit the same morphology and nucleus as those cells cultured on TCP. The tendency for the acid functional polymers to also become stained meant that clear, high magnification images were difficult to obtain on these substrates. The cells that were imaged on the acid functional PBMAs looked healthy and comparable to those cultured on control materials. During culture there was little evidence of cell die-off on the polymers when observed by optical microscopy, and these images confirm the viability assay that fibroblasts can be successfully cultured on PBMA substrates.
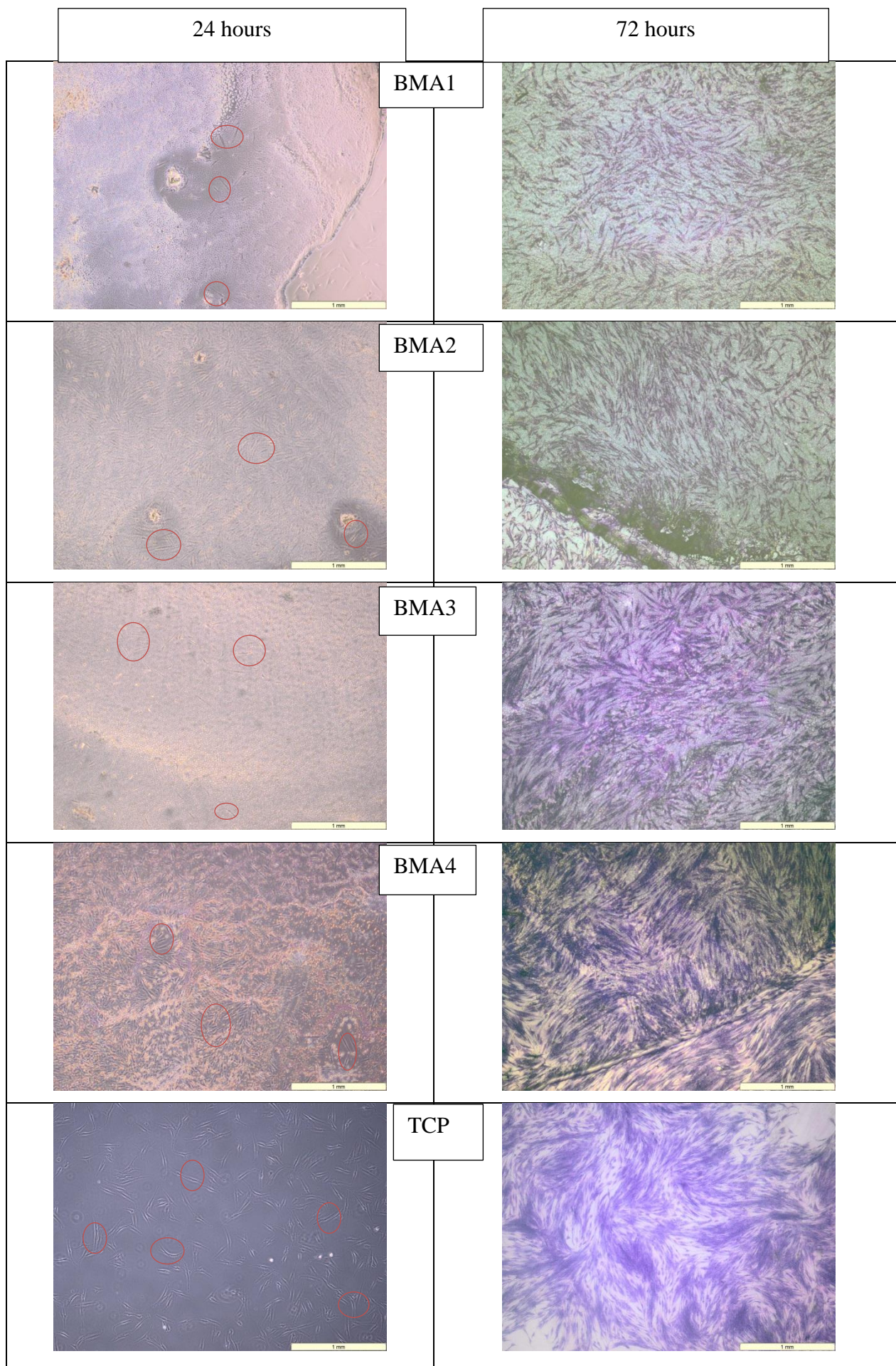
Figure 3.2.4.2- Images comparing fibroblast adhesion on HP(*n*-butyl methacrylate) polymers (BMA1-4) and TCP after 24 and 72 hours at 4x magnification. 24 hours= phase contrast, red circles indicate adhered cells. 72 hours = cells fixed and stained with Giemsa solution.

24 hours	72 hours

BMA1 A

BMA2 A

BMA3 A

TCP

Figure 3.2.4.3 - Images comparing fibroblast adhesion on HP(*n*-butyl methacrylate) polymers with carboxylic acid end groups (BMA1-3 A) and TCP after 24 and 72 hours at 4x magnification. 24 hours= phase contrast, red circles indicate adhered cells. 72 hours = cells fixed and stained with Giemsa solution.
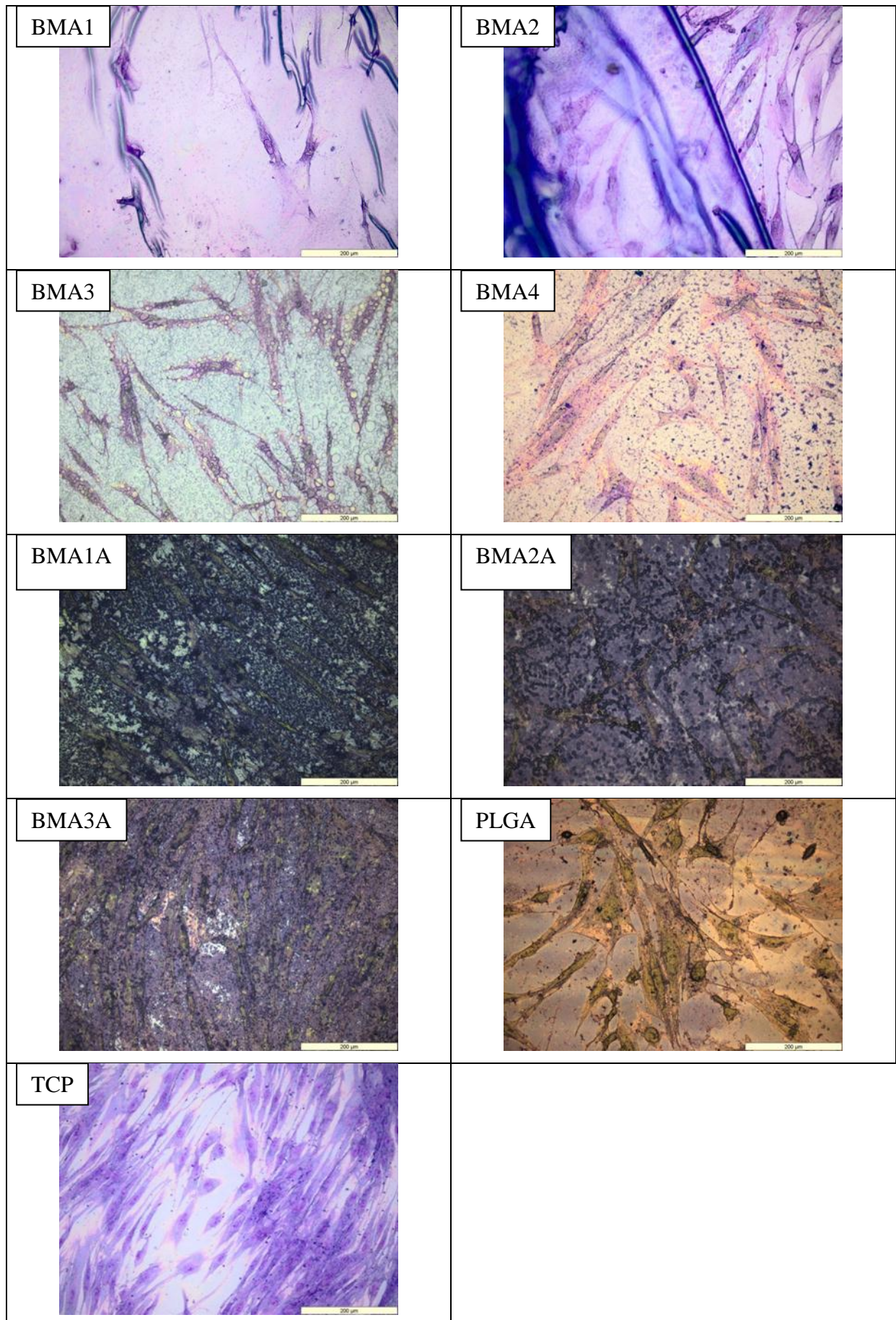
Figure 3.2.3.4 - Images of fibroblast cells on hyperbranched BMA polymers (labelled) after 72 hours culture in direct contact at 20x magnification. Cells fixed and stained with giemsa.

Figure 3.2.4.5 shows fibroblast viability on linear butyl methacrylate polymers; acid functional (due to* the acidic comonomer) or amidated with excess C_{2-4} alkyl diamine. These results show much more starkly the preferential fibroblast growth on acid copolymers compared to those with amine functionality (see the LIN1 polymer series in figure 3.2.4.5 for example). In all three experiments, the amidated polymers had significantly less viable cell growth than TCP and acid polymers after 72 hours. In experiment 3 the LIN2 and 3 polymers (acid functional) also have significantly decreased cell viability. These polymers exhibit satisfactory fibroblast viability in experiments 1 and 2.
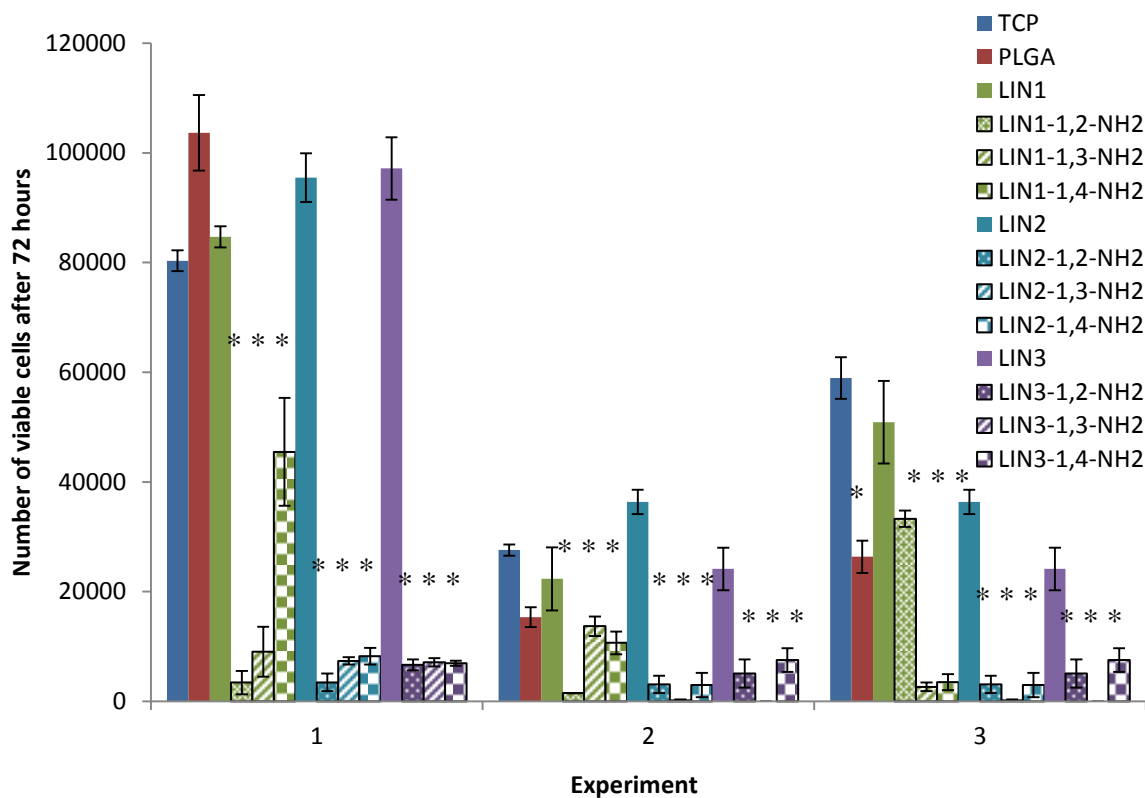
Figure 3.2.4.5 – Human dermal fibroblast cell viability after 72 hours culture in direct contact with linear(BMA) with acid and amine functionality. One-way analysis of variance and post-hoc Tukey's statistical analysis performed. Significant values relative to TCP control marked with *

The fibroblasts observed using optical microscopy were healthy and confluent with visible nuclei on the acid substrates, whilst debris was seen on the amidated polymers. Figure 3.2.4.6-8 show fibroblast visualisation on all of the linear polymers after 24 and 72 hours. In figure 3.2.4.6 the images from the LIN1 polymers are shown, although the acid and 1,4-NH_2 functional polymers could not be satisfactorily imaged using phase contrast after 24 hours.

Some initial fibroblast adhesion is observed on the 1,2-NH_2 functionalised, but none can be seen on the 1,3- functionalised substrate. After 72hours, no fibroblast growth is observed on any of the amidated polymers. The acid functional polymer exhibits the best proliferation of cells after 72hours with a healthy confluence of cells visible.

Figure 3.2.4.7 demonstrates the same 24 and 72 hour images taken on the LIN2 polymer series. Good initial fibroblast adhesion is seen on the acid functional polymer, but there does not appear to be any cells on the amidated materials. After 72 hours a confluence approaching 90% can be seen on the acid polymer (LIN2) whilst the amidated polymers appear to support only the sporadic and spindly growth of fibroblast cells.

The adherence of fibroblasts to the LIN3 polymer series can be seen in figure 3.2.4.8. Once again there is initial cell adherence visible on LIN3 (acid) but none on the amidated polymers. This continues after 72 hours, where a confluence of ~75% is observed on LIN3 but only a few cells are seen on the amidated polymers. These images confirm the viability assay results that polymers with acidic functionality are much preferred for fibroblast culture substrates when to compared the polymer treated with diamine(s).

	24 hours	72 hours
LIN1		
LIN1-1,2-NH$_2$		
LIN1-1,3-NH$_2$		
LIN1-1,4-NH$_2$		
PLGA		
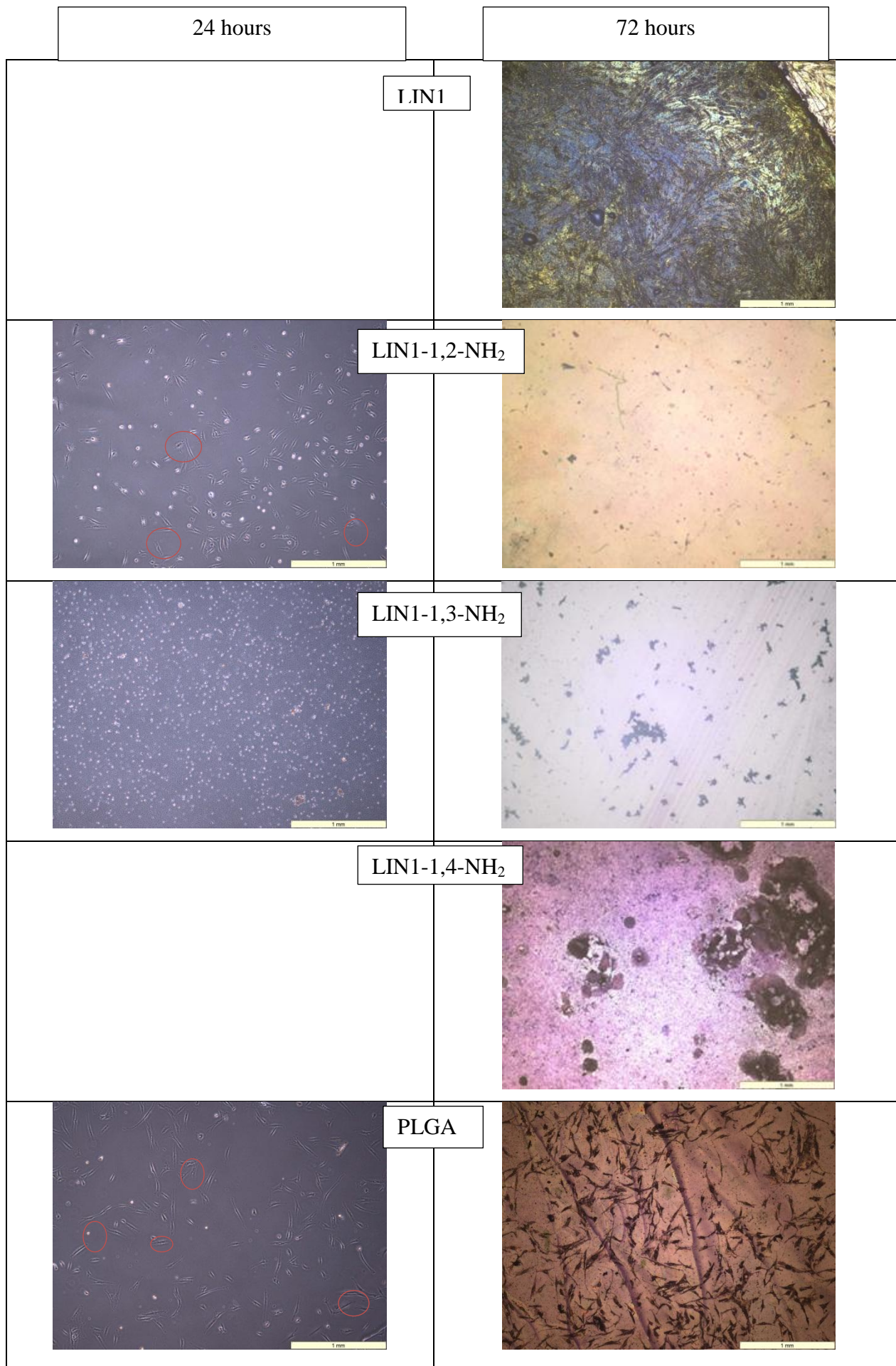
Figure 3.2.4.6 - Images comparing fibroblast adhesion on functionalised linear (*n*-butyl methacrylate) polymer (LIN1) and PLGA after 24 and 72 hours at 4x magnification. 24 hours= phase contrast, red circles indicate adhered cells. 72 hours = cells fixed and stained with Giemsa solution.
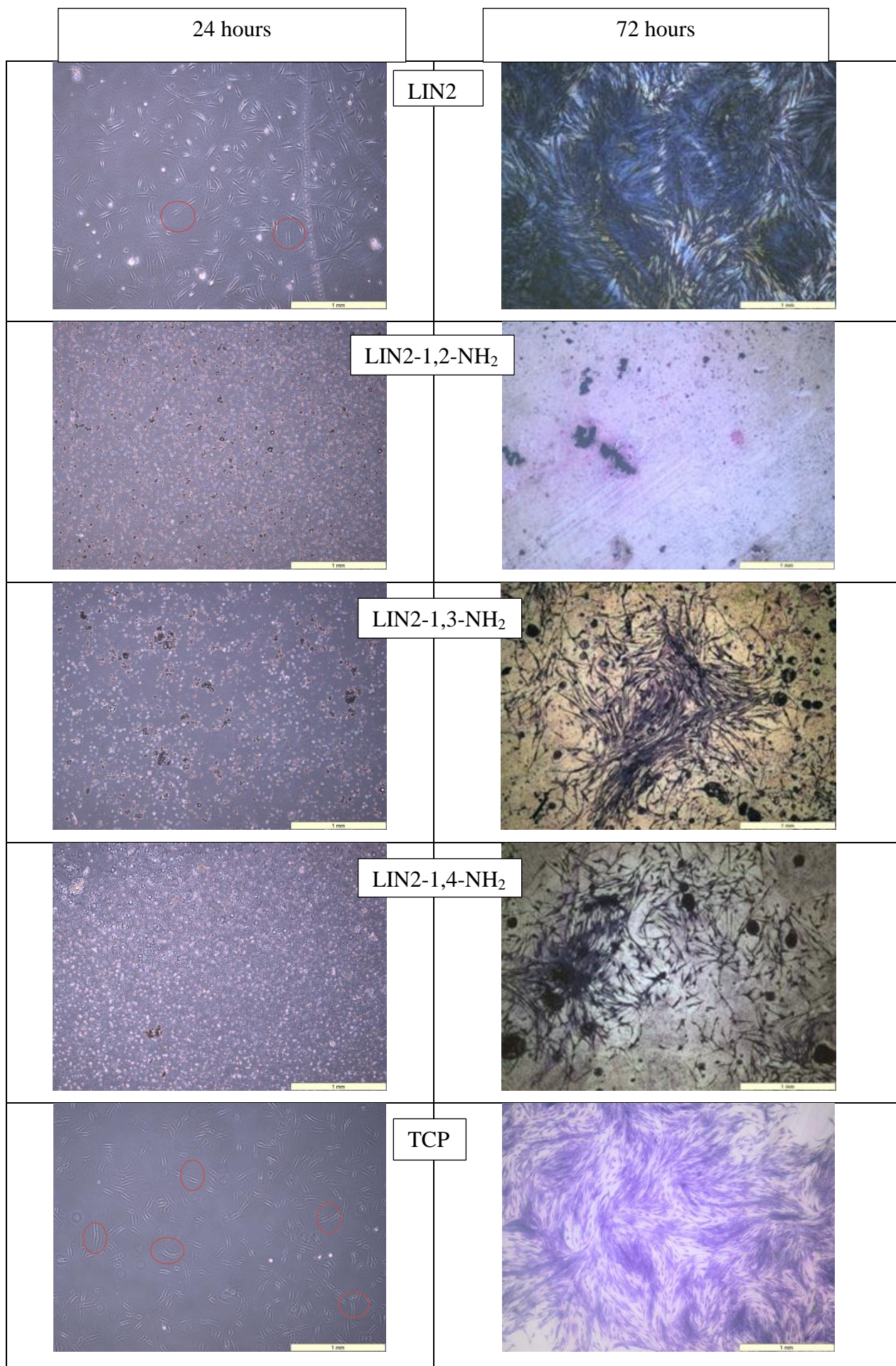
Figure 3.2.4.7- Images comparing fibroblast adhesion on functionalised linear (*n*-butyl methacrylate) polymer (LIN2) and TCP after 24 and 72 hours at 4x magnification. 24 hours= phase contrast, red circles indicate adhered cells. 72 hours = cells fixed and stained with Giemsa solution.

24 hours	72 hours

LIN3

LIN3-1,2-NH$_2$

LIN3-1,3-NH$_2$

LIN3-1,4-NH$_2$

TCP
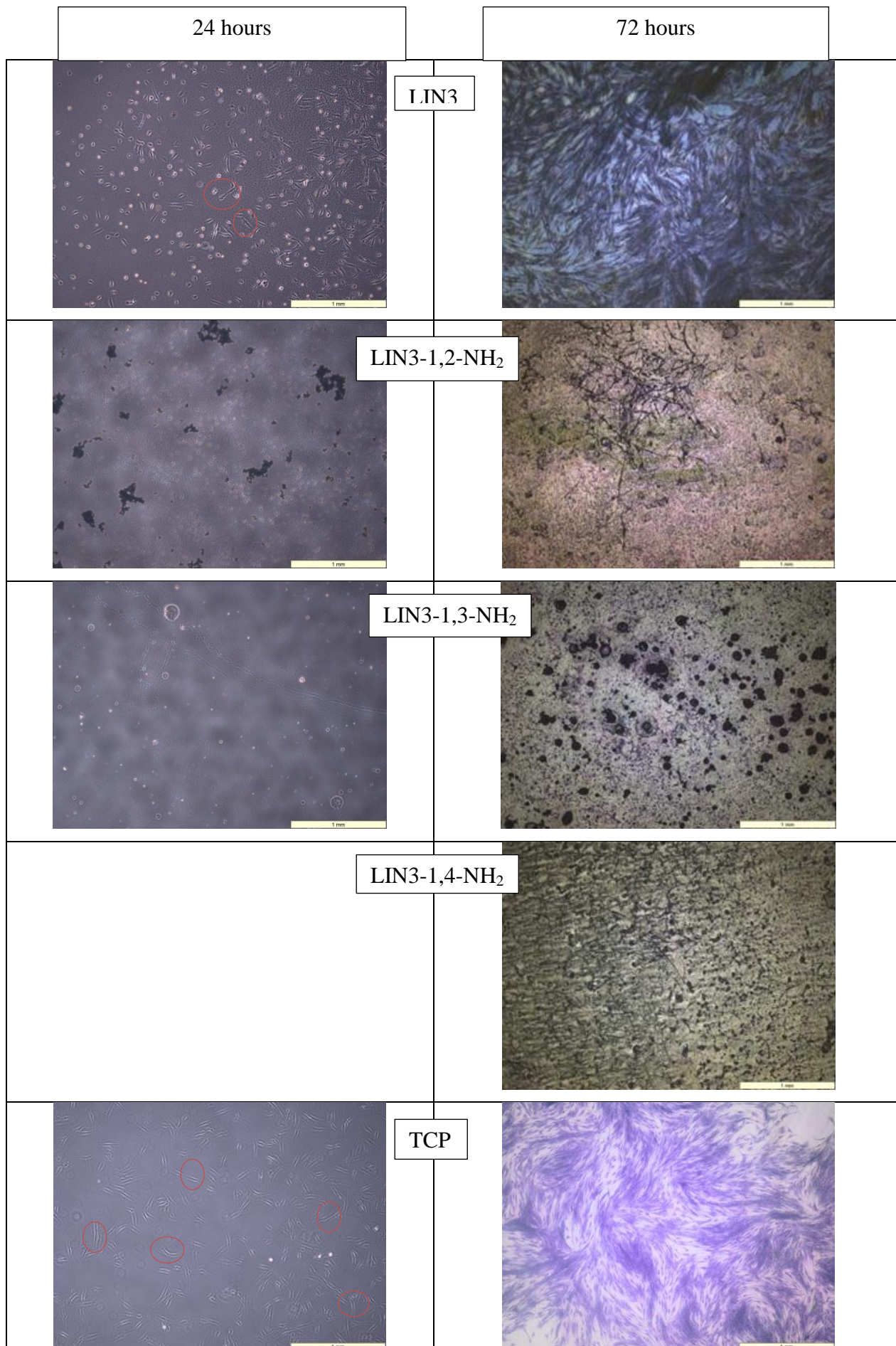
Figure 3.2.4.8 - Images comparing fibroblast adhesion on functionalised linear (*n*-butyl methacrylate) polymer (LIN3) and PLGA after 24 and 72 hours at 4x magnification. 24 hours= phase contrast, red circles indicate adhered cells. 72 hours = cells fixed and stained with Giemsa solution.
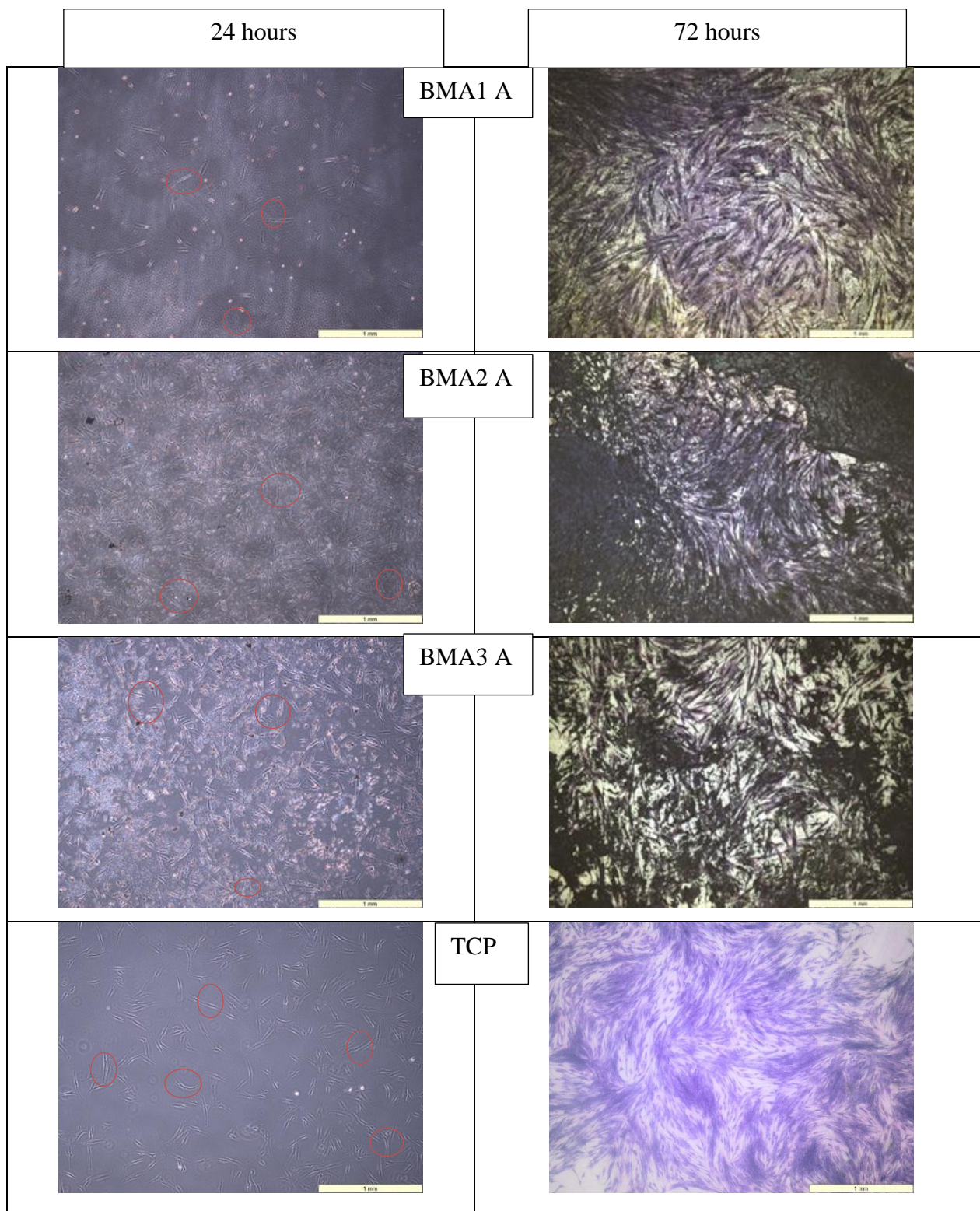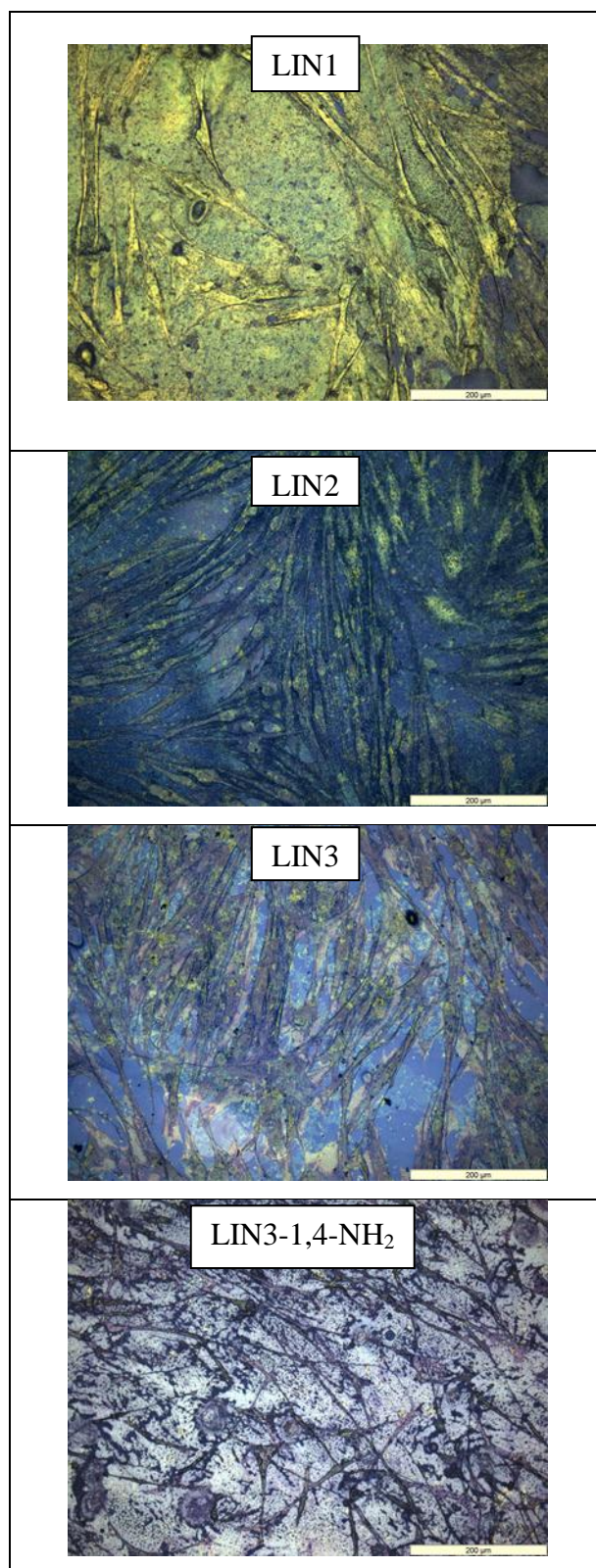
Figure 3.2.4.9 - 20x magnification images of fibroblasts after 72 hours culture on linear polymers (labelled). Those polymers not represented above had no identifiable cells.

Higher magnification images are shown in figure 3.2.4.9. Only debris could be observed for almost all of the amidated polymers. This was partly due to staining of the polymers, but also

due to the death and poor health of the fibroblasts. This is demonstrated for the polymer LIN3 1,4-NH$_2$ which has small and spindly cell growth. However, the acid polymers (LIN1,2,3) can be seen to support healthy fibroblast growth of normal size and with visible nuclei.

Human Renal Epithelial Cells

Figure 3.2.4.10 and subsequent post-hoc analysis indicates that it is hard to determine the optimal polymer chemistry for epithelial adhesion. The data as shown indicates that the acid functional polymers perform poorly in the first two experiments, but large variances are observed throughout. Such inconsistencies are not ideal for cell culture substrates and no particular hyperbranched polymer appears to perform consistently well.

In experiment 1, polymer BMA1 exhibits exceptionally good viability whilst polymers BMA1-3 acid have much lower average cells than TCP. BMA4 also has a greater number of viable cells compared to TCP, whilst BMA2 and 3 do not exceed the standards.
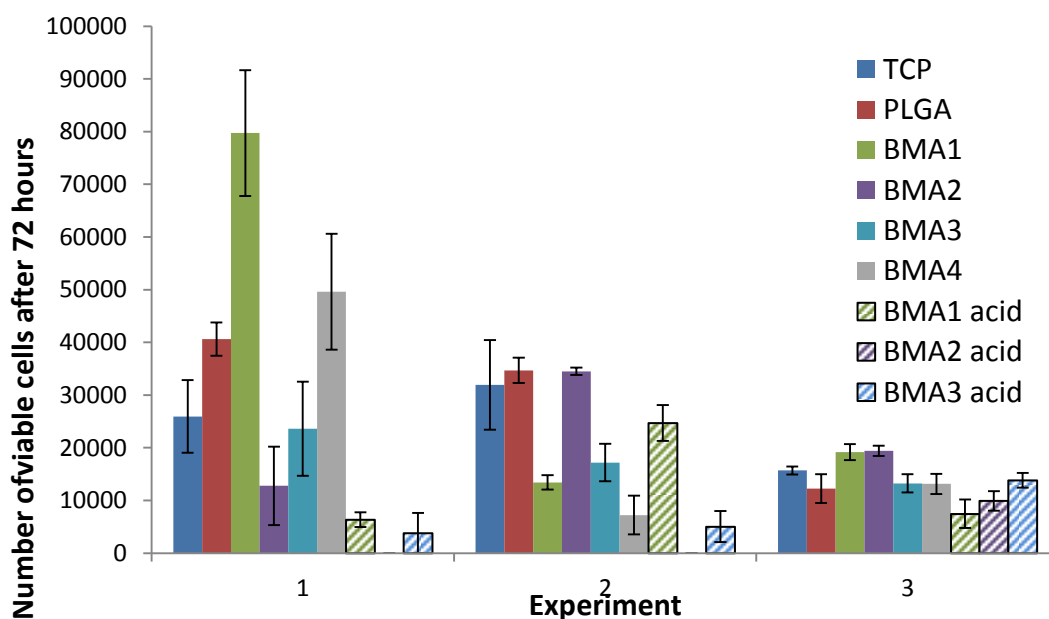
Figure 3.2.4.10 – Epithelial cell viability after 72 hours culture in direct contact with HP(BMA) polymers with dithioate (BMA1-4) and acid functionality (BMA1-3 acid). One-way analysis of variance and post-hoc Tukey's statistical analysis performed.

In experiment 2, BMA2 is the only polymer to perform comparatively to the TCP and PLGA. Experiment 3 offers some complication as BMA3 acid performs almost equally to TCP, and BMA 1 and 2 both perform slightly better. Once again, the proliferation on the acid functional polymers is less than that on the standard materials. Figure 3.2.4.11 compares cell

images taken after 24 and 72 hours culture on the different polymer substrates. The TCP images indicate that there is a good initial adhesion of cells after 24 hours, which continue to proliferate for the remaining time of the experiment. This is a pattern mimicked by the BMA1 polymer, but to a lesser extent. BMA2 does not appear to show many cells adhered after 24hours, but after 72 hours this substrate has a confluence of about 50% - a number which is comparable with the TCP. BMA3 appears to show relatively numerous adhered cells after 24 hours but only a few cells are visible after 72 hours, suggesting that the cells are becoming unadhered or are suffering a toxic effect from this polymer. The polymer itself interfered with the imaging of the cells adhered to BMA4, however after 72 hours there appears to be some adhered cells, but fewer than can be seen on the TCP.

The optical microscopy images of epithelial adhesion on the acid functional HBPs is shown in figure 3.2.4.12. There is very poor initial adhesion visible on all three of the acid substrates after 24 hours. BMA2 acid shows the greatest number of adhered cells after 24 hours but it still performs poorly when compared to TCP. After 72 hours, the TCP can be seen to have approximately 70% confluence whilst only a few sparse cells are observed on the acid functional polymers.
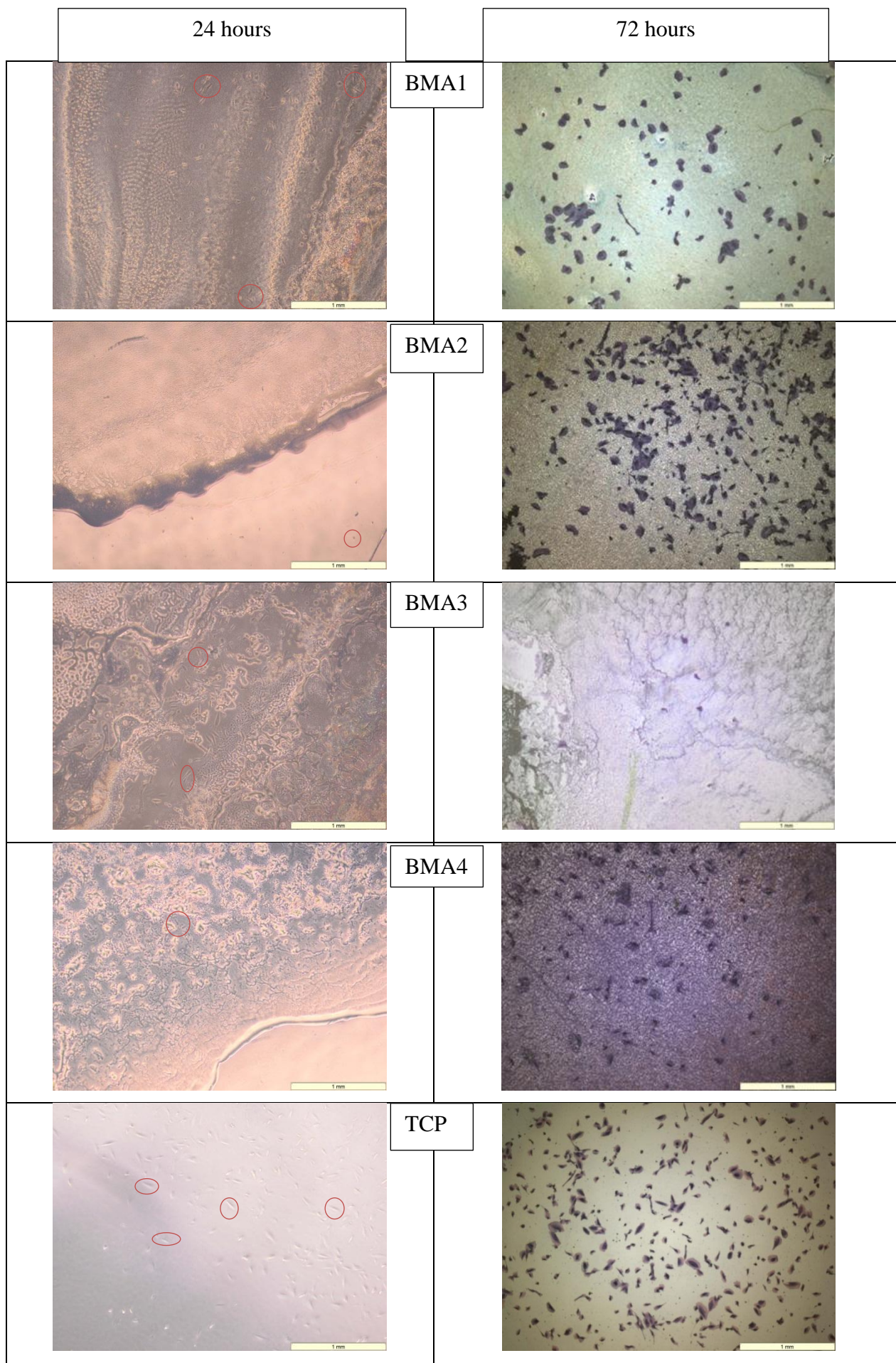
24 hours	72 hours

Figure 3.2.4.11- Images comparing renal epithelial cell adhesion on HP(*n*-butyl methacrylate) polymers (HP1-4) and TCP after 24 and 72 hours at 4x magnification. 24 hours= phase contrast, red circles indicate adhered cells. 72 hours = cells fixed and stained with Giemsa solution.
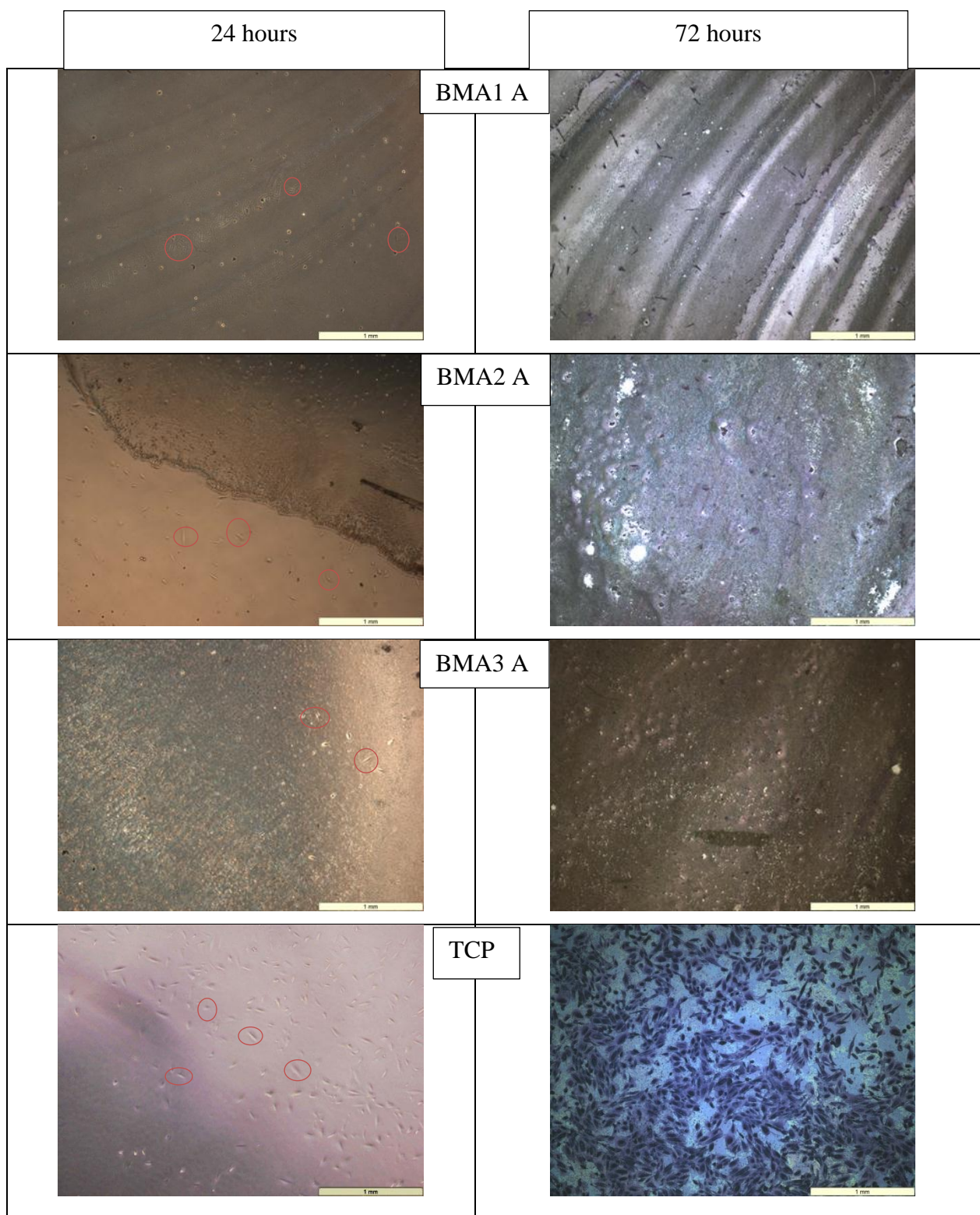
Figure 3.2.4.12 - Images comparing epithelial adhesion on HP(*n*-butyl methacrylate) polymers with carboxylic acid end groups (BMA1-3 A) and TCP after 24 and 72 hours at 4x magnification. 24 hours= phase contrast, red circles indicate adhered cells. 72 hours = cells fixed and stained with Giemsa solution.

Figure 3.2.4.13 compares the cell morphology of the dithioate and acid functional polymers at 20x magnification. From the TCP and PLGA standards it can be seen that epithelial cells generally grow in close proximity, and that approximately $1/3^{rd}$ of the cell area is accounted for by the nucleus. The cells cultured on HBpolymers BMA1 and 2 have healthy cell morphologies comparable with the standards. There are only a few sparse cells on BMA3 and once again the polymer interfered with the quality of images for BMA4. The cells on the acid functional materials appear to have shrunken and malformed morphologies and do not appear healthy.

	Dithioate	Acid
BMA1		
BMA2		
BMA3		
BMA4		Polymer was not acid functional.
PLGA, TCP		
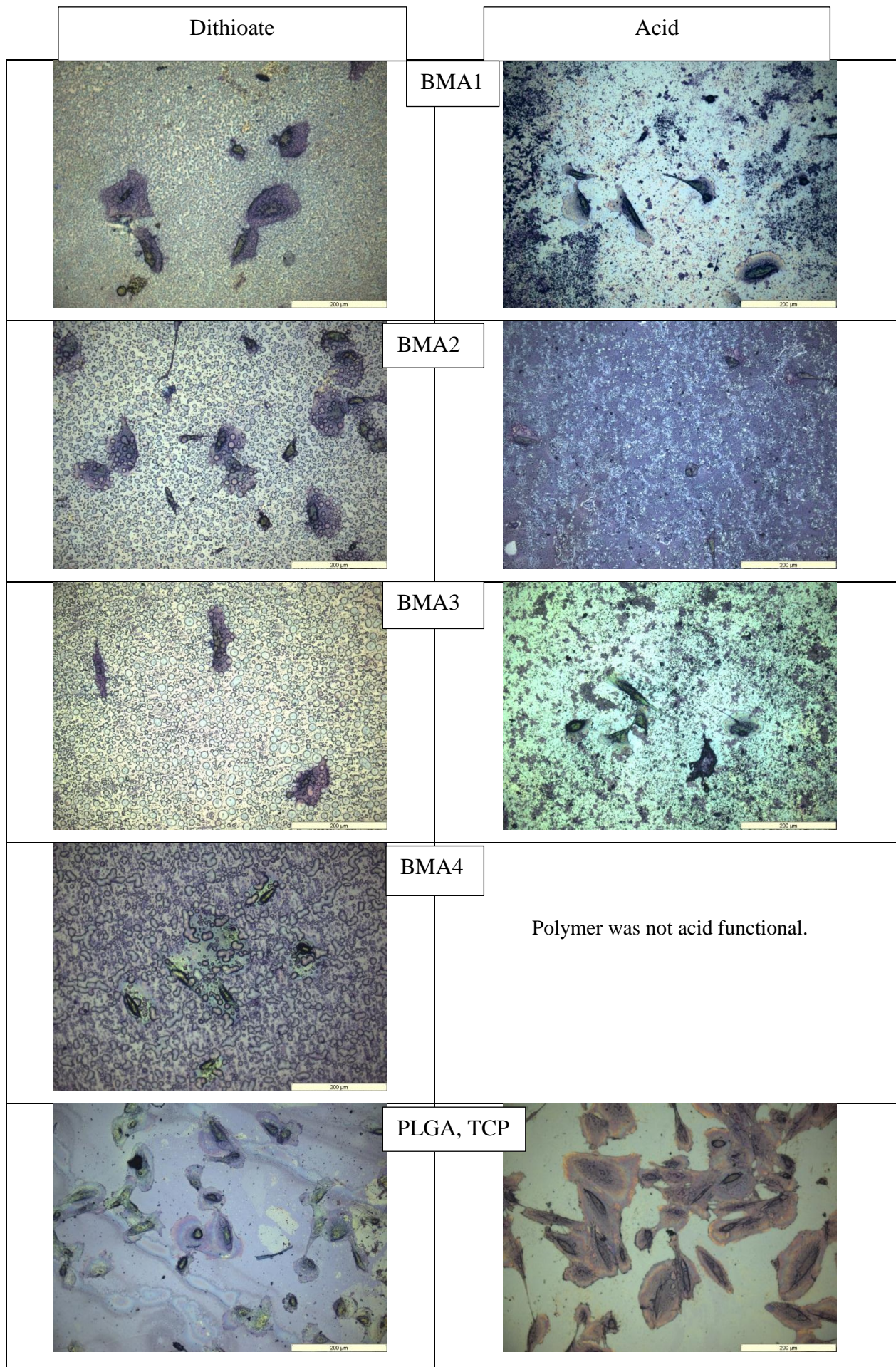
Figure 3.2.4.13 - Images comparing renal epithelial cell adhesion on HP(*n*-butyl methacrylate) polymers (HP1-4) with dithioate and acid functionality with TCP and PLGA after 72 hours at 20x magnification. Cells fixed and stained with Giemsa solution.
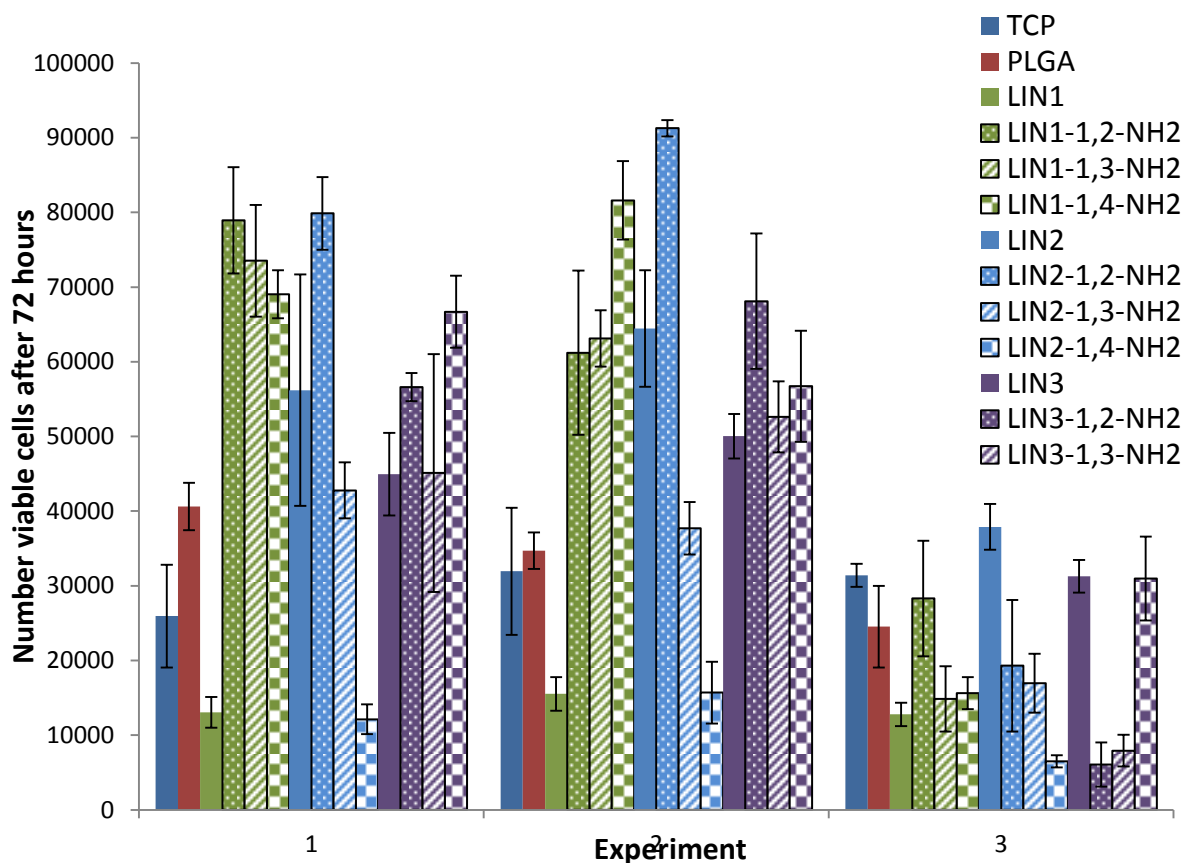
Figure 3.2.4.14 – Human renal epithelial cell viability after 72 hours culture in direct contact with linear(BMA) with acid and amine functionality. One-way analysis of variance and post-hoc Tukey's statistical analysis performed.

This set of experiments shows that amidated polymers are able to outperform tissue culture plastic and poly(lactide-glycolic acid). Of note, is that all amidated polymers have greater average viable cells than TCP in experiments 1 and 2. The acid functional polymers overall do not perform well, although the acidic copolymer LIN2 outperforms TCP in all of the experiments. This could mean that this polymer has the optimal hydrophobic/hydrophilic balance for the adhesion of epithelial cells and it is also in contrast to the contact studies performed with fibroblasts, where acid functional polymers were the best cell culture substrates.

The 'messiness' of this data indicates that epithelial cells are more sensitive to factors such as molar mass and polymer architecture, rather than just functionality as was observed previously for fibroblasts. What is clear is that epithelial cells do not demonstrate the same cytotoxic response when cultured on amine functional materials. We speculate this is because of the actions of lysyl oxidase and transglutaminase in epithelia culture. As discussed in

chapter 1 and chapter 3.1, these two enzymes are vital elements for the construction of the extracellular matrix and action upon lysine residues. The presence of the lysine-like amidated polymers might be triggering ECM formation of the epithelia.

The optical microscope images after 24 and 72 hours are shown in figures 3.2.4.15-17.

Cell adherence is seen after 24 hours on the polymers LIN1, LIN1 1,2-NH_2 and LIN1 1,4-NH_2 at a similar proportion to PLGA. After 72 hours there is some remaining cells, but these seem to have proliferated at a slower rate when compared to PLGA. No cells can be seen on the 1,3- and 1,4-NH_2 functional polymer.

For the LIN2 polymers, only the polymer with acid functionality has adhered cells after 24 hours. After 72 hours the epithelial cells cultured on the TCP are ~75% confluent, whilst much fewer cells are visible on the polymers – and none on the 1,3-NH_2 variant of LIN2.

All of the LIN3 polymers – acid and amine functional – show some epithelial adherence after 24 hours. This continues after 72 hours, with some clustered cell growth on all of the polymers. Some of the cells on the amine functional polymers appear spindly and may not be proliferating normally.

High magnification images of many of the linear polymers proved challenging to the prevalence of 'debris' and interference due to cell staining. Those cells that could be imaged are shown in figure 3.2.4.18. Healthy epithelial morphologies are seen on the acid polymers LIN1 and LN3, but only debris can seen on the 1,3-NH_2 functional LIN2.
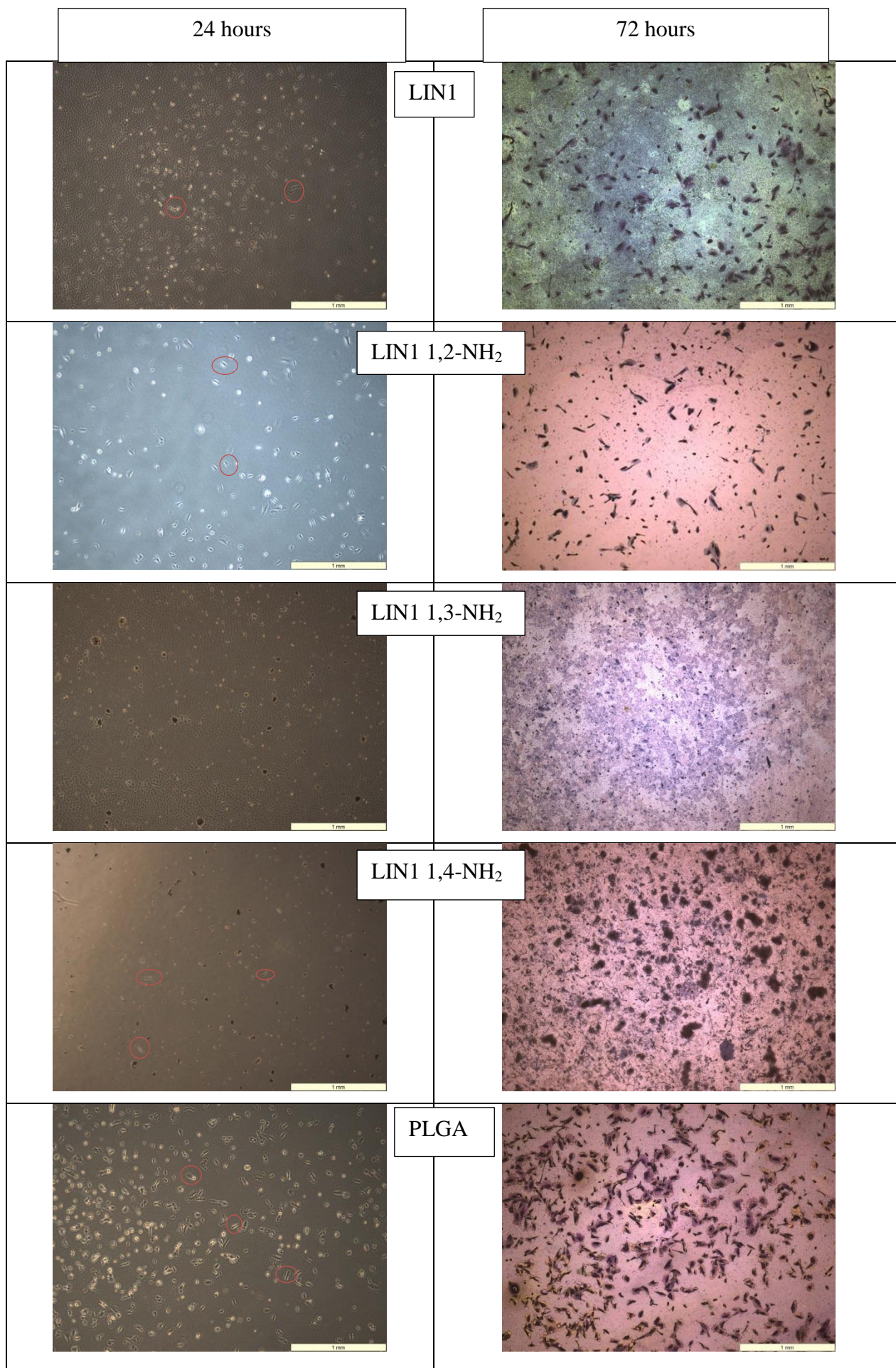
Figure 3.2.4.15- Images comparing epithelial adhesion on functionalised linear (*n*-butyl methacrylate) polymer (LIN1) and PLGA after 24 and 72 hours at 4x magnification. 24 hours= phase contrast, red circles indicate adhered cells. 72 hours = cells fixed and stained with Giemsa solution.
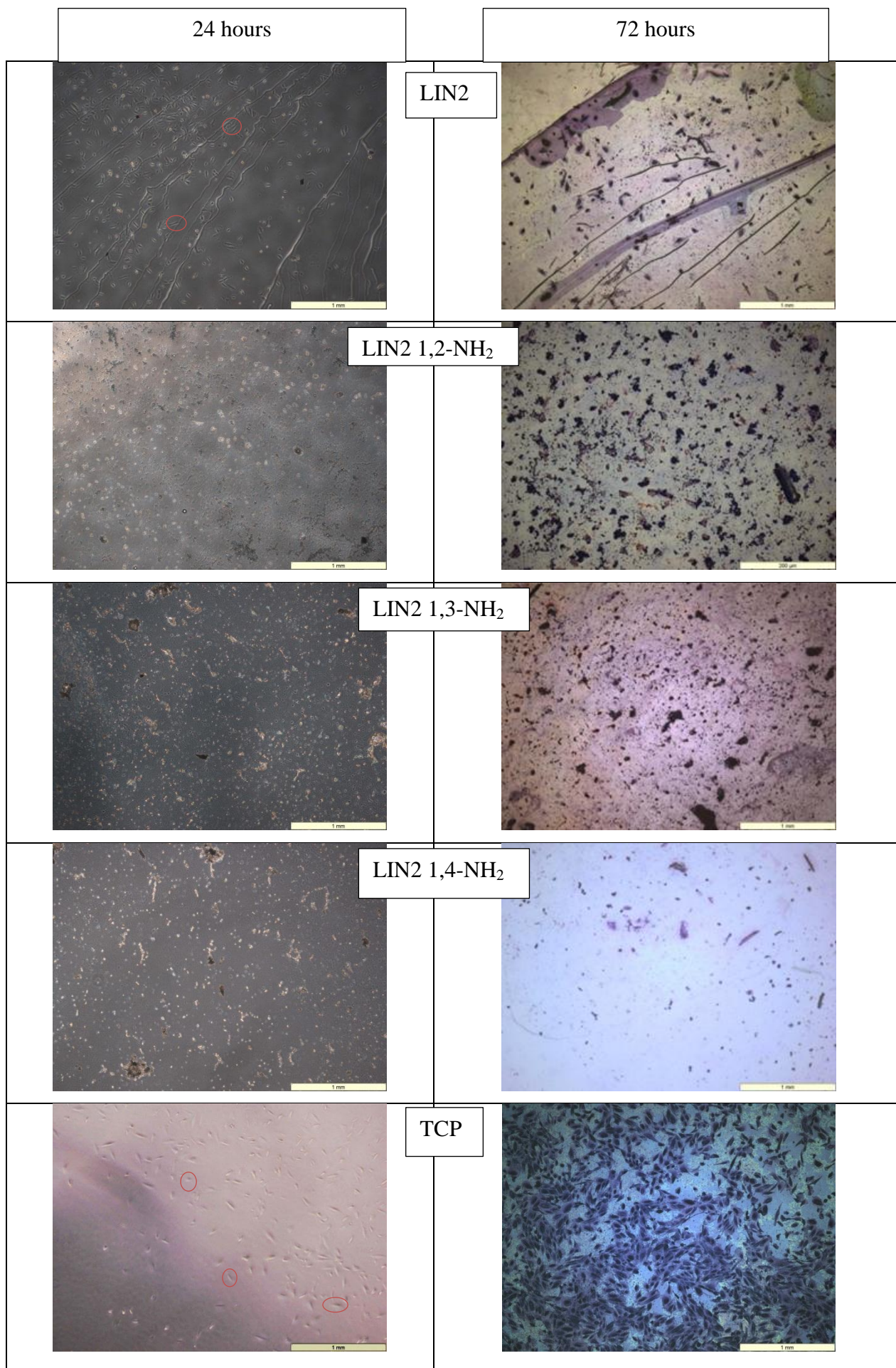
Figure 3.2.4.16- Images comparing epithelial adhesion on functionalised linear (*n*-butyl methacrylate) polymer (LIN2) and TCP after 24 and 72 hours at 4x magnification. 24 hours= phase contrast, red circles indicate adhered cells. 72 hours = cells fixed and stained with Giemsa solution.
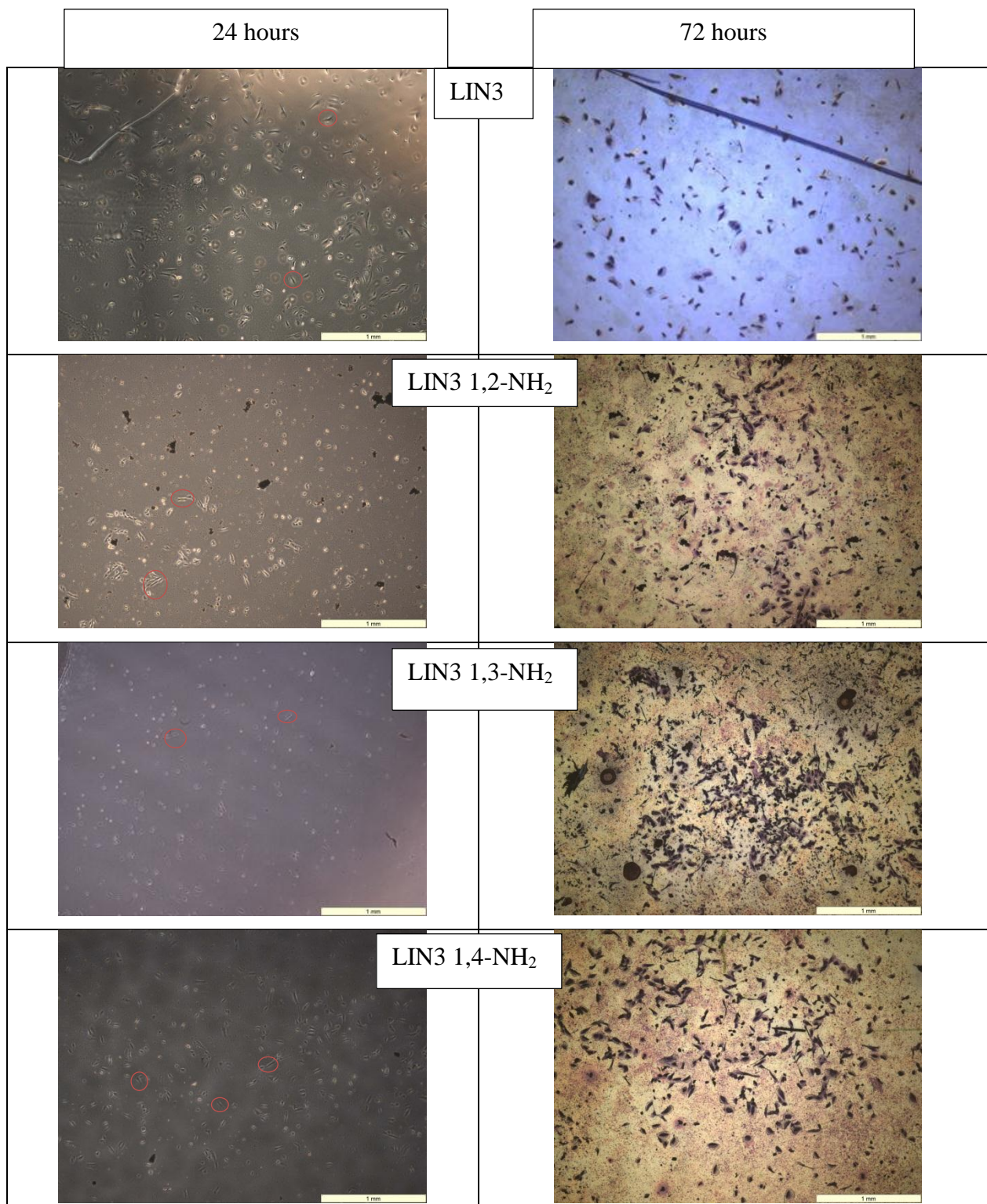
Figure 3.2.4.17- Images comparing epithelial adhesion on functionalised linear (*n*-butyl methacrylate) and polymer (LIN3) after 24 and 72 hours at 4x magnification. 24 hours= phase contrast, red circles indicate adhered cells. 72 hours = cells fixed and stained with Giemsa solution.
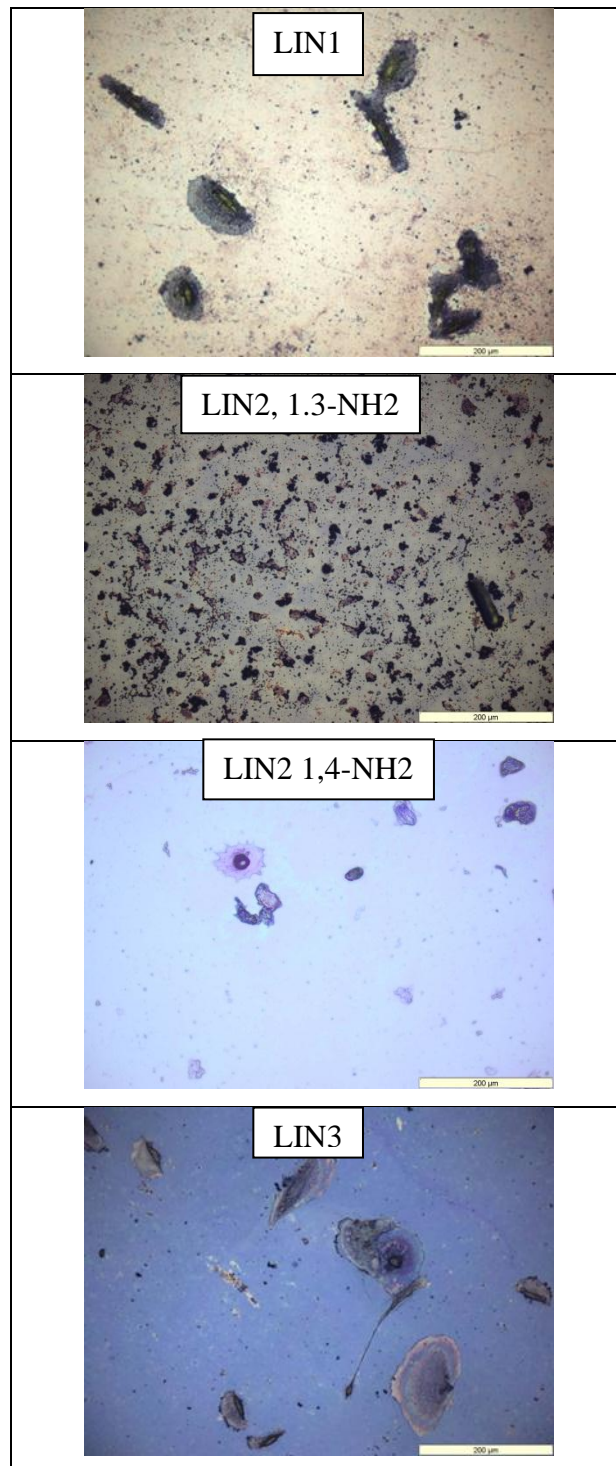
Figure 3.2.4.18 – 20x magnification of stained epithelial cells after 72 hours culture in direct contact with linear polymers.

3.3 Conclusions

Through elemental and chromatographic analysis, we found that 6% of CTA1 in the RAFT polymerisation with *n*-butyl methacrylate was optimal for conversion of monomer and branching of the polymer. Those polymerisations that contained 4 and 3% of CTA1 showed poor conversion as the system was deficient in initiator and flooded with methacrylate monomer. This was also possibly the cause for the suspected crosslinking of BMA4, which was the only polymer that did not successfully react with an excess of ACVA.

The linear polymers supplied for comparison were found to have similar α values to the synthesised hyperbranched polymers, and these were also successfully reacted with a small library of diamines to create a range of functional linear polymers for cell culture studies.

Through the incubation of cells in direct contact with polymers over 72 hours, it was found that HDFs grew equally well on all of the synthesised BMA polymers. The cells cultured on both acid and dithioate end groups show healthy morphologies as on the control materials. There is some evidence, such as greater average cell viabilities, to suggest that dermal fibroblast cells are best cultured in the presence of acid functional materials.

The preference for acid functional polymers is most striking on the linear materials, where very little HDF growth is observed on the amine functional polymers. Some fibroblast growth was seen on the polymer LIN3 1,4-NH_2, but the cells did not appear to be healthy. Further experiments might also expose further nuances between the acid content of polymer and cell proliferation.

Conversely, the epithelial cells were found to show no real preference for any of the dithioate PBMAs. The hyperbranched polymers BMA1 and 2 seem to be relatively better epithelial culture substrates than the 3 and 4 varients, and in some experiments had greater viability than TCP. The epithelial cells showed a strong preference for adherence and proliferation on the amine functional linear polymers. The acid functional polymers – both hyperbranched and linear – showed poor proliferation and cell growth was sparse with unusual morphologies.

These experiments have shown that acid functional linear polymers and hyperbranched poly(BMA) are suitable dermal fibroblast culture substrates. For the culture of renal epithelial cells, the preferred functionality is amine – possibly due to its chemical similarity to lysine which can be utilised by ECM forming enzymes such as lysyl oxidase.

3.4 Experimental

Instrumentation used as described in chapter 2.4

3.4.1 Synthesis of RAFT chain transfer agent: 4-vinylbenzyl-pyrrolecarbodithioate

Materials

Sodium hydride (60% in mineral oil dispersion, Aldrich), carbon disulfide (99+%, Aldrich), 4-vinylbenzyl chloride (90%, Aldrich), diethyl ether (Fisher), hexane (Fisher) were used as received.

Dimethyl formamide (DMF) was obtained from a Grubb's dry solvent system.

Pyrrole (99%, Aldrich) was distilled over calcium hydride (95%, Aldrich) under reduced pressure to give a colourless liquid.

Method

A three-necked round bottom flask was equipped with a condenser and bubbler, pressure equalising dropping funnel and a nitrogen inlet. A magnetic stirrer was also placed inside the flask. The apparatus was heated and purged with nitrogen to remove moisture. Sodium hydride (2.98 g) was added to the flask followed by DMF (80 mL) to form a suspension. Pyrrole (5.0 g) and DMF (10 mL) were then added dropwise over 30 minutes to produce a yellow foam. The solution was stirred at room temperature for 30 minutes and then cooled to 0°C using an ice bath. Carbon disulfide (5.68 g, 4.50 mL) and DMF (10 mL) were added dropwise over 10 minutes to create a dark red solution. This was stirred at room temperature for 30 minutes and then cooled to 0°C. 4-Vinylbenzyl chloride (11.37 g, 10.50 mL) and DMF (10 mL) were then added dropwise over 20 minutes. The brown solution was stirred overnight at room temperature.

The solution product was placed in a 1L separating funnel, with diethyl ether (80 mL) and distilled water (80 mL). The organic layer was recovered and the aqueous layer was extracted with diethyl ether (3 x 160 mL). The organic extracts were combined and dried over magnesium sulfate before filtration, and the solvent was removed by rotary evaporation to give a brown oil.

The oil was purified by flash chromatography, with a column of 6cm diameter, using 100% hexane. The solvent was removed by rotary evaporation to give 5.6 g of a bright yellow oil. The air sensitive product was stored under nitrogen at -18˚C.

Mpt: ~25˚C. **Elemental analysis:** C: 64.7%, H: 5.2%, N: 5.4%, S:24.7%.
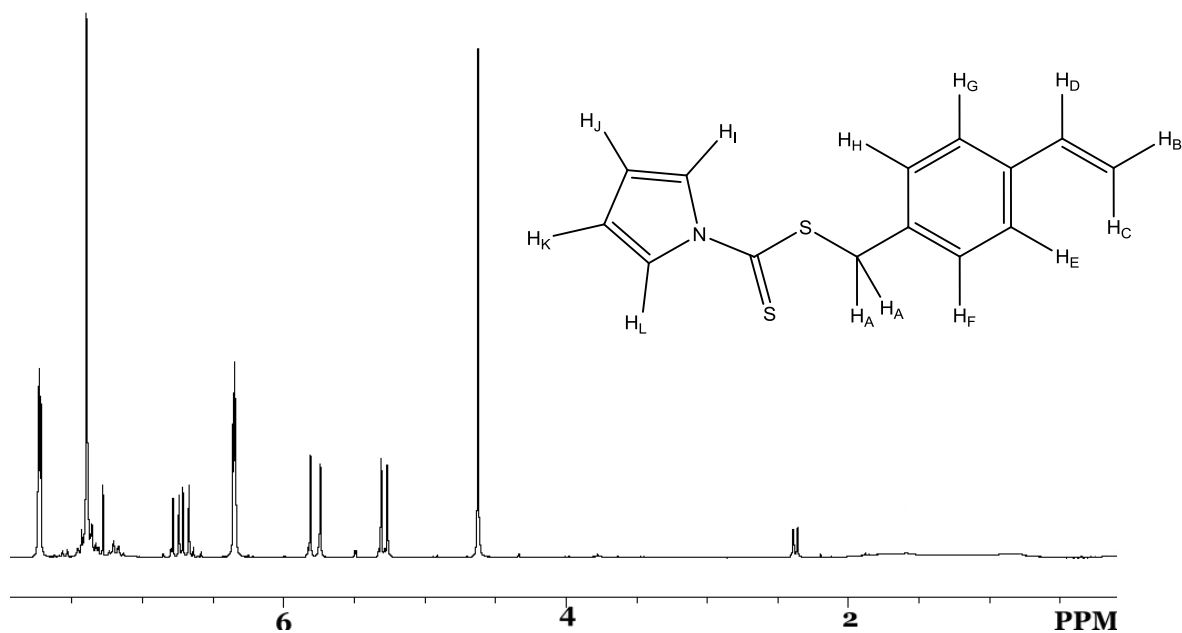
Figure 3.4.1.2 - ^{1}H NMR of 4-vinylbenzyl-pyrrolecarbodithioate (250 MHz, *CDCl₃*) δppm 4.62 (s, H$_A$), 5.29 (d, *J* = 10.81 Hz, H$_C$), 5.78 (d, *J* = 17.57 Hz, H$_B$), 6.35 (H$_J$, H$_K$), 6.73 (dd, *J* = 17.60, 10.90 Hz, H$_D$), 7.20 (H$_I$, H$_L$), 7.28 (solvent), 7.45-7.31 (H$_H$, H$_F$), 7.73 (H$_E$, H$_G$).

3.4.2 RAFT polymerisation of *n*-butyl methacrylate using 4-vinylbenzyl pyrrole carbodithioate chain transfer agent

Materials

4-Vinylbenzyl pyrrole carbodithioate (produced as previously described), *n*-butyl methacrylate (98%, Aldrich), 4,4'-azobis 4-cyanovaleric acid (ACVA, ≥98%, Aldrich), 1,4-dioxane (anhydrous, 99.8%, Sigma-Aldrich), methanol (Fisher) were used as received.

Equipment

Ampoules were degassed on a high vacuum line equipped with a Pirani gauge.

Method

4-vinylbenzyl pyrrole carbodithioate, *n*-butyl methacrylate, dioxane (25 mL) and ACVA were mixed together until the solid initiator had dissolved. The resulting solution was pipetted into a 50 mL ampoule and placed onto the vacuum line but was not exposed to vacuum. The solution was frozen using liquid nitrogen and then opened to the vacuum until the gauge dropped to a steady output. The ampoule's exposure to vacuum was then ceased as its contents were left to thaw. Once thawing was completed, the full process was repeated until a negligible rise in pressure was observed when the ampoule was opened to vacuum. The end pressure in the ampoule was approximately 3×10^{-3} mBar. The ampoule was sealed using a gas/oxygen blowtorch and placed in a water bath at 60 ˚C for up to 24 hrs to undergo polymerisation.

Table 3.4.2.1 summarises the quantities of reagents used.

n-butyl methacrylate /mL	Chain transfer agent /mL	ACVA /g
5 (0.03)	1 (0.004)	1.29 (0.004)
10 (0.06)	1 (0.004)	1.29 (0.004)
15 (0.09)	1 (0.004)	1.29 (0.004)
20 (0.12)	1 (0.004)	1.29 (0.004)
15 (0.09)	1 (0.004)	0.65 (0.002)
20 (0.12)	1 (0.004)	0.65 (0.002)

Table 3.4.2.1 – summary of reagent quantities used in RAFT polymerisation of *n*-butyl methacrylate. Molar values in parenthesis.

Products were precipitated by transferring into 4x by volume of methanol and leaving to stand, followed by filtering and drying in a vacuum oven producing a yellow solid. Dried products were stored in closed sample tubes at room temperature.

Polymers were analysed by ^{1}H and ^{13}C NMR, size exclusion chromatography, FT-IR and elemental analysis.

NMR spectroscopy results:

^{1}H (400 MHz, CDCl3) δppm 0.97 (A), 1.12 (E), 1.42 (B), 1.48 (C), 1.85(F) 4.02 (D), 6.46 (J/I), 7.83 (G/H)

3.4.3 Reaction of hyperbranched butyl methacrylate polymers with excess ACVA

Materials

Acetone (HPLC grade, Fisher), ethanol (absolute, Fisher), methanol (HPLC grade, Fisher), ultrapure water (18.8Ω, MilliQ systems), HBP(*n*-butyl methacrylate) synthesised as described in section 3.3.2 and 4,4'-azobis 4-cyanovaleric acid (ACVA, ≥98%, Aldrich) were used as received. Dimethyl formamide (DMF) was obtained from a Grubb's dry solvent system.

Method

A three necked round bottom flask was equipped with a magnetic stirrer, nitrogen inlet and a condenser. The apparatus was nitrogen purged and heated to 60°C. A known amount of polymer was dissolved in dry DMF and then injected into the warm, dry flask which was kept under a nitrogen atmosphere. 60molar equivalents of ACVA were then dissolved in 10-15mL DMF (up to 1 minute of sonication was used to assist dissolution) and this was then injected into in the flask. The solution was stirred for 16hours at 60°C before the addition of another 60molar equivalents of ACVA. This process was repeated for four additions.

The polymer was purified from ACVA by first removing the DMF under reduced pressure. The solid polymer was then dissolved in ultrapure water (MilliQ) and waste ACVA was removed via vacuum filtration. The polymer was washed with methanol and then further purified by ultrafiltration through a 3kDa cellulose membrane using a solvent system of 9:1 acetone:ethanol.

The reaction was deemed successful when elemental analysis showed that no sulfur was present in the final product, indicating the complete removal of the dithionate protecting groups.

Polymers were analysed by ^{1}H and ^{13}C NMR, size exclusion chromatography, FT-IR and elemental analysis (results shown within this chapter).

3.4.4 Coupling of linear butyl methacrylate copolymers to diamines

Materials

Ethylenediamine (99%, Aldrich), 1,3-diaminopropane (99%, Aldrich) 1,4-diaminobutane (99%, Aldrich), 1,6-diaminohexane (99%, Aldrich), 1-(3-dimethyl-aminopropyl)-3-ethylcarbodiimide hydrochloride (Alfa Aesar) were used as received. Distilled water was used throughout.

Method

A polymer solution was formed by dissolving 2 g of polymer in 10 mL dichloromethane (DCM). To this was added 1g DOWFAX2A1 solvated in 50 mL water with high agitation. The DCM was then removed using nitrogen under high agitation.

10 mL of the resultant polymer in water solution was added to a 3-neck round bottom flask, equipped with a condenser and magnetic stirrer bar. At the same time 1-(3-dimethyl-aminopropyl)-3-ethylcarbodiimide hydrochloride (EDC) was weighed out and dissolved in 45 mL of water. The stirring polymer solution was then submerged into an ice bath and the aqueous solution of EDC was added slowly. The appropriate diamine was then added to the stirring mixture slowly over a period of at least an hour. Substantial effervescence was observed at this stage. The reaction was left to warm to room temperature and continued to stir for 24 hours. The quantities used for each reaction are shown in table 3.4.4.1.

Diamine	Amount used	EDC (g)	DOWFAX2A1 (g)
Ethylenediamine	4.651g (0.08 moles)	3.6971	1.210
1,3-diaminopropane	5.841g (0.08 moles)	3.7123	1.211
1,4-diaminobutane	6.812g (0.09 moles)	3.6991	1.210
1,6-diaminohexane	7.941g (0.09 moles)	3.7114	1.202

Table 3.4.4.1 – Table of reagents used in EDC-mediated diamine-oligomer cross coupling reaction.

1, 6-diaminohexane is a solid and an aqueous solution of this was prepared in 90mL of water which was then added to the reaction mixture.

Purification of amidated polymers

The stable emulsions were removed placed into dialysis visking tubing and placed into distilled water for 2 weeks, with daily changes of water taking place.

The modified polymers were analysed by FT-IR and elemental analysis (results shown within this chapter).

3.4.5 Culture of cells in direct contact with polymers

Materials

Human dermal fibroblasts and human renal epithelial were cultured and prepared as described in chapter 2.

Hyperbranched butyl methacrylate (BMA1-4) as synthesised in section 3.4.2, and with acid end groups as described in section 3.4.3 (BMA1-4 acid). Linear copolymers were used as received from Sarah Canning[230] and also amidated (section 3.4.4), isopropanol (absolute, Fisher), complete media (prepared as described in chapter 2), trypsin-EDTA (Life Technologies), PLGA (50:50, Polysciences), DMSO (Anhydrous, Sigma), Alamarblue® (Life Technologies), phosphate buffered saline (Bioreagent, Sigma), hematoxylin solution according to Weigert (parts A and B, Aldrich), eosin y (99%, Sigma Aldrich), 10% neutral buffered formalin solution (Sigma), giemsa stain modified solution (Sigma), ethanol (absolute, Fisher), glacial acetic acid (99%, Fisher) were all used as received.

Distilled water was used throughout unless otherwise specified.

Equipment

IR spot lamp 75W (Exo Terra), glass coverslip (22x22mm, Menzel).

Glass coverslips were sterilised by autoclave.

Preparation of polymer films and cell seeding

Polymers were dissolved in the solvents listed in table 3.4.5.1 at a concentration of 5mg/mL.

The polymer solutions were well agitated and sonicated for up to 30 seconds if required.

Solvent	Polymer
Isopropylalcohol	Amidated linear copolymers
Tetrahydrofuran	Linear copolymers, BMA1-4
Dimethylsulfoxide	PLGA
Ethanol	BMA1-4 acid

Table 3.4.5.1. – Solvents used to solvate the various polymers prior to casting on glass slips.

100 mL of polymer solution was then pipetted onto each glass coverslip. An IR lamp was used to heat treat the polymer films until the solvent appeared visibly removed. At this point, each covered slip was placed into its own well of a six well plate and washed with sterile PBS to remove any residual solvent.

Fibroblasts or epithelial cells were treated with trypsin as per the protocol for passage, but instead of re-seeding into T-75 flasks, they were seeded directly onto the films at a density 1×10^4 cells/well. 2 mL of complete media was added to each well and the cells were incubated for 24 hours at 37 ºC, 5% CO_2. After 24 hours phase contrast imaging and a full media change was performed. After 72 hours cells were assayed and fixed for staining using the methods in chapter 2.

4 - Hyperbranched Poly(*t*-butyl acrylate)

4.1 Introduction

The purpose of this work was to produce hyperbranched *t*-butyl acrylate using the RAFT procedure already described for *n*-butyl methacrylate. The hypothesis was that having observed the cellular response to acidic polymers, it would be possible to create a polymeric coating that would show good cell adhesion by trapping a branched polymer within a crosslinked coating. The choice of *t*-butyl acrylate monomer was governed by the desire to form a hyperbranched polymer that, along with having functionalised end groups, could also be subjected to further hydrolysis and chemical modifcations to produce either acid or amine functionality at the *t*-butyl sites.

T-butyl acrylate has a glass transition temperature, T*g,* of 43 °C compared to -54 °C for *n*-butyl acrylate and 20 °C for *n*-butyl methacrylate. When a polymer resides at temperatures below its T*g*, it appears crystalline and 'glassy'. At temperatures above the T*g*, individual chains have enough energy to overcome the weak intermolecular forces (usually London dispersion forces and hydrogen bonds) to allow flow to occur. This means that the inclusion of *t*-butyl acrylate can help raise the T*g* and improve the mechanical properties of the polymer. A strong polymer with a reasonably high T*g* is required to prevent wear, especially for the application of a cell-adhesive coating in replacement joints. This has also been exploited in order to control the memory response of polymeric stents. The thermoresponse was induced by warming the polymer stent to above its T*g*, allowing it to be compressed for storage. The polymer could then decompressed by rewarming and softening. A stent was synthesised usng *t*-buyl acrylate that would remain compressed at room temperature but reformed its original shape at body temperature[236]. Control over the T*g* is important not only for issues of storage and application, but also for the form of the polymer at body temperature. Polyurethanes have been extensively studied as so-called shape memory polymers (SMPs) due to excellent biocompatibility and a wide range of available T*g*s[237], [238].

The ease with which it is possible to hydrolyse *t*-BuAc and subsequently subject it to chemical modification makes it an attractive comonomer for polymeric biomaterials[239]–[243].

T-butyl acrylate has previously been reported as a precursor in the formation of poly(acrylic acid). The graft copolymers prepared by Kriegel *et al.* were synthesised using atom-transfer radical polymerisation and ring-opening metathesis techniques[244], which allows for good control over the architecture of the final polymer. Zhou, however, produced hyperbranched polymers using a stepwise graft procedure[245]. The prepared films from both of these reactions showed a high density of carboxylic acid functionality. By employing a weak acid, it has been demonstrated that macrophages and endothelial cells can be corralled into the hydrophobic valleys present on a patterned surface[205]. This finding has implications for controlled 3-dimensional cell culture, allowing cells to grow beyond single layer sheets *in vitro*. The results presented previously in this work indicate that dermal fibroblast and renal epithelial cells would also be suitable for corralling using acid- and amine- function HBP(butyl methacrylate).

The results of cell viability on HBP(*t*-butyl acrylate) also suggests that functionalised Walters and Hirt have previously reported the synthesis of amine functional polymers from *t*-butyl acrylate [224] . Although this work demonstrates the tunability of *t*-butyl acrylate polymers, no cell compatibility work was performed[246]. This is a pattern repeated throughout the current literature and this work hopes to shine some light on the biocompatibility of functionalised *t*-butyl acrylate polymers.

The RAFT polymerisation was carried out as previously described, using four different ratios of monomer to carbodithioate chain transfer agent (4-vinylbenzyldithiobenzoate, CTA 2) in the reaction mix.

After characterisation the polymers were reacted with excess ACVA, as described in chapter 3, to remove the CTA end groups and replace them with acid functionality. The polymers, both in native form and after reaction with excess ACVA, were subjected to the same cell testing as the hyperbranched *n*-butyl methacrylate polymers, so that a direct comparison could be made between the two hyperbranched materials. These polymers are also envisaged to act as a precursor for hyperbranched poly(acrylic acid) by subsequent removal of the tert-butyl group. By reaction with stoichiometric amounts of diamine this could provide carefully tailored amphiphilic biomaterials as previously demonstrated.

The intricacies of IPNs have already been discussed in Chapter 1 section 9. Hydrogels often have limited mechanical properties, and (semi-)IPNs are an emerging alternative. Semi-IPNs

display properties that are often stronger than those of the native polymers due to the combined polymer network and intertwined functional polymer (figure 4.1.1)[247]–[249].
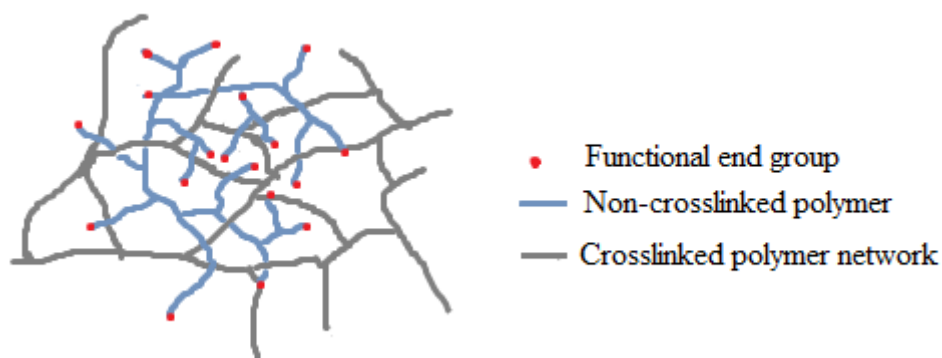
Figure 4.1.1 – Diagram of semi-IPN with a crosslinked polymer network (grey) and a non-crosslinked hyperbranched polymer (blue) with labile, modifiable end groups (red).

The benefit of IPNs and sem-IPNs is that two polymers with different functionality can be combined to form a dual-responsive material as described in chapter 1 section 6.

The HBPs synthesised within this project were also to be investigated for use in semi-interpenetrating networks. Due to their low molecular weights they would not stay trapped within the networks formed, even with increased levels of cross-linker present in the surrounding network.

4.2 Results and discussion

4.2.1 Polymer synthesis and characterisation

The first step of the RAFT polymerisation was synthesis of the RAFT agent 4-vinylbenzyldithiobenzoate (CTA2) shown in scheme 4.2.1.1.
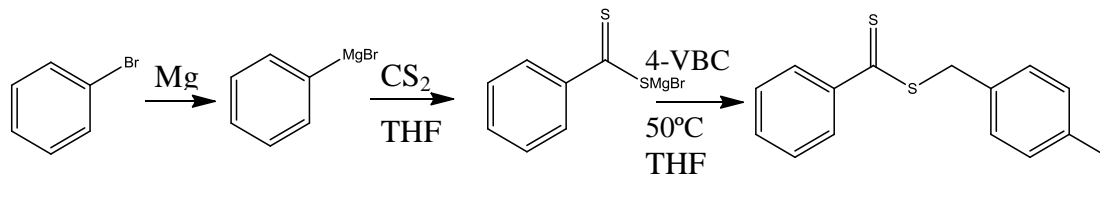
Scheme 4.2.1.1 – Scheme of 4-vinylbenzyl dithiobenzoate synthesis.

Four hyperbranched polymers using *t*-butyl acrylate monomer were synthesised using varying amounts of chain transfer agent 2 (CTA2) and monomer, using a similar methodology as described in chapter 3.

The polymerisation recipes are described in detail in section 4.4.2. Multiple analytical techniques were used to fully characterise the polymers in order to gauge the success of the RAFT polymerisation and the percentage incorporation of CTA2.

^{1}H NMR was first used to observe if the chain transfer agent had successfully copolymerised with *t*-butyl acrylate and a representative spectrum is shown in figure 4.2.1.2. Compared to a homopolymer of the acrylate monomer, the copolymer was expected to exhibit resonances in the region of 7-8.5ppm due to aromatic protons present on CTA2.
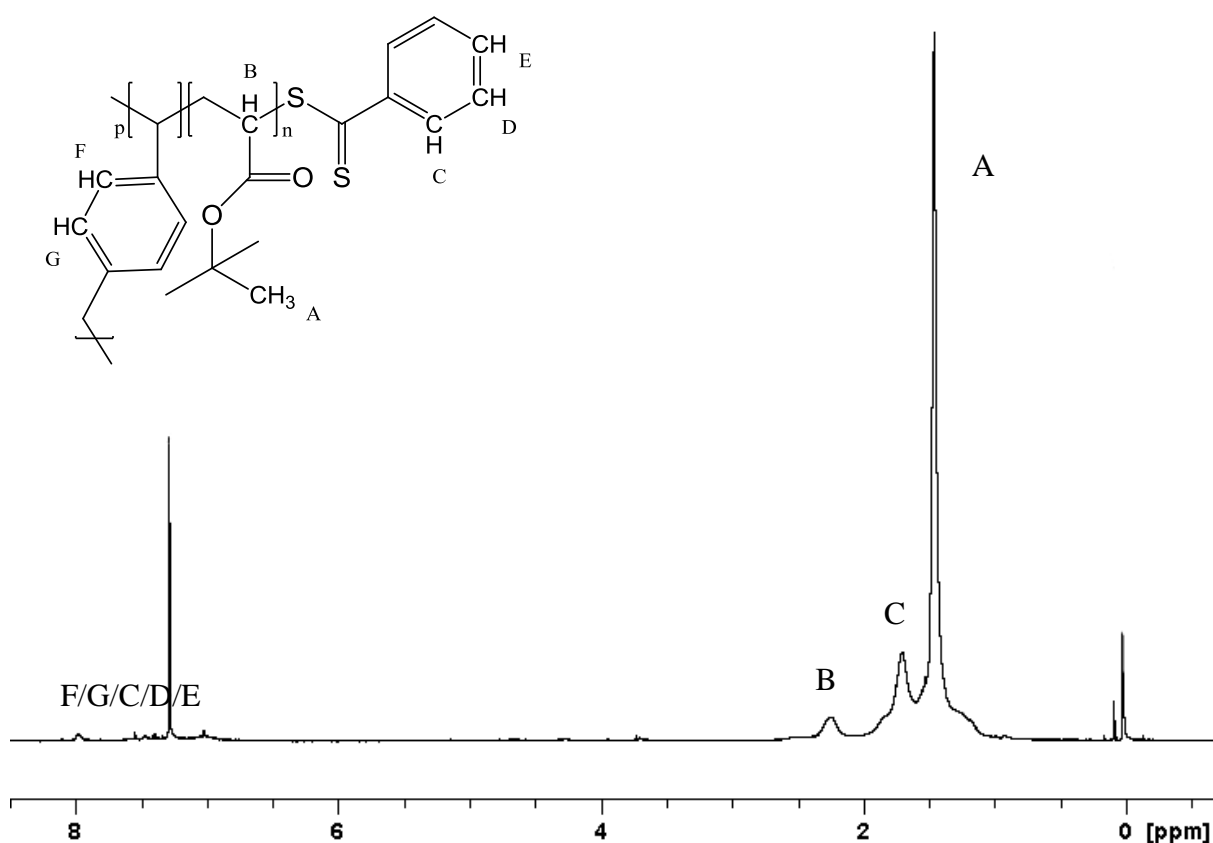
Figure 4.2.1.2 - Representative ^{1}H NMR spectrum of hyperbranched(t-butyl acrylate) polymers. 400 MHz, CDCl$_3$

The spectra showed that the copolymerisation between t-butyl acrylate and the branching chain transfer agent was successful and that aromatic protons are present in the polymer. The only source of the signals seen at 6.5-8ppm is the CTA2 comonomer. The most intense resonance at 1.5ppm can be associated with the sp^3 protons present on the pendant methyl groups of t-butyl acrylate. As this is the monomer present in greatest quantities, it is predictable that these protons will be most numerous. The resonance at 2.1ppm can be assigned to the ArR$_2$C$\underline{H}$ that occurs on the insertion of CTA2 into the polymer backbone, whilst the resonance at 4.9ppm occurs because of the R$_2$(CO)CH protons contributed by t-butyl acrylate. End group analysis was performed using equation 4.2.1.3 in order to quantitatively compare the proton spectra of the polymers and estimate the percentage incorporation of CTA2. This showed that tBuAc4 had an estimated incorporation of 4% CTA2, whilst tBuAC3 and 4 had 7% and 6%, respectively: almost double their predicted maximum amount of CTA2 (table 4.2.1.4).

$$\% \, dithiobenzoate = 100 \; x \; \frac{\int \frac{H_J}{9}}{\int \frac{H_A}{9}}$$

Equation 4.2.1.3 - Equation used to estimate the percentage dithiobenzoate in each polymer using ^{1}H NMR integrals.

	*t*BuAc added (mL)	CTA added (mL)	Moles tBuAc	Moles CTA	Maximum % dithioate	Estimated % dithioate
tBuAc1	5	1	0.034	0.004	12	n/a
tBuAc2	10	1	0.068	0.004	6	4%
tBuAc3	15	1	0.1	0.004	4	7%
tBuAc4	20	1	0.14	0.004	3	6%

Table 4.2.1.4 – Comparison of theoretical and calculated (by ^{1}H NMR end group analysis) % dithioate present in hyperbranched polymers *t*BuAc1-4.

Table 4.2.1.5 compares the monomer conversion for each of the polymers. The monomer conversion of polymers *t*BuAc3 and 4 was extremely low at 22.5% and 7.3%, respectively, which could explain the high presence of CTA2 as indicated by end group NMR analysis.

Polymer	Conversion (% monomer)
*t*BuAc1	75.9±4.3
*t*BuAc2	100.0±11.6
*t*BuAc3	22.5±3.2
*t*BuAc4	7.3±2.5

Table 4.2.1.5 – Percentage monomer conversion for hyperbranched polymers *t*BuAc1-4.

*t*BuAc1 and 2 both showed good monomer conversion and elemental analysis confirmed that both polymers contain over 1% CTA2 (table 4.2.1.6). The percentage of CTA2 calculated by elemental analysis is much lower for all of the polymers when compared to the estimates of

the NMR analysis. Elemental analysis is a much more sensitive technique and it is believed that these results to be more realistic. Analysis by ^{1}H NMR spectroscopy in this manner must be used as a supplement and not as a stand alone technique.

Polymer	Predicted Elemental Analysis	Observed Elemental analysis	% CTA2
*t*BuAc1	C 69.3%, H 8.3%, S 3.9%	C 64.0%, H 8.3%, S 2.7%	1.35%
*t*BuAc2	C 67.7%, H 8.8%, S 2.3%	C 65.3%, H 8.7%, S 2.2%	1.1%
*t*BuAc3	C 67.1%, H 8.9%, S 1.6%	---	---
*t*BuAc4	C 66.8%, H 9.1%, S 1.2%	C 57.4%, H 8.5%, S, 2.5%	1.25%

Table 4.2.1.6 – Elemental analysis results of hyperbranched *t*-butyl acrylate polymers.
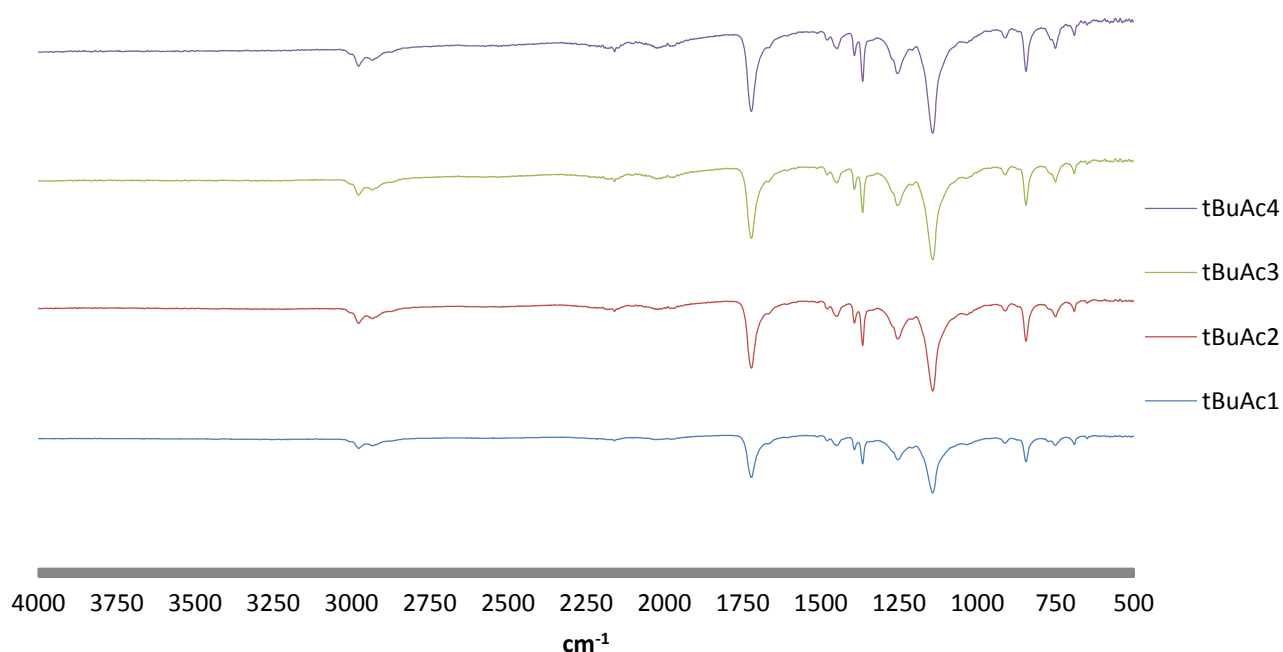
Figure 4.2.1.7 – FT-IR of hyperbranched polymers *t*BuAc1-4.

The FT-IR spectra shows that all four polymers contain the same functionality, with successful inclusion of the RAFT chain transfer agent (figure 4.2.1.7). This is again a strong indicator for the successful copolymerisation between CTA2 and *t*-butyl acrylate in all four polymers. The strong signal seen at 1120cm^{-1} arises due to C=S stretching in CTA2, whilst the two bands at 1220 and 1350cm^{-1} result from C-O stretching in *t*-butyl acrylate. The C=O

of *t*-butyl acrylate is observed as a strong signal at 1700cm^{-1}. Aromatic overtones are observed at 1900-2100cm^{-1} whilst sp[3] and sp[2] C-H stretches are visible at 2980 cm^{-1}.

	$\overline{Mn}$	$\overline{Mw}$	$\overline{Mz}$	PDI
*t*BuAc1	8250	18530	35330	2.24
*t*BuAc2	11030	54230	199420	4.9
*t*BuAc3	3859	8532	18613	2.21
*t*BuAc4	24750	61080	120750	2.47

Table 4.2.1.8 - Molecular weight data (daltons) for HP(tBuAc) polymers as determined by size exclusion GPC using tetrahydrofuran as the mobile phase.
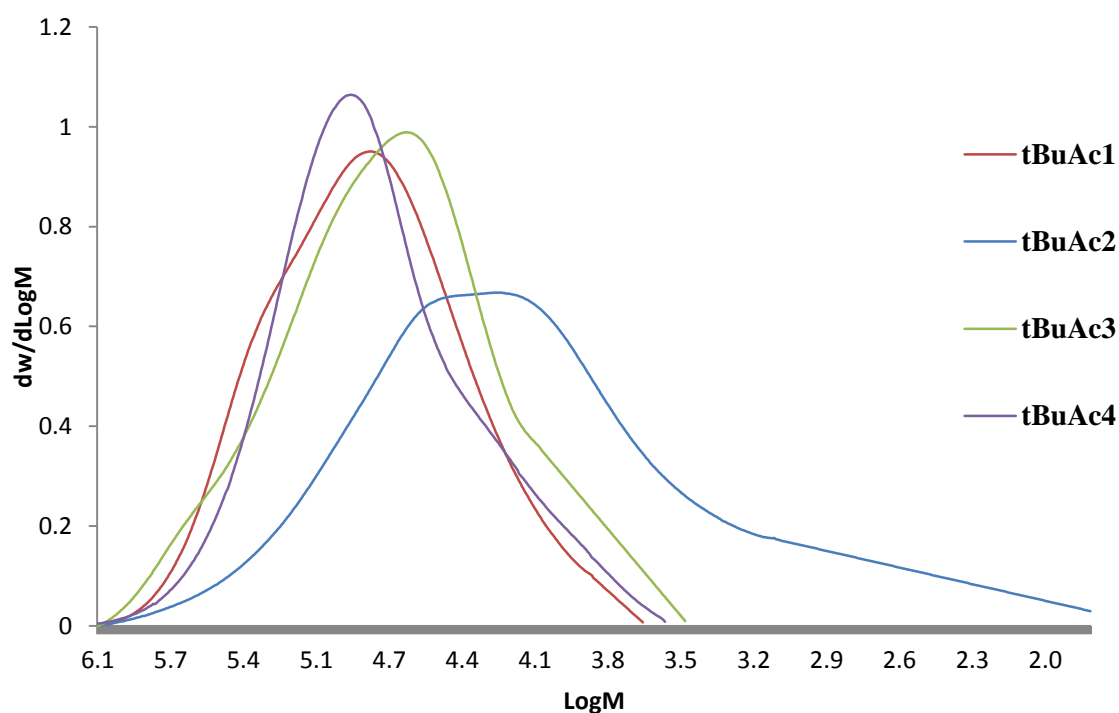
Figure 4.2.1.9 - Molar mass distribution of polymers tBuAc1-4.

Table 4.2.1.8 provides a summary of the polymers' molar masses whilst figure 4.2.1.9 shows the MMD of *t*BuAc1-3. It can be seen that relatively low molar mass averages are obtained with this branching RAFT agent, and this is possibly because higher rate of retardation is experienced when using an aromatic carbodithioester with an acrylate monomer[250]. However, it is unknown if this retardation is caused directly by a low rate of fragmentation or by making side reactions more likely to occur. Ting *et al.* have shown experimentally that the

retardation of styrene does not occur when short chain radicals are not present[251], giving credence to the calculated model proposed by Perrier *et al.*[252]. In addition, Meiser *et al.* observed that fast fragmentation occurred in the RAFT polymerisation of BAc and dithiobenzoate[253] – although it is noted that fragmentation is faster still when using a trithiocarbonate CTA. This still does not explain the wide variances observed in the rate of reaction[254], and the topic has been and continues to be a source of debate[255], [256]. The polydispersity values of the polymers above also suggest at least a bimodal distribution of molar masses. The molar mass distributions in figure 4.2.1.9 are bimodal. The distribution of hyperbranched polymer *t*BuAc3 shows an especially broad distribution and a PDI of 4.9; this sample evidently contains a wide range of polymer chain lengths. As discussed in chapter 3, the broadness in polydispersity is actually considered an advantage in this instance as the low molecular weight chains are expected to migrate to the surface of the films cast on cell culture substrates. However, polymers with low molar mass may not be suitable for incorporation into semi-IPNs due to the lower probability of physical entrapment.

	$\overline{Mn}$	$\overline{Mw}$	$\overline{Mz}$	PDI	α
*t*BuAc1	3800	14100	53500	3.7	0.3
*t*BuAc2	17250	129050	1504000	7.5	0.4
*t*BuAc3	6300	45000	276450	7.2	0.4

Table 4.2.1.10 – Summary of triple detection SEC data of hyperbranched *t*-butyl acrylate polymers *t*BuAc1-3 using tetrahydrofuran mobile phase. *t*BuAc4 was not sufficiently soluble for triple detection analysis.

Despite the low conversions quoted in table 4.2.1.8 the α values in the table above correlate with poly(*N*-isopropyl acrylamide) materials previously prepared in our laboratories; this indicates that some branching has occurred even at low monomer conversion. Rannard *et al.* have used radiolabelled ATRP[257] to demonstrate that initiation occurs even at >90% conversion[258]. Through the combination of these results, it can be concluded that initiation and chain branching occurs throughout the lifetime of the polymerisation.

4.2.2 Characterisation of acid functional polymers and embedding into semi-interpenetrating networks

After characterisation, the hyperbranched polymers were treated with an excess of ACVA in order to remove the carbodithioate end groups and to replace them with acid functionality. The ^{1}H NMR spectra shown in figure 4.2.2.1 of the polymers after this treatment reveals a decrease in the intensity of the benzyl signals at 7-8ppm as would be expected with the loss of CTA2.
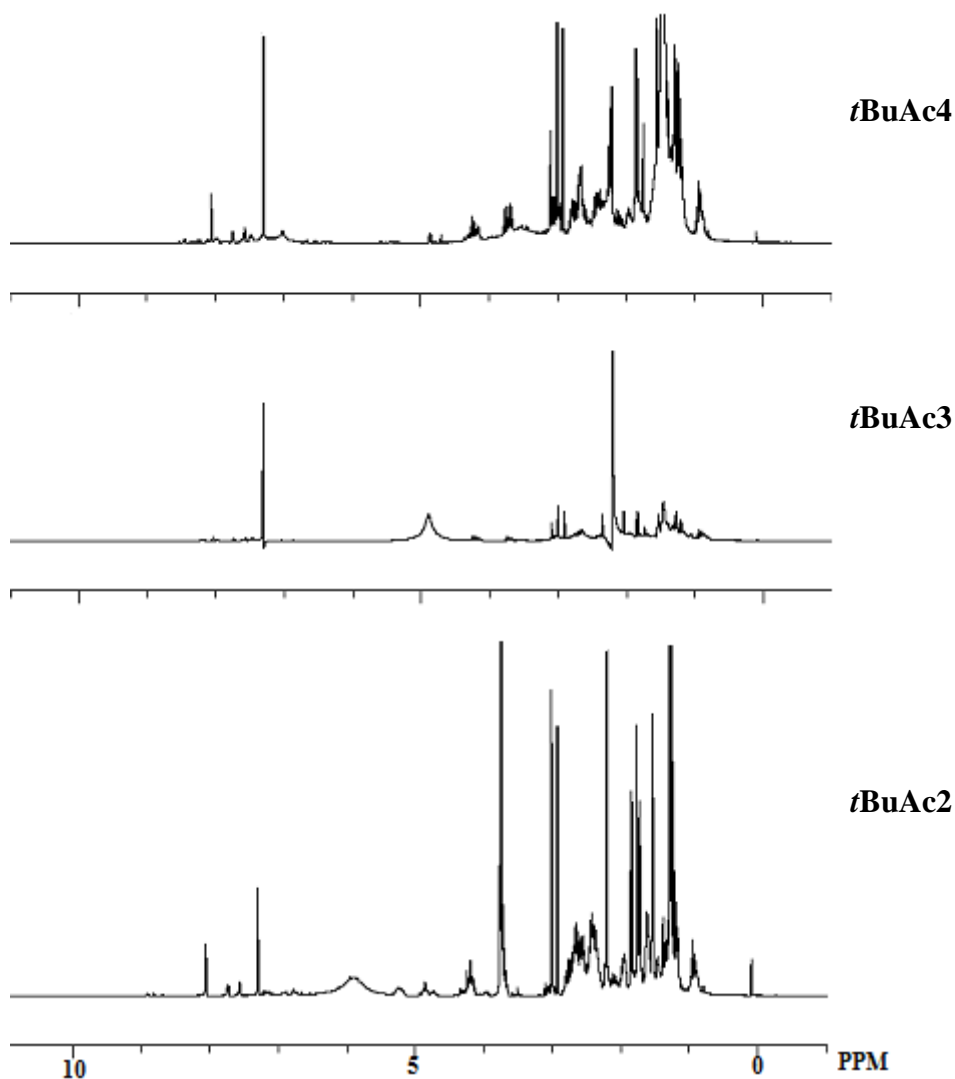
Figure 4.2.2.1 – ^{1}H NMR of hyperbranched *t*-butyl acrylate polymers (tBuAc2-4) after treatment with excess ACVA.
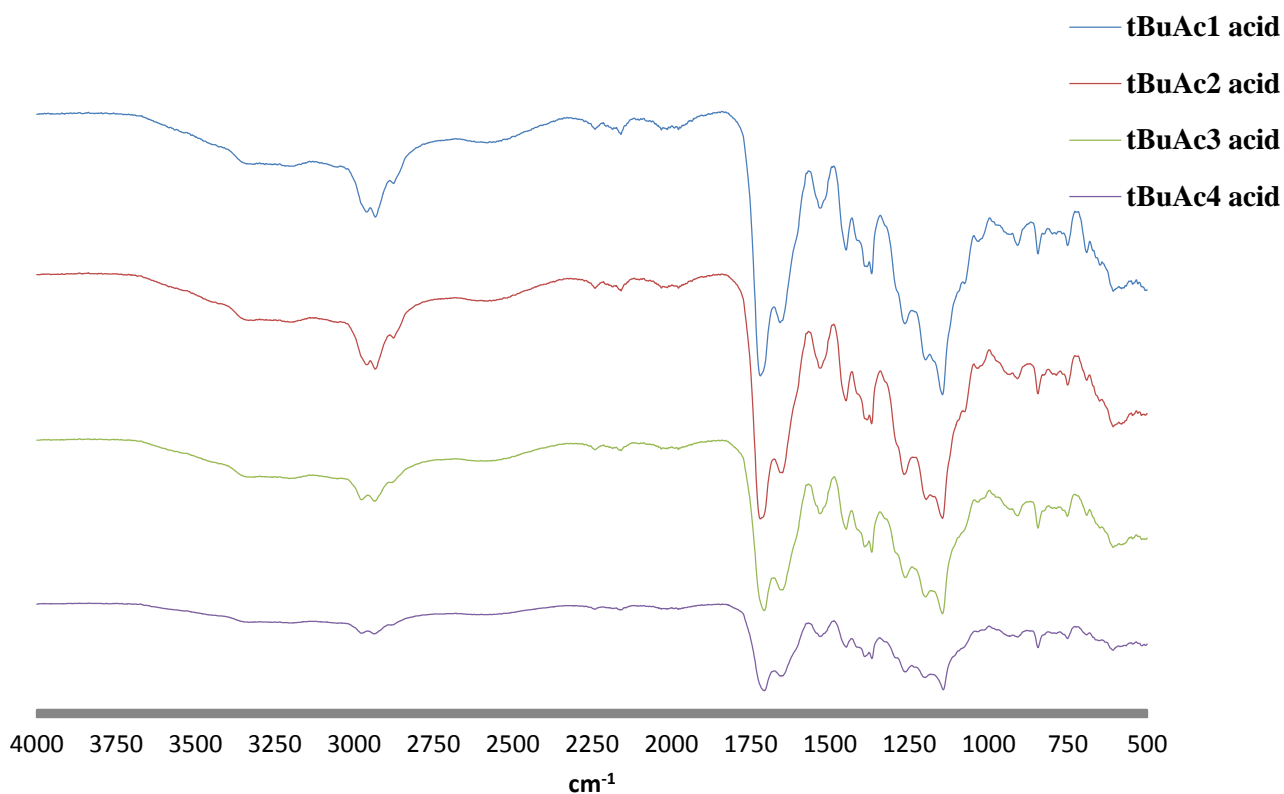
Figure 4.2.2.2 – FT-IR of hyperbranched polymers (*t*BuAc1-4 acid) after treatment with excess ACVA.

As can be seen in figure 4.2.2.2, after work up with the acid-donor group, new weak signals can be observed at 2220cm^{-1} which can be assigned to C≡N in the ACVA molecule. The broad signals at 3000-3500 can be attributed the OH group of carboxylic acid and its associated H bonding. Meanwhile, the signal seen at 2900cm^{-1} arises from the sp^3 carbons of the *t*-butyl acrylate monomer. FT-IR therefore further confirms that all four of the *t*-butyl acrylate polymers were successfully coupled with ACVA.

The hyperbranched polymers were embedded in UV-cured hydrogels using the monomer *n*-butyl acrylate and the crosslinker ethylene glycol dimethacrylate (EGDMA). For recipe details see experimental section 4.4.4 and scheme 4.2.2.3.
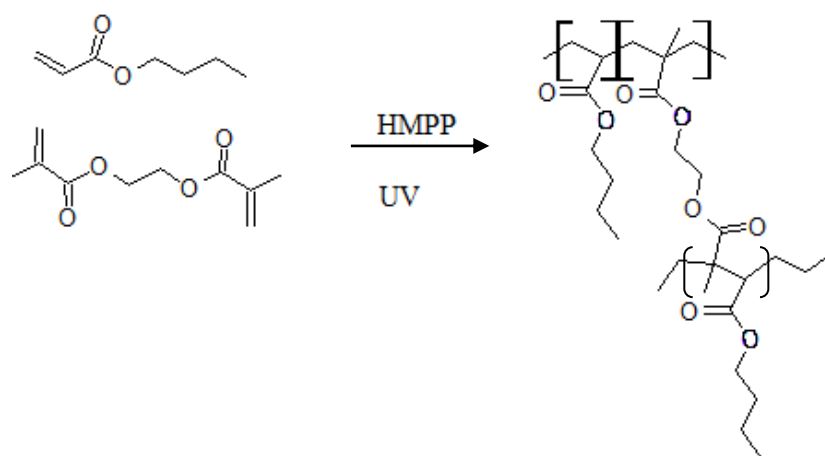
Scheme 4.2.2.3 – Scheme showing the formation of poly(*n*-butyl acrylate) hydrogel network with ethyleneglycol dimethacrylate cross-linker.

The aim was to use a process between the sequential and simultaneous methods to form semi-IPNs by dissolving the hyperbranched polymers in the polymerisation solvent and then forming the crosslinked networks around them. A summary of the networks formed and their properties is shown in table 4.2.2.4.

*n*BuAc /g	DVB /g	EGDMA /g	IPA /mL	HBP /g	HMPP /mg	Properties
3.2	0.3	0	1	0.7	40	Slightly yellow gel, very brittle and crumbled.
3.2	0.3	0	1	0	20	Clear, brittle gel that curled and broke.
3.2	0.15	0	1	0	20	Clear, less brittle gel, sticky.
3.2	0	0.5	1	0	20	Clear, less brittle again, some breakage.
3.2	0	0.25	1	0	20	Clear, not brittle but sticky.
3.2	0.15	0	1	0.5	20	Yellow gel. Slightly brittle, not sticky
3.2	0	0.25	1	0.5	20	Yellow gel. Not brittle or sticky.

Table 4.2.2.4 – Composition and properties of synthesised networks and sem-IPNs.

It was found that the inclusion of HB(*t*BuAc) enhanced the mechanical properties over single network gels. Semi-IPNs were found to increase the rigidity and decrease the 'stickiness' when compared to the single network analogue. This is due to a hardening of the gels, as the HBP is incorporated into the network and reinforces the structure through non-covalent interactions.

The cured gels were washed in isopropyl alcohol overnight in order to remove any residual monomer. However, figure 4.2.2.5 illustrates that the 'embedded' polymer leached from the network over 24 hours. This can be observed as a colour change in the solvent, as the coloured HBP leaves the clear network.
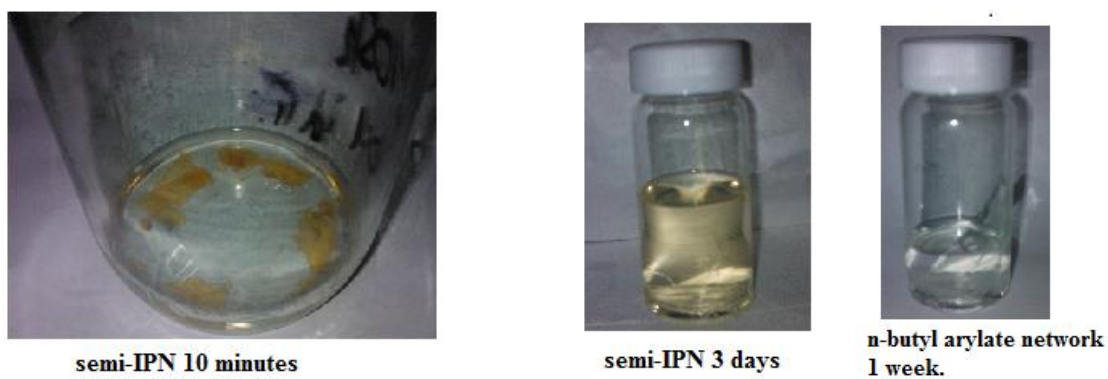
Figure 4.2.2.5 – Photos illustrating the permeation of HB(tBuAc) out of a *n*-butyl acrylate, into the washing solvent (IPA).

As the semi-IPNs were unable to maintain their composition, this route was abandoned and no cell culture work was performed on the gels.

NMR analysis also confirmed the presence of polymer in the isopropanol after a 16 hour wash. It may be possible to embed the hyperbranched polymers with further adjustment of the hydrogel composition, but due to time constraints cell studies were simply performed on films of the HBPs.

4.2.3 Cell contact studies

Human Dermal Fibroblasts

Human dermal fibroblasts were cultured for 72 hours in direct contact with polymer films in order to investigate cell adhesion and proliferation. Cell health was monitored using the Alamarblue™ viability assay and optical microscopy.

Figure 4.2.3.1 shows the cell viability on all materials after 72 hours and it is possible to see a stark contrast between the functionalised and unfunctionalised materials.
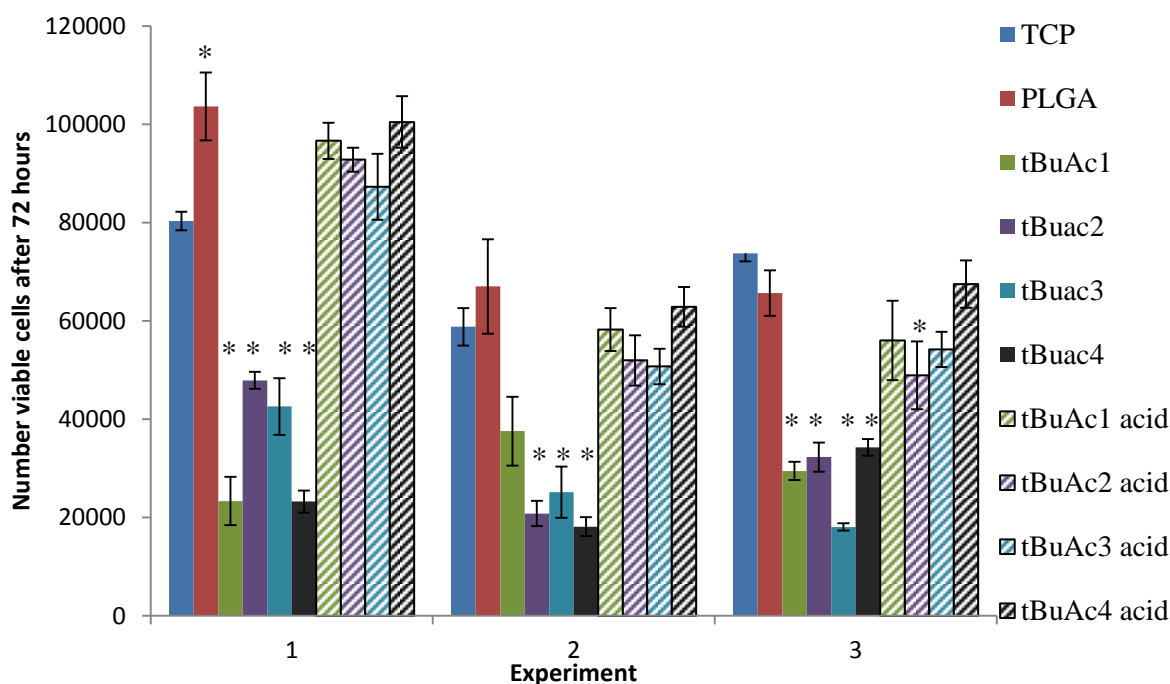
Figure 4.2.3.1 – Human dermal fibroblast viability after 72 hours culture in direct culture with HP(tBuAc)s with carbodithioate (*t*BuAc1-4) or acid (*t*BuAc1-4 acid) functionality. One-way analysis of variance and post-hoc Tukey's statistical analysis performed, significant values relative to TCP marked with *.

In experiment 1 it can be seen that the acid functional polymers have greater average fibroblast viability than TCP. This is to be contrasted with the carbodithioate functional HBpolymers which have not experienced the same levels of cell proliferation. In fact, the polymers *t*BuAc1-4 perform significantly poorly in all three of the experiments, with average viabilities lower than TCP and the acid functional HBPs. This indicates, as in Chapter 3, that fibroblast adherence and proliferation is encouraged with the incorporation of carboxylic acid into the substrate. It is not possible to tell from these results if there is any variance of fibroblast viability between the acid HBPs.

Optical microscopy was performed after 24 hours (phase contrast microscope) and 72 hours (inverted microscope), in order to compare the fibroblast health and confluence between the different substrates. Higher magnification images are also able to show indicators such as morphology and nuclei size that are extremely important in discussions of cell health.

Figure 4.2.3.2 shows the images of the native acrylate polymers and TCP after 24 and 72 hours. It can be seen that after 24 hours, polymers *t*BuAc1, 2 and 3 have a comparable amount of cell adherence to TCP. After 72 hours the number of cells on the TCP has

increased as expected, and this pattern also occurs on the *t*BuAc1 and *t*BuAc3 substrates although there are fewer cells overall than visible on TCP. After 72 hours a reduction in cell number can be seen on the substrate *t*BuAc2 and some degradation (the appearance of holes) is apparent on the polymer film. This could be the consequence of polymer being broken down by the cells. *t*BuAc3 also appears to have suffered some degradation of the polymer, although fibroblasts are present on the remaining polymer. Dead cells are visible after 24 hours on the *t*BuAc4 polymer, and these are seen as small white specks on the image. Poor adherence was also seen after 72 hours on this polymer, although interference from the polymer did reduce the quality of the image.

Figure 4.2.3.3 compares the proliferation of fibroblasts on the acid functional HB polymers after 24 and 72 hours. Images for *t*BuAc3 and 4 acid functional polymers were not possible after 24hours as the polymer interfered with the image quality of the phase contrast microscope. After 72 hours, however, high confluence growth is seen on the *t*BuAc1, 2 and 4 polymers. In fact, these substrates appear to have a greater confluence than the TCP control. The *t*BuAc3 acid functionalised does not appear to have as many adhered cells. This could be a consequence of the low molar mass of *t*BuAc3 leading to cytotoxic effects.

Figure 4.2.3.4 shows higher magnification images of fibroblasts on each of the substrates. The cells on the acidic polymers *t*BuAc1 and 2 were not easily imaged due to staining of the polymer, but no abnormalities seem apparent. The fibroblast cells on the carbodithioate materials have a generally healthy morphology as do those cultured on the acid functional derivatives of *t*BuAc1 2 and 4. The cells cultured on the *t*BuAc3 acid substrate appear to have enlarged nuclei; further evidence that this polymer has a cytotoxic effect.

From the Alamarblue® and microscopy data, it can be suggested that *t*BuAc4 is the most promising functionalised polymer as a cell culture substrate. *t*BuAc4 had the high molar mass and the broadest MMD, and this suggests that the combination of a higher molecular weight polymer to form the structure of the film with lower molar mass chains with numerous functional groups that are able to migrate to the surface is advantageous.

It is believed that the acid functionalised polymers show better cell viability due to the hydrophilic carboxylic acid group which migrates to the surface of the film. This group is able to form essential hydrogen bonds and creates the preferred amphiphilic environment for cell adhesion.

Figure 4.2.3.2- Images comparing fibroblast adhesion on HB(*t*-butyl methacrylate) polymers (*t*BuAc1-4) and TCP after 24 and 72 hours at 4x magnification. 24 hours= phase contrast, red circles indicate adhered cells. 72 hours = cells fixed and stained with Giemsa solution.

24 hours	72 hours	
		*t*BuAc1 A
		*t*BuAc2 A
Unable to image.		*t*BuAc3 A
Unable to image.		*t*BuAc4 A
		TCP
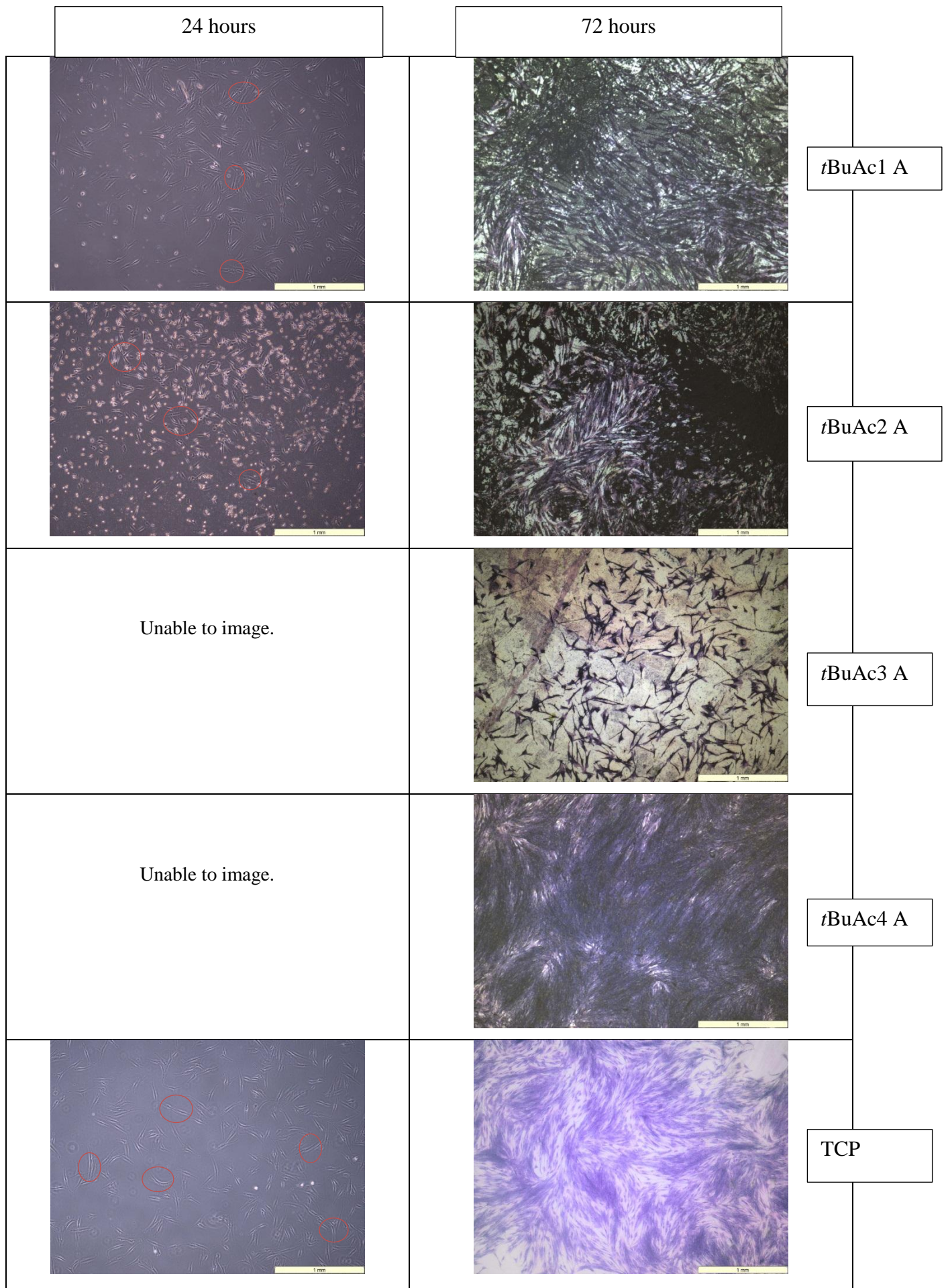
Figure 4.2.3.3- Images comparing fibroblast adhesion on acid functionalised HB(*t*-butyl acrylate) polymers (*t*BuAc1-4A) and TCP after 24 and 72 hours at 4x magnification. 24 hours= phase contrast, red circles indicate adhered cells. 72 hours = cells fixed and stained with Giemsa solution.

	Carbodithionate	Acid	
			tBuAc1
			tBuAc2
			tBuAc3
			tBuAc4
			PLGA, TCP
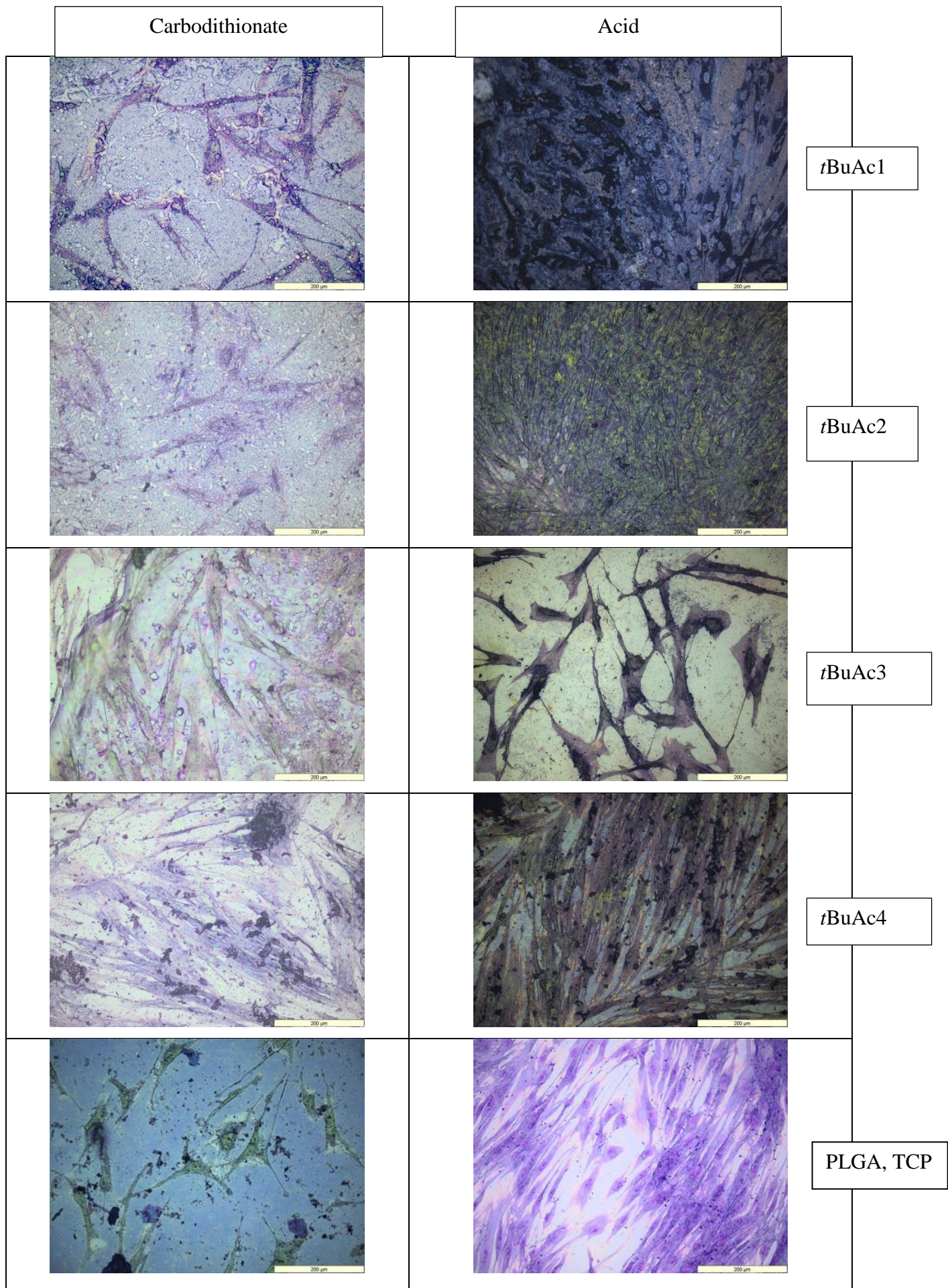
Figure 4.2.3.4- Images comparing fibroblast adhesion on HB(*t*-butyl acrylate) polymers (*t*BuAc1-4) with carbodithioate or acid end groupds, TCP and PLGA after 72 hours at 20x magnification. Cells fixed and stained with Giemsa solution.

Human Renal Epithelial Cells

Renal epithelial cells were cultured on hyperbranched materials for three days, as all previous experiments. The purpose was to compare the growth between the native and acid-functionalised polymers, and to see if the *t*-butyl acrylate monomer had an effect on cytocompatibility. The cell viability results in figure 4.2.3.2 show that compared to the tissue culture plastic, very few of the results were significant. However, this is not a necessarily negative result as it indicates that almost all of these materials could show potential as a cell culture substrate for this cell type.
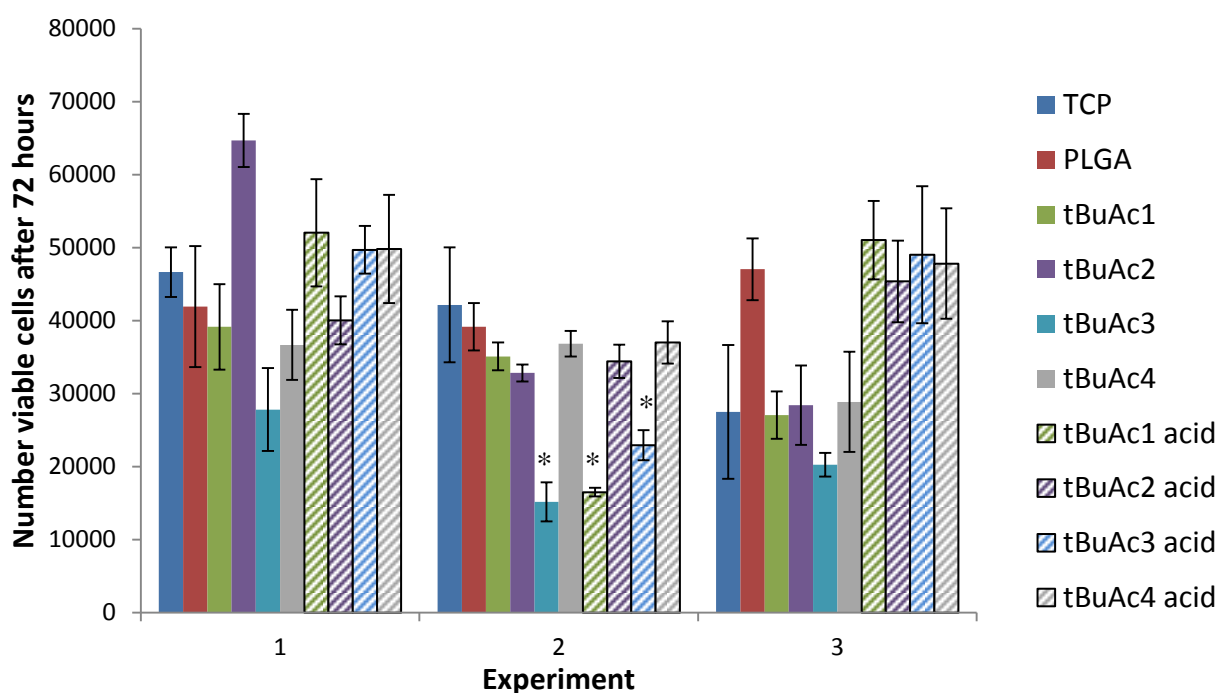
Figure 4.2.3.5 – Human renal epithelial cell viability after 72 hours culture in direct contact with HB(*t*BuAc) with carbodithionate (*t*BuAc1-4) or acid (*t*BuAc1-4 acid) functionality. One-way analysis of variance and post-hoc Tukey's statistical analysis performed, significant values relative to TCP marked with *.

From these results, the epithelial cells appear to have proliferated about equally well on all of the substrates across the 3 experiments. Experiment 1 shows that *t*BuAc2 performs the best, wth an average viability greater than TCP, whilst *t*BuAc3 has the lowest average viabilty. In experiment 2, two of the acid polymers and *t*BuAc2 were found to perform significantly worse than TCP. All of the acid functional films had greater average viabilities than TCP in experiment 3, and this indicates that –like fibroblasts- renal epithelia do exhibit some

preference for an acidic comonomer with *t*-butyl acrylate. Pictures were taken with an optical microscope after 24 and 72 hours of culture in order to visually assess the cells. Figure 4.2.3.6 shows the growth of epithelial cells on CTA2 end group HBPs after 24 and 72 hours. There is some good initial cell adhesion observed on *t*BuAc1 after 24 hours, but proliferation has not occurred and there are only sparse cells present after 72 hours culture. *t*BuAc2 appears to have reasonable cell adhesion after 24 hours, that has proliferated in the 72 hour image. The cells on this polymer have well defined nuclei and cytoplasm and appear to be approaching confluence. Both *t*BuAc3 and 4 show poor initial cell adhesion, and as expected there is little cell growth after 72 hours. These images do not fit harmoniously with the results obtained from the Alamarblue® assay. This could be because of the higher metabolic activity of a few cells.

The cells imaged on the acid functionalised polymers are shown in Figure 4.2.3.7. After 24 hours there is a high percentage of dead cells – visible as white dots - on all four polymers, and little proliferation is seen after 72 hours. The polymer with the most visible cell proliferation is *t*BuAc4 acid, although it still performs poorly when compared to the epithelial cells observed on the TCP.

Higher magnification images (figure 4.2.3.8) show that the cells on *t*BuAc4 acid have a healthy morphology, as do the cells culture on *t*BuAc1 and 2, with carbodithioate end groups. However, the cells on the acid functional *t*BuAc1, 2 and 3 appear to be contracted and dying or becoming unadhered. This again implies that the inclusion of an acid comonomer is not essential, and may even be detrimental, for the adhesion and growth of epithelial cells.

The cell images presented appear to indicate that proliferation as suggested by the Alamarblue® assay has not occurred. This could be due to contamination during the assay, although bacteria would also have been visible using the staining techniques performed.
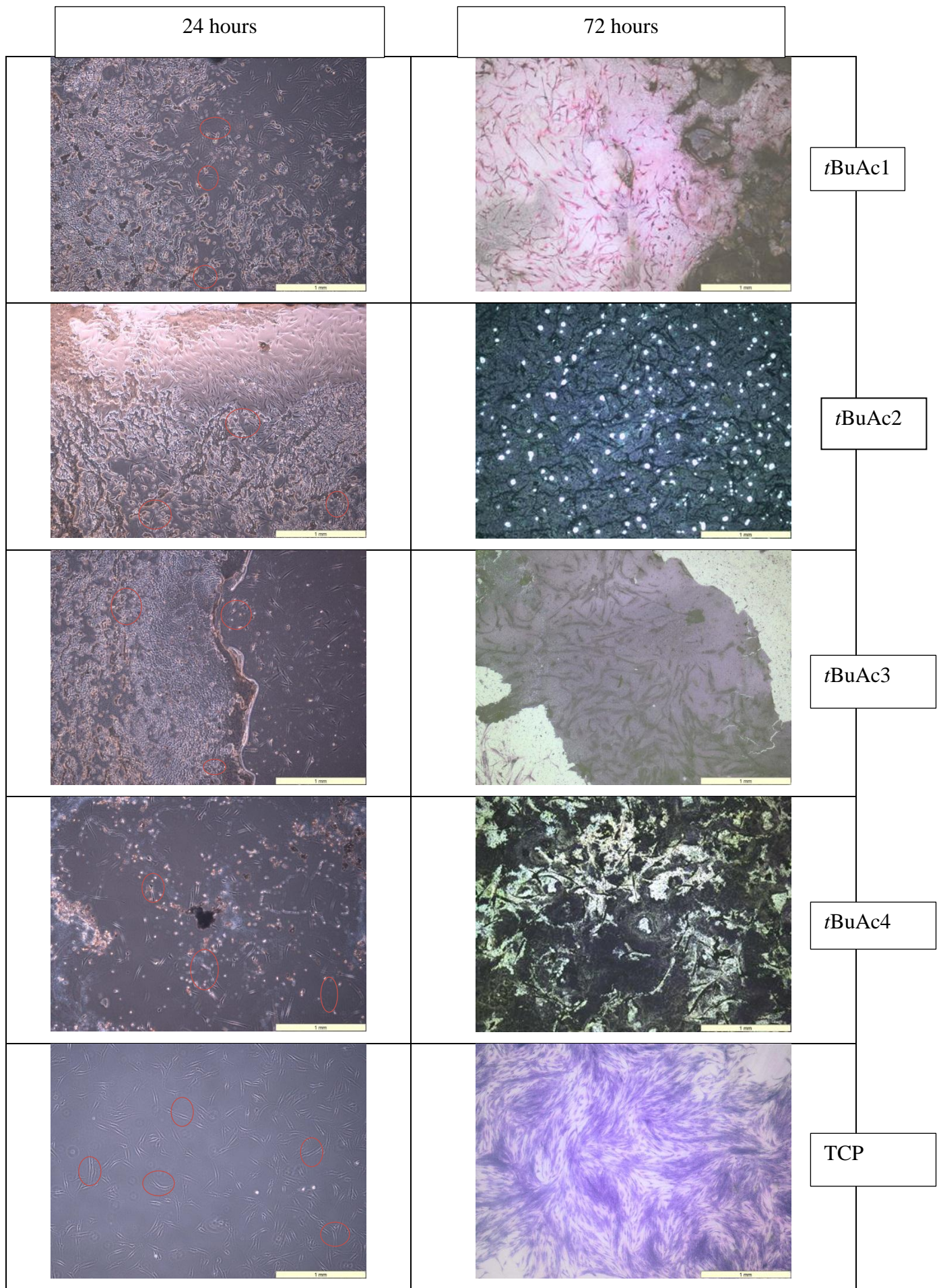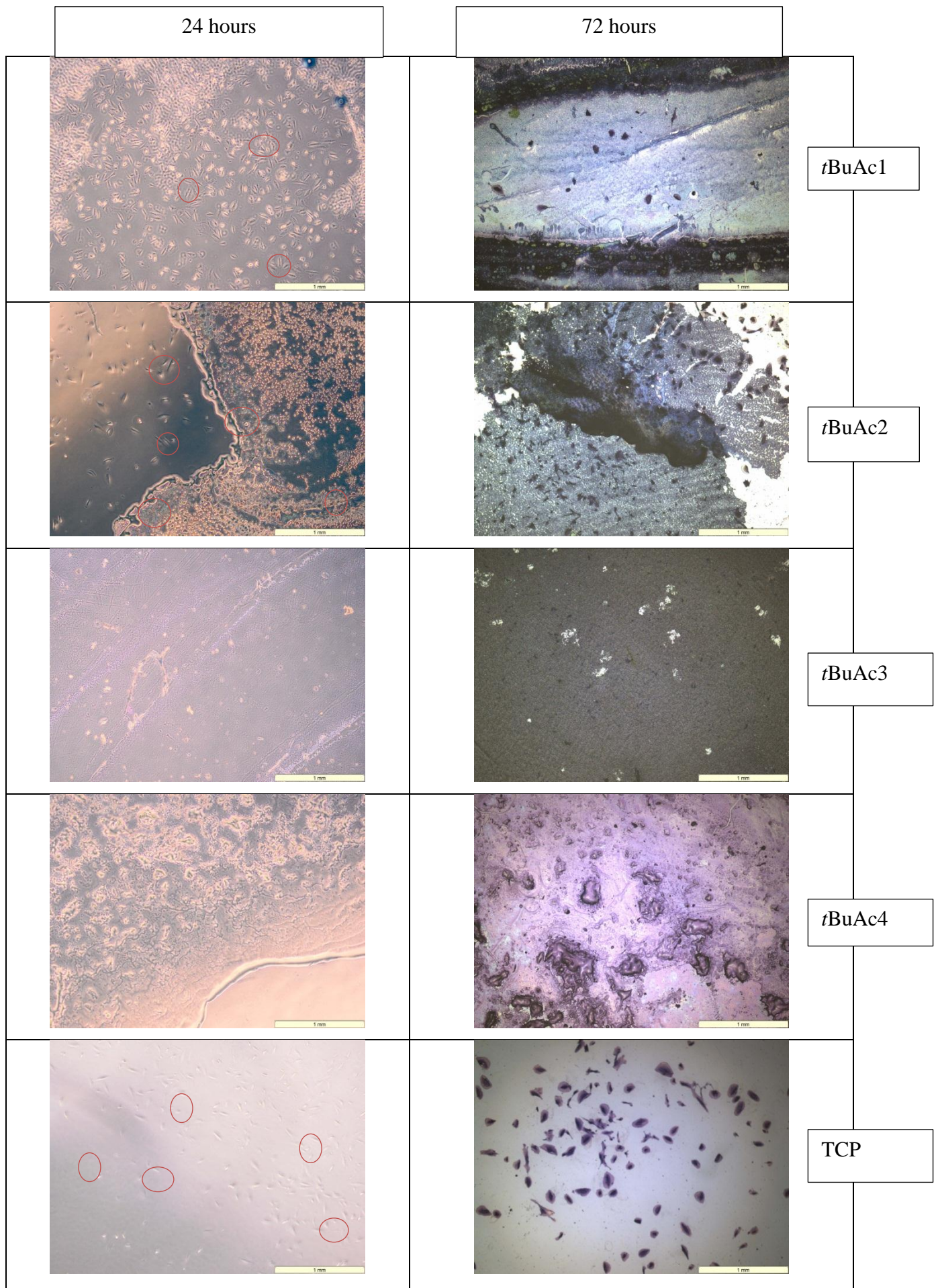
Figure 4.2.3.6- Images comparing epithelial adhesion on HB(*t*-butyl acrylate) polymers (*t*BuAc1-4) and TCP after 24 and 72 hours at 4x magnification. 24 hours= phase contrast, red circles indicate adhered cells. 72 hours = cells fixed and stained with Giemsa solution.

24 hours	72 hours	
		tBuAc1 A
		tBuAc2 A
		tBuAc3 A
		tBuAc4 A
		PLGA
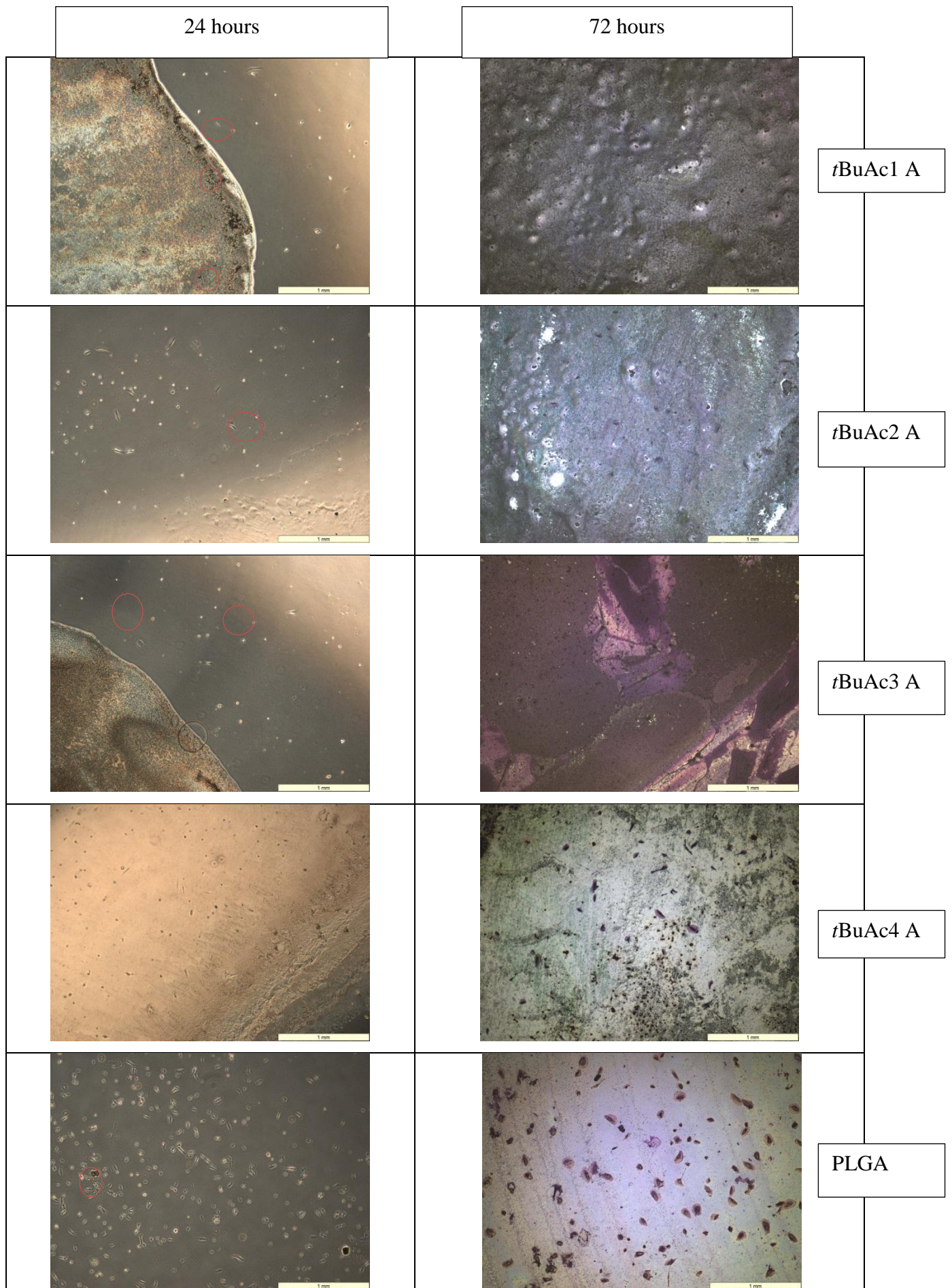
Figure 4.2.3.7 - Images comparing epithelial adhesion on acid functionalised HB(*t*-butyl acrylate) polymers (*t*BuAc1-4 A) and TCP after 24 and 72 hours at 4x magnification. 24 hours= phase contrast, red circles indicate adhered cells. 72 hours = cells fixed and stained with Giemsa solution.

	Carbodithionate	Acid	
			*t*BuAc1
			*t*BuAc2
			*t*BuAc3
			*t*BuAc4
			PLGA/TCP
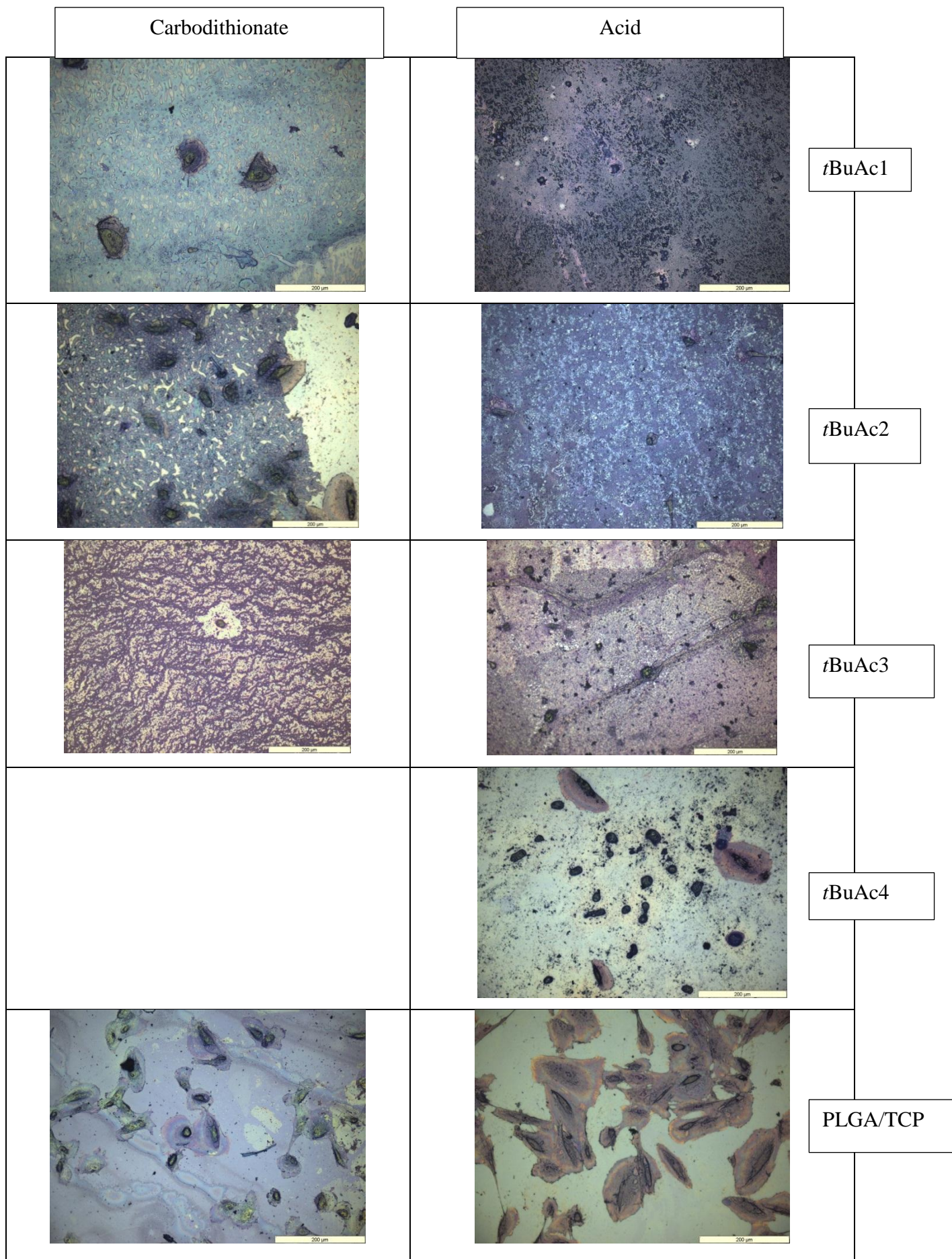
Figure 4.2.3.8 - Images comparing epithelial adhesion on HB(*t*-butyl acrylate) polymers (*t*BuAc1-4), TCP and PLGA after 72 hours at 20x magnification. Cells fixed and stained with Giemsa solution.

4.3 Conclusions

The main aim of this work was to show the successful RAFT polymerisation of *t*-butyl acrylate, and to examine the cytocompatibility before and after hydrolysis of the monomer. The chain transfer agent, CTA2, was especially chosen so that it could also act as a branching agent in the formation of hyperbranched polymers. Four polymers were synthesised with different ratios of monomer:CTA2. The polymer *t*Buac2 showed almost complete conversion of the monomer, whilst *t*BuAc3 and 4 had very low monomer conversion. Elemental analysis of *t*BuAc2 show that it has the lowest level of CTA2 than any of the other polymers, and it also has the broadest molar mass distribution. It is difficult to pinpoint the exact cause of this, as each polymer was made with different levels of monomer, initiator and CTA2.

Despite the lower level of monomer conversion of the polymers *t*BuAc1 and 3, there was still evidence of branching by looking at the Mark-Houwink equation and through the incorporation of CTA2. This is contrary to what is reported in the literature, where it is said that polymers tend to stay linear until higher conversion levels and then begin to branch later in the reaction[257], [258].

All of the synthesised polymers were successfully reacted with ACVA in order to produce HBPs with carboxylic acid end groups. The low molecular weight of the HBPs may subsequently lead to less hindrance and easier access to the polymer end groups.

The incorporation of HBPs into semi-IPNs was not successful. The un-crosslinked polymer could be seen to leech out of the gels over 3 days. However, despite this proof-of-concept was provided as the gels with incorporated HBPs were seen to have beneficial qualities over the single network. This was observed as the gels being less 'sticky' and more rigid.

The cell proliferation assay indicated that fibroblasts have a strong preference for acid functionalised polymers. Fibroblast cells were also seen to adhere and proliferate to all of the polymers tested – both with dithiobenzoate and carboxylic acid end groups. The acid functional derivative of *t*BuAc4 showed the healthiest and most prolific cell growth and it also had the greatest molecular weight as determined by GPC. As previously discussed, low molecular weight polymers can be toxic in their own right[259]. From these results, the synthesised acid functional polymers could be further optimised as fibroblast cell culture substrates.

In contrast, however, renal epithelial cell culture showed a stronger preference for the dithiobenzoate functional polymers. The epithelial cells were seen to both adhere and

proliferate on the dithiobenzoate in a comparable manner to TCP. Epithelials cultured on the acid functional HBPs showed very little to no adherence and proliferation over 72 hours. High magnification images were hampered by polymer staining but the dithiobenzoate polymer *t*BuAc2 did display healthy epithelial growth.

This work has shown that *t*-butyl acrylate can be successfully polymerised using RAFT and dithiobenzoate CTA. The HBPs were all successfully reacted with ACVA to remove the dithiobenzoate group remaining after the polymerisation and replace it with carboxylic acid functionality. Culture with fibroblast cells indicates that these acid functional polymers could be used as cell culture substrates, but none of the polymers were a good substrate for epithelial cells.

4.4 Experimental

Instrumentation used as described in chapter 2.4.

4.4.1 Synthesis of RAFT chain transfer agent: 4-vinylbenzyldithiobenzoate

Materials

Bromobenzene (99%, Aldrich), magnesium turnings (99.95%, Aldrich), carbon disulfide (99+%, Aldrich), 4-vinylbenzyl chloride (90%, Aldrich), diethyl ether (Fischer), hexane (Fischer), ethyl acetate (Fischer) were used as recieved.

THF was obtained from a Grubb's dry solvent system.

Method

A three-necked round bottom flask was equipped with a condenser and bubbler, pressure equalising dropping funnel and a nitrogen inlet. Magnesium turnings (1.7 g) and a magnetic stirrer bar were added to the flask, which was then gently heated and stirred under a nitrogen environment for 40 minutes. The flask was left to cool to room temperature, before the dropwise addition of bromobenzene (10 g) in THF (40 mL) over 30 minutes. Gentle heat was provided to instigate the exothermic reaction, and cooling via an ice bath was provided as required. A green solution was formed, which was left to stir for 30 minutes at room temperature.

Carbon disulfide (5 g) and THF (30 mL) were then added dropwise over 10minutes, and an orange to red colour change of the reaction solution was observed. The flask contents were cooled to 0 °C using an ice bath and stirred for 30 minutes, before being heated to 50 °C and stirred for a further 30 minutes. At this higher temperature, 4-vinylbenzyl chloride (10 g) in THF (30 mL) was added dropwise over 10 minutes.

The solution was left to cool to room temperature and stirred overnight. The red liquid product was placed in a 1 L separating funnel, with diethyl ether (80 mL) and distilled water (80 mL). The organic layer was recovered and the aqueous layer was extracted with diethyl ether (3 x 100 mL). The organic extracts were combined and dried over magnesium sulfate before filtration and the solvent was removed by rotary evaporation to give a red oil.

The oil was purified by flash chromatography, with a column of 6cm diameter, using 0.5-2 % hexane in ethyl acetate. The solvent was removed was removed by rotary evaporation to give 5.6 g of a red oil. The product was stored at -18 ˚C.

Elemental analysis: C: 70.6%, H: 5.9%, N: 0%, S:23.5%.
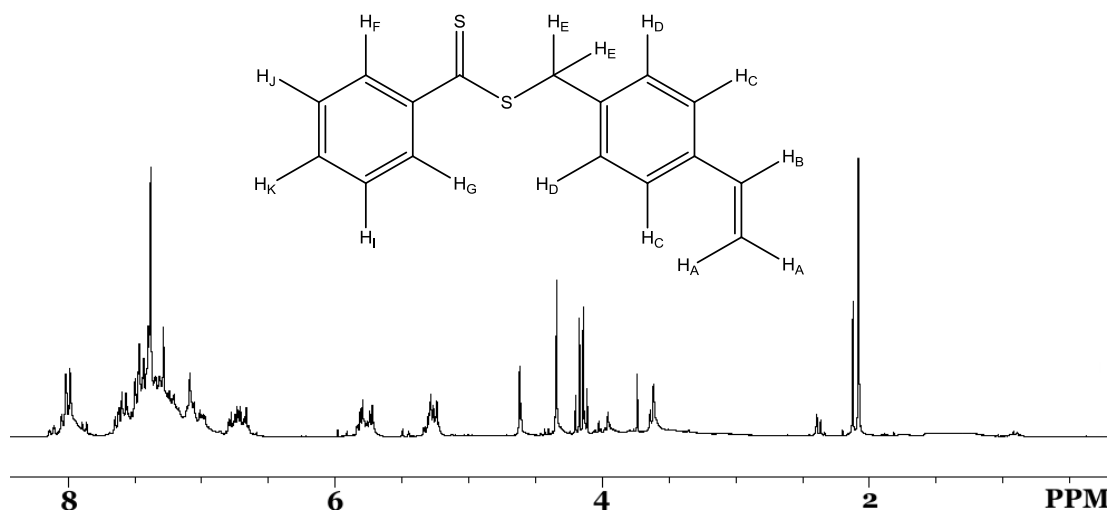
Figure 4.4.1.2 – ^{1}H NMR of 4-vinylbenzyl dithiobenzoate (250 MHz, *CDCl$_3$*) δppm 4.33 (H$_E$), 5.28 (H$_A$), 5.79 (H$_A$), 6.70 (H$_B$), 7.08 (H$_D$), 7.28 (H$_C$), 7.38 (H$_J$), 7.53 (H$_I$, H$_K$), 7.98 (H$_F$, H$_G$).

4.4.2 RAFT polymerisation of *t*-butyl acrylate using 4-vinylbenzyl dithiobenzoate chain transfer agent

Materials

4-Vinylbenzyl dithiobenzoate (produced as previously described), *t*-butyl acrylate (98%, Aldrich), 4,4'-azobis 4-cyanovaleric acid (ACVA, ≥98%, Aldrich), 1,4-dioxane (anhydrous, 99.8%, Sigma-Aldrich), methanol (Fisher) were used as recieved.

Equipment

Ampoules were degassed on a high vacuum line equipped with a Pirani gauge.

Method

4-Vinylbenzyl dithiobenzoate, *t*-butyl acrylate, dioxane (25 mL) and ACVA were mixed together until the solid initiator had dissolved. The resulting solution was pipetted into a 50 mL ampoule and placed onto the vacuum line but was not exposed to vacuum. The solution was frozen using liquid nitrogen and then opened to the vacuum until the gauge dropped to a steady output. The ampoule's exposure to vacuum was then ceased as its contents were left to thaw. Once thawing was completed, the full process was repeated until a negligible rise in pressure was observed when the ampoule was opened to vacuum. The end pressure in the ampoule was approximately 3×10^{-3} mBar. The ampoule was sealed using a gas/oxygen blowtorch and placed in a water bath at 60°C for up to 24 hrs to undergo polymerisation.

Table 4.4.2.1 summarises the quantities of reagents used.

t-**Butyl acrylate /mL**	**Chain transfer agent /mL**	**ACVA /g**
5 (0.034)	1 (4.0×10^{-3})	0.025 (8.9×10^{-5})
10 (0.068)	1 (4.0×10^{-3})	0.025 (8.9×10^{-5})
15 (0.1)	1 (4.0×10^{-3})	0.025 (8.9×10^{-5})
20 (0.14)	1 (4.0×10^{-3})	0.025 (8.9×10^{-5})
5 (0.034)	1 (4.0×10^{-3})	1.29 (4.6×10^{-3})
10 (0.068)	1 (4.0×10^{-3})	1.29 (4.6×10^{-3})
15 (0.1)	1 (4.0×10^{-3})	1.29 (4.6×10^{-3})
20 (0.14)	1 (4.0×10^{-3})	1.29 (4.6×10^{-3})
15 (0.1)	1 (4.0×10^{-3})	0.65 (2.3×10^{-3})
20 (0.14)	1 (4.0×10^{-3})	0.65 (2.3×10^{-3})

Table 4.4.2.1 – summary of reagent quantities used in RAFT polymerisation of *t*-Butyl acrylate. Moles shown in parenthesis.

Products were precipitated by transferring into 4x by volume of methanol and leaving to stand, followed by filtering and drying in a vacuum oven producing an orange solid. Dried products were stored in closed sample tubes at room temperature.

4.4.3 Reaction of hyperbranched *t*-butylacrylate polymers with excess ACVA

Materials

Acetone (HPLC grade, Fisher), ethanol (absolute, Fisher), methanol (HPLC grade, Fisher), ultrapure water (18.8Ω, MilliQ systems), HBP(*t*-butyl acrylate) synthesised as described in 4.4.2 and 4,4'-azobis 4-cyanovaleric acid (ACVA, ≥98%, Aldrich) were used as received. Dimethyl formamide (DMF) was obtained from the Grubb's dry solvent system.

Method

A three necked round bottom flask was equipped with a magnetic stirrer, nitrogen inlet and a condenser. The apparatus was nitrogen purged and heated to 60 °C. A known amount of polymer was dissolved in dry DMF and then injected into the warm, dry flask which was kept under a nitrogen atmosphere. 60 molar equivalents of ACVA were then dissolved in 10-15mL DMF (up to 1 minute of sonication was used to assist dissolution) and this was then injected into in the flask. The solution was stirred for 16hours at 60 °C before the addition of another 60molar equivalents of ACVA. This process was repeated for four additions.

The polymer was purified from ACVA by first removing the DMF under reduced pressure. The solid polymer was then dissolved in ultrapure water (MilliQ) and waste ACVA was removed via vacuum filtration. The polymer was washed with methanol and then further purified by ultrafiltration through a 3 kDa cellulose membrane using a solvent system of 9:1 acetone:ethanol.

The reaction was deemed successful when elemental analysis showed no sulfur present in the final product, indicating the complete removal of the carbodithioate groups.

4.4.4 Embedding of hyperbranched polymers into semi-interpenetrating networks

Materials

HBP(*t*-butyl acrylate) as synthesised in 4.4.4.2, isopropanol (IPA, absolute, Fisher), *n*-butyl acrylate (>99%, Aldrich), 2-hydroxy-2-methylpropiophenone (HMPP, 97%, Aldrich), divinyl benzene (80%, Aldrich), ethylene glycol dimethacrylate (98%, Aldrich) were used as received.

Preparation of semi-IPNs

The monomers were mixed together in the ratios shown in table 4.4.1 and flushed with nitrogen for 30 minutes, and at the same time the HBP was dissolved in isopropanol and also nitrogen flushed.

nBuAc /g	DVB /g	EGDMA /g	IPA /mL	HBP /g	HMPP /mg	Properties
3.2	0.3	0	1	0.7	40	Slightly yellow gel, very brittle and crumbled.
3.2	0.3	0	1	0	20	Clear, brittle gel that curled and broke.
3.2	0.15	0	1	0	20	Clear, less brittle gel, sticky.
3.2	0	0.5	1	0	20	Clear, less brittle again, some breakage.
3.2	0	0.25	1	0	20	Clear, not brittle but sticky.
3.2	0.15	0	1	0.5	20	Yellow gel. Slightly brittle, not sticky
3.2	0	0.25	1	0.5	20	Yellow gel. Not brittle or sticky.

Table 4.4.4.1 – Quantities of monomers used in the synthesis of hydrogels and sem-IPNs.

The polymerisation mould was constructed from two 4mm glass sheets, covered with 100μm PET film fixed using the minimum amount of Spray-Mount® (3-M) adhesive. A 500μm PTFE spacer was used to separate the plates, leaving a gap into which the polymerisation mixture was injected. The mould was secured around all edges using crocodile clips. The monomer and HBP mixtures were then combined, and finally the initiator (HMPP) was added. This solution was then quickly transferred into the mould using a syringe. The polymerisation was performed in a UV oven over 150secs, turning the mould every 30sec until a gel had been formed.

The semi-IPN was then removed from the mould and washed with IPA for 24 hours, before being stored in IPA. The hydrating solvent was replaced every 7 days thereon.

4.4.5 Culture of cells in direct contact with polymers

Materials

Human dermal fibroblasts and human renal epithelial were cultured and prepared as described in chapter 2.

Hyperbranched tbutyl acrylate (tBuAc1-4) as synthesised in section 4.4.2, and with acid end groups as described in section 4.4.3 (tBuAc1-4 acid). isopropanol (absolute, Fisher), complete media (prepared as described in chapter 2), trypsin-EDTA (Life Technologies), PLGA (50:50, Polysciences), DMSO (Anhydrous, Sigma), Alamarblue® (Life Technologies), phosphate buffered saline (Bioreagent, Sigma), hematoxylin solution according to Weigert (parts A and B, Aldrich), eosin y (99%, Sigma Aldrich), 10% neutral buffered formalin solution (Sigma), giemsa stain modified solution (Sigma), ethanol (absolute, Fisher), glacial acetic acid (99%, Fisher) were used as received. Distilled water was used throughout unless otherwise specified.

Equipment

IR spot lamp 75W (Exo Terra), glass coverslip (22x22mm, Menzel).
Glass coverslips were sterilised by autoclave.

Preparation of polymer films and cell seeding

Polymers were dissolved in the solvents listed in table 4.4.5.1 at a concentration of 5 mg/mL. The polymer solutions were well agitated and sonicated for up to 30 seconds if required.

Solvent	Polymer
Tetrahydrofuran	*t*BuAc1-4
Dimethylsulfoxide	PLGA
Ethanol	*t*BuAc1-3 acid

Table 4.4.5.1. – Solvents used to solvate the various polymers prior to casting on glass slips.

100mL of polymer solution was then pipetted onto each glass coverslip. An IR lamp was used to heat treat the polymer films until the solvent appeared visibly removed. At this point, each covered slip was placed into its own well of a six well plate and washed with sterile PBS to remove any residual solvent.

Fibroblasts or epithelial cells were treated with trypsin as per the protocol for passage, but instead of re-seeding into T-75 flasks, they were seeded directly onto the films at a density 1×10^4 cells/well. 2 mL of complete media was added to each well and the cells were incubated for 24 hours at 37ºC, 5% CO_2. After 24 hours phase contrast imaging and a full media change was performed. After 72 hours cells were assayed and fixed for staining using the methods in chapter 2.

5 - Overall conclusions and future work

The aim of this thesis was to develop new synthetic procedures for hyperbranched polymers, and also further our understanding into how imposing end group functionality can impact upon biocompatibility. Other properties that were assessed were polymer mass and degree of branching.

The greatest challenge in the synthesis of oligo(BMA) laid with the initial copolymerisation with butadiene. A series of experiements were performed in an unpressurised reactor, allowing the determination of optimal reaction conditions. It was found that the use of α- or β-cyclodextrin and a carefully controlled reaction temperature of 75-80 °C was essential for copolymerisation to occur. The amount of cyclodextrin included in the reaction was not found to have any significant effect above 0.003 moles; this is because cyclodextrin acts as a carrier molecule for butadiene and is not used up during the course of the polymerisation. The presence of cyclodextrin contaminant in the final product is not a barrier to cell based studies as these molecules do possess some cytocompatibility.

The copolymer was successfully cleaved at the sites of 1,4-butadiene insertion using the well-established technique of ozonolysis and oxidative cleavage. The creation of oligomers in this way allowed further reaction of the end groups to carboxylic acid and diamine functionality. GPC confirmed the successful polymer cleavage as the oligomers had a decrease in molecular weight and FT-IR and elemental analysis was used to confirm the end group functionality.

Cell adhesion studies of oligomers with fibroblast and epithelial cells showed that different functionality is preferred by different cell types. When cultured on the synthesised materials, fibroblast cells showed the greatest proliferation on the acid functionalised oligomer whilst epithelial cells performed best on the 1,6-amidated oligomer. This is most likely due to differences in protein expression which are observed as variances in adhesion mechanism and ECM formation. None of the oligomers showed as great cell adhesion as the control materials TCP and PLGA – indicating that further work is required to produce fully biocompatible oligomers.

Hyperbranched polymers of *n*-butyl methacrylate and t-butyl acrylate were produced using RAFT polymerisation via two different chain transfer agents (CTA1 and 2).

Again a series of polymerisations were performed and the optimal amount of CTA1 in the polymerisation with BMA was found to be 4%, which gave almost total monomer conversion. CTA2, a benzyl carbodithioate, was employed with the tBuAc monomer. These polymerisations had relatively low conversion and it is believed this is due to a retardation effect that is experienced when copolymerising acrylates with a benzyl CTA. During the polymerisation of mixes with higher levels of monomer, gelation indicated the occurance of cross-linking and therefore the amount of initiator in the feed was decreased.

Triple detection GPC was successfully used to substantiate the claimed hyperbranched structure of the polymer. Using excess ACVA, the end groups of each polymer were replaced with carboxylic acid functionality, which was confirmed by elemental analysis and FT-IR. The linear n-butyl methacrylate copolymers supplied by Sarah Canning were characterised and found to be sufficient for comparison with HB(BMA). These linear polymers already possessed acid functionality through the incorporation of the comonomer 4-divinyl benzoic acid. Linear polymers were amidated at the 4-vinyl benzoic acid groups through work up with excess diamines. All of the functionalised polymers were assessed for their biocompatibility, where it was found that fibroblast cells show a significant preference for acid functional polymers and not the amidated varients. This echoes the response observed on the shorter chain oligo(BMA)s - fibroblast cells grown on the amine functional materials either did not grow, or displayed unhealthy morphologies.

When compared together, it can be seen that there is no significant differences in the fibroblast viabilities between linear, oligomeric and hyperbranched P(BMA) – except in the cases where amine functionality were present. Amine functional linear polymers and unmodified HP polymers show a significant decrease in cell adhesion compared to standard materials such as tissue culture plastic (TCP) and poly(lactide-glycolic acid) (PLGA). When the functionality was preferable fibroblast cells were able to proliferate equally as well on linear and HB polymers, showing that HBPs are a viable substrate for new biomaterials.

The strong preference of fibroblasts for acid functional polymers was not observed for renal epithelial cells. The epithelial cells also showed higher average viabilities on linear(BMA) when compared to hyperbranched and oligomeric analogues – although it should be cautioned that lower viabilities were also seen on the control materials. There was also an overall increase in proliferation seen on the HB(tBuAc). It is very likely that the percentage functionality and hydrophilicity, which are related to the structure, of the polymer contribute to the ability of cells to adhere.

It is not surprising that the two cell types displayed different reactions when exposed to the same material, due to their differences in phenotype and gene expression. As discussed previously, the differences in cell genotype can be seen as differences in the localised extracellular matrix and its formation.

An attempt to produce semi-IPNs using n-butyl acrylate network with HBP(tBuAc) was made. Although these semi-IPNs showed enhanced properties over the single networks, the HBPs leached into the storage solvent over a few days.

This evidence shows that the formation of a new biomaterial is highly complex, and one functionality is unlikely to be harmonious with all cell types, indicating that the thoughtful functionalisation of polymers can increase their cytocompatibilty. When developing new materials for use in cell culture and tissue regeneration, it is important to consider the cell types to make sure that optimal polymer architecture and functionality is used. For instance, one would pick an amine functionalised polymer for use with epithelial cells, and acid functionality for fibroblast cells.

Future work

It is thought that some low Mw toxicity was observed during cell culture with oligo(BMA). A better method for the synthesis and purification of these molecules is required if further cell adhesion experiements are to be performed. Fine tuning of the polymerisation may produce a more regular distributon of butadiene so that the cleaved oligomers are of similar chain length. Meanwhile, purification techniques such as filtration and dialysis could be used to further remove very short chain oligomers.

Functional polymers can be subjected to titration, in order to assess the amount of acid functionality, which can then be used to find the optimal %acid required for fibroblast adherence.

By work up of the acid functional HBPs with diamines, it would be possible to form amine functional HBPs. These may show an increase in cell proliferation when used as a substrate for epithelial cells.

The RAFT polymerisation of t-BuAc could be repeated with a more compatible CTA – this would produce higher molecular weight HBPs that may be better suited for both cell culture and inclusion in semi-IPNs.

With increased time it would be beneficial to repeat the cell culture experiments with more sophisticated assays and imaging. For instance, fluorescent dyes are available that stain specific proteins and methods such as ELISA can be used to observe protein expression. Assaying for the presence of small molecules such as ATP can also provide valuable insight into cells' metabolic rate.

HB(BMA) polymers may not show the same leaching effects as HB(tBuAc) when incorporated into semi-IPNs. These polymers showed some agreeable cell adherence and proliferaton, and it would be interesting to see how this is affected on inclusion in a non-toxic n-butyl acrylate network. Once the optimal polymer/IPN composition had been found, this would be suitable for use as a structured cell culture substrate in the laboratory, or as a biomaterial with applications in wound healing and tissue regeneration.

6 - References

[1]   H. Frey and R. Haag, "Dendritic polyglycerol: a new versatile biocompatible material," *Rev. Mol. Biotechnol.*, vol. 90, no. 3–4, pp. 257–267, May 2002.

[2]   Y. Lim, S.-M. Kim, Y. Lee, W. Lee, T. Yang, M. Lee, H. Suh, and J. Park, "Cationic Hyperbranched Poly(amino ester): A Novel Class of DNA Condensing Molecule with Cationic Surface, Biodegradable Three-Dimensional Structure, and Tertiary Amine Groups in the Interior," *J. Am. Chem. Soc.*, vol. 123, no. 10, pp. 2460–2461, Feb. 2001.

[3]   G. Shen, C. Cai, K. Wang, and J. Lu, "Improvement of antibody immobilization using hyperbranched polymer and protein A," *Anal. Biochem.*, vol. 409, no. 1, pp. 22–27, Feb. 2011.

[4]   G. Shen, M. Liu, X. Cai, and J. Lu, "A novel piezoelectric quartz crystal immnuosensor based on hyperbranched polymer films for the detection of α-Fetoprotein," *Anal. Chim. Acta*, vol. 630, no. 1, pp. 75–81, Dec. 2008.

[5]   M. E. Cosulich, S. Russo, S. Pasquale, and A. Mariani, "Performance evaluation of hyperbranched aramids as potential supports for protein immobilization," *Polymer (Guildf).*, vol. 41, no. 13, pp. 4951–4956, Jun. 2000.

[6]   Y. Lin, K.-Y. Zhang, Z.-M. Dong, L.-S. Dong, and Y.-S. Li, "Study of Hydrogen-Bonded Blend of Polylactide with Biodegradable Hyperbranched Poly(ester amide)," *Macromolecules*, vol. 40, no. 17, pp. 6257–6267, Aug. 2007.

[7]   H. Tian, C. Deng, H. Lin, J. Sun, M. Deng, X. Chen, and X. Jing, "Biodegradable cationic PEG–PEI–PBLG hyperbranched block copolymer: synthesis and micelle characterization," *Biomaterials*, vol. 26, no. 20, pp. 4209–4217, Jul. 2005.

[8]   S. Kumar, N. Prakash, and D. Datta, "Biopolymers Based on Carboxylic Acids Derived from Renewable Resources," in in *Biopolymers*, John Wiley & Sons, Inc., 2011, pp. 167–182.

[9]   R. M. France, R. D. Short, R. A. Dawson, and S. Macneil, "Attachment of human keratinocytes to plasma co-polymers of acrylic acid/octa-1,7-diene and allyl amine/octa-1,7-diene," *J. Mater. Chem.*, vol. 8, no. 1, pp. 37–42, 1998.

[10]   R. Daw, S. Candan, A. J. Beck, A. J. Devlin, I. M. Brook, S. MacNeil, R. A. Dawson, and R. D. Short, "Plasma copolymer surfaces of acrylic acid/1,7 octadiene: Surface characterisation and the attachment of ROS 17/2.8 osteoblast-like cells," *Biomaterials*, vol. 19, no. 19, pp. 1717–1725, Oct. 1998.

[11]   P. Deshpande, R. McKean, K. A. Blackwood, R. A. Senior, A. Ogunbanjo, A. J. Ryan, and S. MacNeil, "Using poly(lactide-co-glycolide) electrospun scaffolds to deliver cultured epithelial cells to the cornea," *Regen. Med.*, vol. 5, no. 3, pp. 395–401, May 2010.

[12]   I. Cantón, R. Mckean, M. Charnley, K. A. Blackwood, C. Fiorica, A. J. Ryan, and S. MacNeil, "Development of an Ibuprofen-releasing biodegradable PLA/PGA electrospun scaffold for tissue regeneration," *Biotechnol. Bioeng.*, vol. 105, no. 2, pp. 396–408, 2010.

[13]   M. Jaiswal, V. Koul, A. K. Dinda, S. Mohanty, and K. G. Jain, "Cell adhesion and proliferation studies on semi-interpenetrating polymeric networks (semi-IPNs) of polyacrylamide and gelatin," *J. Biomed. Mater. Res. Part B Appl. Biomater.*, vol. 98B, no. 2, pp. 342–350, 2011.

[14]   K. Y. Lee and D. J. Mooney, "Hydrogels for Tissue Engineering," *Chem. Rev.*, vol. 101, no. 7, pp. 1869–1880, Jul. 2001.

[15]   O. Sadanao and O. Teruaki, "Emulsion ink for stencil printing," *US Pat. 5,779,777*, 1998.

[16]   H. Warson and C. A. Finch, *Applications of Synthetic Resin Latices: Fundamental Chemistry of Latices and Applications in Adhesives. Volume 1*. Chichester: John Wiley & Sons, Ltd., 2001, p. 730.

[17]   P. P. Constantinides, A. Tustian, and D. R. Kessler, "Tocol emulsions for drug solubilization and parenteral delivery," *Adv. Drug Deliv. Rev.*, vol. 56, no. 9, pp. 1243–1255, May 2004.

[18]   L. C. Collins-Gold, R. T. Lyons, and L. C. Bartholow, "Parenteral emulsions for drug delivery," *Adv. Drug Deliv. Rev.*, vol. 5, no. 3, pp. 189–208, Sep. 1990.

[19]   N. C. Lehman, S. W. Rhein, and J. T. Anderson, "One part woodworking adhesive compostion," 68722782005.

[20]   T. Tsutsumi, M. Sawada, and Y. Nakano, "Polymer Emulsion-Based Ink Jet Colorant and Ink," in *International Conference on Digital Printing Technologies*, 1999, pp. 133–136.

[21]   R. Wang, P.-M. Wang, and X.-G. Li, "Physical and mechanical properties of styrene-butadiene rubber emulsion modified cement mortars," *Cem. Concr. Res.*, vol. 35, no. 5, pp. 900–906, 2005.

[22]   R. Jovanović and M. A. Dubé, "Emulsion-Based Pressure-Sensitive Adhesives: A Review," *J. Macromol. Sci. - Polym. Rev.*, vol. 44, no. 1, pp. 1–51, 2004.

[23]   F. Chu and a. Guyot, "High solids content latexes with low viscosity," *Colloid Polym. Sci.*, vol. 279, no. 4, pp. 361–367, Apr. 2001.

[24]   H. Y. Erbil, *Vinyl Acetate Emulsion Polymerization and Copolymerization With Acrylic Monomers*. Boca Raton: CRC Press LLC, 2000, p. 324.

[25]   H. Warson and C. A. Finch, *Applications of Synthetic Resin Lattices Volume 2: Lattices in Surface Coatings; Emulsion Paints*. Chichester: John Wiley & Sons, Ltd., 2001.

[26]   W. D. Harkins, "A General Theory of the Mechanism of Emulsion Polymerization 1," *J. Am. Chem. Soc.*, vol. 69, no. 6, pp. 1428–1444, 1947.

[27]   W. D. Harkins, "A General Theory Of The Reaction Loci In Emulsion Polymerization. 2," *J. Chem. Phys.*, vol. 14, no. 1, pp. 47–48, 1946.

[28]   W. V. Smith and R. H. Ewart, "Kinetics of Emulsion Polymerization," *J. Chem. Phys.*, vol. 16, no. 6, p. 592, 1948.

[29]   C. S. Chern, "Emulsion polymerization mechanisms and kinetics," *Prog. Polym. Sci.*, vol. 31, no. 5, pp. 443–486, May 2006.

[30]   J. Chiefari, Y. K. B. Chong, F. Ercole, J. Krstina, J. Jeffery, T. P. T. Le, R. T. A. Mayadunne, G. F. Meijs, C. L. Moad, G. Moad, E. Rizzardo, S. H. Thang, and C. South, "Living Free-Radical Polymerization by Reversible Addition-Fragmentation Chain Transfer : The RAFT Process," *Macromolecules*, vol. 31, pp. 5559–5562, 1998.

[31]   G. Moad, E. Rizzardo, and S. H. Thang, "Living radical polymerization by the RAFT process - A first update," *Aust. J. Chem.*, vol. 59, no. 10, pp. 669–692, 2006.

[32]   G. Moad, E. Rizzardo, and S. H. Thang, "Living Radical Polymerization by the RAFT Process – A Second Update," *Australian Journal of Chemistry*, vol. 62 , no. 11. pp. 1402–1472, 2009.

[33]   G. Moad, E. Rizzardo, and S. H. Thang, "Toward Living Radical Polymerization," *Acc. Chem. Res.*, vol. 41, no. 9, pp. 1133–1142, Aug. 2008.

[34]   G. Moad, J. Chiefari, B. Y. K. Chong, J. Krstina, R. T. A. Mayadunne, A. Postma, E. Rizzardo, and S. H. Thang, "Living free radical polymerization with reversible addition – fragmentation chain transfer (the life of RAFT)," *Polym. Int.*, vol. 1001, no. January, pp. 993–1001, 2000.

[35]   G. Moad, E. Rizzardo, and S. H. Thang, "Radical addition-fragmentation chemistry in polymer synthesis," *Polymer (Guildf).*, vol. 49, no. 5, pp. 1079–1131, 2008.

[36]   C. Barner-Kowollik, *Handbook of RAFT polymeristion*. Weinheim, Germany: WILEY-VCH Verlag, 2009.

[37]   A. Gregory and M. H. Stenzel, "Complex polymer architectures via RAFT polymerization: From fundamental process to extending the scope using click chemistry and nature's building blocks," *Prog. Polym. Sci.*, vol. 37, no. 1, pp. 38–105, Jan. 2012.

[38]   Y. K. Chong, T. P. T. Le, G. Moad, E. Rizzardo, and S. H. Thang, "A More Versatile Route to Block Copolymers and Other Polymers of Complex Architecture by Living Radical Polymerization: The RAFT Process," *Macromolecules*, vol. 32, no. 6, pp. 2071–2074, Feb. 1999.

[39]   P. Sébastien and T. Pittaya, "Macromolecular design via reversible addition-fragmentation chain transfer (RAFT)/xanthates (MADIX) polymerization," *J. Polym. Sci. Part A Polym. Chem.*, vol. 43, no. 22, pp. 5347–5393, 2005.

[40]   G. Moad, E. Rizzardo, and S. H. Thang, "Living Radical Polymerization by the RAFT Process," *Aust. J. Chem.*, vol. 58, no. 6, p. 379, 2005.

[41]   J. M. Pelet and D. Putnam, "High Molecular Weight Poly(methacrylic acid) with Narrow Polydispersity by RAFT Polymerization," *Macromolecules*, vol. 42, no. 5, pp. 1494–1499, Feb. 2009.

[42]   D. B. Thomas, A. J. Convertine, L. J. Myrick, C. W. Scales, A. E. Smith, A. B. Lowe, Y. A. Vasilieva, N. Ayres, and C. L. McCormick, "Kinetics and Molecular Weight Control of the Polymerization of Acrylamide via RAFT†," *Macromolecules*, vol. 37, no. 24, pp. 8941–8950, Nov. 2004.

[43]   J. Clayden Nick Greeves, Stuart Warren and Peter Wothers, *Organic Chemistry*. Oxford: Oxford University Press, 2001, p. 1264.

[44]   J. Chiefari, R. T. A. Mayadunne, C. L. Moad, G. Moad, E. Rizzardo, A. Postma, M. A. Skidmore, and S. H. Thang, "Thiocarbonylthio Compounds (SdC(Z)S-R) in Free Radical Polymerization with Reversible Addition-Fragmentation Chain Transfer (RAFT Polymerization). Effect of the Activating Group Z," *Macromolecules*, vol. 36, pp. 2273–2283, 2003.

[45]   Sigma-Aldrich, "RAFT Polymerisation," 2012. [Online]. Available: http://www.sigmaaldrich.com/materials-science/polymer-science/raft-polymerization.html. [Accessed: 10-Dec-2012].

[46]   B. Y. K. Chong, J. Krstina, T. P. T. Le, G. Moad, A. Postma, E. Rizzardo, and S. H. Thang, "Thiocarbonylthio Compounds [SdC (Ph) S-R] in Free Radical Polymerization with Reversible Addition-Fragmentation Chain Transfer (RAFT Polymerization). Role of the Free-Radical Leaving Group (R)," vol. 36, pp. 2256–2272, 2003.

[47]   M. R. Wood, D. J. Duncalf, S. P. Rannard, and Sã©. Perrier, "Selective One-Pot Synthesis of Trithiocarbonates, Xanthates, and Dithiocarbamates for Use in RAFT/MADIX Living Radical Polymerizations," *Org. Lett.*, vol. 8, no. 4, pp. 553–556, 2006.

[48]   J. Skey and R. K. O'Reilly, "Facile one pot synthesis of a range of reversible addition-fragmentation chain transfer (RAFT) agents," *Chem. Commun.*, no. 35, pp. 4183–4185, 2008.

[49]   B. Liu, A. Kazlauciunas, J. T. Guthrie, and S. Perrier, "One-Pot Hyperbranched Polymer Synthesis Mediated by Reversible Addition Fragmentation Chain Transfer (RAFT) Polymerization," *Macromolecules*, vol. 38, no. 6, pp. 2131–2136, 2005.

[50]   B. Liu, A. Kazlauciunas, J. T. Guthrie, and S. Perrier, "Influence of reaction parameters on the synthesis of hyperbranched polymers via reversible addition

fragmentation chain transfer (RAFT) polymerization," *Polymer (Guildf).*, vol. 46, no. 17, pp. 6293–6299, 2005.

[51]   Y. Kwak, A. Goto, K. Komatsu, Y. Sugiura, and T. Fukuda, "Characterization of Low-Mass Model 3-Arm Stars Produced in Reversible Additionâˆ'Fragmentation Chain Transfer (RAFT) Process," *Macromolecules*, vol. 37, no. 12, pp. 4434–4440, 2004.

[52]   V. Philipp, P. D. Thomas, and B.-K. Christopher, "Kinetic Analysis of Reversible Addition Fragmentation Chain Transfer (RAFT) Polymerizations: Conditions for Inhibition, Retardation, and Optimum Living Polymerization," *Macromol. Theory Simulations*, vol. 11, no. 8, pp. 823–835, 2002.

[53]   R. Wang, Aileen, S. Zhu, Y. Kwak, A. Goto, T. Fukuda, and S. Monteiro, Michael, "A difference of six orders of magnitude: A reply to the magnitude of the fragmentation rate coefficient," *J. Polym. Sci. Part A Polym. Chem.*, vol. 41, no. 18, pp. 2833–2839, 2003.

[54]   S. R. Carter, R. M. England, B. J. Hunt, S. Rimmer, R. C. Steven, M. E. Richard, J. H. Barry, and R. Stephen, "Functional Graft Poly(N-isopropyl acrylamide)s Using Reversible Addition-Fragmentation Chain Transfer (RAFT) Polymerisation," *Macromol. Biosci.*, vol. 7, no. 8, pp. 975–986, Aug. 2007.

[55]   J. Rosselgong, S. P. Armes, W. R. S. Barton, and D. Price, "Synthesis of Branched Methacrylic Copolymers: Comparison between RAFT and ATRP and Effect of Varying the Monomer Concentration," *Macromolecules*, vol. 43, no. 5, pp. 2145–2156.

[56]   N. O'Brien, A. McKee, D. C. Sherrington, A. T. Slark, and A. Titterton, "Facile, versatile and cost effective route to branched vinyl polymers," *Polymer (Guildf).*, vol. 41, no. 15, pp. 6027–6031, Jul. 2000.

[57]   P. A. Costello, I. K. Martin, A. T. Slark, D. C. Sherrington, and A. Titterton, "Branched methacrylate copolymers from multifunctional monomers: chemical composition and physical architecture distributions," *Polymer (Guildf).*, vol. 43, no. 2, pp. 245–254, Jan. 2002.

[58]   F. Isaure, P. A. G. Cormack, and D. C. Sherrington, "Facile synthesis of branched poly(methyl methacrylate)s," *J. Mater. Chem.*, vol. 13, no. 11, pp. 2701–2710, 2003.

[59]   A. T. Slark, D. C. Sherrington, A. Titterton, and I. K. Martin, "Branched methacrylate copolymers from multifunctional comonomers: the effect of multifunctional monomer functionality on polymer architecture and properties," *J. Mater. Chem.*, vol. 13, no. 11, pp. 2711–2720, 2003.

[60]   S. Graham, P. A. G. Cormack, and D. C. Sherrington, "One-Pot Synthesis of Branched Poly(methacrylic acid)s and Suppression of the Rheological 'Polyelectrolyte Effect'," *Macromolecules*, vol. 38, no. 1, pp. 86–90, Dec. 2004.

[61]   G. Saunders, P. A. G. Cormack, S. Graham, and D. C. Sherrington, "Use of Rapid Triple Detection Size Exclusion Chromatography To Evaluate the Evolution of Molar

Mass and Branching Architecture during Free Radical Branching Copolymerization of Methyl Methacrylate and Ethylene Glycol Dimethacrylate," *Macromolecules*, vol. 38, no. 15, pp. 6418–6422, Jul. 2005.

[62] S. Carter, S. Rimmer, A. Sturdy, and M. Webb, "Highly Branched Stimuli Responsive Poly[(N-isopropyl acrylamide)-co-(1,2-propandiol-3-methacrylate)]s with Protein Binding Functionality," *Macromol. Biosci.*, vol. 5, no. 5, pp. 373–378, 2005.

[63] S. Reichelt, K.-J. Eichhorn, D. Aulich, K. Hinrichs, N. Jain, D. Appelhans, and B. Voit, "Functionalization of solid surfaces with hyperbranched polyesters to control protein adsorption," *Colloids Surfaces B Biointerfaces*, vol. 69, no. 2, pp. 169–177, Mar. 2009.

[64] J. Xu, L. Tao, J. Liu, V. Bulmus, and T. P. Davis, "Synthesis of Functionalized and Biodegradable Hyperbranched Polymers from Novel AB2 Macromonomers Prepared by RAFT Polymerization," *Macromolecules*, vol. 42, no. 18, pp. 6893–6901, 2009.

[65] L. Tao, J. Liu, B. H. Tan, and T. P. Davis, "RAFT Synthesis and DNA Binding of Biodegradable, Hyperbranched Poly(2-(dimethylamino)ethyl Methacrylate," *Macromolecules*, vol. 42, no. 14, pp. 4960–4962, Jun. 2009.

[66] G. Moad, Y. K. Chong, A. Postma, E. Rizzardo, and S. H. Thang, "Advances in RAFT polymerization: the synthesis of polymers with defined end-groups," *Polymer (Guildf).*, vol. 46, no. 19, pp. 8458–8468, Sep. 2005.

[67] Y. K. Chong, G. Moad, E. Rizzardo, and S. H. Thang, "Thiocarbonylthio End Group Removal from RAFT-Synthesized Polymers by Radical-Induced Reduction," *Macromolecules*, vol. 40, no. 13, pp. 4446–4455, May 2007.

[68] J.-F. Baussard, J.-L. Habib-Jiwan, A. Laschewsky, M. Mertoglu, and J. Storsberg, "New chain transfer agents for reversible addition-fragmentation chain transfer (RAFT) polymerisation in aqueous solution," *Polymer (Guildf).*, vol. 45, no. 11, pp. 3615–3626, May 2004.

[69] C. L. McCormick and A. B. Lowe, "Aqueous RAFT Polymerization: Recent Developments in Synthesis of Functional Water-Soluble (Co)polymers with Controlled Structures†," *Acc. Chem. Res.*, vol. 37, no. 5, pp. 312–325, Mar. 2004.

[70] S. E. Shim, H. Lee, and S. Choe, "Synthesis of Functionalized Monodisperse Poly(methyl methacrylate) Nanoparticles by a RAFT Agent Carrying Carboxyl End Group," *Macromolecules*, vol. 37, no. 15, pp. 5565–5571, Jul. 2004.

[71] D. Bontempo, K. L. Heredia, B. A. Fish, and H. D. Maynard, "Cysteine-Reactive Polymers Synthesized by Atom Transfer Radical Polymerization for Conjugation to Proteins," *J. Am. Chem. Soc.*, vol. 126, no. 47, pp. 15372–15373, Nov. 2004.

[72] A. Vega-rios, A. Licea-claveríe, C. De Graduados, and I. T. De Tijuana, "Controlled Synthesis of Block Copolymers containing N-isopropylacrylamide by Reversible Addition-Fragmentation Chain-Transfer (RAFT) Polymerization," *J. Mex. Chem. Soc.*, vol. 55, no. 1, pp. 21–32, 2011.

[73] S. Boisse, J. Rieger, K. Belal, A. Di-Cicco, P. Beaunier, M.-H. Li, and B. Charleux, "Amphiphilic block copolymer nano-fibers via RAFT-mediated polymerization in aqueous dispersed system," *Chem. Commun.*, vol. 46, no. 11, pp. 1950–1952, 2010.

[74] S. Boissé, J. Rieger, A. Di-Cicco, P.-A. Albouy, C. Bui, M.-H. Li, and B. Charleux, "Synthesis via RAFT of Amphiphilic Block Copolymers with Liquid-Crystalline Hydrophobic Block and Their Self-Assembly in Water," *Macromolecules*, vol. 42, no. 22, pp. 8688–8696, Oct. 2009.

[75] S. Kulkarni, C. Schilli, B. Grin, A. H. E. Müller, A. S. Hoffman, and P. S. Stayton, "Controlling the Aggregation of Conjugates of Streptavidin with Smart Block Copolymers Prepared via the RAFT Copolymerization Technique," *Biomacromolecules*, vol. 7, no. 10, pp. 2736–2741, Sep. 2006.

[76] A. S. Hoffman, "Applications of thermally reversible polymers and hydrogels in therapeutics and diagnostics," *J. Control. Release*, vol. 6, no. 1, pp. 297–305, Dec. 1987.

[77] A. S. Hoffman, "'intelligent' polymers in medicine and biotechnology," *Macromol. Symp.*, vol. 98, no. 1, pp. 645–664, 1995.

[78] S. Kulkarni, C. Schilli, A. H. E. Müller, A. S. Hoffman, and P. S. Stayton, "Reversible Meso-Scale Smart Polymer−Protein Particles of Controlled Sizes," *Bioconjug. Chem.*, vol. 15, no. 4, pp. 747–753, Jun. 2004.

[79] C. Harries, "Über die Einwirkung des Ozons auf organische Verbindungen. [Zweite Abhandlung.]," *Liebigs Ann. Chem.*, vol. 374, p. 288, 1910.

[80] C. Harries, "Über die Einwirkung des Ozons auf organische Verbindungen," *Liebigs Ann. Chem.*, vol. 343, p. 311, 1905.

[81] C. Harries, "Über die Einwirkung des Ozons auf organische Verbindungen," *Liebigs Ann. Chem.*, vol. 390, p. 235, 1912.

[82] C. Harries, "Über die Einwirkung des Ozons auf organische Verbindungen," *Liebigs Ann. Chem.*, vol. 410, p. 1, 1915.

[83] P. S. Bailey, *Organic Chemistry - A series of Monographs - Vol 39-1 Ozonoation In Organic Chemistry, Vol 1 Olefinic Compounds*. Academic Press, 1978.

[84] R. Criegee, "Mechanism of Ozonolysis," *Angew. Chem. internat. Ed.*, vol. 14, no. 11, pp. 745–752, 1975.

[85] P. S. Bailey, "The Reactions of Ozone With Organic Compounds," *Chem. Rev*, vol. 58, pp. 925–1010, 1958.

[86] T. H. Lowry and K. Schueller-Richardson, *Mechanism and Theory in Organic Chemistry* , 3rd ed. Harper and Row, 1987.

[87] R. B. Grossman, *The Art of Writing Reasonable Organic Reaction Mechanisms*. Springer, 2002.

[88] S. Gäb, W. V Turner, S. Wolff, K. H. Becker, L. Ruppert, and K. J. Brockmann, "Formation of alkyl and hydroxyalkyl hydroperoxides on ozonolysis in water and in air," *Atmos. Environ.*, vol. 29, no. 18, pp. 2401–2407, 1995.

[89] M. Nobis and D. M. Roberge, "Mastering ozonolysis: production from laboratory to ton scale in continuous flow," *Chem. Today*, vol. 29, pp. 56–58, 2011.

[90] R. H. Kienle and A. G. Hovey, "The polyhydric alcohol-polybasic acid reaction. I. Glycerol-phthalic anhydride," *J. Am. Chem. Soc.*, vol. 51, no. 2, pp. 509–519, Feb. 1929.

[91] R. H. Kienle, P. A. van der. Meulen, and F. E. Petke, "The Polyhydric Alcohol-Polybasic Acid Reaction. III. Further Studies of the Glycerol-Phthalic Anhydride Reaction," *J. Am. Chem. Soc.*, vol. 61, no. 9, pp. 2258–2268, Sep. 1939.

[92] R. H. Kienle, P. A. van der. Meulen, and F. E. Petke, "The Polyhydric Alcohol-Polybasic Acid Reaction. IV. Glyceryl Phthalate from Phthalic Acid," *J. Am. Chem. Soc.*, vol. 61, no. 9, pp. 2268–2271, Sep. 1939.

[93] G. Odian, *Principles of Polymerization*, 4th ed. Hoboken: Wiley, 2004, p. 832.

[94] P. J. Flory, "Molecular Size Distribution in Three Dimensional Polymers. I. Gelation1," *J. Am. Chem. Soc.*, vol. 63, no. 11, pp. 3083–3090, Nov. 1941.

[95] P. J. Flory, "Molecular Size Distribution in Three Dimensional Polymers. II. Trifunctional Branching Units," *J. Am. Chem. Soc.*, vol. 63, no. 11, pp. 3091–3096, Nov. 1941.

[96] P. J. Flory, "Molecular Size Distribution in Three Dimensional Polymers. III. Tetrafunctional Branching Units," *J. Am. Chem. Soc.*, vol. 63, no. 11, pp. 3096–3100, Nov. 1941.

[97] P. J. Flory, "Molecular Size Distribution in Three Dimensional Polymers. V. Post-gelation Relationships," *J. Am. Chem. Soc.*, vol. 69, no. 1, pp. 30–35, Jan. 1947.

[98] P. J. Flory, "Molecular Size Distribution in Three Dimensional Polymers. VI. Branched Polymers Containing A—R—Bf-1 Type Units," *J. Am. Chem. Soc.*, vol. 74, no. 11, pp. 2718–2723, Jun. 1952.

[99] H. R. Kricheldorf, Q.-Z. Zang, and G. Schwarz, "New polymer syntheses: 6. Linear and branched poly(3-hydroxy-benzoates)," *Polymer (Guildf).*, vol. 23, no. 12, pp. 1821–1829, Nov. 1982.

[100] Y. H. Kim and O. W. Webster, "Water soluble hyperbranched polyphenylene: 'a unimolecular micelle?'," *J. Am. Chem. Soc.*, vol. 112, no. 11, pp. 4592–4593, May 1990.

[101] E. Burakowska, J. R. Quinn, S. C. Zimmerman, and R. Haag, "Cross-Linked Hyperbranched Polyglycerols as Hosts for Selective Binding of Guest Molecules," *J. Am. Chem. Soc.*, vol. 131, no. 30, pp. 10574–10580, Jul. 2009.

[102] D. of C. E. University of Utah, "A Viscosity Primer: Viscosity Definitions," 2012. [Online]. Available: http://www.che.utah.edu/department_equipment/Projects_Lab/A_Viscometers/ViscosityDefinitions.pdf. [Accessed: 10-Dec-2012].

[103] J. Jang, J. H. Oh, and S. I. Moon, "Crystallization Behavior of Poly(ethylene terephthalate) Blended with Hyperbranched Polymers: The Effect of Terminal Groups and Composition of Hyperbranched Polymers," *Macromolecules*, vol. 33, no. 5, pp. 1864–1870, Mar. 2000.

[104] G. Ajroldi, G. Pezzin, and G. Palma, "Influence of branching on melt viscosity of polydisperse polymers," *Rheol. Acta*, vol. 10, no. 3, pp. 418–421 LA – English, 1971.

[105] W. F. Busse and R. Longworth, "Effect of molecular weight distribution and branching on the viscosity of polyethylene melts," *J. Polym. Sci.*, vol. 58, no. 166, pp. 49–69, 1962.

[106] Z. Grubisic, P. Rempp, and H. Benoit, "A universal calibration for gel permeation chromatography," *J. Polym. Sci. Part B Polym. Lett.*, vol. 5, no. 9, pp. 753–759, 1967.

[107] P. M. Wood-Adams and J. M. Dealy, "Using Rheological Data To Determine the Branching Level in Metallocene Polyethylenes," *Macromolecules*, vol. 33, no. 20, pp. 7481–7488, Sep. 2000.

[108] I. Vittorias, M. Parkinson, K. Klimke, B. Debbaut, and M. Wilhelm, "Detection and quantification of industrial polyethylene branching topologies via Fourier-transform rheology, NMR and simulation using the Pom-pom model," *Rheol. Acta*, vol. 46, no. 3, pp. 321–340 LA – English, 2007.

[109] J. M. Hernández, M. Gaborieau, P. Castignolles, M. J. Gidley, A. M. Myers, and R. G. Gilbert, "Mechanistic Investigation of a Starch-Branching Enzyme Using Hydrodynamic Volume SEC Analysis," *Biomacromolecules*, vol. 9, no. 3, pp. 954–965, Feb. 2008.

[110] K. Klimke, M. Parkinson, C. Piel, W. Kaminsky, H. W. Spiess, and M. Wilhelm, "Optimisation and Application of Polyolefin Branch Quantification by Melt-State 13C NMR Spectroscopy," *Macromol. Chem. Phys.*, vol. 207, no. 4, pp. 382–395, 2006.

[111] P. Castignolles, R. Graf, M. Parkinson, M. Wilhelm, and M. Gaborieau, "Detection and quantification of branching in polyacrylates by size-exclusion chromatography (SEC) and melt-state 13C NMR spectroscopy," *Polymer (Guildf).*, vol. 50, no. 11, pp. 2373–2383, May 2009.

[112] M. Jikei and M. Kakimoto, "Hyperbranched polymers: a promising new class of materials," *Prog. Polym. Sci.*, vol. 26, no. 8, pp. 1233–1285, Oct. 2001.

[113] C. R. Yates and W. Hayes, "Synthesis and applications of hyperbranched polymers," *Eur. Polym. J.*, vol. 40, no. 7, pp. 1257–1281, Jul. 2004.

[114] B. Voit, "New developments in hyperbranched polymers," *J. Polym. Sci. Part A Polym. Chem.*, vol. 38, no. 14, pp. 2505–2525, 2000.

[115] M. Nic, J. Jirat, and B. Kosata, "IUPAC. Compendium of Chemical Terminology, 2nd ed. (the 'Gold Book')."[Online]. Available: XML on-line corrected version: http://goldbook.iupac.org . [Accessed: 10-Dec-2012].

[116] M. S. Sánchez, G. G. Ferrer, C. T. Cabanilles, J. M. Meseguer Dueñas, M. M. Pradas, and J. L. Gómez Ribelles, "Forced compatibility in poly(methyl acrylate)/poly(methyl methacrylate) sequential interpenetrating polymer networks," *Polymer (Guildf).*, vol. 42, no. 25, pp. 10071–10075, 2001.

[117] T. Trakulsujaritchok and D. J. Hourston, "Damping characteristics and mechanical properties of silica filled PUR/PEMA simultaneous interpenetrating polymer networks," *Eur. Polym. J.*, vol. 42, no. 11, pp. 2968–2976, 2006.

[118] A. Ortega, E. Bucio, and G. Burillo, "New Interpenetrating Polymer Networks of N-isopropylacrylamide/ N-acryloxysuccinimide: Synthesis and Characterization," *Polym. Bull.*, vol. 60, no. 4, pp. 515–524, 2008.

[119] J. P. Gong, Y. Katsuyama, T. Kurokawa, and Y. Osada, "Double-Network Hydrogels with Extremely High Mechanical Strength," *Adv. Mater.*, vol. 15, no. 14, pp. 1155–1158, 2003.

[120] D. Myung, W. U. Koh, J. M. Ko, Y. Hu, M. Carrasco, J. Noolandi, C. N. Ta, and C. W. Frank, "Biomimetic strain hardening in interpenetrating polymer network hydrogels," *Polymer (Guildf).*, vol. 48, no. 18, pp. 5376–5387, 2007.

[121] P. S. K. Murthy, Y. Murali Mohan, K. Varaprasad, B. Sreedhar, and K. Mohana Raju, "First successful design of semi-IPN hydrogel-silver nanocomposites: a facile approach for antibacterial application.," *J. Colloid Interface Sci.*, vol. 318, no. 2, pp. 217–24, Feb. 2008.

[122] P. S. Gils, D. Ray, and P. K. Sahoo, "Designing of silver nanoparticles in gum arabic based semi-IPN hydrogel," *Int. J. Biol. Macromol.*, vol. 46, no. 2, pp. 237–244, Mar. 2010.

[123] S. Park, P. S. K. Murthy, S. Park, Y. M. Mohan, and W.-G. Koh, "Preparation of silver nanoparticle-containing semi-interpenetrating network hydrogels composed of pluronic and poly(acrylamide) with antibacterial property," *J. Ind. Eng. Chem.*, vol. 17, no. 2, pp. 293–297, Mar. 2011.

[124] H. Pan, H. Pu, D. Wan, M. Jin, and Z. Chang, "Proton exchange membranes based on semi-interpenetrating polymer networks of fluorine-containing polyimide and Nafion®," *J. Power Sources*, vol. 195, no. 10, pp. 3077–3083.

[125] K.-Y. Cho, H.-Y. Jung, S.-S. Shin, N.-S. Choi, S.-J. Sung, J.-K. Park, J.-H. Choi, K.-W. Park, and Y.-E. Sung, "Proton conducting semi-IPN based on Nafion and crosslinked poly(AMPS) for direct methanol fuel cell," *Electrochim. Acta*, vol. 50, no. 2–3, pp. 588–593, Nov. 2004.

[126] A. K. Bajpai, J. Bajpai, and S. Shukla, "Water sorption through a semi-interpenetrating polymer network (IPN) with hydrophilic and hydrophobic chains," *React. Funct. Polym.*, vol. 50, no. 1, pp. 9–21, Jan. 2002.

[127] Y. H. Bae and S. W. Kim, "Hydrogel delivery systems based on polymer blends, block co-polymers or interpenetrating networks," *Adv. Drug Deliv. Rev.*, vol. 11, no. 1–2, pp. 109–135, Jul. 1993.

[128] W. Wu, J. Liu, S. Cao, H. Tan, J. Li, F. Xu, and X. Zhang, "Drug release behaviors of a pH sensitive semi-interpenetrating polymer network hydrogel composed of poly(vinyl alcohol) and star poly[2-(dimethylamino)ethyl methacrylate]," *Int. J. Pharm.*, vol. 416, no. 1, pp. 104–109, Sep. 2011.

[129] X.-Z. Zhang, D.-Q. Wu, and C.-C. Chu, "Synthesis, characterization and controlled drug release of thermosensitive IPN-PNIPAAm hydrogels," *Biomaterials*, vol. 25, no. 17, pp. 3793–3805, 2004.

[130] Z. Xing, C. Wang, J. Yan, L. Zhang, L. Li, and L. Zha, "Dual stimuli responsive hollow nanogels with IPN structure for temperature controlling drug loading and pH triggering drug release," *Soft Matter*, vol. 7, no. 18, pp. 7992–7997, 2011.

[131] Y.-Y. Liu, X.-D. Fan, B.-R. Wei, Q.-F. Si, W.-X. Chen, and L. Sun, "pH-responsive amphiphilic hydrogel networks with IPN structure: A strategy for controlled drug release," *Int. J. Pharm.*, vol. 308, no. 1–2, pp. 205–209, 2006.

[132] I. Ratcliffe, P. A. Williams, C. Viebke, and J. Meadows, "Physicochemical Characterization of Konjac Glucomannan," *Biomacromolecules*, vol. 6, no. 4, pp. 1977–1986, 2005.

[133] X. Wen, X. L. Cao, Z. H. Yin, T. Wang, and C. S. Zhao, "Preparation and characterization of konjac glucomannan-poly(acrylic acid) IPN hydrogels for controlled release," *Carbohydr. Polym.*, vol. 78, no. 2, pp. 193–198, 2009.

[134] M. Heskins and J. E. Guillet, "Solution Properties of Poly(N-isopropylacrylamide)," *J. Macromol. Sci. Part A - Chem.*, vol. 2, no. 8, pp. 1441–1455, 1968.

[135] J. Su, S. T. Wall, K. E. Healy, and C. F. Wildsoet, "Scleral Reinforcement Through Host Tissue Integration with Biomimetic Enzymatically Degradable Semi-Interpenetrating Polymer Network," *Tissue Eng. Part A*, vol. 16, no. 3, pp. 905–916, 2010.

[136] K. Seon Jeong, P. Sang Jun, L. Sang Min, L. Young Moo, K. Hee Chan, and I. K. Sun, "Electroactive characteristics of interpenetrating polymer network hydrogels composed of poly(vinyl alcohol) and poly(*N*-isopropylacrylamide)," *J. Appl. Polym. Sci.*, vol. 89, no. 4, pp. 890–894, 2003.

[137] K. Seon Jeong and et al., "Properties of smart hydrogels composed of polyacrylic acid/poly(vinyl sulfonic acid) responsive to external stimuli," *Smart Mater. Struct.*, vol. 13, no. 2, p. 317, 2004.

[138] K. Seon Jeong, L. Chang Kee, and I. K. Sun, "Electrical/pH responsive properties of poly(2-acrylamido-2-methylpropane sulfonic acid)/hyaluronic acid hydrogels," *J. Appl. Polym. Sci.*, vol. 92, no. 3, pp. 1731–1736, 2004.

[139] L. K. Kostanski, R. Huang, C. D. M. Filipe, and R. Ghosh, "Interpenetrating polymer networks as a route to tunable multi-responsive biomaterials: Development of novel concepts," *J. Biomater. Sci. Polym. Ed.*, vol. 20, no. 3, pp. 271–297, 2009.

[140] M. J. Mahoney and K. S. Anseth, "Three-dimensional growth and function of neural tissue in degradable polyethylene glycol hydrogels," *Biomaterials*, vol. 27, no. 10, pp. 2265–2274, 2006.

[141] Y. X. Liu and M. B. Chan-Park, "Hydrogel based on interpenetrating polymer networks of dextran and gelatin for vascular tissue engineering," *Biomaterials*, vol. 30, no. 2, pp. 196–207, 2009.

[142] C. Deng, F. Li, J. M. Hackett, S. H. Chaudhry, F. N. Toll, B. Toye, W. Hodge, and M. Griffith, "Collagen and glycopolymer based hydrogel for potential corneal application," *Acta Biomater.*, vol. 6, no. 1, pp. 187–194.

[143] J. F. Hester, P. Banerjee, Y. Y. Won, A. Akthakul, M. H. Acar, and A. M. Mayes, "ATRP of Amphiphilic Graft Copolymers Based on PVDF and Their Use as Membrane Additives," *Macromolecules*, vol. 35, no. 20, pp. 7652–7661, 2002.

[144] J. Groll, E. V Amirgoulova, T. Ameringer, C. D. Heyes, C. Rocker, G. U. Nienhaus, and M. Moller, "Biofunctionalized, Ultrathin Coatings of Cross-Linked Star-Shaped Poly(ethylene oxide) Allow Reversible Folding of Immobilized Proteins," *J. Am. Chem. Soc.*, vol. 126, no. 13, pp. 4234–4239, 2004.

[145] C. S. Gudipati, J. A. Finlay, J. A. Callow, M. E. Callow, and K. L. Wooley, "The antifouling and fouling-release perfomance of hyperbranched fluoropolymer (HBFP)-poly(ethylene glycol) (PEG) composite coatings evaluated by adsorption of biomacromolecules and the green fouling alga ulva," *Langmuir*, vol. 21, no. 7, pp. 3044–3053, 2005.

[146] K. T. Powell, C. Cheng, and K. L. Wooley, "Complex amphiphilic hyperbranched fluoropolymers by atom transfer radical self-condensing vinyl (Co)polymerization," *Macromolecules*, vol. 40, no. 13, pp. 4509–4515, 2007.

[147] J. W. Bartels, P. L. Billings, B. Ghosh, M. W. Urban, C. Michael Greenlief, and K. L. Wooley, "Amphiphilic cross-linked networks produced from the vulcanization of nanodomains within thin films of poly(N-vinylpyrrolidinone)-b-poly (isoprene)," *Langmuir*, vol. 25, no. 16, pp. 9535–9544, 2009.

[148] C. M. Magin, S. P. Cooper, and A. B. Brennan, "Non-toxic antifouling strategies," *Mater. Today*, vol. 13, no. 4, pp. 36–44.

[149] A. Rosenhahn, S. Schilp, H. J. Kreuzer, and M. Grunze, "The role of 'inert' surface chemistry in marine biofouling prevention," *Phys. Chem. Chem. Phys.*, vol. 12, no. 17, pp. 4275–4286.

[150] R. Baier, "Surface behaviour of biomaterials: The theta surface for biocompatibility," *J. Mater. Sci. Mater. Med.*, vol. 17, no. 11, pp. 1057–1062, 2006.

[151] M. E. Callow, J. A. Callow, L. K. Ista, S. E. Coleman, A. C. Nolasco, and G. P. Lopez, "Use of Self-Assembled Monolayers of Different Wettabilities To Study Surface Selection and Primary Adhesion Processes of Green Algal (Enteromorpha) Zoospores," *Appl. Environ. Microbiol.*, vol. 66, no. 8, pp. 3249–3254, 2000.

[152] J. A. Finlay, M. E. Callow, M. P. Schultz, G. W. Swain, and J. A. Callow, "Adhesion Strength of Settled Spores of the Green Alga *Enteromorpha*," *Biofouling J. Bioadhesion Biofilm Res.*, vol. 18, no. 4, pp. 251–256, 2002.

[153] E. Ostuni, R. G. Chapman, R. E. Holmlin, S. Takayama, and G. M. Whitesides, "A Survey of Structureâˆ'Property Relationships of Surfaces that Resist the Adsorption of Protein," *Langmuir*, vol. 17, no. 18, pp. 5605–5620, 2001.

[154] B. G. Ilagan and B. G. Amsden, "Surface modifications of photocrosslinked biodegradable elastomers and their influence on smooth muscle cell adhesion and proliferation," *Acta Biomater.*, vol. 5, no. 7, pp. 2429–2440, 2009.

[155] S. Rimmer, C. Johnson, B. Zhao, J. Collier, L. Gilmore, S. Sabnis, P. Wyman, C. Sammon, N. J. Fullwood, and S. MacNeil, "Epithelialization of hydrogels achieved by amine functionalization and co-culture with stromal cells," *Biomaterials*, vol. 28, no. 35, pp. 5319–5331, 2007.

[156] Y. Sun, J. Maughan, R. Haigh, S. A. Hopkins, P. Wyman, C. Johnson, N. J. Fullwood, J. Ebdon, S. MacNeil, and S. Rimmer, "Polymethacrylate Networks as Substrates for Cell Culture," *Macromol. Symp.*, vol. 256, no. 1, pp. 137–148, 2007.

[157] R. A. Marklein and J. A. Burdick, "Controlling Stem Cell Fate with Material Design," *Adv. Mater.*, vol. 22, no. 2, pp. 175–189, 2010.

[158] B. Alberts, A. Johnson, M. Raff, K. Roberts, and P. Walter, *Molecular Biology of the Cell*, 5th ed. Garland Science, 2008, p. 1728.

[159] S. F. Badylak, "The extracellular matrix as a scaffold for tissue reconstruction," *Semin. Cell Dev. Biol.*, vol. 13, no. 5, pp. 377–383, Oct. 2002.

[160] C. Yeaman, K. K. Grindstaff, M. D. H. Hansen, and W. J. Nelson, "Cell polarity: Versatile scaffolds keep things in place," *Curr. Biol.*, vol. 9, no. 14, pp. R515–R517, Jul. 1999.

[161] R. J. McAnulty, "Fibroblasts and myofibroblasts: Their source, function and role in disease," *Int. J. Biochem. Cell Biol.*, vol. 39, no. 4, pp. 666–671, 2007.

[162] T. a Baudino, W. Carver, W. Giles, and T. K. Borg, "Cardiac fibroblasts: friend or foe?," *Am. J. Physiol. Heart Circ. Physiol.*, vol. 291, no. 3, pp. H1015–26, Oct. 2006.

[163] G. Tettamanti, A. Grimaldi, L. Rinaldi, F. Arnaboldi, T. Congiu, R. Valvassori, and M. de Eguileor, "The multifunctional role of fibroblasts during wound healing in Hirudo medicinalis (Annelida, Hirudinea).," *Biol. Cell*, vol. 96, no. 6, pp. 443–55, Aug. 2004.

[164] J. H.-C. Wang, G. Yang, Z. Li, and W. Shen, "Fibroblast responses to cyclic mechanical stretching depend on cell orientation to the stretching direction," *J. Biomech.*, vol. 37, no. 4, pp. 573–576, Apr. 2004.

[165] E. C. Breen, "Mechanical strain increases type I collagen expression in pulmonary fibroblasts in vitro Mechanical strain increases type I collagen expression in pulmonary fibroblasts in vitro," pp. 203–209, 2012.

[166] J. Gaston, B. Quinchia Rios, R. Bartlett, C. Berchtold, and S. L. Thibeault, "The response of vocal fold fibroblasts and mesenchymal stromal cells to vibration.," *PLoS One*, vol. 7, no. 2, Jan. 2012.

[167] R. Kalluri and R. A. Weinberg, "The basics of epithelial-mesenchymal transition," *J. Clin. Invest.*, vol. 119, no. 6, pp. 1420–1428, Jun. 2009.

[168] D. Radisky, "Epithelial-mesenchymal transition," *J. Cell Sci.*, vol. 118, pp. 4325–4326, 2005.

[169] E. Janda, K. Lehmann, I. Killisch, M. Jechlinger, M. Herzig, J. Downward, H. Beug, and S. Grünert, "Ras and TGFβ cooperatively regulate epithelial cell plasticity and metastasis: dissection of Ras signaling pathways ," *J. Cell Biol.* , vol. 156 , no. 2 , pp. 299–314, Jan. 2002.

[170] J. P. Thiery, "Epithelial–mesenchymal transitions in development and pathologies," *Curr. Opin. Cell Biol.*, vol. 15, no. 6, pp. 740–746, Dec. 2003.

[171] Y. Shi and J. Massagu, "Mechanisms of TGF-B Signaling from Cell Membrane to the Nucleus," *Cell*, vol. 113, no. 6. Cell Press, pp. 685–700, 13-Jun-2003.

[172] D. C. Radisky, D. D. Levy, L. E. Littlepage, H. Liu, C. M. Nelson, J. E. Fata, D. Leake, E. L. Godden, D. G. Albertson, M. Angela Nieto, Z. Werb, and M. J. Bissell, "Rac1b and reactive oxygen species mediate MMP-3-induced EMT and genomic instability," *Nature*, vol. 436, no. 7047, pp. 123–127, 2005.

[173] Y. Nakaya, S. Kuroda, Y. T. Katagiri, K. Kaibuchi, and Y. Takahashi, "Mesenchymal-Epithelial Transition during Somitic Segmentation Is Regulated by Differential Roles of Cdc42 and Rac1," *Developmental cell*, vol. 7, no. 3. Cell Press,, pp. 425–438, 01-Sep-2004.

[174] Y. Nakajima, T. Yamagishi, S. Hokari, and H. Nakamura, "Mechanisms involved in valvuloseptal endocardial cushion formation in early cardiogenesis: Roles of transforming growth factor (TGF)-β and bone morphogenetic protein (BMP)," *Anat. Rec.*, vol. 258, no. 2, pp. 119–127, 2000.

[175] B. Baum, J. Settleman, and M. P. Quinlan, "Transitions between epithelial and mesenchymal states in development and disease," *Semin. Cell Dev. Biol.*, vol. 19, no. 3, pp. 294–308, Jun. 2008.

[176] R. Li, J. Liang, S. Ni, T. Zhou, X. Qing, H. Li, W. He, J. Chen, F. Li, Q. Zhuang, B. Qin, J. Xu, W. Li, J. Yang, Y. Gan, D. Qin, S. Feng, H. Song, D. Yang, B. Zhang, L. Zeng, L. Lai, M. A. Esteban, and D. Pei, "A Mesenchymal-to-Epithelial Transition Initiates and Is Required for the Nuclear Reprogramming of Mouse Fibroblasts," *Cell stem cell*, vol. 7, no. 1. Cell Press, pp. 51–63, 02-Jul-2010.

[177] J. Poole, S. MacNeil, and S. Rimmer, "Semicontinuous Emulsion Polymerization of Butyl Methacrylate and 1, 3-Butadiene in the Presence of Cyclodextrins and Cytocompatibility of Dicarboxylic Acid Telechelic Oligo(butyl Methacrylate)s Derived from Ozonolysis of the Latexes," *Macromol. Chem. Phys.*, vol. 212, no. 18, pp. 2043–2051, Sep. 2011.

[178] J. Poole, "Functional Oligo(butylmethacrylates): Synthesis and Cytocompatibility," *Chemistry*, vol. PhD. The University of Sheffield, 2008.

[179] X. Han and J. Pan, "Polymer chain scission, oligomer production and diffusion: a two-scale model for degradation of bioresorbable polyesters.," *Acta Biomater.*, vol. 7, no. 2, pp. 538–47, Feb. 2011.

[180] Y. Sun, J. Collett, N. J. Fullwood, S. Mac Neil, and S. Rimmer, "Culture of dermal fibroblasts and protein adsorption on block conetworks of poly(butyl methacrylate-block-(2,3 propandiol-1-methacrylate-stat-ethandiol dimethacrylate)).," *Biomaterials*, vol. 28, no. 4, pp. 661–70, Feb. 2007.

[181] S. Rimmer, M. J. German, J. Maughan, Y. Sun, N. Fullwood, J. Ebdon, and S. MacNeil, "Synthesis and properties of amphiphilic networks 3: preparation and characterization of block conetworks of poly(butyl methacrylate-block-(2,3 propandiol-1-methacrylate-stat-ethandiol dimethacrylate)).," *Biomaterials*, vol. 26, no. 15, pp. 2219–30, May 2005.

[182] J. Szejtli, "Introduction and General Overview of Cyclodextrin Chemistry," *Chem. Rev.*, vol. 98, no. 5, pp. 1743–1754, 1998.

[183] W. Lau, "Emulsion Polymerization of Hydrophia Monomers," *Macromol. Symp.*, vol. 182, pp. 283–289, 2002.

[184] R. Leyrer and W. Mächtle, "Emulsion polymerization of hydrophobic monomers like stearyl acrylate with cyclodextrin as a phase transfer agent," *Macromol. Chem. Phys.*, vol. 1243, pp. 1235–1243, 2000.

[185] J. Storsberg and H. Ritter, "Cyclodextrins in polymer synthesis: free radical polymerization of cyclodextrin host-guest complexes of methyl methacrylate or styrene from homogenous aqueous solution," *Macromol. Rapid Commun.*, vol. 21, no. 5, pp. 236–241, Mar. 2000.

[186] J. Storsberg, H. van Aert, C. van Roost, and H. Ritter, "Cyclodextrins in Polymer Synthesis: A Simple and Surfactant Free Way to Polymer Particles Having Narrow Particle Size Distribution," *Macromolecules*, vol. 36, no. 1, pp. 50–53, Jan. 2003.

[187] S. Bernhardt, P. Glo, A. Theis, and H. Ritter, "Cyclodextrins in Polymer Synthesis : Influence of Acrylate Side Groups on the Initial Rate of Radical Polymerization of Various Acrylate / Methylated -cyclodextrin Complexes in Water," no. Table 1, pp. 1647–1649, 2001.

[188] N. Metz and H. Ritter, "Cyclodextrins in Polymer Synthesis: Free-Radical Polymerization of Methylated -Cyclodextrin Complexes of Methyl Methacrylate and Styrene Controlled by," pp. 4288–4290, 2000.

[189] P. Casper, P. Glo, and H. Ritter, "Cyclodextrins in Polymer Synthesis : Free Radical Copolymerization of Methylated -Cyclodextrin Complexes of Hydrophobic Monomers with N-Isopropylacrylamide in Aqueous Medium †," pp. 4361–4364, 2000.

[190] T. Loftsson, P. Jarho, M. Masson, and T. Jarvinen, "Cyclodextrins in drug delivery," *Expert Opin. Drug Deliv.*, vol. 2, no. 2, pp. 335–351, 2005.

[191] T. Loftsson and D. Duchêne, "Cyclodextrins and their pharmaceutical applications.," *Int. J. Pharm.*, vol. 329, no. 1–2, pp. 1–11, Feb. 2007.

[192] T. Loftsson and M. Brewster, "Pharmaceutical applications of cyclodextrins. 1. Drug solubilization and stabilization," *J. Pharm. Sci.*, vol. 85, no. 10, pp. 1017–1025, 1996.

[193] D. Leroylechat, F., Wouessidjewe, D., Andreux, J. P., Puisieux, F., Duchene, "Evaluation Of The Cytotoxicity Of Cyclodextrins And Hydroxypropylated Derivatives.," *Int. J. Pharm.*, vol. 101, no. 1–2, pp. 97–103, 1994.

[194] K. Irie, T., Uekama, "Pharmaceutical applications of cyclodextrins. Toxicological issues and safety evaluation.," *J. Pharm. Sci.*, vol. 86, no. 2, pp. 147–162, 1997.

[195] P. Bellringer, M. E., Smith, T. G., Read, R., Gopinath, C., Olivier, "Beta-Cyclodextrin - 52-Week Toxicity Studies In The Rat And Dog.," *Food Chem. Toxicol.*, vol. 33, no. 5, pp. 367–376, 1995.

[196] E. R. Santee, R. Chang, and M. Morton, "300 MHz proton NMR of polybutadiene: Measurement of cis-trans isomeric content," *J. Polym. Sci. Polym. Lett. Ed.*, vol. 11, no. 7, pp. 449–452, 1973.

[197] L. A. Fraga and M. I. B. Tavares, "NMR Characterization of High cis Polybutadiene," *Ann. Magn. Reson.*, vol. 3, no. 3, pp. 68–72, 2004.

[198] K. Matyjaszewski and T. P. Davis, *Handbook of radical polymerization*, 1st ed. Wiley-Interscience, 2002, p. 936.

[199] N. Nakajima and Y. Ikada, "Mechanism of amide formation by carbodiimide for bioconjugation in aqueous media.," *Bioconjug. Chem.*, vol. 6, no. 1, pp. 123–30, 1995.

[200] H. Swaisgood and M. Natake, "Effect of Carboxyl Group Modification on Some of the Enzymatic Properties of L-Glutamate Dehydrogenase," *J. Biochem.*, vol. 74, no. 1, pp. 77–86, Jul. 1973.

[201] B. D. Ratner, A. S. Hoffman, F. J. Schoen, and J. E. Lemons, *Biomaterials Science: An Introduction to Materials in Medicine*, 3rd ed. California: Elsevier Academic Press, 2004, p. 851.

[202] J. Chandra, J. D. Patel, J. Li, G. Zhou, P. K. Mukherjee, T. S. Mccormick, J. M. Anderson, M. A. Ghannoum, C. E. T. Al, and A. P. P. L. E. N. M. Icrobiol, "Modification of Surface Properties of Biomaterials Influences the Ability of Candida albicans To Form Biofilms," *Appl. Environ. Microbiol.*, vol. 71, no. 12, pp. 8795–8801, 2005.

[203] L. Wightman, R. Kircheis, V. Rössler, S. Carotta, R. Ruzicka, M. Kursa, and E. Wagner, "Different behavior of branched and linear polyethylenimine for gene delivery in vitro and in vivo," *J. Gene Med.*, vol. 3, no. 4, pp. 362–372, 2001.

[204] W. T. Godbey, K. K. Wu, and a G. Mikos, "Size matters: molecular weight affects the efficiency of poly(ethylenimine) as a gene delivery vehicle.," *J. Biomed. Mater. Res.*, vol. 45, no. 3, pp. 268–75, Jun. 1999.

[205] M. L. Amirpour, P. Ghosh, W. M. Lackowski, R. M. Crooks, and M. V Pishko, "Mammalian cell cultures on micropatterned surfaces of weak-acid, polyelectrolyte hyperbranched thin films on gold.," *Anal. Chem.*, vol. 73, no. 7, pp. 1560–6, Apr. 2001.

[206] H. Huang, C. Ho, T. Lee, T. Lee, K. Liao, and F. Chen, "Effect of surface roughness of ground titanium on initial cell adhesion," vol. 21, pp. 93–97, 2004.

[207] D. D. Deligianni, N. D. Katsala, P. G. Koutsoukos, and Y. F. Missirlis, "Effect of surface roughness of hydroxyapatite on human bone marrow cell adhesion , proliferation , differentiation and detachment strength," *Biomaterials*, vol. 22, pp. 87–96, 2001.

[208] J. E. Folk, M. H. Park, S. I. Chung, J. Schrode, E. P. Lester, and H. L. Cooper, "Polyamines as physiological substrates for transglutaminases," *J. Biol. Chem.*, vol. 255, no. 8, pp. 3695–3700, Apr. 1980.

[209] L. Lorand and S. Conrad, "Transglutaminases," *Mol. Cell Biochem.*, vol. 58, no. 1–2, pp. 9–35, Aug. 1984.

[210] A. Ichinose, R. E. Bottenus, and E. W. Davie, "Structure of transglutaminases.," *J. Biol. Chem.*, vol. 265, no. 23, pp. 13411–4, Aug. 1990.

[211] J. C. Byrd and U. Lichtin, "Two Types of Transglutaminase in the PC12 Pheochromocytoma Cell," *J. Biol. Chem.*, vol. 262, no. 24, pp. 11699–11705, 1987.

[212] K. Nara, K. Nakanishi, H. Hagiwara, K. Wakita, S. Kojima, and S. Hirose, "Retinol-induced morphological changes of cultured bovine endothelial cells are accompanied

by a marked increase in transglutaminase.," *J. Biol. Chem.*, vol. 264, no. 32, pp. 19308–12, Nov. 1989.

[213] S. G. Priglinger, "TGF-B2-Induced Cell Surface Tissue Transglutaminase Increases Adhesion and Migration of RPE Cells on Fibronectin through the Gelatin-Binding Domain," *Invest. Ophthalmol. Vis. Sci.*, vol. 45, no. 3, pp. 955–963, Mar. 2004.

[214] L. Technologies, "Alamarblue(R) Cell Viability Assay Protocol," 2012. [Online]. Available: http://www.invitrogen.com/site/us/en/home/References/protocols/cell-and-tissue-analysis/cell-profilteration-assay-protocols/cell-viability-with-alamarblue.html. [Accessed: 07-Oct-2012].

[215] D. C. Martin, J. L. Semple, and M. V Sefton, "Poly(methacrylic acid-co-methyl methacrylate) beads promote vascularization and wound repair in diabetic mice," *J Biomed Mater Res A.*, vol. 93, no. 2, pp. 484–492, 2010.

[216] M. J. Butler and M. Sefton, "Poly(butyl methacrylate-co-methacrylic acid) tissue engineering scaffold with pro-angiogenic potential in vivo," *J Biomed Mater Res A.*, vol. 82, no. 2, pp. 265–273, 2007.

[217] E. Ruoslahti, "Integrins," *J. Clin. Investig.*, vol. 87, pp. 1–5, 1991.

[218] E. Ruoslahti, "Proteoglycans in cell regulation.," *J. Biol. Chem.*, vol. 264, no. 23, pp. 13369–13372, Aug. 1989.

[219] R. G. LeBaron and K. a Athanasiou, "Extracellular matrix cell adhesion peptides: functional applications in orthopedic materials.," *Tissue Eng.*, vol. 6, no. 2, pp. 85–103, Apr. 2000.

[220] C. Johnson, L. Perlin, P. Wyman, B. Zhao, N. J. Fullwood, S. MacNeil, and S. Rimmer, "Cell Adhesion to Polymethacrylate Networks Prepared by Photopolymerization and Functionalized with GRGDS Peptide or Fibrinogen," *Macromol. Symp.*, vol. 291–292, no. 1, pp. 314–325, 2010.

[221] L. Perlin, S. MacNeil, and S. Rimmer, "Cell adhesive hydrogels synthesised by copolymerisation of arg-protected Gly-Arg-Gly-Asp-Ser methacrylate monomers and enzymatic deprotection," *Chem. Commun.*, no. 45, pp. 5951–5953, 2008.

[222] L. Perlin, S. MacNeil, and S. Rimmer, "Production and performance of biomaterials containing RGD peptides," *Soft Matter*, vol. 4, no. 12, pp. 2331–2349, 2008.

[223] Z. Song and W. E. Baker, "Chemical reactions and reactivity of primary, secondary, and tertiary diamines with acid functionalized polymers," *J. Polym. Sci. Part A Polym. Chem.*, vol. 30, no. 8, pp. 1589–1600, 1992.

[224] K. B. Walters and D. E. Hirt, "Synthesis and Characterization of a Tertiary Amine Polymer Series from Surface-Grafted Poly(tert-butyl acrylate) via Diamine Reactions," *Macromolecules*, vol. 40, no. 14, pp. 4829–4838, Jun. 2007.

[225] M. J. Betts and R. . Russell, "Amino acid properties and consequences of subsitutions.," in in *Bioinformatics For Geneticists*, Wiley, 2003.

[226] M. S. Searle, S. R. Griffiths-Jones, and H. Skinner-Smith, "Energetics of Weak Interactions in a β-hairpin Peptide: Electrostatic and Hydrophobic Contributions to Stability from Lysine Salt Bridges," *J. Am. Chem. Soc.*, vol. 121, no. 50, pp. 11615–11620, Nov. 1999.

[227] N. Errington and A. J. Doig, "A Phosphoserine−Lysine Salt Bridge within an α-Helical Peptide, the Strongest α-Helix Side-Chain Interaction Measured to Date†," *Biochemistry*, vol. 44, no. 20, pp. 7553–7558, Apr. 2005.

[228] R. B. Rucker and J. Murray, "Cross-linking amino acids in collagen and elastin. ," *Am. J. Clin. Nutr.* , vol. 31 , no. 7 , pp. 1221–1236, Jul. 1978.

[229] R. C. Siegel and G. R. Martin, "Collagen Cross-linking. Enzymatic synthesis of lysine-derived aldehydes and the production of cross-linked components," *J. Biol. Chem.*, vol. 245, no. 7, pp. 1653–1658, Apr. 1970.

[230] S. Canning, "Synthesis and characterisation of highly branched poly(butyl methacrylate)s with acid functional end groups," The University of Sheffield, Master's Thesis, 2011.

[231] K. Matyjaszewski and A. H. E. Müller, *Controlled and Living Polymerizations: From Mechanisms to Applications*. Weinheim, Germany: John Wiley & Sons, 2009.

[232] J. Bandrup and E. H. Immergut, *Polymer Handbook*, 2nd Ed. New York: Wiley, 1975, p. SEC IV.

[233] S. B. Kharchenko, R. M. Kannan, J. J. Cernohous, and S. Venkataramani, "Role of Architecture on the Conformation, Rheology, and Orientation Behavior of Linear, Star, and Hyperbranched Polymer Melts. 1. Synthesis and Molecular Characterization," *Macromolecules*, vol. 36, no. 2, pp. 399–406, Jan. 2003.

[234] E. T. F. Geladé, B. Goderis, C. G. de Koster, N. Meijerink, R. A. T. M. van Benthem, R. Fokkens, N. M. M. Nibbering, and K. Mortensen, "Molecular Structure Characterization of Hyperbranched Polyesteramides," *Macromolecules*, vol. 34, no. 11, pp. 3552–3558, Apr. 2001.

[235] P. F. W. Simon, A. H. E. Müller, and T. Pakula, "Characterization of Highly Branched Poly(methyl methacrylate) by Solution Viscosity and Viscoelastic Spectroscopy," *Macromolecules*, vol. 34, no. 6, pp. 1677–1684, Feb. 2001.

[236] C. M. Yakacki, R. Shandas, C. Lanning, B. Rech, A. Eckstein, and K. Gall, "Unconstrained recovery characterization of shape-memory polymer networks for cardiovascular applications.," *Biomaterials*, vol. 28, no. 14, pp. 2255–63, May 2007.

[237] H. M. Wache, D. J. Tartakowska, A. Hentrich, and M. H. Wagner, "Development of a polymer stent with shape memory effect as a drug delivery system," *J. Mater. Sci. Mater. Med.*, vol. 14, no. 2, pp. 109–112 LA − English, 2003.

[238] A. Metcalfe, A.-C. Desfaits, I. Salazkin, L. Yahia, W. M. Sokolowski, and J. Raymond, "Cold hibernated elastic memory foams for endovascular interventions," *Biomaterials*, vol. 24, no. 3, pp. 491–497, Feb. 2003.

[239] B. Masař and P. Vlček, "Block copolymers by sequential group transfer polymerization: poly(methyl methacrylate)-block-poly(2-ethylhexyl acrylate) and poly(methyl methacrylate)-block-poly(tert-butyl acrylate)," *Macromol. Chem. Phys.*, vol. 195, no. 2, pp. 671–678, 1994.

[240] J. P. Hautekeer, S. K. Varshney, R. Fayt, C. Jacobs, R. Jerome, and P. Teyssie, "Anionic polymerization of acrylic monomers. 5. Synthesis, characterization and modification of polystyrene-poly(tert-butyl acrylate) di- and triblock copolymers," *Macromolecules*, vol. 23, no. 17, pp. 3893–3898, Aug. 1990.

[241] J. W. Klein, J.-P. Lamps, Y. Gnanou, and P. Rempp, "Synthesis and characterization of block copolymers containing poly(tert.butyl acrylate) blocks," *Polymer (Guildf).*, vol. 32, no. 12, pp. 2278–2282, 1991.

[242] S. K. Varshney, C. Jacobs, J. P. Hautekeer, P. Bayard, R. Jerome, R. Fayt, and P. Teyssie, "Anionic polymerization of acrylic monomers. 6. Synthesis, characterization, and modification of poly(methyl methacrylate)-poly(tert-butyl acrylate) di- and triblock copolymers," *Macromolecules*, vol. 24, no. 18, pp. 4997–5000, Sep. 1991.

[243] M. Bednarek, T. Biedroń, and P. Kubisa, "Synthesis of block copolymers by atom transfer radical polymerization of tert-butyl acrylate with poly(oxyethylene) macroinitiators," *Macromol. Rapid Commun.*, vol. 20, no. 2, pp. 59–65, 1999.

[244] R. M. Kriegel, W. S. Rees, and M. Weck, "Synthesis and Hydrolysis of Poly (norbornene)/ Poly (acrylic acid) Graft Copolymers Synthesized via a Combination of Atom-Transfer Radical Polymerization and Ring-Opening Metathesis Polymerization Graft copolymers offer the unique possibility of tailo," *Macromolecules*, vol. 37, pp. 6644–6649, 2004.

[245] Y. Zhou, M. L. Bruening, D. E. Bergbreiter, R. M. Crooks, and M. Wells, "Preparation of Hyperbranched Polymer Films Grafted on Self-Assembled Monolayers," *J. Am. Chem. Soc.*, vol. 118, pp. 3773–3774, 1996.

[246] K. B. Walters and D. E. Hirt, "Grafting of end-functionalized poly(tert-butyl acrylate) to poly(ethylene-co-acrylic acid) film," *Polymer (Guildf).*, vol. 47, no. 19, pp. 6567–6574, Sep. 2006.

[247] D. H. Wertz and D. C. Prevorsek, "Dicyanate semi IPNs—A new class of high performance, high temperature plastics," *Polym. Eng. Sci.*, vol. 25, no. 13, pp. 804–806, 1985.

[248] L. Pescosolido, W. Schuurman, J. Malda, P. Matricardi, F. Alhaique, T. Coviello, P. R. van Weeren, W. J. A. Dhert, W. E. Hennink, and T. Vermonden, "Hyaluronic Acid and Dextran-Based Semi-IPN Hydrogels as Biomaterials for Bioprinting," *Biomacromolecules*, vol. 12, no. 5, pp. 1831–1838, Mar. 2011.

[249] D. Myung, D. Waters, M. Wiseman, P. Duhamel, C. N. Ta, and C. W. Frank, "Progress in the development of interpenetrating polymer network hydrogels," *Polym. Adv. Technol.*, vol. 19, no. 6, pp. 647–657, 2009.

[250] D. J. Keddie, G. Moad, E. Rizzardo, and S. H. Thang, "RAFT Agent Design and Synthesis," *Macromolecules*, vol. 45, no. 13, pp. 5321–5342, Jul. 2012.

[251] S. R. S. Ting, T. P. Davis, and P. B. Zetterlund, "Retardation in RAFT Polymerization: Does Cross-Termination Occur with Short Radicals Only?," *Macromolecules*, vol. 44, no. 11, pp. 4187–4193, May 2011.

[252] D. Konkolewicz, B. S. Hawkett, A. Gray-Weale, and S. Perrier, "RAFT polymerization kinetics: How long are the cross-terminating oligomers?," *J. Polym. Sci. Part A Polym. Chem.*, vol. 47, no. 14, pp. 3455–3466, 2009.

[253] W. Meiser, J. Barth, M. Buback, H. Kattner, and P. Vana, "EPR Measurement of Fragmentation Kinetics in Dithiobenzoate-Mediated RAFT Polymerization," *Macromolecules*, vol. 44, no. 8, pp. 2474–2480, Mar. 2011.

[254] T. Junkers, "RAFT kinetics revisited: Revival of the RAFT debate," *J. Polym. Sci. Part A Polym. Chem.*, vol. 49, no. 19, pp. 4154–4163, 2011.

[255] C. Barner-Kowollik, M. Buback, B. Charleux, M. L. Coote, M. Drache, T. Fukuda, A. Goto, B. Klumperman, A. B. Lowe, J. B. Mcleary, G. Moad, M. J. Monteiro, R. D. Sanderson, M. P. Tonge, and P. Vana, "Mechanism and kinetics of dithiobenzoate-mediated RAFT polymerization. I. The current situation," *J. Polym. Sci. Part A Polym. Chem.*, vol. 44, no. 20, pp. 5809–5831, 2006.

[256] C. Barner-Kowollik, M. L. Coote, T. P. Davis, L. Radom, and P. Vana, "The reversible addition-fragmentation chain transfer process and the strength and limitations of modeling: Comment on 'the magnitude of the fragmentation rate coefficient'," *J. Polym. Sci. Part A Polym. Chem.*, vol. 41, no. 18, pp. 2828–2832, 2003.

[257] M. Long, D. W. Thornthwaite, S. H. Rogers, G. Bonzi, F. R. Livens, and S. P. Rannard, "Utilising (14)C-radiolabelled atom transfer radical polymerisation initiators.," *Chem. Commun. (Camb).*, no. 42, pp. 6406–8, Nov. 2009.

[258] M. Long, S. H. Rogers, D. W. Thornthwaite, F. R. Livens, and S. P. Rannard, "Monitoring Atom Transfer Radical Polymerisation using 14C-radiolabelled initiators," *Polym. Chem.*, vol. 2, no. 3, p. 581, 2011.

[259] O. Biondi, S. Motta, and P. Mosesso, "Low molecular weight polyethylene glycol induces chromosome aberrations in Chinese hamster cells cultured in vitro," *Mutagen.* , vol. 17 , no. 3 , pp. 261–264, May 2002.